Plasmachemical Functionalisation for Modification of Surfaces with Biomolecules and Metals

MCGETTRICK, JAMES,DOUGLAS

Plasmachemical Functionalisation for Modification of Surfaces with Biomolecules and Metals

By

James Douglas McGettrick

A thesis submitted as part of the degree of Doctor of Philosophy, Department of Chemistry, University of Durham.

2010

Table of Contents

List of Figures

4. A substrate independent route for DNA microarray manufacture using 3-vinylbenzaldehyde

5. A substrate independent route for DNA microarray manufacture using 2-bromoethylacrylate

6. A plasmachemical route to smart wound dressings – some initial results

7. Plasmachemical functionalisation of single walled carbon nanotubes

Publications and Patents

This work has contributed to the following journal publications and patents.

Journal Publications

A Substrate-Independent Approach for the Surface Immobilization of Oligonucleotides using Aldehyde Functionalized Surfaces.
McGettrick, J. D.; Schofield, W. C. E.; Garrod, R. P.; Badyal, J. P. S
Chemical Vapour Deposition **2009**, *15*, 122

Bromine-containing functional nanolayers for biomolecule immobilization.
McGettrick, J. D.; Crockford, T.; Schofield, W. C. E.; Badyal, J. P. S. *Applied Surface Science* **2009**, *256S*, S30

Patents

A Method for Producing an Aldehyde Containing Coating
Badyal, J. P. S.; Schofield, W. C. E.; McGettrick, J.
WO 2006 100480

Article, and a Method for Creating the Atricle, with a Chemically Patterned Surface
Badyal, J. P. S.; McGettrick, J.; Harris, L. G.
US Application 2010 0055413

Acknowledgements

I would like to thank my supervisor Professor J. P. S. Badyal for both his faith and support. I would also like to thank all of my co-workers in the Durham Surface Science group. Special mentions are deserved for Dr. W. C. E. Schofield for his tireless advice, conversation and support. Thanks also to T. J. Bradley and R. P. Garrod for fluorescence and Raman microscopy work, and to Dr. C. Spanos for introducing me to the practicalities of plasma polymerisation. A special mention also to T. Crockford and S. M. D. Watson for work with brominated monomers.

Thanks to S. Przyborski of the School of Biomedical Sciences in Durham for the use of the microarray scanner, and to Dr. D. R. W. Hodgson for useful discussions concerning the surface tethering of biomolecules. Thanks to Dr. P. W. Dyer for lab space, practical help and conversation on the surface tethering of MTO.

My thanks also go to EPSRC for funding.

Dedication

To Mum.

Abstract

Plasmachemical functionalisation offers a versatile route to surface functionalisation, allowing a wide variety of functional groups to be deposited in a substrate independent process. This thesis presents the application of pulsed plasmachemical functionalisation in two areas.

Firstly, the construction of covalently tethered DNA or protein arrays is examined, and novel routes are presented based on the introduction of aldehyde and bromine functions onto substrates such as glass, silicon, polystyrene beads and carbon nanotubes.

Secondly, the use of plasmachemical layers for the tethering of metal centres is also presented, with aldehyde and vinylpyridine functional surfaces presented, and their use in the metallization of substrates such as carbon nanotubes demonstrated. The functionalisation and reaction of plasmachemical surfaces is monitored by a variety of surface sensitive methods including XPS, FT-IR, contact angles, and reflectometry.

Overview

In order to put the experimental chapters into some context, chapter one contains a brief overview of plasmachemical functionalisation and plasmas, and a general literature survey on the subject of DNA microarray technology, and acts as an introduction to the three chapters dealing with biological molecule interactions with plasmachemical surfaces. As discussed in more depth in the chapters themselves, plasmachemical technology offers a promising route to circumvent the often complex chemistries used in DNA microarrays with a single, substrate-independent functionalisation. This is followed by an overview of typical surface analysis techniques such as XPS, FT-IR, contact angle analysis and reflectometry in chapter two.

Chapter three describes the use of undec-1-enal to introduce aldehyde functions onto the substrate surface, and the use of this aldehyde surface to tether DNA onto via the well known reductive amination route. Chapter four follows a similar route, using the 3-vinylbenzaldehyde monomer to introduce the aldehyde surface functions, and extending the repertoire of biological molecules to include proteins and dextrans. Both of these approaches allowed the formation of DNA microarrays, showing the potential of pulsed plasmachemical technology in the manufacture of biological systems. Chapter five describes a novel approach using 2-bromoethyl acrylate as a precursor to generate bromine functionalised surfaces, which are then suitable for reaction with thiol-terminated oligonucleotides. Chapter sixincludes some initial results based on the surface immobilisation of a biologically derived chloromethyl ketone

The work on metallization of SWCNT's follows on from chapters three and four, where silver deposition onto the aldehyde surfaces showed promise, and was extended to the use of vinylpyridine surfaces, both for metallization (chapter seven) and tethering of the methyl rhenium trioxide catalyst, where preliminary results are presented in the appendix.

1. An introduction to plasmas and DNA microarray technology.

1.1 What is a plasma?

Plasma is the fourth state of matter alongside the solid, liquid and gas states. A plasma is defined as a quasi-neutral gas of both neutral and ionised particles, displaying a collective behaviour[1]. The ions in this gas consist mainly of positively charged atoms or molecules, with negatively charged electrons.

Plasmas are classified into one of three types:

1) Complete Thermal Equilibrium (CTE) Plasmas. The plasma is in total thermal equilibrium, so that the temperatures of electrons (T_e) and all of the temperatures associated with heavier species (e.g. translational energy, T_g) are equal. Stars contain CTE plasmas, but they do not exist in controlled laboratory conditions.

2) Local Thermodynamic Equilibrium (LTE) Plasmas, also known as "thermal" or "equilibrium" plasmas. These plasmas are formed when heavy particles within the plasma are particularly energetic. T_e and the temperatures of heavy particles are equal. Electric arcs and plasma torches are an example of LTE plasmas. They exist at temperatures <6000K.

3) Non-local thermodynamic equilibrium plasmas (non-LTE), also known as "cold" or "non-equilibrium" plasmas. In a cold plasma T_e is much greater than that of the ions, and the temperature of the overall gas (T_g) is lower still. These cold plasmas have found much use in chemistry[2,3].

1.2 Interactions in plasmas

Plasmas contain a variety of particles. Before the plasma is ignited, a small amount of initial free electrons are present in the system, arising from ionisation of gaseous molecules by naturally occurring radioactivity or cosmic rays[4]. Electrons are the lightest particles in the plasma; they are easily accelerated and absorb the largest amount of energy from any

external source. When an electric field is initially applied to a gas, it is the acceleration of electrons and the resultant ionisation events that result in the plasma.

Electrons and large particles will undergo many interactions, with kinetic energy being lost by ionisation, excitation in inelastic collisions. Collisions involving no change in excitation are described as elastic. Some of the more common interactions are outlined below.

Elastic electron-large particle energy transfer: As energy is conserved, the energy transfer, W_{Tr} is simply determined by the mass ratio of the particles[1]:

$$W_{Tr} = \frac{2m_e}{M} W$$

Where M is the mass of the heavy particle, W is the energy of the electron and m_e is the mass of the electron. The mass of the electron is so small however, that the target heavy particle will be virtually unaffected by the collision.

For inelastic collision, the fraction of energy transferred is given by[1]

$$\frac{W_{Tr}}{W} = \frac{M}{m_{in} + M}$$

where m_{in} is the mass of the particle losing energy.

Excitation: An electron impact promotes an electron from the target into a higher energy level in an atom.

Relaxation: Excited atoms and molecules relax back into their ground states and as they do so, they release photons of energy. This process causes plasmas to glow distinctively, and photons are emitted from the deep UV to the visible spectrum to the far infrared region[5].

Dissociation is the breaking apart of a molecule by electron impact, often leaving highly reactive radical species:

Electron Attachment can also result in the generation of radicals. Halogen atoms in particular will easily form radicals:

Other processes include charge transfers and collisions involving excited molecules[6].

Ionisation: Electron impact ionisation results from an electron collision that also ionises an atom, to produce a positive ion and two electrons[5].

$$e^- + Ar \rightarrow 2e^- + Ar^+$$

Electron impact ionisation is the most common ionisation within the plasma. The electrons are accelerated to velocities that can induce ionisation by the external electric field. The reverse process of *recombination* also takes place.

$e^- + CF_4 \rightarrow e^- + \bullet CF_3 + \bullet F$ (dissociation)

$e^- + CF_4 \rightarrow 2e^- + {}^+CF_3 + \bullet F$ (dissociative ionisation)

$SF_6 + e^- \rightarrow SF_5^- + \bullet F$

Thus, plasmas contain a ready sea of radical species that can initiate polymerisation by reaction with molecules within the plasma.

1.3 Cold Plasmas for Chemical Modification

The functionalisation of surfaces with polymeric species occurs when suitable organic precursors are introduced into the cold plasma. The collision mechanisms described above result in the generation of active species both in the plasma itself and on the surface of any local substrate, which can then react to form an organic film.

Plasma polymerisation allows tailoring of surface properties such as surface energy or wear resistance, or the introduction of new chemical functionality. The plasmachemical layers are also transparent and can act as barrier layers[7].

Plasma polymerisation differs markedly from conventional polymerisation. In a conventional polymerisation there is very little molecular rearrangement and the polymers consist of orderly repeat units. In plasma there is an abundance of reactive species such as radicals and ions which leads to highly branched, cross-linked species. Plasma polymerisation is characterised by several features[1]:

1) A lack of distinct repeat units such as those in conventional polymers.

2) Properties of a given plasma polymer can vary depending on the plasma conditions.

3) Functional groups such as double bonds are not essential for polymerisation to occur.

Considering plasma polymerisation as consisting of a series of steps, initiation, propagation and termination, we see in the initiation phase bonds are opened and free radicals formed by the processes already discussed above. Where molecules and radicals are adsorbed onto the surface formation of the polymer film can begin (Figure 1.1, reaction 1). The propagation of the reaction can continue both in the plasma itself and on the surface by reaction of radicals with species in the plasma (Reactions 2 & 3). Termination occurs when radical species react together to give a neutral species (Reactions 4, 5 & 6). However, plasmas can generate new radicals which will re-initiate polymerisation.

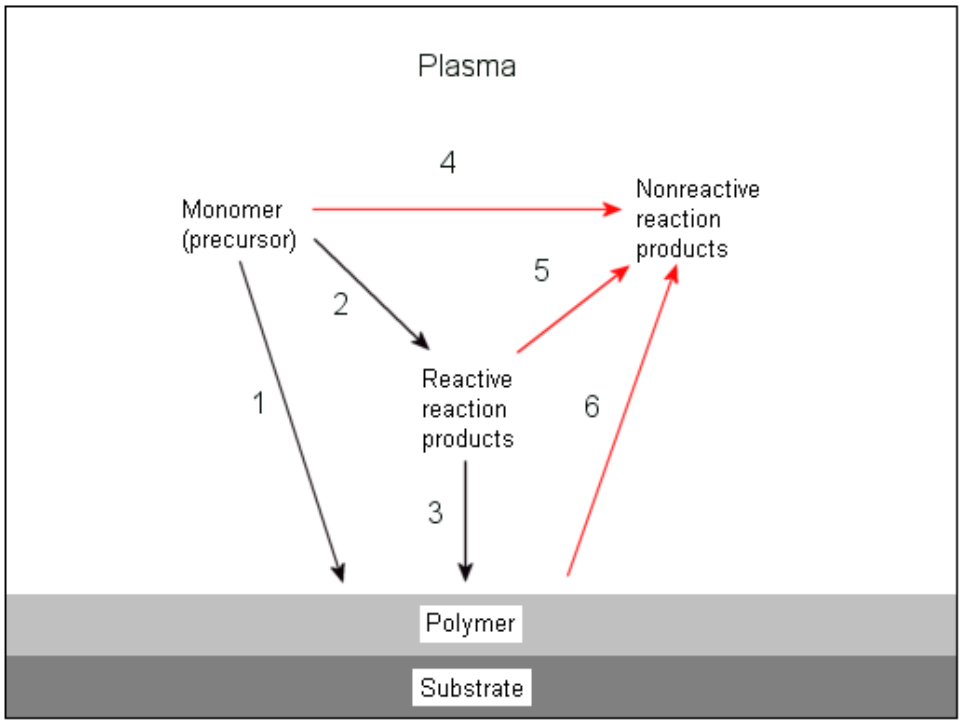

Figure 1.1. Interactions in a plasma[1]

1.4 Pulsed Plasma Polymerisation

Pulsed plasma polymerisation is a technique that is becoming widely used. The pulsing of the power input to the plasma has several advantages[8]:

The overall efficiency of the plasma polymerisation process is increased. The average power <P> delivered to the system during pulsing can be calculated[9]

$$< P >= P_P \left(\frac{t_{on}}{t_{on} + t_{off}}\right)$$

Where variables include the peak power (P_P) delivered to the glow discharge, on time (t_{on}) and off time (t_{off}).

It has also been found that structural retention can be improved by carefully tailoring these parameters for a given monomer. During the pulse on-time, plasma polymerisation occurs and radical populations increase. In the off-period radical initiated chain growth takes place[10]. This reduces the time

during which the monomer is exposed to destructive dissociation reactions, whilst still applying enough energy to maintain the plasma itself.

1.5 Introduction to DNA microarrays

DNA microarrays have found application in many fields, as diverse as computing[11,12] drug discovery[13], cancer research[14], and the elucidation of the human genome[15]. In particular, they allow simultaneous screening of large numbers of oligonucleotides, thereby reducing both the time and expense for DNA based diagnostics[16]. Typically, the oligonucleotides are assembled onto a solid surface either by in situ synthesis[17,18] or mechanical spotting[16]. Surface functionality plays a key role during microarray fabrication[19], and has in the past been limited to specific substrate materials and geometries, e.g. self-assembled monolayers (SAMs on glass[20,21,22], silicon[23], or gold[24,25,26]), Schiff-base derivatisation of aminated PMMA polymer[27], and alcoholysis of surface-generated acyl halides on diamond[28].

In the following chapters a route for constructing DNA chips is presented in which a substrate is plasmachemically functionalized by utilizing undec-1-enal, 3-vinylbenzaldehyde, and 2-bromoethylacrylate precursors. The obtained surface functionalities are shown to be suitable for the immobilization and hybridization of 15-base oligonucleotides, and the readout of hybridization via microarray fabrication.

1.6 DNA

Deoxyribose nucleic acid (DNA) is a powerful information encoder which forms the basis of life.

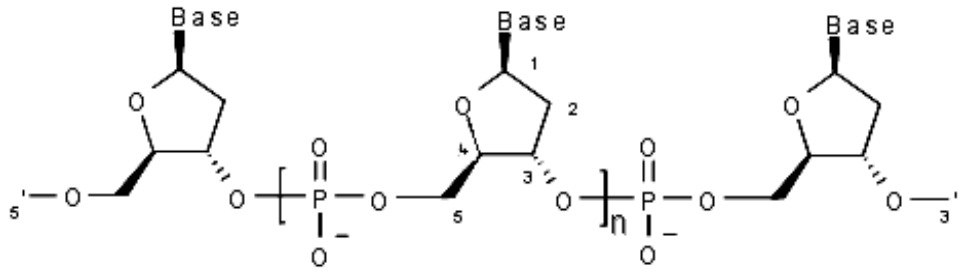

Figure 1.2. DNA sugar-phosphate backbone

The DNA molecule itself is formed from a polymeric backbone comprising of a chain of 2-deoxyribose sugars linked by phosphodiester linkages between the 5' and 3' carbons on adjacent 2-deoxyribose sugars (Figure 1.2). Attached to the 1' carbon of the deoxyribose unit is one of four bases: the purines Adenine (A) and Guanine (G), or pyrimidines Cytosine (C) and Thymine (T). The order of these bases along the DNA strand is known as the primary structure, which forms the information encoding for life in the form of genes[29,30,19].

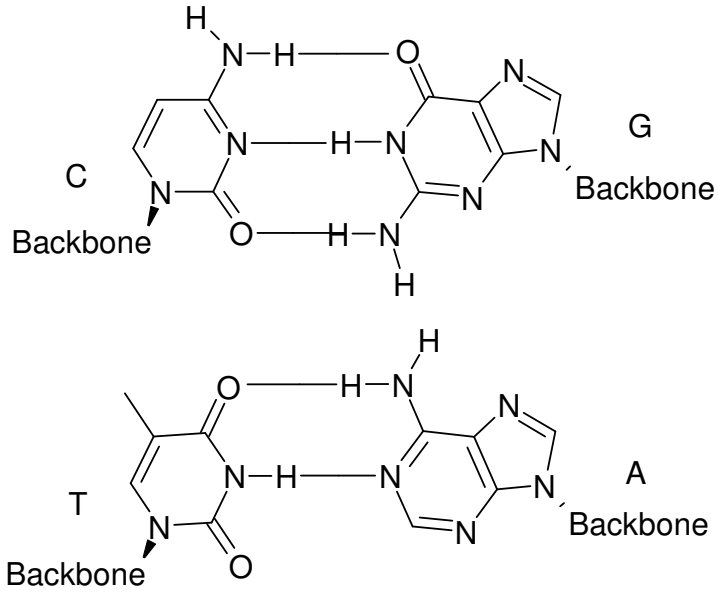

Figure 1.3. Base Pairing in DNA

Part of the versatility of DNA as an information storage medium is the ability of a single strand of DNA to selectively couple, or hybridise, with another complimentary strand of DNA. Two DNA strands hybridise such that the bases pair together via hydrogen bonding to form the well-known double helical structure[31], A-T via two hydrogen bonds and C-G via three[32] (Figure 1.3). This helix can be opened and each strand copied for cell mitosis, coupled with Ribose Nucleic Acid (RNA, a macromolecule similar in primary structure to DNA but containing a hydroxyl group at the 2' position[30], used as an information transfer vector in protein synthesis) for reading the DNA in a process called transcription.

1.7 DNA microarrays and their application

A DNA chip or microarray16[33] is a flat substrate on which a large number of single-stranded DNA oligonucleotide strands are immobilised at specific points to form a regular array of well defined spots. Each spot contains an oligonucleotide with a specific base sequence such that by passing an oligonucleotide target probe of over the array and studying both the extent and location of hybridisation, the structure of the probe may be elucidated. Probes are typically labelled with fluorescent markers to allow swift detection of hybridization.

Such high interest and usage stems directly from the highly parallel nature of such DNA chips and the consequent savings in time and expense[34]. Microarrays can contain thousands of individual spots of a size <500µm[19] meaning that many experiments can be carried out on one chip and at one time, with spot size limiting the number of different base sequences that can be accommodated onto the chip[35]. This highly parallel approach has been used widely in gene mapping[36], gene expression monitoring[16], identifying SNPs (single nucleotide polymorphisms)[37], cancer research[14], drug discovery13[38], and computing[11,12,39]

1.8 Design of DNA microarrays

1.8.1 Substrate choice and surface functionalisation

The microarray substrate must fulfil a range of criteria such as stability to commonly used reagents, low background fluorescence, smooth surface, chemical homogeneity and low cost[40].

DNA hybridisation experiments involving various membrane systems such as nitrocellulose or nylon filters have traditionally been used for macroscopic parallel analysis, such as Southern blotting of gel electrophoresis products[41,42]. The porous nature, and resultant large surface area of the substrate, allows immobilisation of large amounts of DNA with relative ease[43] which gave good, strong signals. However, the porous nature of the filter and

membrane hybridisation substrates makes it a difficult substrate to miniaturise as internal diffusion along the nylon membrane has been reported[29].

Glass substrates are widely used where high temperatures are needed[20] and do not suffer from the problem of internal diffusion[44]. Glass is transparent, with a relatively smooth surface and has a low intrinsic fluorescence[16,17,18], which allows study of reactions in which the active surface is in solution by fluorescence spectroscopy and by microscopy. Like glass, silicon is resistant to temperature and diffusion but is also a semiconducting substrate that is well known for its use in microtechnology, and its relatively smooth surface improves reproducibility[45]. For glass or silicon, by far the most common surface functionalisation method involves the use of silane SAMs[20,46,47,48,49,50,51,52,53,54,55,56,57]. Glass is also a low cost substrate.

Gold is widely used for immobilizations due to the ready formation of self assembled monolayers (SAMs) by thiolated compounds[24,46 58,59,60,61,62.] The use of long chained ‘dilution thiols’ to form SAMs with hydroxyl-terminated thiols has also been explored[63]. Thiol-terminated oligonucleotides can also be immobilized directly to the surface[64]. A gold substrate is also useful in techniques such as surface plasmon resonance[65,66].

1.8.2 Immobilisation chemistry

The immobilisation chemistry must result in a minimum of ‘noise’ in the form of non-reproducible immobilisations, and strong (preferably covalent) bonding to allow repeated use of the immobilised probes without array deterioration over time[42,67].

Avidin-biotin complexations are commonly used in immobilisation of DNA[68]. Avidin is a large biomolecule with four identical binding sites. The smaller molecule biotin attaches to the binding sites of avidin or streptavidin with an affinity which approaches that of a covalent bond. These methods use a surface bound avidin molecule to couple a biotinylated oligonucleotide. These biological molecules are stable in aqueous solutions and thus are

easy to handle. However, the thick molecular layers that are formed contain a large number of sites for non-specific binding which may result in some loss of sensitivity and selectivity[69].

The exact methodology used for covalent immobilisations varies depending on the terminal chemistry of the linker arm. In the case of amine or hydroxyl termination, formation of a phosphoramidate bond between the arm and 5'-phospate group has been reported[49,70] and bromoacetamide surfaces can be reacted with 5'-phopsphorthioate DNA[57.] Other methods include amide bond formation[71] by use of succinimide esters[51,63], amine reaction with isothiocyanates[56], conversion of amines to diazonium salts and subsequent reaction[48], formation of disulphide bonds[52,53,54,55,60], thiolated DNA attack of malimides[47.72].

More exotic methods include use of phosphoramidite chemistry[73] to form linkers of various lengths on aminated polypropylene surfaces. Titanium oxide layers have been used to bind the phosphate groups in the DNA backbone[67]. Polypyrrole has been electropolymerised onto platinum electrodes and aminated DNA bound to the polymer, via amide bond formation[71]. Diamond has been functionalised to give acid chloride surfaces to which DNA has been directly attached[28].

1.8.3 Linkers

The ability of the surface immobilised probes to hybridise is improved with the addition of a flexible linker[74]. This usually takes the form of a hydrocarbon chain that is engineered between the probe and surface. The additional flexibility offered by chains of 28Å length have been reported to increase hybridisation yields four-fold[48], with longer linkers (>40atoms) yielding 150-fold improvement[49,73]. This has encouraged the use of flexible molecules such as dendrimers to form a surface-immobilised layer for hybridisation[21].

1.9 Delivery of oligonucleotide probes

1.9.1 In-situ synthesis by photolithography

This technique, originally pioneered by Affymetrix[18,75], is capable of forming arrays with feature down to 50µm in size[42] and is favourable for high density microarrays. It builds on standard DNA syntheses, such as those used in porous glass columns in current commercial oligonucleotide synthesis utilising phosphoramidite chemistry[19], but utilises a photosensitive protecting group. The deprotection is only effective where light is directed onto the molecule. Precise masking allows each area for reaction to be carefully selected (Figure 1.4).

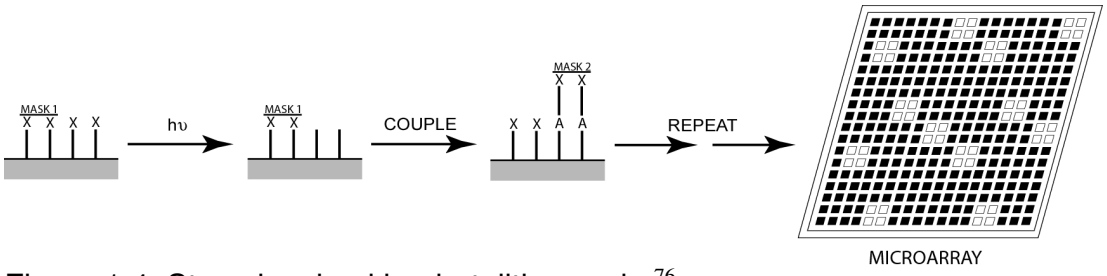

Figure 1.4. Steps involved in photolithography[76].

By sequential protection, deprotection and oligomer extension, thousands of oligomers can be built on a surface. For instance, in 32 cycles, 65,536 8-mer DNA strands can be synthesised. However, incomplete reactions limit the maximum sequence length and the accuracy of results as they leave incomplete DNA strands on the surface. Such high density arrays are excellent for high through-put screening to identify sequences of interest, but detailed study may require longer oligomers and custom microarrays.

1.9.2 Mechanical microspotting of pre-synthesised Oligonucleotides

Mechanical microspotting allows pre-synthesised oligomer strands to be delivered to different areas of a surface. The pre-synthesised oligomers can be rigorously purified prior to use and hence longer oligomer strands are possible[30]. Commonly, a robot will dispense nanovolumes of reagents in a prearranged pattern onto the substrate surface, using a variety of methods

such as drop-touch systems[16], automatic nano-pipetteing, microvalves or piezoelectric injection devices (developed from ink-jet processes)[77,78].

1 Grill, A.; *Cold Plasmas in Materials Technology: From Fundamentals to Applications*; IEEE Press: New York, **1994**.

2 Lee, W. W.; d'Agostino, R.; Wertheimer, M. R. (ed) *Materials Research Society Symposium Proceedings* **1999**, *544*.

3 Chan, C.-M.; Ko, T.-M., Hiraoka, H. *Surface Science Reports* **1996**, *24*, 1

4 *Plasma Deposition Treatment, and Etching of Polymers*, d'Agostino, R., Ed.; Academic Press : Boston, **1990**

5 Chapman, B. *Glow Discharge Processes Sputtering and Plasma Etching*; Wiley-Interscience, New York **1980**

6 Liebermann, M. A.; Lichtenberg, A. J. *Principles of Plasma Discharges and Materials Processing 2nd ed.*; Wiley-Interscience, New Jersey, **2005**.

7 Reece Roth, J.; *Industrial Plasma Engineering Volume 2: Applications to Nonthermal plasma processing*; Institute of Physics Publishing: Bristol, **2001**

8 Han, L. M.; Timmons, R. B. *J. Polymer Science Part A: Polymer Chemistry* **1998**, *36*, 3121

9 Nakajima, K.; Bell, A. T.; Shen, M. *J. Vac. Sci. Technol.* **1992**, *A10*, 1

10 Ryan, M. E.; Hynes, A. M.; Badyal, J. P. S. *Chem. Mater.* **1996**, *8*, 37

11 Aldeman, M. *Science* (Washington, DC, U.S.) **1994**, 266, 1021.

12 Frutos, A. G.; Liu, Q.; Thiel, A. J.; Sanner, A. M. W.; Condon, A. E; Smith, L. M.; Corn, R. M. *Nucleic Acids Res.* **1997**, *25*, 4748.

13 Debouck, C.; Goodfellow, P. N. *Nat. Genet.* **1999**, *1(suppl.)* 48.

14 van't Veer, L. J.; Dai, H.; van de Vijver, M. J.; He, Y. D.; Hart, A. A. M.; Mao, M.; Peterse, H. L.; van der Kooy, K.; Marton, M. J.; Witteveen, A. T.; Schreiber, G. J.; Kerkhoven, R. M.; Roberts, C.; Linsley, P. S.; Bernards, R.; Friend, S. H. *Nature* (London, U.K.) **2002**, 415, 530.

15 McGlennen, R. C. *Clin. Chem* .(Washington, DC, U.S.) **2001**, 47, 393.

16 Schena, M.; Shalon, D.; Davis, R. W.; Brown, P. O. *Science (Washington, DC. U.S.)* **1995**, *270*, 467.

17 Maskos, U.; Southern, E. M. *Nucleic. Acids Res.* **1992**, *20*, 1679.

18 Fodor, S. P. A.; Read, J. L.; Pirrung, M. C.; Stryler, L.; Tsai Lu, A.; Solas, D. *Science* (Washington, DC, U.S.)**1991**, 251, 767.

19 Souteyrand, E.; Cloarec, J. P.; Martin, J. R.; Cabrera, M.; Bras, M.; Chauvet, J. P.; Dugas, V.; Bessueille, F. *Appl. Surf. Sci.* **2000**, *164*, 246.

20 Zammatteo, N.; Jeanmart, L.; Hamels, S.; Courtois, S.; Louette, P.; Hevesi, L.; Remacle, J. *Anal. Biochem.* **2000**, *280*, 143.

21 Le Berre, V.; Trévisiol, E.; Dagkessamanskaia, A.; Sokol, S.; Caminade, A.; Majoral, J. P.; Meunier, B.; François, J. *Nucleic Acids Res.* **2003**, *31*, e88.

22 Guo, Z.; Guilfoyle, R. A.; Thiel, A. J.; Wang, R.; Smith, L. M. *Nucleic Acids Res.* **1994**, *22*, 5456.

23 Souteyrand, E.; Cloarec, J. P.; Martin, J. R.; Wilson, C.; Lawrence, I.; Mikkelsen, S.; Lawrence, M. F. *J. Phys. Chem. B* **1997**, *101*, 2980.

24 Bain, C. D.; Whitesides, G. M. *Science* **1988**, *240*, 62.

25 Zhao, Y.; Pang, D; Hu, S.; Wang, Z.; Cheng, J.; Dai, H. *Talanta* **1999**, *49*, 751.

26 Kelley, S. O.; Boon, E. M.; Barton, J. K.; Jackson, N. M.; Hill, M. G. *Nucleic Acids Res.* **1999**, *27*, 4830.

27 Waddell, E.; Wang, Y.; Stryjewski, W.; McWhorter, S.; Henry, A. C.; Evans, D.; McCarley, R. L.; Soper, S. A. *Anal. Chem.* **2000**, *72*, 5907.

28 Ushizawa, K.; Sato, Y.; Mitsumori, T.; Machinami, T.; Ueda, T.; Ando, T. *Chem. Phys. Lett.* **2002**, 351, 105.

29 M. Schena (ed.) *DNA Microarrays: A Practical Approach* Oxford University Press, Oxford 1999

30 Gillmor, S. D.; Rugheimer, P. P.; Lagally, M. G.; *Surface Science* **2002**, *500*, 699

31 Watson, J. D.; Crick, H. H. C. *Nature* **1953**, *131*, 737

32 Chargaff, E.; Brawerman, G.; Zamenhof, S. *Biochim. Biophys. Acta* **1952**, 9, 402.

33 MacBeath, G.; Schrieber, S. L. *Science* **2000**, *289*, 1760

34 M. Thompson; *Analyst* **1999**, *32*, 2353 and S. F. Y. Li; *Analyst* **2000**, *16*, 107

35 Wang, D. G.; Fan, J.; Siao, C.; Berno, A.; Young, P.; Sapolsky, R.; Ghandour, G.; Perkins, N.; Winchester, E.; Spencer J.; Kruglyak L.; Stein, L.; Hsie, L.; Topaloglou, T.; Hubbell, E.; Robinson, E.; Mittmann, M.; Morris, M. S.; Shen, N.; Kilburn, D.; Rioux, J.; Nusbaum, C.; Rozen, S.; Hudson, T. J.; Lipshutz, R.; Chee, M.; Lander, E.S. *Science* **1995**, 280, 1077.

36 Kallioniemi, A.; Kallioniemi, O.; Sudar, D.; Rutovitz, D.; Gray, J. W.; Waldman, F.; Pinkel, D. *Science* **1992**, 258, 818

37 Zhong, X.; Reynolds, R.; Kidd, J. R.; Kenneth, K.; Jenison, R.; Marlar, R. A.; Ward, D. C. *Proc. Natl. Acad. Sci. USA*, **2003**, 100, 11559.

38 Yang, M.; McGovern, M. E.; Thompson, M.; *Anal. Chim. Acta* **1997**, 346, 259

39 Ogihara, M.; Ray, A. *Nature* **2000**, 403, 143

40 Elder, J. K.; Johnson, M.; Milner, N.; Sohal, M.; Southern, E.M. In *DNA Microarrays: A Practical Approach*, Schena, M., Ed.; Oxford University Press: New York, **1999**, pp 77 - 99.

41 G. H. Keller, M. M. Manak *DNA Probes* Stockton Press, New York, 1989

42 Beier, M.; Hoheisel, J. D. *Nucleic Acids Research* **1999**, *27(9)*, 1970

43 Zhang, Y.; Coyne, M. Y.; Will, S. G.; Levenson, C. H.; Kawasaki, E. S. *Nucleic Acids Research* **1991**, *19*, 3929

44 Southern, E.; Mir, K.; Shchepinov, M. *Nature Genetic (suppl.)* **1999**, *21*, 5

45 G. Childs *Nature Biotechnology* **2000**, *18*, 384

46 Demers, L. M.; Ginger, D. S.; Park, S.-J Li, Z.; Chung, S.-W.; Mirkin, C. A. *Science* **2002**, *296*, 1836

47 Chrisey, L. A.; Lee, G. U.; O'Ferrall, C. E. *Nucleic Acids Research* **1996**, *24(15)*, 3031

48 Dolan, P. L.; Wu, Y.; Ista, L. K.; Metzenberg, R. L.; Nelson, M. A.; Lopez, G. P. *Nucleic Acids Research* **2001**, *29(21)*, e107

49 Henke, L.; Piunno, P. A. E.; McClure, A. C.; Krull, U. J. *Analytica Chimica Acta* **1997**, *344*, 201

50 Lamture, J. B.; Beattie, K. L.; Burke, B. E.; Eggers, M. D.; Ehrlich, D. J.; Fowler, R.; Hollis, M. A.; Kosicki, B. B.; Reich, R. K.; Smith, S. R.; Varma, R. S.; Hogan, M. E. *Nucleic Acids Research* **1994**, *22(11)*, 2121

51 Jung, A.; Stemmler, I.; Brecht, A.; Gauglitz, G. *Fresenius Journal of Analytical Chemistry* **2001**, *371*, 128

52 Kumar, A.; Liang, Z.; *Nucleic Acids Research* **2001**, *29(2)*, e2

53 Lenigk, R.; Carles, M.; Ip, N. Y.; Sucher, N. J. *Langmuir* **2001**, *17*, 2497

54 Rogers, Y.-H.; Jiang-Baucom, P.; Huang, Z.-J.; Bogdanov, V.; Anderson, S.; Boyce-Jacino, M. T. *Analytical Biochemistry* **1999**, *266*, 23

55 Hilliard, L. R.; Zhao, X.; Tan, W. *Analytica Chimica Acta* **2002**, *470*, 51

56 Lindroos, K.; Liljedahl, U.; Raitio, M.; Syvänen, A.-C. *Nuc. Acids Res.* **2001**, *29(13)*, e69

57 Pirrung, M. C.; Davis, J. D.; Odenbaugh, A. L. *Langmuir* **2000**, *16*, 2185

58 Gerion, D.; Parak, W. J.; Williams, S. C.; Zanchet, D.; Micheel, C. M.; A. P. Alivisatos *J. Am. Chem. Soc.* **2002**, *124*, 7070

59 Heaton, R. J.; Peterson, A. W.; Georgiadis, R. M. *Proceedings of the National Academy of Sciences USA* **2001**, *98*, 3701

60 Nelson, B. P.; Grimsrud, T. E.; Liles, M. R.; Goodman, R. M.; Corn, R. M. *Anal. Chem.* **2001**, *73*, 1

61 Smith, E. A.; Wanat, M. J.; Cheng, Y., Barreira, S. V. P.; Frutos, A. G.; Corn, R. M. *Langmuir* **2001**, *17*, 2502

62 Ijiro, K.; Sunami, H.; Arai, K.; Matsumoto, J.; Karthaus, O.; Kraemer, S.; Mittler, S.; Nishi, N.; Juskowiak, B.; Takenaka, S.; Knoll, W.; Shimomura, M. *Colloids and Surfaces A: Physiochemical and Engineering Aspects* **2002**, *198-200*, 677

63 Boncheva, M.; Schreibler, L.; Lincoln, P.; Vogel, H.; Akerman, B. *Langmuir* **1999**, *15*, 4317

64 Mourougou-Candoni, N.; Naud, C.; Thibaudau, F. *Langmuir* **2003**, 19, 682.

65 Nagata, K.; Handa, H. (eds.) *Real-Time Analysis of Biomolecular Interactions* Springer-Verlag, Tokyo, **2000**.

66 Brockman, J. M.; Nelson, B. P.; Corn, R. M. *Annual Reviews of Physical Chemistry* **2000**, *51*, 41

67 Wang, J.; Fernandes, J. R.; Kubota, L. T. *Anal. Chem.* **1998**, *70*, 3699

68 Su, X. *Biochemical and Biophysical Research Communications* **2002**, *290*, 962.

69 Shea, L. D.; Segura, T.; *Bioconjugate Chemistry* **2002**, *13*, 621.

70 Lyttle, M .H.; Adams, H.; Hudson, D.; Cook, R. M.; *Bioconjugate Chem.* **1997**, *8*, 193

71 Korri-Youssoufi, H.; Garnier, F.; Srivastava, P.; Godillo, P.; Yassar, A. *J. Am. Chem. Soc.* **1997**, *119*, 7388

72 Lin, Z.; Strother, T.; Cai, W; Cao, X.; Smith, L. M.; Hamers, R. J. *Langmuir* **2002**, *18*, 788

73 Shchepinov, M. S.; Case-Green, S. C.; Southern, E. M. *Nucleic Acids Research* **1997**, *25(6)*, 1155

74 Case-Green, S.; Pritchard, C.; Southern, E. M. In *DNA Microarrays: A Practical Approach*, Schena*, M., Ed.;* Oxford University Press: New York, **1999,** pp 61 - 76.

75 Chee, M.; Yang, R.; Hubbel, E.; Berno, A.; Huang, X. C.; Stern, D.; Winkler, J.; Lockhart, D. J.; Morris, M. S.; Fodor, S. P. A. *Science* **1996**, *274*, 610

Schena, M.; Theriault, T. P.; Konrad, K.; Lachenmeier, E.; Davis, R. W. *Trends in Biotechnology* **1998**, 16, 301.

77 Shoji, T.; Nisshinbo Industries Inc., **2004**, *Method for Producing a Microarray*, Eur. Pat. EP 1380338 A2

78 Manning, J. H.; Array-Jet Limited, **2002**, *Highly Parallel Fabrication of Microarrays by Ink-Jet Printheads*, Int. Pat. WO 02/11889 A1

2 Plasmachemical and surface analysis methods

2.1 The plasma reactor

Several types of reactors have been used in plasma polymerisation, and these can be summarised into three broad categories[1]:

1) electrodeless microwave (MW) or high frequency (HF) reactors which make use of a resonant cavity to create the plasma.
2) internal electrodes, parallel plates: containing an RF driven electrode and a grounded electrode between which is placed the substrate.
3) external electrodes, tubular reactors. Power is passed into a coil that is wrapped around the reactor and the plasma created by inductive coupling of the energy from the coils.

A reactor of type 3 is used in this work (Figure 2.1). The simplicity of the setup and plasma generation is advantageous, especially as the electrodes do not require removal of deposited polymer. It allows the maintenance of a pressure of <0.2mbar by use of a vacuum pump and monomer can be introduced via a Youngs tap. The sample is easily accessible as the reactor can be easily opened when not under vacuum.

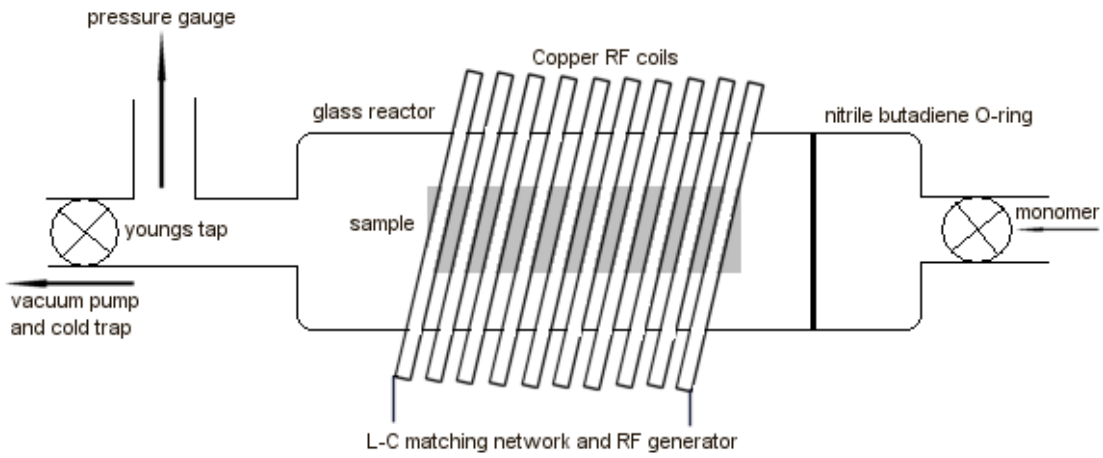

Figure 2.1. A typical external electrode reactor, such as the one used in this work.

Plasma polymerization of precursors in this work was carried out in an electrodeless cylindrical glass reactor[2] (5 cm diameter, 520 cm^3 volume, base pressure = 3 x 10^{-2} mbar, leak rate = 1 x 10^{-9} mol s^{-1})[3] enclosed in a Faraday cage. The chamber was fitted with a gas inlet, a thermocouple pressure gauge, and a 30 L min^{-1} two-stage rotary pump connected to a liquid nitrogen cold trap. All joints were grease free. An externally wound 4 mm diameter copper coil spanned 8 – 15 cm from the gas inlet with 9 turns. The output impedance of a 13.56 MHz RF power supply was matched to the partially ionized gas load using an L-C matching network. In the case of pulsed plasma deposition, the RF source was triggered from an external signal generator, and the pulse shape monitored with a cathode ray oscilloscope. Prior to each deposition, the reactor was scrubbed with detergent, rinsed in water followed by propan-2-ol, and finally dried in an oven. Further cleaning entailed running a 0.2 mbar pressure air plasma operating at 40 W for a period of 30 min.

Each substrate was ultrasonically cleaned in a 50:50 mixture of cyclohexane and propan-2-ol for 10 min and then placed onto a flat glass plate located in the center of the reactor. Substrates used in this work include silicon wafer, borosilicate glass microscope slides and coverslips, single walled carbon nanotubes as outlined in experimental chapters. This was followed by evacuation to base pressure and introduction of precursors at a pressure of 0.20 mbar and a flow rate of 4.1 x 10^{-7} mol s^{-1} for 5 min. Precursors were purified by several freeze-pump-thaw cycles prior to use. Upon extinction of the electrical discharge, the precursor was allowed to continue to pass through the apparatus for a further 5 min prior to venting to atmosphere, to allow quenching of any remaining active sites.

2.2 X-Ray Photoelectron Spectroscopy (XPS)

XPS is a quantitative ultrahigh vacuum technique for investigation and characterisation of the composition of solid surfaces[4,5]. The surface is irradiated with X-Ray photons which causes ejection of core electrons from the surface, where the kinetic energy, *KE*, of the electron can be described as[6]

$$KE = hv - BE - \varphi_f - \varphi_s$$

where *BE* is the binding energy of the ejected electron. φ_f is the work function of the spectrometer, a term which takes corrects the *KE* for extra energy gained in the vacuum/detector interface which can be measured experimentally and is characteristic of the spectrometer. φ_s is a correction term for surface charging, to take into account the loss in *KE* when photo-electrons are ejected from a charge surface. φ_f and φ_s can be considered constant for a given sample. Only electrons that leave the sample without inelastic collisions give recognisable peaks, meaning that the effective sampling depth of XPS is 3-10nm, as defined by the mean-free path of the electron.

As no two elements have the same set of binding energies[7], it is possible to differentiate between different elements using XPS. Moreover, variation in chemical environment can also be examined with XPS as the binding energy of a given level will vary with oxidation state, giving a chemical shift. XPS allows quantitative analysis as the intensity of photoelectron emission is directly proportional to the atomic distribution of emitting atoms.

The holes left in the core levels by photoelectron emission give rise to two de-excitation mechanisms, X-Ray fluorescence and Auger emission (Figure 2.2). In the case of fluorescence an outer shell electron fills the core electron hole and excess energy is released in the form of an X-Ray photon. Auger emission occurs when the excess energy is imparted to another electron, which then leaves the atom. Auger emission energy is thus independent of source as it is governed not by the energy of the incident radiation, but by the energy levels of the atom itself.

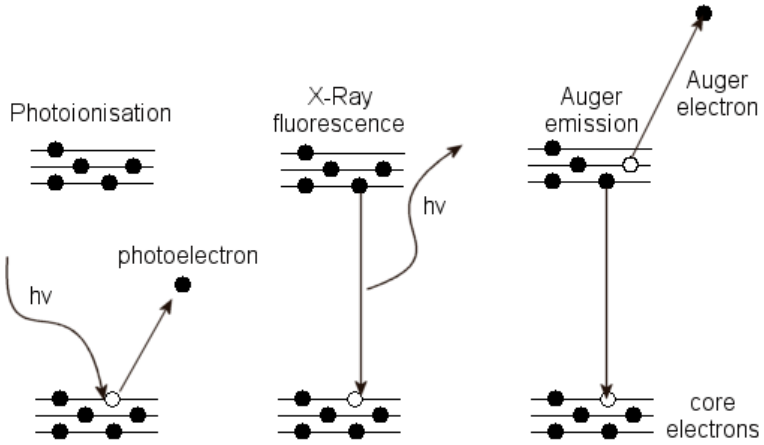

Figure 2.2. Emission processes in XPS

Typical spectra then show sharp peaks based on photoelectron emission, with a series of source-independent edges based on Auger emissions.

The two commonly used X-ray sources are Mg and Al, which fit the two main requirements of an XPS soft X-ray source. In order to minimise the signal to noise ratio, to produce clear spectra, the source must have a low emission width as the width of any peak in a spectrum will be related to the width of the X-ray emission. The energy of the emission must also be sufficient to eject photoelectrons from the sample in the first place[7].

The specimen is excited by unmonochromatised $K\alpha_{1,2}$ lines from the Al or Mg source[8], giving a spectrum of characteristic X-ray lines superimposed over bremsstrahlung radiation (caused by the deceleration of electrons impinging on the anode of the X-ray gun). This broad background and satellite peaks in the x-ray emission, such as the $K\alpha_{3,4}$ and $K\beta$ will cause the appearance of satellite peaks in the XPS spectrum. Where resolution is paramount, the x-rays can be passed through a monochromator, such as a quartz crystal, which can separate the desired $K\alpha_{1,2}$ line, but this will result in a loss of signal intensity.

Emitted electrons are collected, retarded and analyzed as a function of their kinetic energy. The concentric hemispherical analyser (Figure 2.3) is widely used in XPS. It consists of two hemispherical surfaces positioned concentrically. The plates are charged electrostatically so that the negative potential V2 (outer) is greater than V1 (inner). Electrons entering the analyser with the correct energy and at the right angle follow the hemisphere and are focused into a channeltron device.

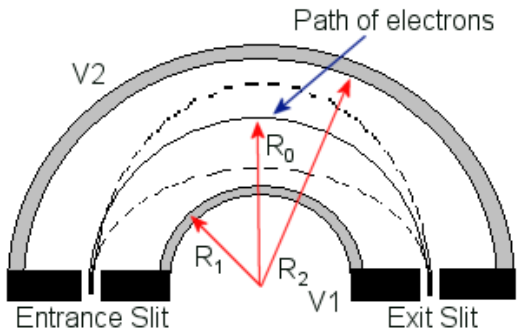

Figure 2.3. The concentric hemispherical analyser.

The absolute resolution of the analyser is defined as

$$R=\Delta E/E_0$$

where R is the absolute resolution, ΔE is the full width at half maximum (FWHM) of the peak and E_0 is the energy of the peak. In order to maintain a constant resolution for any peak in the XPS spectrum, an electrostatic lens at the entrance to the analyser is used to retard incoming photoelectrons. There are two commonly used modes CAE: Constant Analyser Energy, in which electrons are retarded by a constant amount, and CRR: Constant Retard Ratio, in which electrons are retarded proportionally to their energy.

The channeltron device acts as both a detector and an amplifier of the incoming electron current, which is extremely small. A small spiral glass tube is coated on the inside with a high resistance material and a potential of 3kV applied to the ends. Incoming electrons collide with the walls and emission of

a number of secondary electrons. Multiple collisions result in a cascade effect and results in gains of $>10^7$.

For this work XPS analysis of the functionalized surfaces was performed using a VG ESCALAB I spectrometer equipped with an unmonochromated Mg $K\alpha_{1,2}$ X-ray source (1253.6 eV) and a concentric hemispherical analyzer (operating in constant analyzer energy (CAE) mode with a pass energy of 20 eV, and set to a take-off angle of 30° to the substrate normal). To account for any sample charging, a constant offset was applied to each peak based on the deviation of the C_xH_y signal from the defined 285 eV. Instrument sensitivity (multiplication) factors were derived using chemical standards. Peak areas were determined after subtraction of a linear background from high resolution spectra of the envelope, with fitting performed using Marquardt minimisation computer software. High resolution envelopes were fitted with a minimum number of Gaussian peaks, wherever possible limited to one. Where more peaks were judged necessary to provide a satisfactory fit, all FWHM were constrained to be equal, and additional gaussian peaks only added where the chemical shift corresponds to a chemically plausible species, based on the precursor structure. The absence of any Si(2p) signal from the underlying silicon substrate was indicative of a pinhole free film[9], whilst the disappearance of Na(1s) and Cl(2p) peaks corresponded to the complete removal of buffer salts from the surface during washing.

2.3 Fourier Transform Infrared (FT-IR) spectroscopy

IR spectroscopy is a method of studying the vibrations of the various functional groups within a molecule that contain dipole moments. Many chemical groups have distinctive vibrational modes whose frequency is equivalent to an infrared photon (wavelength in µm). Thus irradiation of a sample with infrared radiation (typically in the region of 4000 – 200cm^{-1}) achieves vibrational excitation as the molecule absorbs the infrared energy. By comparing the incident IR beam with the transmitted IR beam it is then possible to plot the relative transmission (T) at a given wavenumber.

$$T = I / I_0$$

Where I is the intensity of transmitted radiation and I_0 is the intensity of the incident radiation.

Vibrational modes are active only if there is a change in the molecular dipole moment during the vibration, so that antisymmetric vibrations and vibrations involving polar groups (such as carbonyls) are more likely to produce strong IR absorption bands[10].

The FT-IR method has several advantages over normal infra-red spectroscopy.

1) The whole spectrum is scanned at once, so the time taken to acquire a spectrum with identical S/N ratio to a conventional IR spectrometer is drastically reduced in comparison to slowly scanning through the entire wavenumber range and collection of data is rapid.
2) There are no slits required in the optics of the spectrometer which results in a much higher radiation throughput.
3) Resolving power in an FT-IR instrument is constant and does not vary with wavenumber.

FT-IR can be combined with the optical phenomenon of total internal reflection to study thin films (Figure 2.4). The IR beam is capable of passing through the polymer film and will reflect from the dense substrate media (gold, silicon, glass).

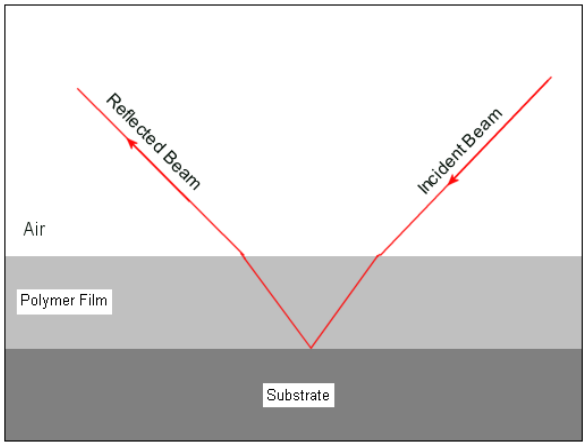

Figure 2.4. Grazing Angle Reflection in FT-IR

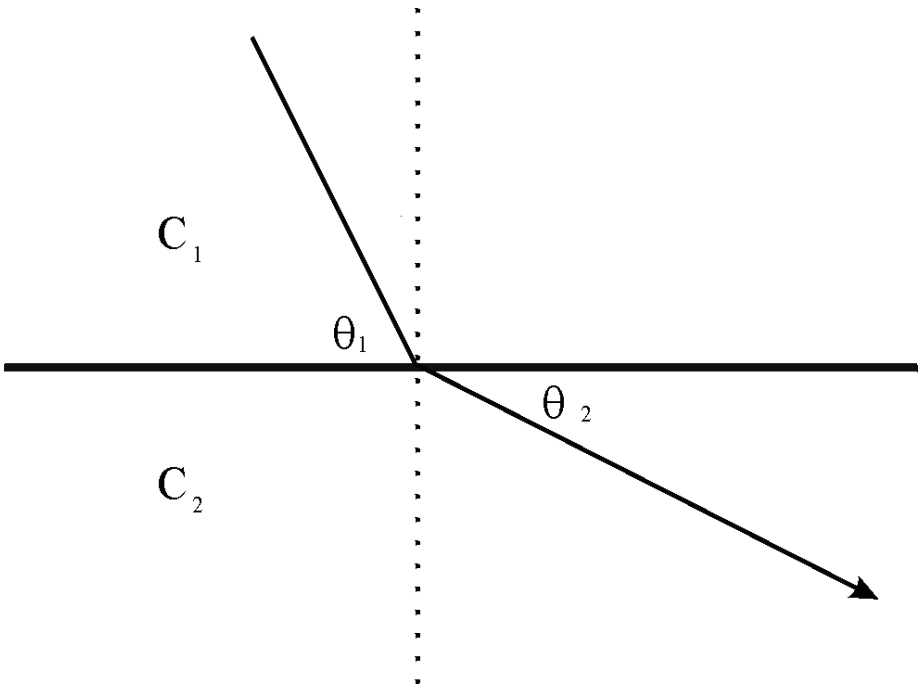

Fig 2.5. A beam of light at an interface[11]

Snells law[11] states that

$$\frac{c_1}{\cos(\theta_1)} = \frac{c_2}{\cos(\theta_2)} = \text{constant}$$

However, when the grazing angle reaches a certain level Snells law fails and none of the incident energy propagates into the lower layer. The angle at which Snells law fails is known as the critical angle θ_{crit}, and using this angle in FT-IR guarantees total external reflection.

$$\theta_{crit} = \cos^{-1}\left(\frac{c_1}{c_2}\right)$$

An FT-IR spectrometer usually consists of a source of infrared radiation and a Michelson interferometer before the sample and a detector to examine the intensity of the IR beam after is has passed through the sample.

The Nernst Glower (composed mainly of rare earth oxides) and the Globar (a silicon carbide rod) have been used as IR sources in the past due to their near-black body emission[12]. Generally sources such as these are placed at

the focal point of a parabolic mirror so that the reflected light produces a parallel beam.

The Michelson interferometer (Figure 2.6) consists of a beam splitter, a fixed mirror and a mirror free to move backwards and forwards. The beam splitter transmits half of the radiation striking it and reflects the other half. One beam is transmitted onto the stationary mirror; the other is reflected onto the moving mirror. Both beams then reflect back to the beamsplitter, which again transmits half and reflects half, which results in one beam returning to the source and the other beam passes through the sample and onto the detector.

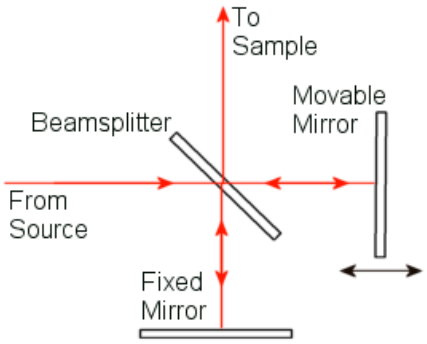

Figure 2.6. The Michelson Interferometer

This second beam now consists of a combination of the two separate beams, but the introduction of a varying path difference by the moving mirror means that the two beams are no longer in phase at all times. This phase difference results in constructive or destructive interference, giving peaks or troughs in the beam signal at the detector to give an interferogram. By application of a Fourier transform procedure and reference to an interferogram in which there is no sample present (a background), it is possible to separate this total signal into its components.

There are two types of detectors commonly employed in FT-IR instruments, thermal detectors and quantum or photon detectors. Thermal detectors such as TGS (triglycine sulphate) have good responses over a wide range of IR frequencies and are relatively cheap in terms of cost. The MCT (mercury

cadmium telluride) detector is a quantum detector that has much better sensitivity and response, but over a smaller range and is cooled with liquid nitrogen to improve he signal/noise ratio[12].

Infrared analysis was carried out using a Fourier Transform spectrometer (Perkin Elmer Spectrum One) fitted with a liquid nitrogen-cooled MCT detector and a total external reflection accessory (SPECAC). Coated silicon wafers were examined at a reflection angle of 66°, with spectra averaged over 256 scans at a resolution of 4 cm^{-1} and baseline corrected.

2.4 Sessile drop contact angle

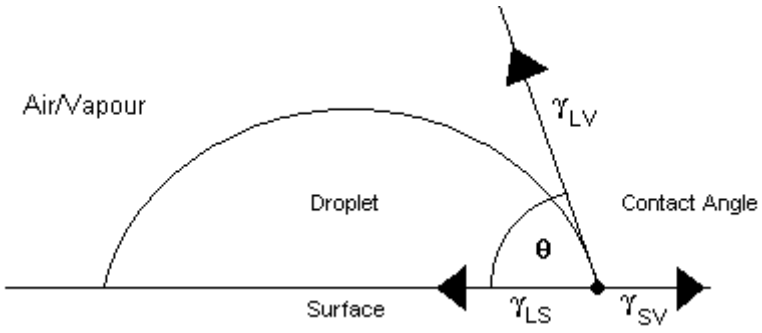

Figure 2.7. The contact angle of a sessile drop.

Measurement of contact angles is an extremely surface sensitive technique, sampling the first 5-10 Å of a surface[13]. A droplet of a liquid such as water is placed in the surface and the contact angle measured (Figure 2.7). The contact angle on the surface is related to the surface energy, or interfacial tension of the surface, and the relationship between the different surface tensions is based on Youngs equation[14]:

$$\gamma_{SV} = \gamma_{LV}\cos\theta_e + \gamma_{SL}$$

γ_{SV} is the surface-vapour interfacial tension, γ_{LV} is the liquid-vapour interfacial tension, γ_{SL} is the surface-liquid interfacial tension and θ_e is the contact angle. Youngs equation can be related to a spreading coefficient, S[14].

$$S = \gamma_{SV} - \gamma_{SL} - \gamma_{LV}$$

This is essentially the difference between the completely dry solid-vapour interface and the moist surface covered in a macroscopic film of fluid (positive S), to give partial coverage (negative S). So, the greater the attraction between the surface and the liquid, the lower γ_{SL} will be, therefore there is a greater spreading tendency and the contact angle will increase.

Sessile drop contact angle measurements in this work were performed with 2 µL droplets of high-purity water (B.S. 5978 Grade 1) using video capture apparatus (A.S.T. Products VCA2500XE).

2.5 Spectrophotometry

The technique of spectrophotometry involves measurement of the changes in reflection and/or transmission of the sample thin film over a range of wavelengths of light. By examining the changes in reflection and/or transmission it is possible to elucidate the thickness of a film.

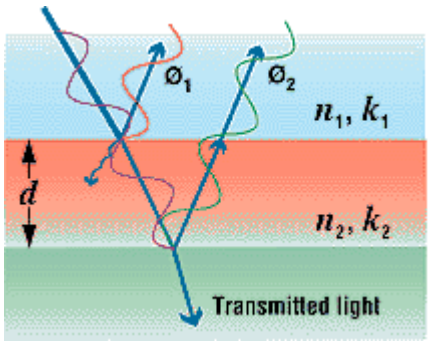

Figure 2.8. Reflections from a thin film on a substrate.

Incident light can be reflected by the air/film interface (blue/red), the film/substrate interface (red/green) or transmitted. Different wavelengths of light will give constructive/destructive interference depending on the film thickness, d[15].

The reflectivity, R, at the air-sample interface is defined as[16]

$$R = [(n-1) / (n+1)]^2$$

Where *n* is the refractive index of the sample, and the sample is non-absorbing.

The light that is has passed through the sample will now be out of phase with the light reflected directly from the sample surface as is has travelled an extra distance, *d*, through the sample. Taking into account the differing refractive index of air and sample we can define the beams optical path [*d*]

$$[d] = nd$$

And the optical path difference, [*p*] between the two beams as

$$[p] = 2[d] = 2nd$$

Where the path difference of the beams is equal to an integer (m=1, 2, 3 …) the two beams are exactly out of phase, giving destructive interference

$$[p] = m\lambda$$

Where the path difference is equal to a half-integer then constructive interference occurs.

$$[p] = (m+1/2)\lambda$$

As the path difference varies with the angle of the incident light, θ, the path difference can be written as

$$[p] = 2nd\cos\theta$$

The situation is complicated somewhat by the assumption that the film does not absorb light. Where light is absorbed, the complex refractive index is used

$$N = n + ik$$

However, where the Cauchy method for modelling n(λ) is used, k(λ) is assumed to be zero[15]

$$n(\lambda) = A + B/\lambda^2 + C/\lambda^4$$

Leaving three variables to model the reflectivity.

In general, the amplitude of the oscillations is related to the refractive index difference between film and substrate. The period of oscillations with is connected to the thickness of the film and vertical positioning of the curves gives us information about the absorption in the film and substrate. The model can then be refined to present a truer example of the film parameters.

Typically, reflectometry can measure minimum film thicknesses in the 10-300Å range, depending on the film in question, although this is increased significantly where optical measurements are needed also.

For thinner layers, ellipsometry should be used. Ellipsometry works is the measurement of the change in polarisation of a beam of light on reflection from a surface. Ellipsometry measures the reflectance at much lower angles and is thus more sensitive to thin layers (e.g. 75° from the normal).

A spectrophotometer was used for film thickness measurements (nkd-6000 Aquila Instruments Ltd). Transmittance-reflectance curves over the 350-1000 nm wavelength range were fitted to a Cauchy material model using a modified Levenburg-Marquardt method[17].

2.6 Fluorescence Microscopy

Fluorescence microscopy operates on the principle that molecules, excited by irradiation with light of a specific excitation wavelength, may emit energy detectable as visible light upon relaxation back to their ground state. Sources such as lasers are used to excite fluorescent materials, and the intensity of the resultant fluorescent light is recorded.

The principle components of a fluorescence microscope are a light source, optics, filters and a detector. Filters are present to give a monochrome excitation source function to monochromise the excitation light, and to filter any excitation light back scattered from the sample surface, which would otherwise swamp the fluorescent emission signal.

A photomultiplier detector is used to count the emitted fluorescent photons and amplify the generated signal. The emitted photons collected by the detector are transformed into a series of electrical signals, which can then be digitally recorded and displayed on a computer interfaced to the microscope. Additionally, the microscope includes a precise xy stage to allow rastering across a sample surface and hence the formation of a three dimensional map.

Fluorescent labelled oligonucleotides or antibodies attached to solid surfaces were identified using a Raman microscope system (LABRAM, Jobin Yvon Ltd) fitted with a 10x lens and a 20 mW HeNe laser (632.817 nm wavelength) which corresponds to the excitation range of the Cy5 fluorophore. A polarization of 500:1 was employed, and the laser beam passed through a diffraction grating of 1800 lines mm^{-1}; a filter permitting 1% laser energy transmission was used for all experiments, except for those found in Figure 7 where a 10% transmission was used. In the case of glass slides, a low-level fluorescence background was noted, with a broad shallow peak at approximately 2800 cm^{-1}. In all cases, the signals are normalized to the typical glass background signal of 225 counts recorded with untreated slides.

In typical mapping experiments, the sample on a motorized stage is rastered under the beam over a 500 µm by 500 µm area, recording a 50 x 50 lattice of points. Composite images were examined using LabSpec Pro software.

Both the DNA and protein microarrays were screened using a Genomic Solutions Gene Tac LS IV Microarray Scanner.

2.7 Estimation of errors

The main expected source of errors in the data was expected to be in sample variability due to potential uncontrolled environmental variables during sample preparation. The results presented are the mean averages of a given data set, with errors reported as one standard deviation of the data. Errors presented for XPS peak fitting and growth rate of layers by

reflectometry are based on a minimum data set of three separately generated samples. For sessile drop contact angle and fluorescence microscopy errors are estimated based on ten separate readings for each sample, with the presented error being one standard deviation of the data.

3. A substrate independent route for DNA microarray manufacture using undec-1-enal

3.1 Precursor choice and immobilisation chemistry

Imine formation is known to produce relatively stable bonds. It proceeds via an addition-elimination mechanism, with the amine adding to the carbonyl followed by the elimination of water. The reaction is acid catalysed, with the amine addition to the carbonyl usually being rate determining. Note that the reverse reaction is also acid catalysed and that excess acid can reverse the reaction (Figure 3.1).

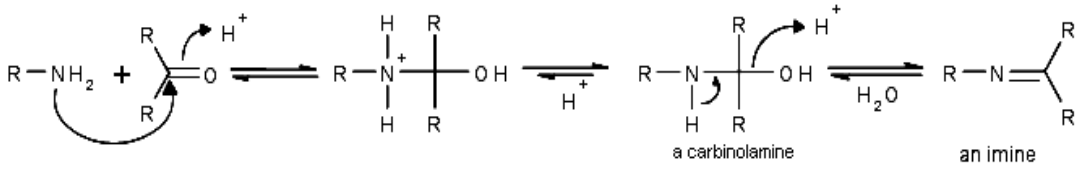

Figure 3.1. Mechanism of imine formation.

It is also known that aldehydes can be used to form imines for the immobilization of amine terminated DNA[29]. This particular methodology requires pre-synthesis of $Cl_3Si(CH_2)_{10}COOCH_2CF_3$ (TETU) in a reaction scheme involving ice-cooled reactions under an argon atmosphere in a many step process. TETU is then grafted onto glass and reduced to an alcohol by $LiAlH_4$ and finally oxidised to an aldehyde. In all, five separate reactive steps are required. In this section it will be demonstrated that simple imine chemistry can be utilised in combination with the plasma polymerisation of a suitable monomer such as undecenal (Figure 3.2).

Undecenal presents the precursor which combined a commercially available molecule with long and flexible aliphatic chain, a classically polymerisable bond in the terminal alkene function, and yet remained volatile enough to generate a vapour within the plasma reactor. Thus it was desirable to combine functionality in availability and deposition with the maximum chance of generating a flexible layer on the substrate.

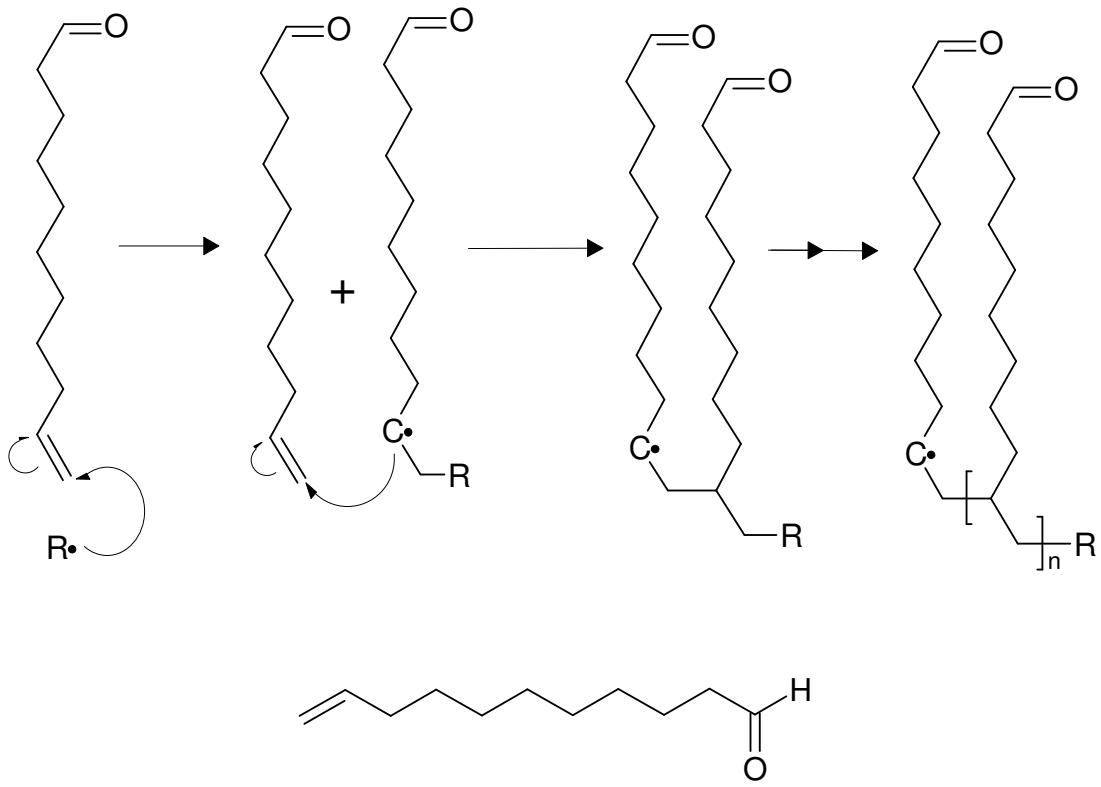

Figure 3.2. Radical chain growth polymerization mechanism of an undecenal precursor to yield an aldehyde plasmachemical functionalized surface.

A plasmachemical surface provides many of the important factors for DNA hybridisation. An undecenal modified surface offers a flexible linkage to the surface due to its long chain. The long carbon chains and relative lack of polar groups will offer a high contact angle – preventing spreading of droplets during the microarraying process.

3.2 Experimental

Plasma polymerization of undec-1-enal (Aldrich, +99%, $H_2C{=}CH(CH_2)_8CHO$, purified by several freeze-pump-thaw cycles) was carried out in an electrodeless cylindrical glass reactor as described in Chapter 2.

Substrates included borosilicate glass cover slips (BDH), glass slides (VWR International, SuperFrost), polished silicon wafer (MEMC Electronics Materials).

Optimum plasmachemical pulsing conditions were established by varying t_{on} (between 5 and 50 µs) and t_{off} (between 0.5 and 50 ms), with typical

deposition times varying between 10 – 70 minutes. Upon extinction of the electrical discharge, the precursor was allowed to continue to pass through the apparatus for a further 5 min prior to venting to atmosphere. Based on the results presented later in this chapter, the optimum deposition corresponded to a pulsed plasma duty cycle of t_{on} = 15 µs, t_{off} = 20 ms, and a peak power of 40 W. All subsequent immobilization experiments used undec-1-enal substrates modified using this duty cycle.

3.2.1 DNA immobilization and hybridization

DNA immobilization entailed immersing the poly(3-vinylbenzaldehyde) plasma polymer surfaces into 1.0 µmol dm^{-3} of fluorescently tagged oligonucleotide (Sigma-Genosys Ltd, oligonucleotide sequence: 5'-3' AACGATGCACGAGCA, desalted, reverse phase purified, with 3' terminal primary amine and 5' terminal Cy5 fluorophore) at 42 ºC for 16 h in saline sodium citrate buffer at pH4.5 (citric acid 99%, Aldrich; NaCl 99.9%, Sigma). Subsequently, 3.5 mg ml^{-1} $NaCN(BH_3)$ (Aldrich, 99%) was added, and the solution gently stirred for 3 h. Any excess physisorbed oligonucleotides were removed by sequential washing in high purity water, saline sodium citrate buffer (SSC, 0.3M sodium citrate, 3M NaCl, pH7, Sigma) containing 1% (w/v) sodium dodecyl sulphate (Sigma, 10% solution), high purity water, a solution of 10% (v/v) stock SSC buffer in high purity water with 0.1% (w/v) sodium dodecyl sulphate, high purity water, 5% (v/v) stock SSC buffer in high purity water, and finally high purity water.

For the hybridization studies, oligonucleotide (sequence: 5'-3' GCTTATCGAGCTTTC with 5' terminal primary amine, desalted, reverse phase purified, Sigma-Genosys Ltd) was attached onto the poly(3-vinylbenzaldehyde) plasma polymer surfaces as described above. These surfaces were then immersed in a solution of 50% (v/v) pre-hybridization solution (Sigma, from 2x concentrate) and 50% (v/v) formamide (Sigma, molecular biology grade) for 1 h. Subsequent removal from solution was followed by rinsing in high purity H_2O, immersion in a 50% (v/v) high purity H_2O/50% (v/v) hybridization solution (Sigma, from 2x concentrate) containing 200 nM oligonucletide (sequence: 5'-3' GAAAGCTCGATAAGC, desalted,

reverse phase purified with 5' terminal Cy5 fluorophore, Sigma-Genosys Ltd) at 20 ℃ for 1 h. Final washing of these hybridized surfaces was carried out sequentially as outlined previously.

Undecenal plasmachemically functionalized slides were compared to commercially available aldehyde functionalized substrates (ALS-25, batch 03154, CEL Associates Inc., Pearland, Texas).

3.2.2 Microarray fabrication

Amine terminated oligonucleotides were microarrayed onto pulsed plasma poly(undec-1-enal) coated glass microscope slides using a robotic spotter (Genepak). The respective probe solutions were placed into a 384-well plate and spotted onto the functionalized slides using a stainless steel pin. Typically, four identical 500 µm print pitch arrays were constructed onto each slide, using a pin pick-up time of 1 s and a 0.01 s dwell time. The spotted arrays were incubated in an oven at 42 ℃ over a saturated solution of K_2SO_4 (96% relative humidity to keep spotted samples solvated over the period of the experiment) for 16 h followed by cleaning as described above in order to dislodge any noncovalently-bound material.

3.3 Results

3.3.1 Optimisation of duty cycle

The continuous wave functionalisation (5W) of undec-1-enal yields a surface that is oxygen poor in comparison to the theoretical surface based on the monomer structure (Figure 3.3). Pulsed plasmachemical functionalisation at 15 µs t_{on}, 20 ms t_{off}, 40W PP, yields a surface composition that corresponds with that expected from the monomer structure (Table 3.1). Additional oxygen observed in the case of some pulsed plasmachemical layers is attributed to the incorporation of atmospheric oxygen into the coating either via minor leaks in the reactor, or via reaction with atmospheric oxygen when the reactor is brought up to atmosphere.

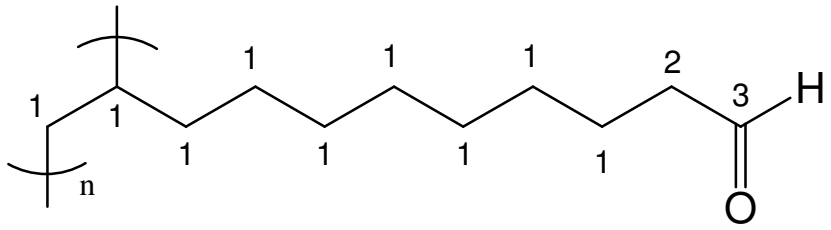

Figure 3.3. Theoretical surface polymer structure indicating the three expected carbon environments 1) $\underline{C}_yH_x$ 2) $\underline{C}$-C=O 3) $\underline{C}$=O

	C(1s) %	O(1s) %
Continuous Wave (5 W)	93 ± 1	6.9 ± 1
Pulsed (15 µs t_{on}, 20 ms t_{off}, 40 W PP)	91 ± 1	9.1 ± 1
Theoretical	91.7	8.3

Table 3.1. XPS atomic composition of plasma polymerised undec-1-enal surfaces.

Examination of the C(1s) envelopes of the continuous wave and pulsed plasma polymer of undec-1-enal both consist primarily of CyHx (285.00 eV), with a theoretical contribution from C-C=O (285.40 eV) that is not resolved in practice (Figure 3.4). The C=O band is more pronounced (287.80 eV) in the pulsed plasma polymer (8.8 ± 0.7 % of the C(1s) envelope area), being somewhat obscured in the broader tail on the continuous wave envelope (6.7 ± 0.6 % of the C(1s) envelope area)[18,19]. Similar examination of the O(1s) envelope (Figure 3.5) confirms a similar oxygen chemical environment in both the pulsed plasmchemical and continuous wave layers. The only resolvable peak in each spectrum is a single signal at 532.6 eV which is consistent with C=$\underline{O}$ functions[20]. However, instrumental resolution may not be enough to identify any peaks associated with C-$\underline{O}$H (531.7 eV) or COOH (~534.0 eV), especially if these signals of low intensity.

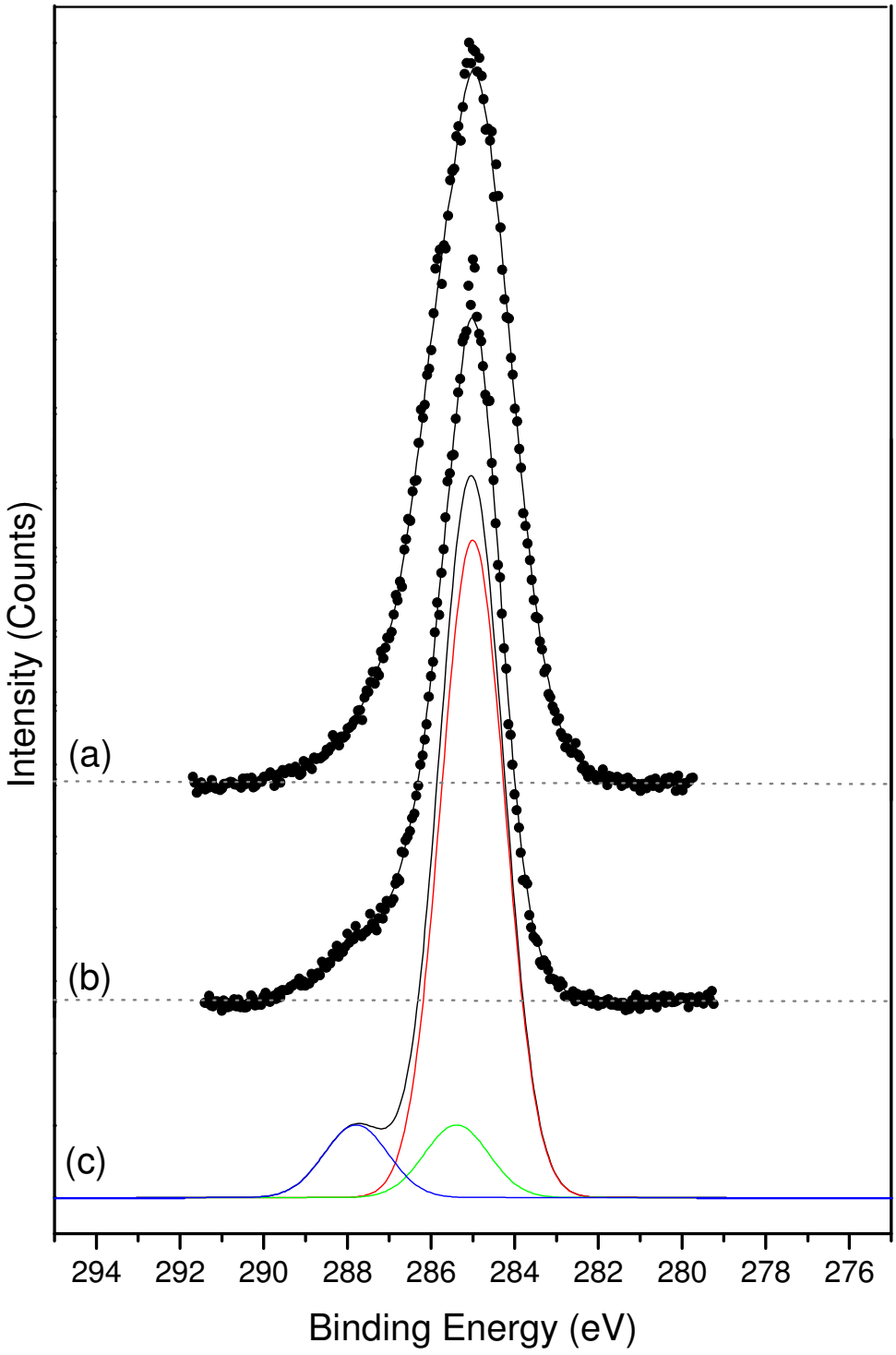

Figure 3.4. C(1s) Envelopes on by XPS for (a) continuous wave (5 W), (b) pulsed plasma (15 μs t_{on}, 20 ms t_{off}, 40W P_P) and (c) theoretical poly(undec-1-enal) on Si wafers.

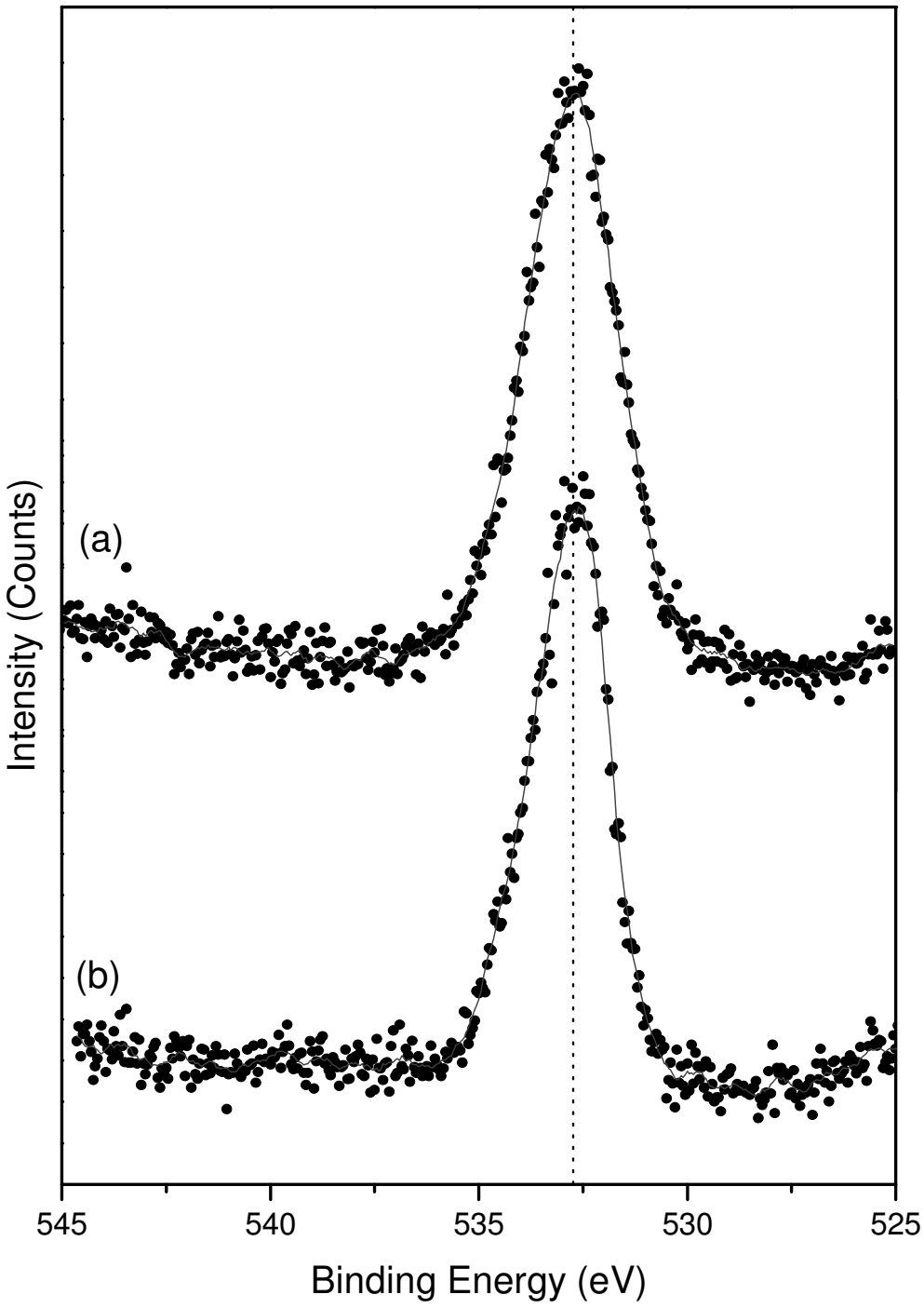

Figure 3.5. O(1s) Envelopes on by XPS for (a) continuous wave (5 W), (b) pulsed plasma (15 μs t_{on}, 20 ms t_{off}, 40W P_P) poly(undec-1-enal) on Si wafers. Peak highlighted is at 532.6 eV.

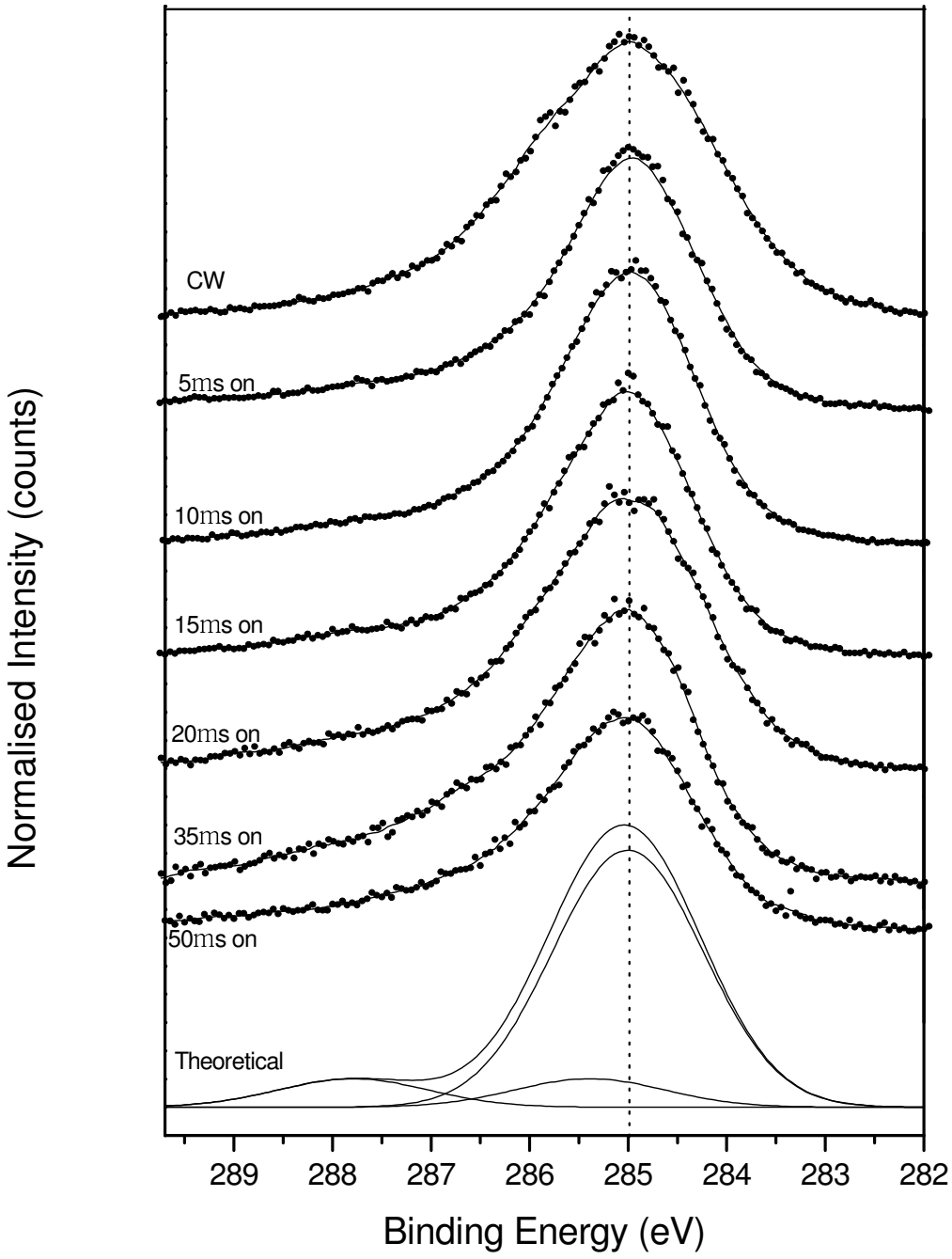

Figure 3.6 Variation of the C(1s) envelope with varied pulse on time.

The effect of variation in duty cycle was monitored by XPS. Variation of pulse t_{on} was shown to have a considerable effect on the composition of plasmachemically functionalised surfaces (Figs 3.6, 3.7 and Table 3.2). Longer t_{on} durations show increased oxygen content at the surface, with larger oxygenated tails observed in the C(1s) envelope. The theoretical polymer oxygen content of 8.3 atomic % corresponds most closely to a t_{on} of 10 or 15 µs. Additionally, fitting the high-resolution C(1s) envelopes with the three expected carbon environments (Fig 3.6, Table 3.2), shows a similar trend, with a larger C=O signal at 287.8 eV relative to the total carbon signal.

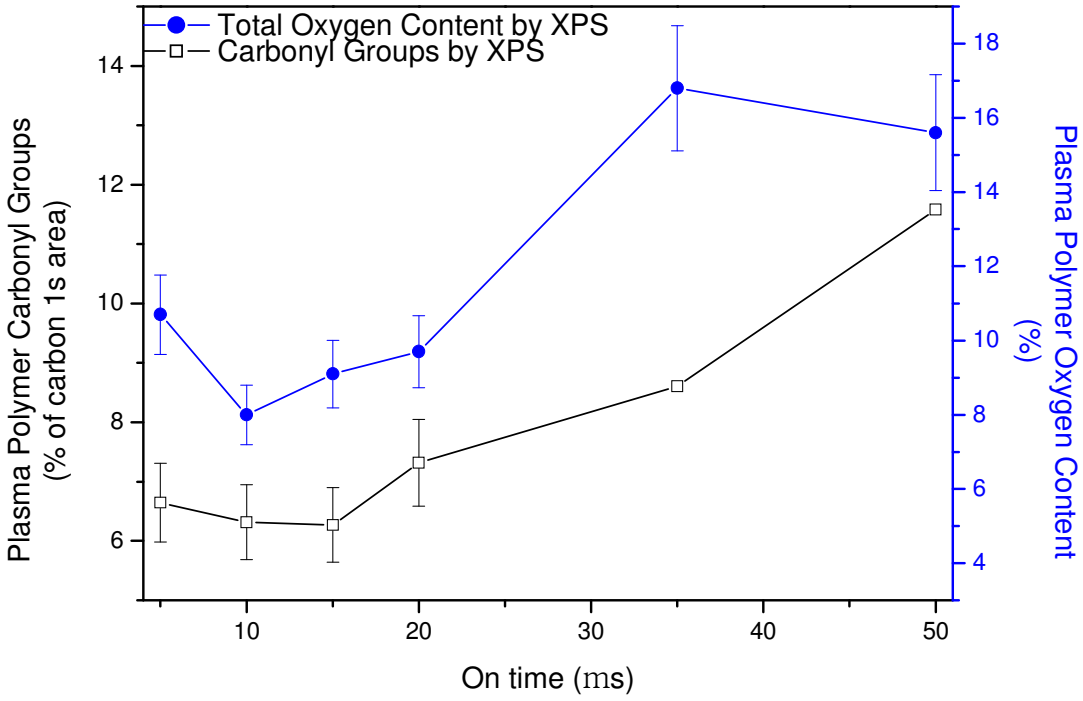

Figure 3.7 Variation in the surface atomic oxygen content (Atomic %) and the intensity of the C=O signal (% of the total carbon signal), with varied pulse on time.

Time on / µs	Time off / ms	C %	O %
5	20	89.3	10.7
10	20	92.0	8.0
15	20	90.9	9.1
20	20	90.3	9.7
35	20	83.2	16.8
50	20	84.8	15.6
Theoretical		91.7	8.3

Table 3.2 Variation in the surface atomic oxygen content (Atomic %) and the intensity of the C=O signal (% of the total carbon signal), with varied pulse on time.

The effect of pulse off time was similarly monitored by XPS with the surface elemental compositions shown in Figure 3.8 and Table 3.3. The extremely long and extremely short pulse off-time durations again show increased oxygen content, with oxygen signals significantly higher than those predicted based on the undec-1-enal structure. The intensity of the C=O peak in the carbon 1s envelope follows the same trend (Figure 3.9). In practice, the t_{off} of 20 ms, was observed to give a relatively strong structural retention.

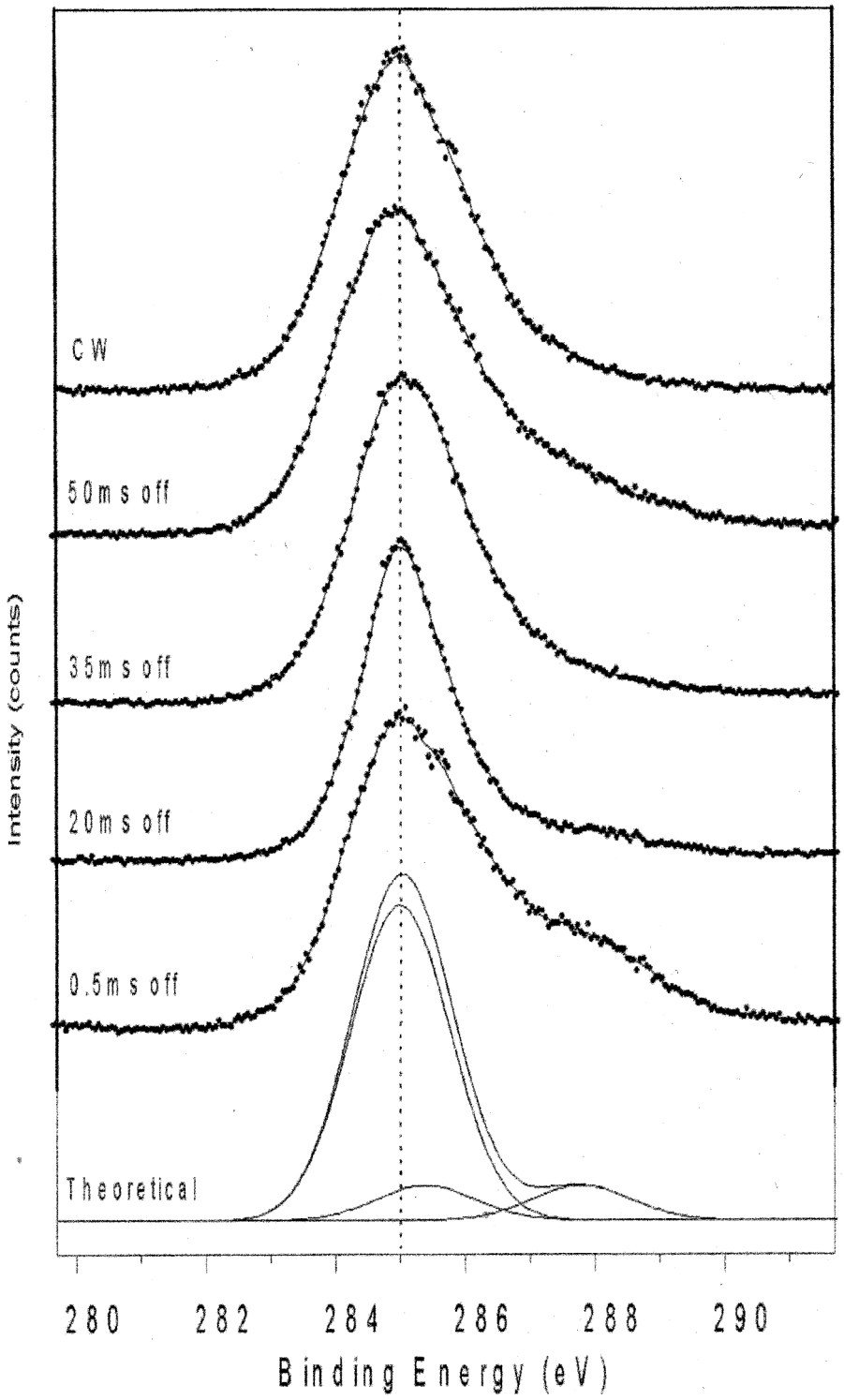

Figure 3.8 Variation of the C(1s) envelope with varied pulse off time.

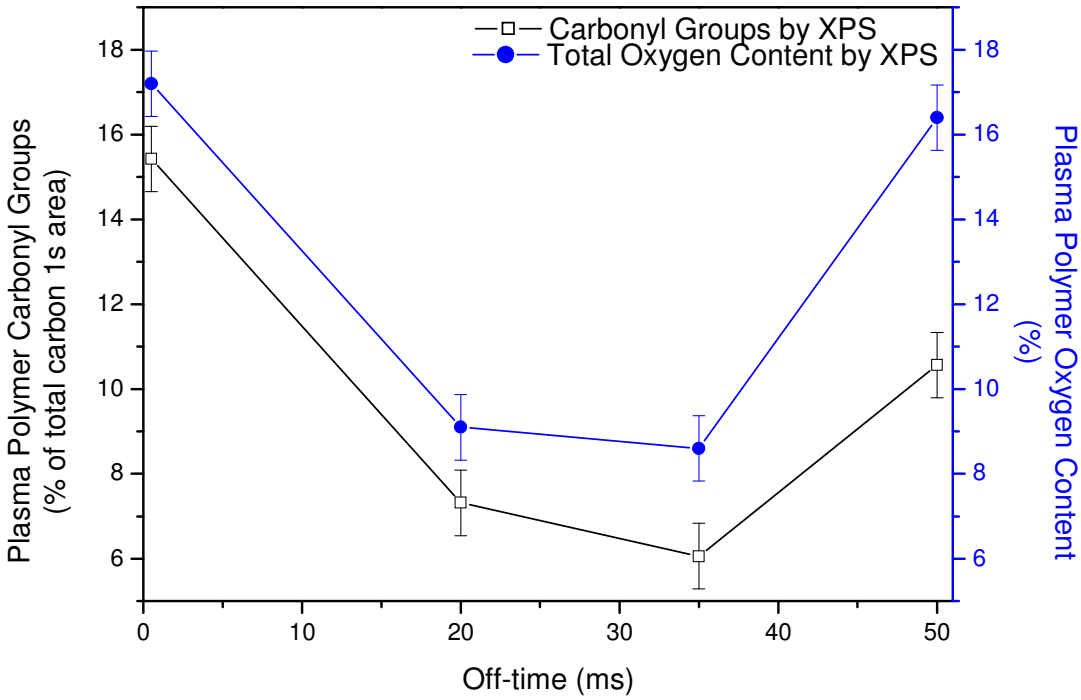

Figure 3.9 Variation in the surface atomic oxygen content (Atomic %) and the intensity of the C=O signal (% of the total carbon signal) with pulse off time.

Time on / µs	Time off / ms	C %	O %
15	0.5	82.8	17.2
15	20	90.9	9.1
15	35	91.4	8.6
15	50	83.6	16.4
Theoretical		91.7	8.3

Table 3.3 Variation in the surface atomic oxygen content (Atomic %) and the intensity of the C=O signal (% of the total carbon signal) with pulse off time.

A comparison of the functionalized surfaces with the undec-1-enal monomer by grazing angle FT-IR shows that functionalisation results in the complete disappearance of the monomer vinyl C=C stretch at 1637 cm^{-1} in the case of the pulsed plasmachemical layer. Otherwise, the pulsed plasmachemical undec-1-enal surface retains the same general profile as the monomer, in particular the aldehyde C=O carbonyl band at 1709 cm^{-1}, and the aldehyde CHO rock bands at 2810 cm^{-1} and 2715 cm^{-1}.

Continuous wave plasmachemical functionalisation results in significant peak broadening and the total loss of the aldehyde CHO rock bands. The broad C=O stretching mode may also include some retained vinyl C=C stretch at 1637 cm^{-1} (Figure 3.10).

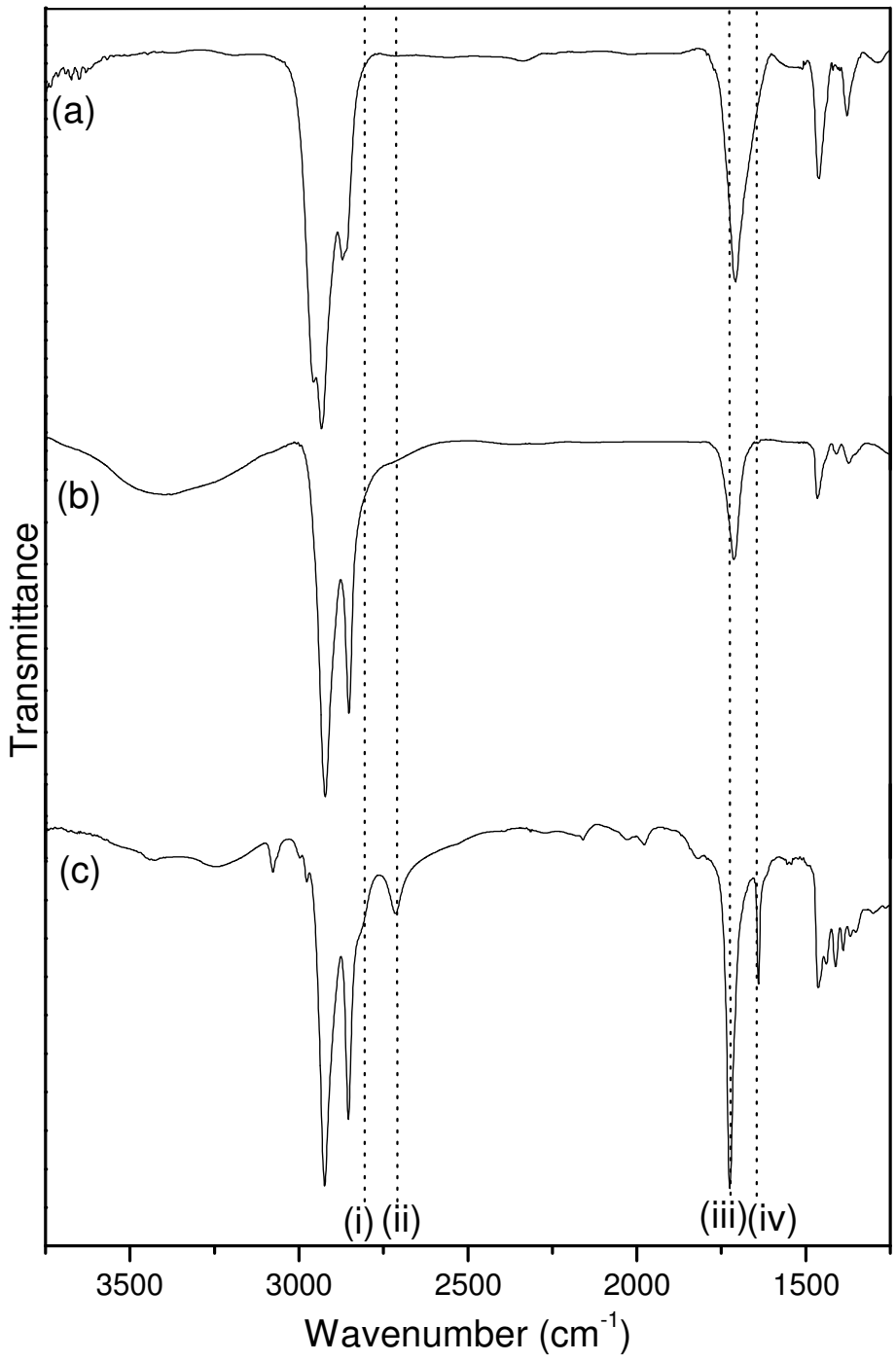

Figure 3.10. FT-IR of (a) continuous wave plasmachemical functionalised surface (5 W), (b) pulsed plasmachemical functionalised surface (15 μs t_{on}, 20 ms t_{off}, 40W PP) and (c) undec-1-enal monomer. Highlighted bands are (i) & (ii) aldehyde CH stretches (2810 & 2715 cm^{-1}); (iii) carbonyl C=O stretch (1717 cm^{-1})'; (iv) vinyl C=C stretch (1637 cm^{-1}).

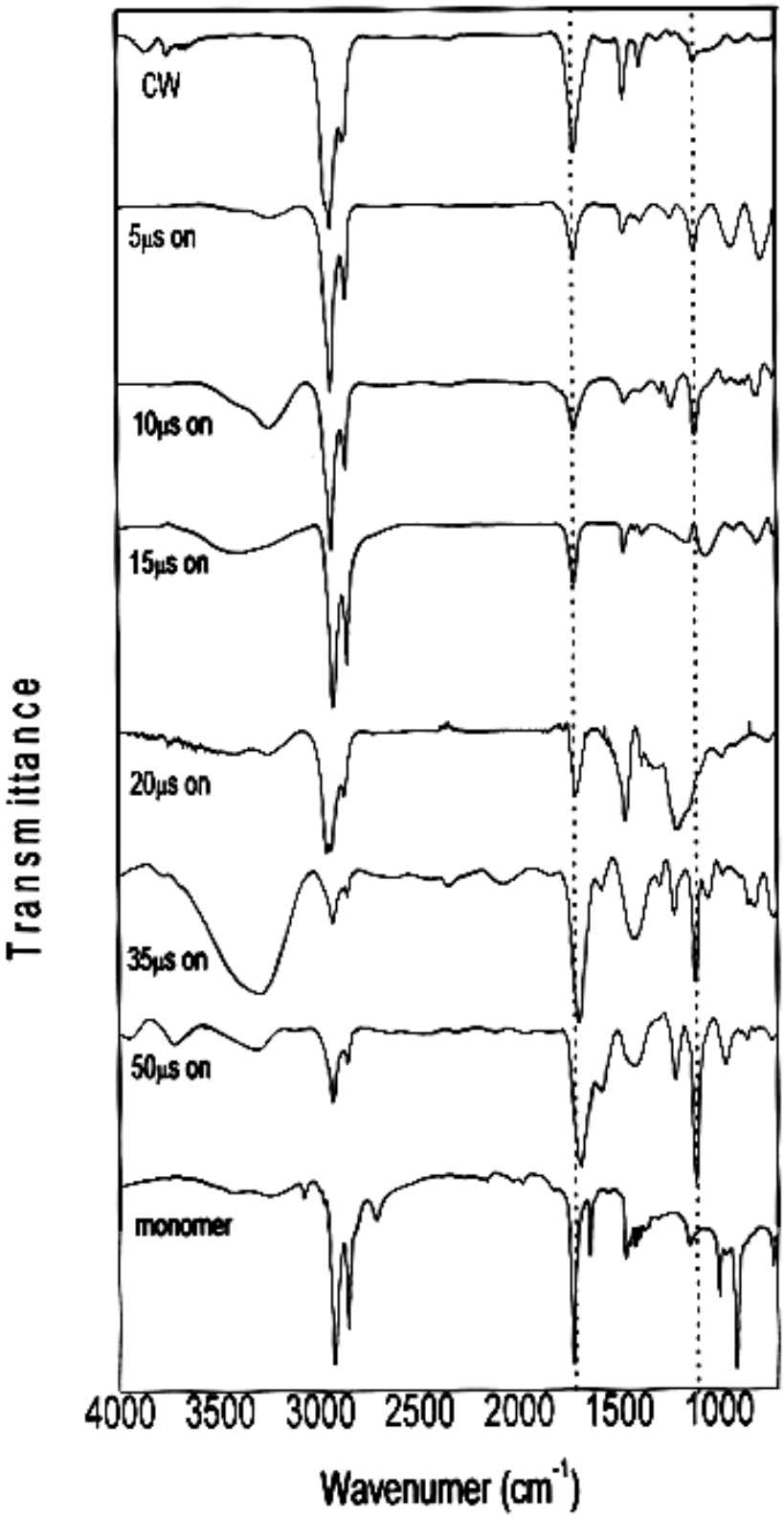

Figure 3.11 Variation of FTIR spectra of plasmachemical layers with varied pulse on time.

The effect of the pulse duty cycle was also monitored by grazing angle FT-IR of plasmachemical surfaces on silicon wafers. At longer on-times the carbonyl shifts to the 1680cm-1 region (Figure 3.11), probably due to incorporation of extra oxygen to give carboxylic acid groups. Note also the inclusion of extra bands in the C-H stretch region in higher on-time samples. There is also a general broadening of all bands within the spectra at on-times greater than 15μs. Simultaneously, the carbonyl stretching region is increased with respect to the C-H stretch region (Table 3.4).

Time on	Time off	Ratio of C-H:C=O areas
5	20	1.5
10	20	3.1
15	20	4.1
20	20	2.0
35	20	0.4
50	20	0.3
CW		6.8
monomer		2.2

Table 3.4. A comparison of the area of C-H stretching bands and carbonyl bands (1680cm^{-1} to 1717cm^{-1}) in undec-1-enal polymers, with varied pulse on time.

The FT-IR data (Figure 3.11) correspond closely with the XPS data. The oxygenation in several samples is clearly demonstrated by the large carbonyl bands in the 1700cm-1 region (Figure 3.11). The broad peak in the 3230cm-1 region is suggestive of hydrogen bonded C-O-H on the surface. Examination of the C-H stretch and C=O stretching envelopes corroborates this, and at 20-35 ms off-time suggests only a slight increase in the number of carbonyl units present. The relatively sharp IR spectra at 20ms off suggests that this off time offers good structural retention. The broad bands at 1576cm-1 and 1340cm-1 are suggestive of R-CO_2- formation.

Time on	Time off	Ratio: C-H:C=O areas
15	50	1.4
15	35	2.1
15	20	4.1
15	0.5	0.4
CW		6.8
monomer		2.2

Table 3.5. A comparison of the area of C-H stretching bands and carbonyl bands (1680cm^{-1} to 1717cm^{-1}) in undec-1-enal polymers, with varied pulse off time.

The sessile drop contact angle of the continuous wave surface is 88 ± 2 ° and the deposition rate observed by reflectometry is 36 ± 2 nm min^{-1}. Pulsed plasmachemical functionalisation yields a contact angle of 87 ± 3° and a deposition rate of 1.5 ± 0.6 nm min^{-1}. From a practical perspective, both surfaces are at the cusp of wetting – non-wetting. It is advantageous that surfaces are not too wetting as this can result in downstream processing problems when spotted aqueous solutions can spread, particularly under humid conditions. Conversely interactions of aqueous reaction solutions with excessively hydrophobic surfaces could be expected to produce poor reactions with small spot contact areas.

Tagging of the surface aldehyde functions for further XPS quantification of functional group retention proved inconclusive. Reaction with aqueous ammonium hydroxide (pH 9.04) or propylamine (0.25 M, pH 9.12) caused complete film destruction. Whilst plasma polymer films are generally stable in aqueous solutions, the chemistry of the polymer and the strength of the plasma polymer – substrate interface will dictate stability. Higher cross-linking is commonly used to stabilise acrylic acid plasma polymers for instance. For undec-1-enal coatings, such an approach was undesirable as it also results in increased fragmentation of functional groups.

Exposure of the substrate to TFA vapour in a sealed plasma deposition rig produced no change by XPS, presumably as any imines formed are destabilised by the subsequent vacuum used to clear the reactor of acid.

However, exposure of the substrates to a concentrated cresyl violet perchlorate ($C_{12}ON_3ClO_4$, Figure 3.12) solution for 24h at room temperature did result in the appearance of nitrogen signals in the XPS survey scans, which were 69% higher for the pulsed plasma polymer (Table 3.6). Cresyl violet can interact with the surface aldehyde groups via the two amine functions.

		Surface Elemental Composition (Atomic %)		
		C (1s)	O (1s)	N (1s)
CW	Before	94.6	5.4	-
	After	81.4	17	1.6
Pulsed	Before	89.5	10.5	-
	After	81.8	15.5	2.7

Table 3.6. Exposure of continuous wave (CW, 5 W) and pulsed (15 µs t_{on}, 20 ms t_{off}, 40 W PP) plasmachemical layers to a cresyl violet solution.

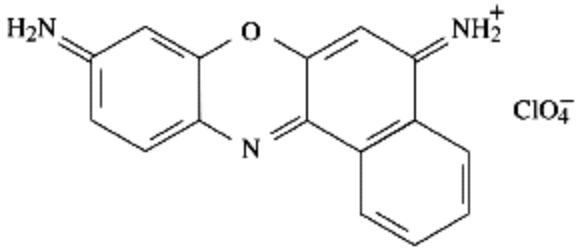

Figure 3.12. Cresyl violet perchlorate.

3.3.2 Immobilization of oligonucleotides to undec-1-enal functionalised surfaces

The extent of immobilization of the 5' Cy5 tagged, 3' primary amine oligonucleotide AM1 (see Table 3.7 for oligonucleotide structures) with undec-1-enal functionalized surfaces was examined by fluorescence spectroscopy. The effect of temperature on fluorescence intensity was examined, showing that 42℃ was the optimal temperature for AM1 probe immobilization (Figure 3.13). The intensity of the observed fluorescence signal was also shown to vary strongly with pH, with the signal remaining low at most pH values but showing a marked increase at pH 4.50 and 5.03 (Figure 1.14).

	5' Modification	5'-3' Base Sequence	3' Modification
AM1	Cy5	AACGATGCACGAGCA	C13 Amine
AM2	C13 Amine	GCTTATCGAGCTTTC	-
AM3	Cy5	GAAGCTCGATAAGC	-

Table 3.7. Oligonucleotide Probe Structures

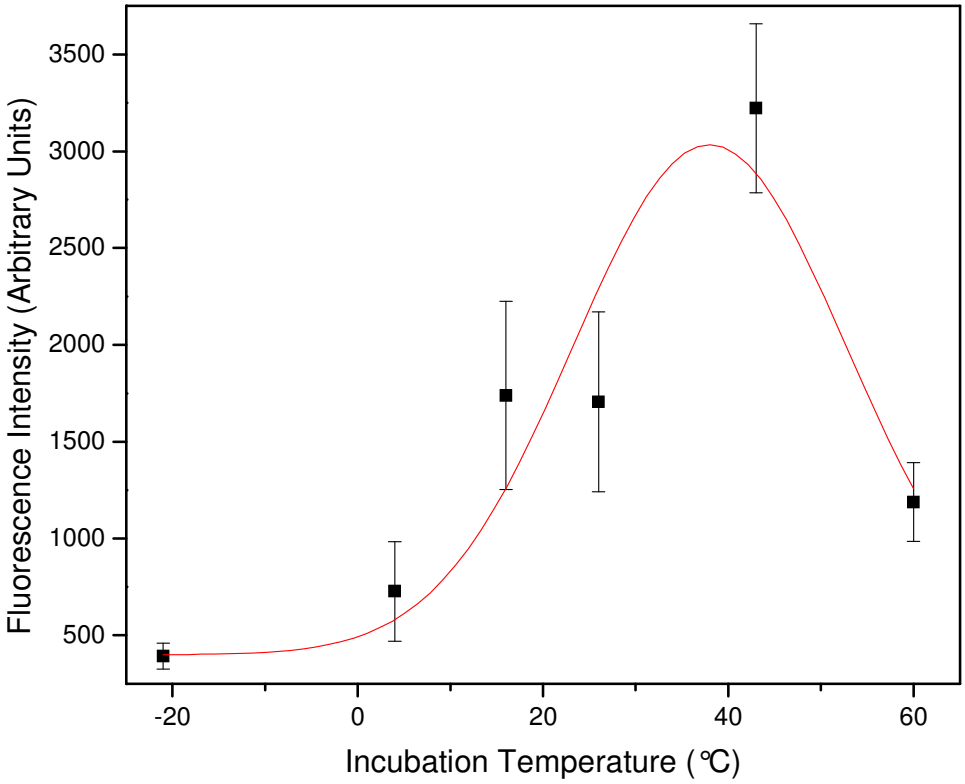

Figure 3.13. Fluorescence intensity as a function of temperature for Cy5 tagged oligonucleotide reaction with pulsed plasmachemical undec-1-enal surfaces (15 μs t_{on}, 20 ms t_{off}, 40W PP). Probe concentration 1.04 μmol dm^{-3}, incubation time 24 hours, pH 4.47.

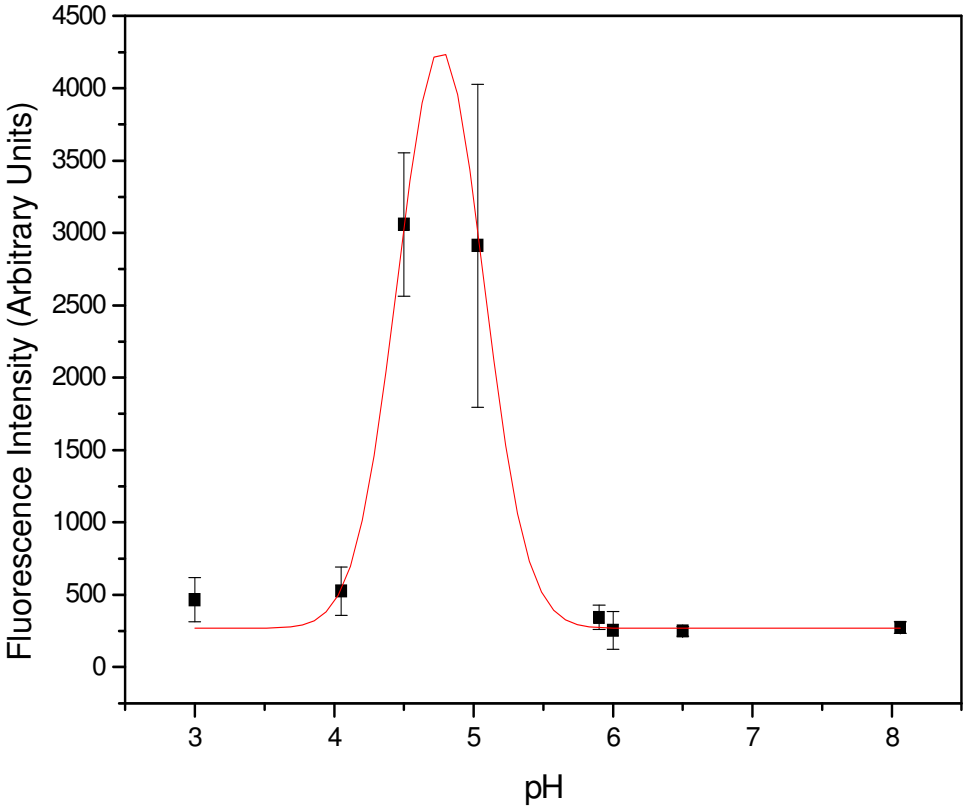

Figure 3.14. Fluorescence intensity as a function of pH for Cy5 tagged oligonucleotide reaction with pulsed plasmachemical undec-1-enal surfaces (15 µs t_{on}, 20 ms t_{off}, 40W P_P). Probe concentration 1.04 µmol dm^{-3}, incubation time 24 hours, incubation temperature 42℃.

An increase in AM1 probe concentration yields increased fluorescence intensity only above 500 n mol dm^{-3}. The intensity plateaus after 1 µmoldm^{-3}, with addition of extra AM1 probe showing no significant increase in signal (Figure 3.15). The immobilization reaction was demonstrated to be largely complete after about 4 hours (Figure 3.16).

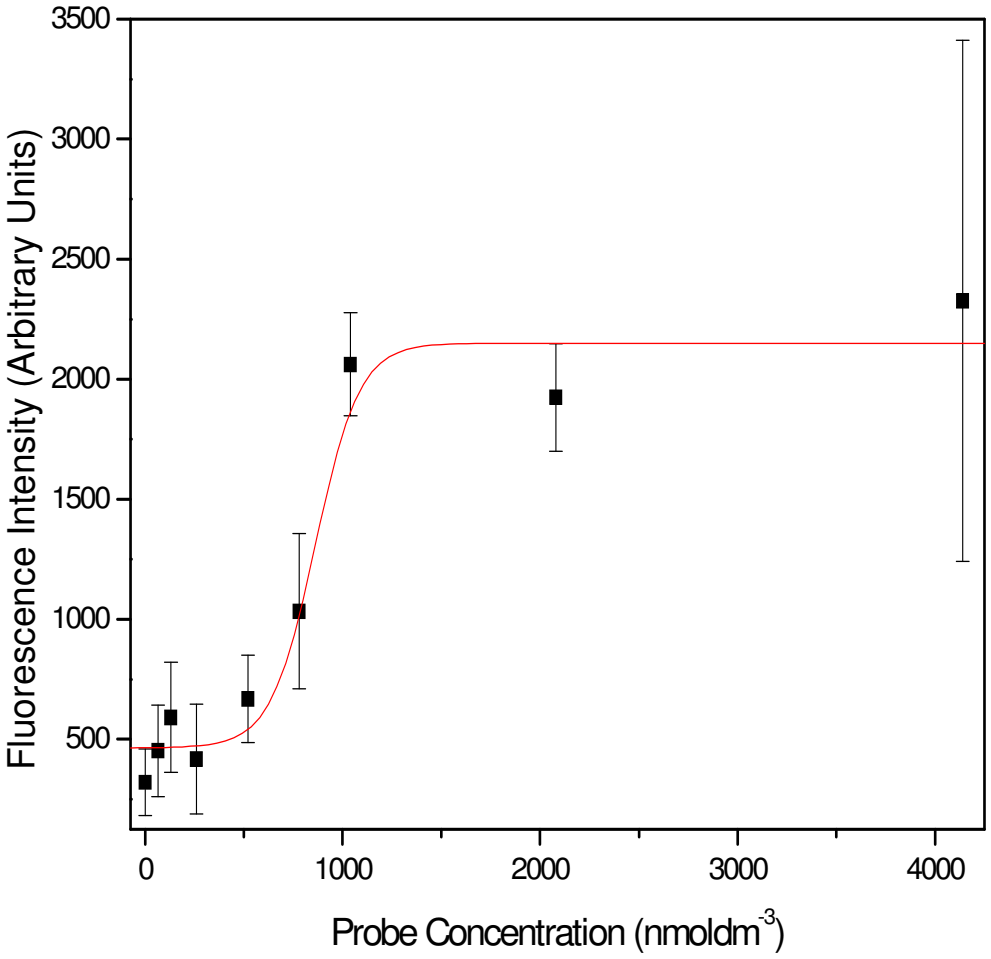

Figure 3.15. Fluorescence intensity as a function of probe concentration for Cy5 tagged oligonucleotide reaction with pulsed plasmachemical undec-1-enal surfaces (15 μs t_{on}, 20 ms t_{off}, 40W P_P). pH 4.47, incubation time 24 hours, incubation temperature 42℃.

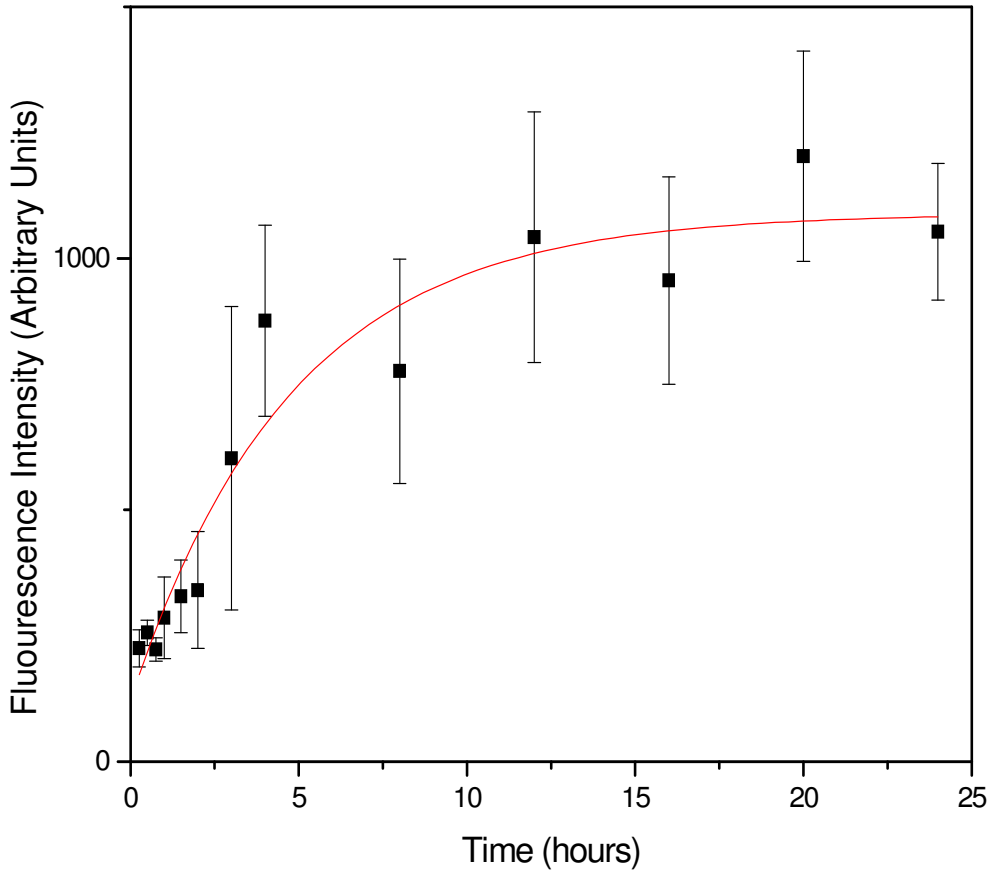

Figure 3.16. Fluorescence intensity as a function of time for Cy5 tagged oligonucleotide reaction with pulsed plasmachemical undec-1-enal surfaces (15 µs t_{on}, 20 ms t_{off}, 40W P_P). Probe concentration 1.04 µmol dm^{-3}, incubation temperature 24 hours, pH 4.55.

Immobilization of AM1 probe to the surface aldehyde functions using optimal conditions (temperature 42°C, pH 4.50, probe concentration 1 µmoldm^{-3}, time > 4h) was followed by XPS (Figure 3.17). On reaction with an oligonucleotide probe containing a primary amine function, AM1, a small N(1s) band is observed in the survey scan at 398 eV. This band is not observed when control oligonucleotide AM3 that lacks the primary amine is used under otherwise identical immobilization conditions, indicating minimal non-specific adsorption. The O(1s) band at 533 eV is also observed to increase relative to the C(1s) envelope at 285 eV. Occasional trace Na(1s) and Cl(2p) bands were also observed (Table 3.8).

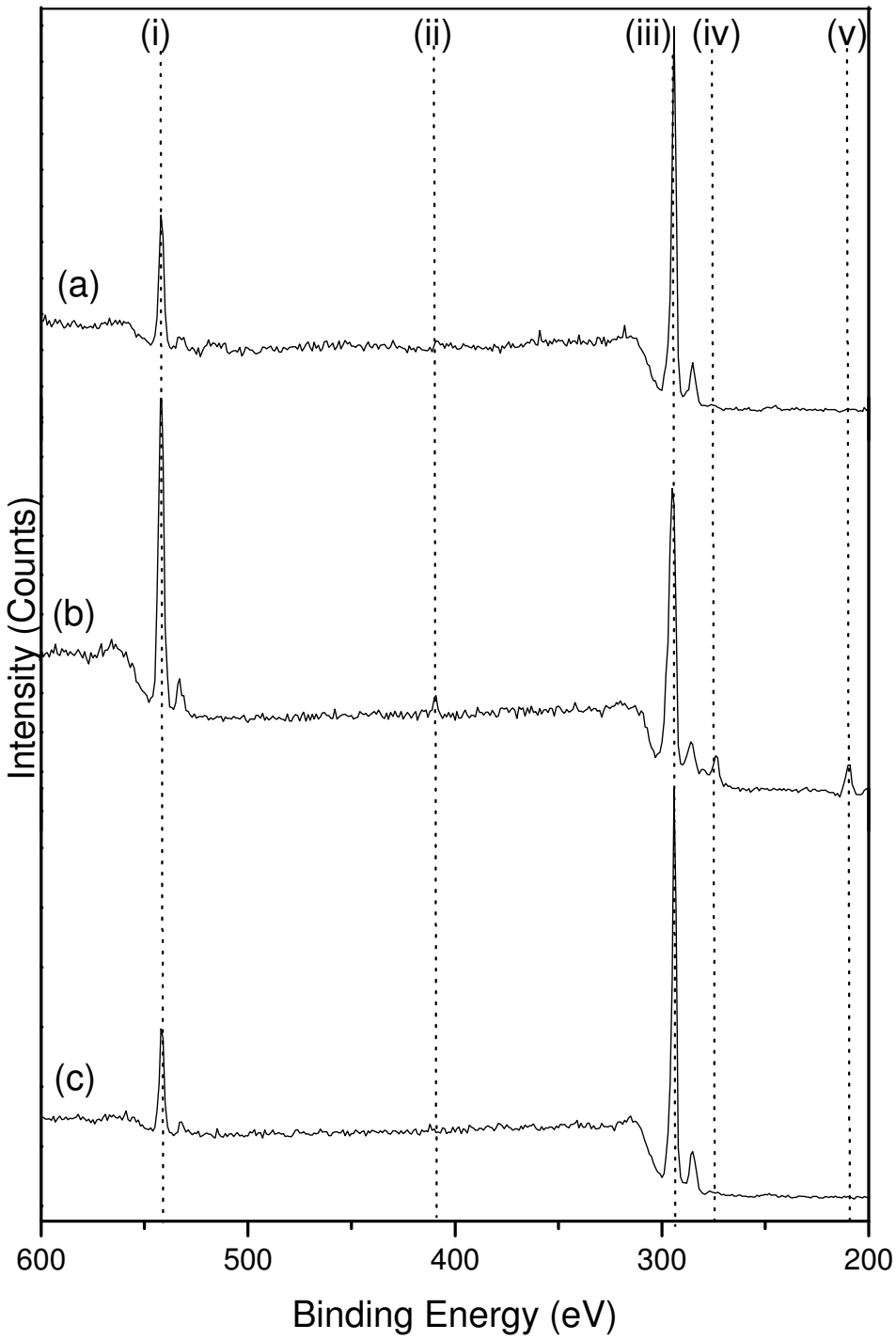

Figure 3.17. XPS surveys of DNA interaction with aldehyde plasmachemical surfaces (a) Surface after treatment with 1.04 μmoldm^{-3} probe. (b) Surface after reaction with 1.04 μmoldm^{-3} probe containing carbon linker to a primary amine. (c) As produced plasmachemical functionalised surface. The dashed lines highlight (i) O(1s); (ii) N(1s); (iii) C(1s); (iv) Cl(2s); (v) Cl(2p)

Atom	Amount (%)
C (1s)	82 ± 4.0
N (1s)	2.4 ± 1.3
O (1s)	15 ± 4.1
Na (1s)	0.086 ± 0.086
Cl (2p)	0.40 ± 0.22

Table 3.8 Observed XPS bands of AM1 oligonucleotide immobilized (1.04 µmol dm^{-3} concentration in pH4.5 SSC at 42ºC) onto functionalised undec-1-enal surfaces (15 µs t_{on}, 20 ms t_{off}, 40W PP)

The reaction was also followed using FT-IR. Again, reaction with oligonucleotide probe is not observed unless the terminal primary amine group is present (Figure 3.18). In the case where a terminal amine group is present, AM1, a strong change is observed in the spectrum of the surface (Figure 3.18b). In particular, a strong broad band is observed due to primary amine stretching in the 3250 cm-1 and amide stretching[21] at 3400 cm-1. The observed aldehyde CHO shoulder (2815, 2710 cm-1) on the C-H region is absent although a strong, broad carbonyl C=O peak is retained at 1722cm-1. A strong, broad band is also observed at 1509 cm-1 is attributed to a mix of C-N-H in-plane deformation and C-N stretches. Finally, the strong peak at 1254 cm-1 is attributed to the amide III band[22,23].

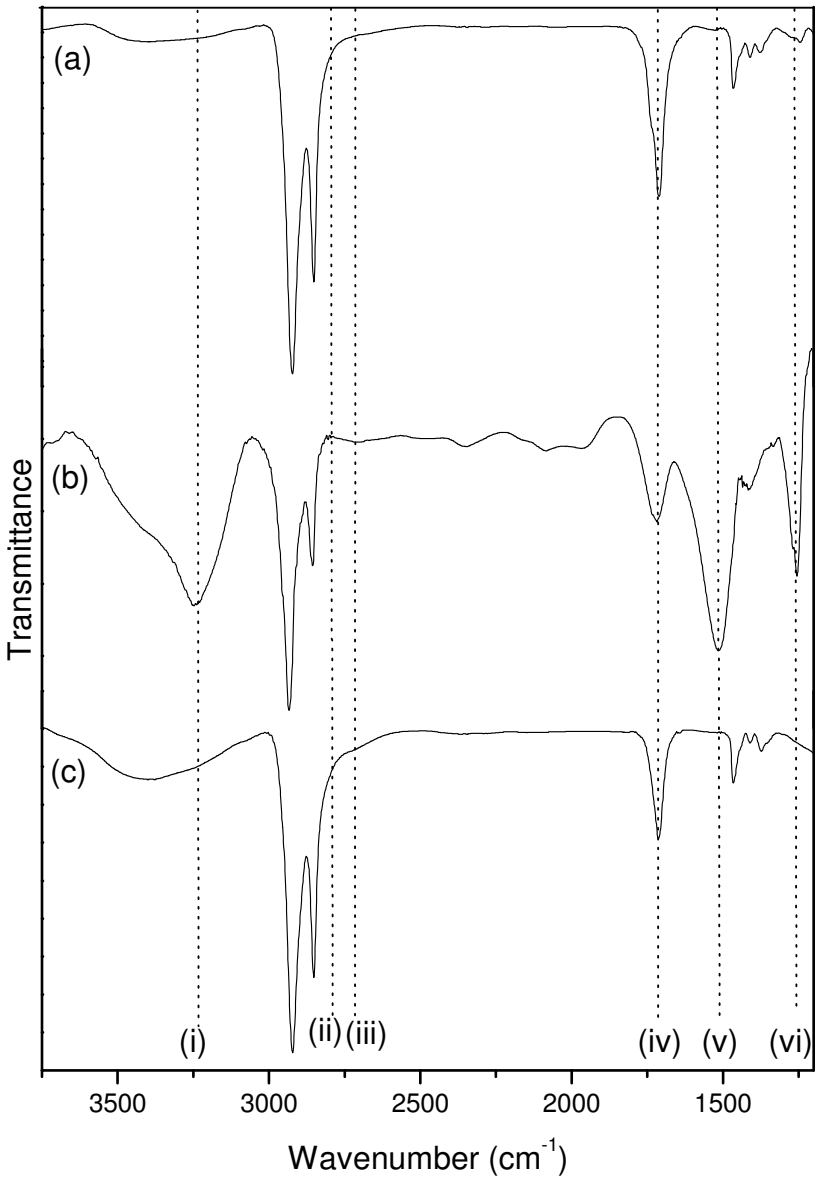

Figure 3.18. FT-IR of chemically immobilised DNA probes on plasmachemically functionalised undec-1-enal surfaces (15 µs t_{on}, 20 ms t_{off}, 40W P_P): (a) Surface after treatment with 1.04 µmol dm^{-3} probe. (b) Surface after reaction with 1.04 µmol dm^{-3} probe containing carbon linker to a primary amine. (c) As produced plasmachemical functionalised surface. Highlighted bands are (i) amide stretching bands, 3200-3400 cm^{-1}; (ii) aldehyde CHO stretch, 2815cm^{-1}; (iii) aldehyde CHO stretch, 2710 cm^{-1}; (iv) carbonyl C=O, 1722 cm^{-1}; (v) C-N-H & C-N stretches, 1509 cm^{-1}; (vi) amide III band, 1254 cm^{-1}

3.3.3. Hybridization of oligonucleotides on undec-1-enal functionalized surfaces

The hybridization of probe AM3 to surface immobilized probe AM2 was monitored by fluorescence spectroscopy as a function of probe concentration (Figure 4.19). Hybridization was observed with as little as 200 nmoldm^{-3} probe in a pH7.5 SSC buffer. Addition of probe up to 1 μmoldm^{-3} resulted in a small increase in the overall fluorescence signal.

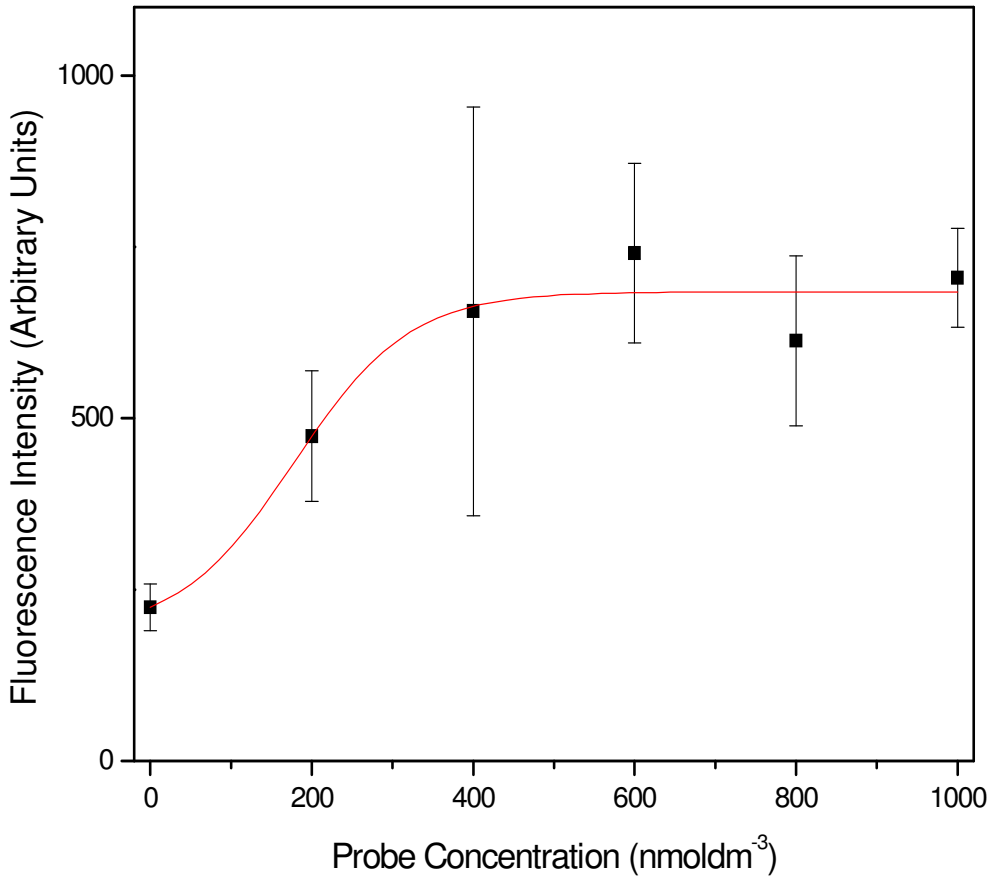

Figure 3.19. Fluorescence intensity as a function of probe concentration for Cy5 tagged oligonucleotide hybridisation with a complimentary partner surface immobilised on pulsed plasmachemical undec-1-enal surfaces (15 μs t_{on}, 20 ms t_{off}, 40W P_P). Hybridisation in pH 7.50 SSC buffer at room temperature for 1 hour.

The optimal conditions for constructing an oligonucleotide surface for hybridization studies were then used in the fabrication of a DNA array of AM2 probe onto the aldehyde functionalized surface (Figure 3.20). Clearly defined and regularly spaced fluorescent spots are observed after hybridization with AM3, with signals due to non-specific adsorption of the Cy5-tagged oligonucleotide minimized to minor background noise. Otherwise, the fluorescent spots display strong contrast when compared to the low signal from the background. In several cases a 'coffee ring' effect is observed wherein the outer edges of the spot record a higher fluorescence signal than observed in the centre.

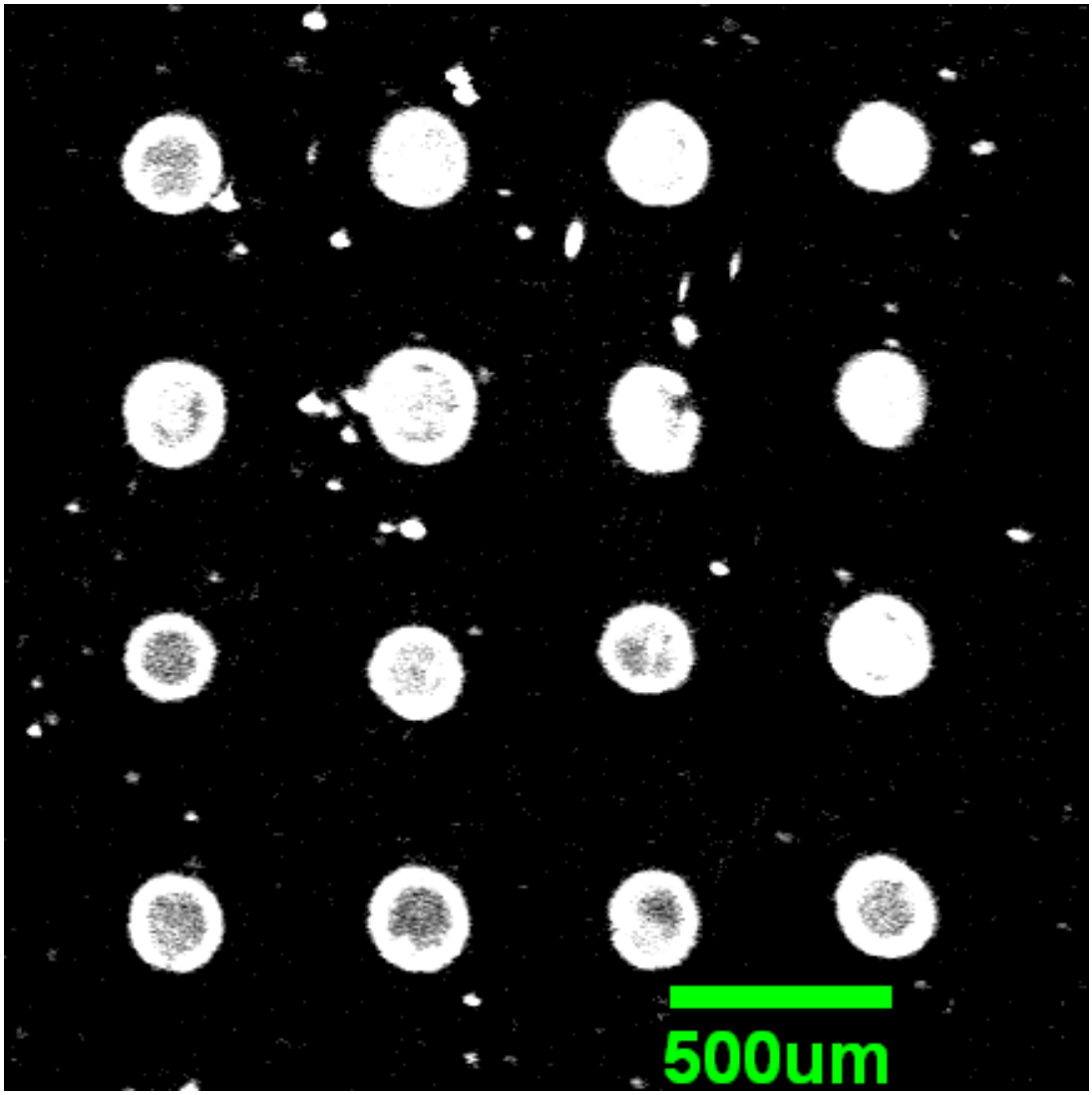

Figure 3.20. An array of Cy5 modified oligonucleotides immobilised onto an undec-1-enal pulsed plasma polymer surface (15 μs t_{on}, 20 ms t_{off}, 40W P_P).

3.4. Discussion

3.4.1. Plasmachemical functionalisation with undec-1-enal

The introduction of aldehyde functions to surfaces via plasmachemical functionalisation of undec-1-enal has been demonstrated. Pulsed plasmachemical technology in particular offered several beneficial features over continuous wave methods.

Although there have been previous attempts at plasma depositing aldehyde groups from precursors such as acrolein[24,25,26], acetaldehyde[27], or benzaldehyde[28], they have all suffered from poor aldehyde group incorporation due to either extensive fragmentation of the monomer or the absence of a polymerizable carbon-carbon double bond. Silane SAM technology for generation of aldehyde functions is not widely used although some examples have been generated. The highly-reactive trichlorosilane SAM precursors tend to be unstable with aldehydes and some common precursors such as alcohols. A typical strategy to overcome this problem is to surface immobilize a suitable SAM and subsequently generate an aldehyde function on the surface with a second reaction step[29,30,31], detection limits for DNA are reported by fluorescence microscopy are in sub nM levels. The ozonolysis of terminal vinyl groups, resulting in 36% of available surface vinyl groups reacting to give surface aldehyde functions[32]. Deposition of thiol SAMs for aldehyde functions is reported, although here the need for a gold or thiol substrate surface has limited application for DNA chips. However, where the substrate is gold or thiol, the availability of molecules such as di-(10-decanal)-disulfide allow the direct introduction of aldhehyde functions, including also a suitable flexible linker [33,34,35].

Using the analogy with classical polymerisation, the pulse on time is the period in which the free radicals that initiate chain growth are generated. Long on-time periods allow for greater radical generation, increasing the rate of polymerisation, but also increasing the likelihood that extensive cross-linking of the polymer chains can take place and that the carbonyl double bond will be attacked by radical species.

The off-time is the period in which radical initiated chain growth takes place, but an increase in off-times allows more time for termination reactions and inefficient polymerisation as radical populations decrease. Equally, if the off-time is too short then the concentration of radicals present will be high leading to fast reactions, but possibly less selective polymerisations.

The complete disappearance of the alkene functionalities in FT-IR and the retention of the carbonyl functions in the pulsed polymer strongly suggests that polymerisation has proceeded predominantly via the alkene, although there is a noticeable increase in oxygenation, as witnessed both in XPS and FT-IR with increasing on time. The increasing ether C-O stretch in the IR and the presence of a C-O contribution in the XPS indicate that the plasma conditions are opening some of the carbonyl bonds leading to an overall loss in aldehyde groups. The shifting of the carbonyl in the polymer from ~1720cm^{-1} to ~1680cm^{-1} is also indicative of increased oxygenation and is attributed to increased hydrogen bonding and even some CO2- formation on the surface. Again, this is most noticeable at high on-times. Both 15µs and 10µs on-times produce relatively sharp IR spectra and XPS spectra suggest their composition is close to that of a theoretical undecenal polymer. The increase in oxygenation at on-times >20µs and the good retention of carbonyl groups by the 15µs, as well as the clear presence of aldehyde C-H stretch in the IR spectrum were taken to indicate that 15µs on offered the best retention of aldehydes and, unless otherwise stated, 15µs on has been used for the DNA immobilisations.

With off time variation, the degree of oxygenation proved to be problematic, with excessive broadening of the carbonyl group and appearance of extra bands suggesting poor retention of monomer structure. Both 20ms and 35ms off-times showed excellent XPS data, both approaching the theoretical monomer composition. However IR showed that the carbonyl in 35ms off is noticeably broadened and contains a broad side peak. 20ms off-times therefore offered the best retention of carbonyl functionality and were retained as optimum.

In the case of 15 µs t_{on}, 20 ms t_{off}, 40W P_P, composition of the pulsed plasmachemical surface by XPS remained close to that of the monomer indicating that the structure of the monomer is retained. Continuous wave functionalisation resulted in a significant reduction in the O(1s) band and reduction in the carbonyl C=O contribution to the C(1s) envelope, indicating that the monomer undergoes some fragmentation under these conditions (Figure 3.4 and Table 3.1)[36].

The superior structural retention using pulsed technology was also discernable in the FT-IR spectrum. Crucially, not only is the carbonyl retained, but the bands at 2815 and 2710 cm^{-1} indicate that the aldehyde function is retained. The total loss of these functions in the continuous wave functionalisation is accompanied by significant broadening of the remaining bands in the spectra, indicating again that fragmentation and crosslinking have occurred. The broadening of the carbonyl band itself is indicative of the generation of multiple, similarly structured, carbonyl environments.

This loss of structure in the continuous wave functionalisation is due to the relatively strong power input <P>=5W, which compared to that calculated by equation (1) as <P>=0.03W

$$< P >= \frac{P_P t_{on}}{t_{on} + t_{off}} \quad (1)$$

Where P_P is the peak power, t_{on} is the pulse on-time and t_{off} is the pulse off-time.

The relative efficiency of the pulsed technology is demonstrated by the deposition rate of 50 ± 2 nm min^{-1} W^{-1} compared to that of the continuous wave method of 7.2 ± 0.4 nm min^{-1} W^{-1}.

3.4.2. Immobilization of oligonucleotides to undec-1-enal functionalised surfaces

Reductive amination via imine intermediates is a well characterized synthetic route in classic organic chemistry (Figure 3.1). It is also widely used in the construction of biomolecule chips[37]. The use of a reducing agent is effectively traps the imine product, and the use of sodium cyanoborohydride is well known from classical chemistry[38]. The optimal conditions obtained for the immobilization of oligonucleotide probe AM1 on to plasmachemically deposited aldehyde function correspond to those of the Schiff-Base reaction (Figures 3.13-3.16), confirming that imine formation is the mechanism of immobilization. The temperature dependence is typical of that observed for the Schiff-base reaction[39]. The acid catalysis of imine formation is well known (Figure 3.1). The peak at relatively mild pH values (Figure 3.14) stems from the reaction kinetics of the protonated tetrahedral intermediate. Increasing proton concentration increases the formation of the intermediate in the first place, but an excess of protons will act to stabilise this intermediate, reducing the formation of the carbinolamine intermediate[40].

The optimal concentration of probe was observed to be at 1000 $nmoldm^{-3}$. The time dependence of the immobilisation is in agreement with literature observations and methodology where reaction protocols tend to be in the order of hours[41].

Covalent immobilizations are favoured over physisorption methods as the non-specific nature of DNA adsorption can cause poor hybridisation efficiency, and there is a tendency for the DNA to desorb under hybridisation conditions[42,43,44].

The observed hybridisation of surface immobilised AM2 to its complimentary oligonucleotide AM3 is also a strong confirmation that the immobilization proceeds primarily through the terminal amine and via amine functions in the DNA base-pairs. Immobilization via the base pairs would result in extremely poor hybridisation efficiency in the case of the 15-base oligonucleotides used in this study, as T_m for the AM2 – AM3 pair would drop below room

temperature if even one base was inaccessible. Crucially, the as-prepared plasmachemical layer also demonstrated minor non-specific adsorption of the control probe AM3, thus confirming that the terminal primary amine was necessary for efficient immobilization.

Low non-specific adsorption of probe AM3 was also essential for the excellent contrast observed in the final AM2-AM3 arrays (Figure 3.20). The inhomogeneity observed in the array spots ('coffee ring' effect) is a commonly observed feature of arrays caused by drying of the liquid droplet on the substrate surface, which causes preferential immobilization at the outer ring of the droplet[45]. A plasmachemical layer utilising a lower contact angle was demonstrated to reduce occurrence of this artefact as will be discussed in Chapter 4.

A comparison of fluorescence intensities between plasmachemically functionalised aldehyde surfaces and commercially available aldehyde functionalised slides showed that, after hybridisation, plasmachemical slides yielded 700 ± 70 arbitrary units, whilst commercially available slides yielded 70 ± 11 arbitrary units. This improvement is attributed to strong functional group retention and the ability of the plasmachemical layers to re-arrange to allow the oligonucleotides suitable orientation for hybridisation. This relative flexibility of plasmachemical layers is a further desirable feature in the design of the plasmachemical-based biochip. It has been shown that whilst the 13 carbon linkers such as those employed in this study can improve hybridisation four-fold, the introduction of a more flexible linker (>40 atoms) can increase efficiency 150-fold[46]. That an identical chemical approach can be applied to varying substrate compositions and geometries (e.g. beads, wires or well plates) is also advantageous.

3.5. Conclusion

Pulsed plasmachemical functionalisation can be used to prepare aldehyde functionalised surfaces utilizing an undecenal precursor. The pulsed plasmachemical functionalisation of undec-1en-al had been demonstrated, and the deposition duty cycle optimised to 15 µs t_{on}, 20 ms t_{off}, 40W PP.

These aldehyde functions have been optimised to immobilize and subsequently hybridise oligonucleotide DNA strands via the Schiff base reaction. The surfaces were also suitable for the generation of DNA microarrays, with limited non-specific adsorption and spatial resolution of immobilised DNA functions.

1 *Plasma Deposition Treatment, and Etching of Polymers,* d'Agostino, R. (ed.); Academic Press, Boston **1990**

2 Shard, A. G.; Munro, H. S.; Badyal, J. P. S. *Polym. Commun.* **1991**, *32*, 152.

3 Ehrlich, C. D.; Basford, J. A. *J. Vac. Sci. Technol., A* **1992**, *10*, 1.

4 Briggs, D.; Seah M. P (eds) *Practical Surface Analysis 2nd Edition*, John Wiley and Sons, Chichester, **1994**

5 Kibel, M. H. in *Surface Analysis Methods in Materials Science*, 2nd ed., O'Connor, D. J.; Sexton, B. A.; Smart, R. St. C (eds), Springer-Verlag Heidelberg, **2003**, p175

6 Sabbatini, L.; Zambonin, P. G. *Surface Characterization of Advanced Polymers* VCH Publishers, New York, **1993**

7 Christie, A. B. in *Method of Surface Analysis* Walls, J. M. (ed.), Cambridge University Press, Cambridge, **1989**

8 Smith, G. C. in *Handbook of Surface and Interface Analysis*, Riviere, J. C.; Myhra, S., Eds.; Marcel Dekker : New York, **1997**.

9 Briggs, D.; Seah, M. P. (eds) Auger, X-Ray Photoelectron Spectroscopy, John Wiley, **1990**.

10 Colthup, N. B.; Daly, L. H.; Wiberley, S. E. *Introduction to Infrared and Raman Spectroscopy 3 ed.* Academic Press, San Diego **1990**.

11 Carson, F. A. *Basic Optics and Optical Intruments* Dover Publications Inc., Mineola, **1997**

12 Behrning, S.; Bley, H.; Braun, P.; *Proceedings of the 10th International Colloquium on Surfaces* p.230-238, Chemnitz, Germany, **2000**

13 Domingue J. *American Laboratory* **1990**, *22*, 50

14 De Gennes, P. G. in *Les Houches 1988 Session XLVIII liquids at interfaces*, Charvolin, J.; Joanny, J. F., Zinn-Justin, J. (eds.), North-Holland, Amsterdam, **1990**

15 *Taking the Mystery out of Thin Film Measurements* Filmetrics Inc. San Diego, **2003**, available at http://www.filmetrics.com/refl.php November **2009**

16 Tilley, R. *Colour and the Optical Properties of Materials* Wiley, Chichester, **2000**

17 Gauthier-Manuel, B. *Meas. Sci. Technol.* **1998**, *9*, 485.

18 Beamson, G.; Briggs, D. *High Resolution XPS of Organic Polymers The Scienta ESCA300 Database*, Wiley, Chichester **1992**.

19 McMurry, J. *Organic Chemistry* 3rd ed. Brooks/Cole Publishing Company, **1992**

20 Beamson, G.; Briggs, D. *High Resolution XPS of Organic Polymers The Scienta ESCA300 Database*, Wiley, Chichester **1992**.

21 Colthup, N. B.; Daly, L. H.; Wiberley, S. E. *Introduction to Infrared and Raman Spectroscopy* 3rd ed. Academic Press, San Diego, **1990**.

22 Blout, E. R.; Fields, M. *J. Am. Chem. Soc.* **1950**, *72*, 479.

23 Tsuboi, M.; Kubo, Y.; Ikeda, T.; Overman, S. A.; Osman, O.; Thomas, G. J. *Biochemistry* **2003**, *42*, 940.

24 Griesser, H. J.; McClean, K. M.; Beumer, G. J.; Gong, X.; Kingshott, P.; Johnson, G.; Steele, J. G. *Mater. Res. Soc. Symp. Proc.* **1999**, *544*, 9.

25 Gong, X.; Dai, L.; Griesser, H. J.; Mau, A. W. H. *J. Polym. Sci., Part B: Polym. Phys.* **2000**, *38*, 2323.

26 Chen, Q.; Dai, L.; Gao, M.; Huang, S.; Mau, A. *J. Phys. Chem. B* **2001**, *105*, 618.

27 McLean, K. M.; Johnson, G.; Chatelier, R. C.; Beumer, G. J.; Steele, J. G.; Griesser, H. J. *Colloids Surf., B.* **2000**, *18*, 221.

28 Leich, M. A.; Mackie, N. M.; Williams, K. L.; Fisher, E. R. *Macromolecules* **1998**, *31*, 7618.

29 Zammatteo, N.; Jeanmart, L.; Hamels, S.; Courtois, S.; Louette, P.; Hevesi, L.; Remacle, J. *Anal. Biochem.* **2000**, *280*, 143.

30 Le Berre, V.; Trévisiol, E.; Dagkessamanskaia, A.; Sokol, S.; Caminade, A.; Majoral, J. P.; Meunier, B.; François, J. *Nucleic Acids Res.* **2003**, *31*, e88.

31 Guo, Z.; Guilfoyle, R. A.; Thiel, A. J.; Wang, R.; Smith, L. M. *Nucleic Acids Res.* **1994**, *22*, 5456.

32 Razong, A.; Bergman, R. G.; Sukenik, C. N. *Langmuir* **2008**, *24*, 2545

33 Bain, C. D.; Whitesides, G. M. *Science* **1988**, *240*, 62.

34 Zhao, Y.; Pang, D; Hu, S.; Wang, Z.; Cheng, J.; Dai, H. *Talanta* **1999**, *49*, 751.

35 Kelley, S. O.; Boon, E. M.; Barton, J. K.; Jackson, N. M.; Hill, M. G. *Nucleic Acids Res.* **1999**, *27*, 4830.

36 Yasuda, H.; Hsu, T. J. *Polym. Sci. Part A: Polym. Chem*. **1977**, *15*, 81.

37 Taylor, J. R.; Nie, S. *Conference Proceedings, Bioengineering Conference*, **2001**, Snowbird, Utah. http://asme.pinetec.com/bio2001/data/pdfs/a0222568.pdf

38 Andersson, P. G.; Munslow, I. J. (eds) *Modern Reduction Methods* **2008**, Wiley-VCH Verlag GmbH & Co., Weinheim.

39 Xing, W-L.; Chenge, J. *Frontiers in Biochip Technology* **2006**, Springer, New York

40 McMurry, J.; Begley, T. P. *The Organic Chemistry of Biological Pathways* **2005**, Roberts and Company Publishers, Greenwood Village, Colorado.

41 Zammatteo, N.; Jeanmart, L.; Hamels, S.; Courtois, S.; Louette, P.; Hevesi, L.; Remacle, J. *Anal. Biochem.* **2000**, *280*, 143.

42 Bünemann, H.; Westhoff, P.; Herrmann, R. G. *Nuc. Acids Res.* **1982**, *10*, 7163.

43 Bünemann, H. *Nuc. Acids Res.* **1982**, *10*, 7181.

44 Pividori, M. I.; Merkoçi, A.; Alegret, S. *Biosensors and Bioelectronics* **2000**, *15*, 291

45 Dolan, P. L.; Wu, Y.; Ista, L. K.; Metzenberg, R. L.; Nelson, M. A.; Lopez, G. P. *Nuc. Acids. Res.* **2001**, *29*, e107

46 Shchepinov, M. S.; Case-Green, S. C.; Southern, E. M. *Nuc. Acids*

*Res.***1997**, *25*, 1155

4. A Substrate Independent Route for DNA Microarray Manufacture using 3-vinylbenzaldehyde

In this section a substrate-independent methodology for covalent immobilization of single-strand oligonucleotides onto solid surfaces is presented (Scheme 4.1). This entails the immobilization of DNA molecules onto pulsed plasma deposited poly(3-vinylbenzaldehyde) surfaces via the Schiff-base reaction. The substrate independence of this methodology is demonstrated by the functionalisation of substrates including glass, silicon, SWCNT's, polystyrene microspheres. The methodology also allows the formation of microwells on the surface of a flat substrate.

The use of the surface aldehyde functions is also extended to similar biological systems. Protein-protein screening chips are demonstrated by the use of the IgG – protein G interaction as a model system[10]. Similarly the use of the plasmachemical layer as a substrate for sugar immobilization is demonstrated with the model system of amino dextran[1]. Whilst the strict function of DNA molecules is widely understood, and the main interest is in identifying the order of the base pairs, for the case of other biomolecules the critical interest is in the function of the molecules themselves. By surface immobilization of appropriate biomolecules and the study of their interactions it is possible to elucidate details about the mechanism of biological processes, such as enzymatic activity, immune system interactions.

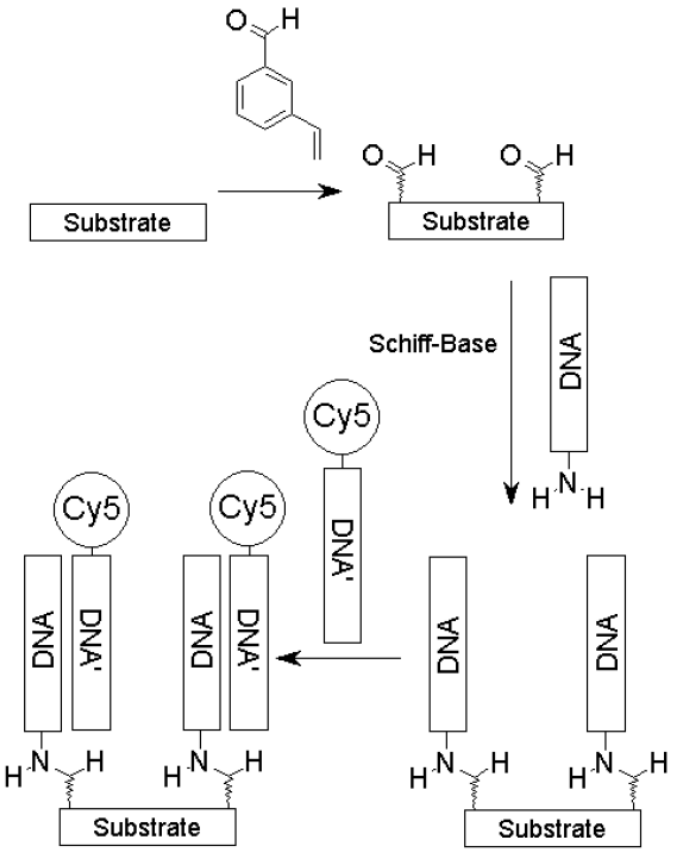

Scheme 4.1. DNA hybridization onto aldehyde functionalized surfaces

4.1 Precursor Choice and Immobilisation Chemistry

The success in functionalising surfaces with an undecenal precursor (Chapter 3) demonstrated the applicability of aldehyde precursors for pulsed plasmachemical functionalisation and subsequent use in DNA array manufacture. Another aldehyde containing precursor is 3-vinylbenzaldehyde which offers identical surface functionalisation and DNA immobilisation chemistry (Scheme 4.1).

The use of conjugated double bonded structures such as acrylic acids or styrenes potentially offer several benefits over the simple vinyl group present in undec-1-enal. Firstly, the delocalisation of radical species potentially gives a more stable active species, allowing greater radical generation for a given power input, and more efficient, faster deposition. Additionally it is speculated that the stability of the aromatic structure will offer some protection to the aldehydye carbonyl, to give superior structural retention. An ideal case would give an aldehyde functional group independent of the conjugated structure of the polymerisable bond, but no such precursor was identified.

The use of the relatively inflexible aromatic group in the precursor will be expected to reduce the flexibility of the resultant plasmachemical layer. Limiting the degree of cross-linking in the plasmachemical layer will therefore be critical in retaining flexibility and thus immobilisation and hybridisation efficiency of DNA reactions.

The ability of plasma functionalisation to functionalise three-dimensional substrates such as beads and carbon nanotubes is also demonstrated.

4.2 Experimental

Unless otherwise stated, reaction conditions and surface characterisation were as outlined in Chapter 2. Identical DNA oligonucleotides and associated chemistry were utilised to those in Chapter 3.

Plasma polymerization of 3-vinylbenzaldehyde (Aldrich, 97%, H2C=CH(C6H4)CHO, purified by several freeze-pump-thaw cycles) was carried out in an electrodeless cylindrical glass reactor as described in chapter 2. 3-vinylbenzaldehyde was introduced into the reactor at a pressure of 0.15 mbar and a flow rate of 7.5 x 10^{-8} mol s^{-1} for 5 min prior to reaction. Substrates included borosilicate glass cover slips, glass slides, polished silicon wafer, SWNT (singlewalled carbon nanotubes +92%, MicroTechNano), and polystyrene microspheres (Biosearch Technologies, Inc., macroporous, 50 µm).

Optimum aldehyde functionality incorporation corresponded to a pulsed plasma duty cycle of t_{on} = 50 µs, t_{off} = 4 ms, and a peak power of 40 W.

DNA immobilization, hybridization and microarray construction were carried out as outlined in Chapter 3. As well as 3-vinylbenzaldehyde functionalized surfaces, commercially available aldehyde functionalized slides were examined (ALS-25, batch 03154, CEL Associates Inc., Pearland, Texas).

4.2.1 Protein immobilization and interaction

The immobilization of protein G to a commercially available aldehyde-silane SAM surface and its subsequent interaction with antibody IgG has been described previously[10]. In this study, a solution of 100 µg ml^{-1} purified recomb protein G (Pierce) in 60% (v/v) SSC/40% (w/v) glycerol was arrayed onto the aldehyde pulsed plasma polymer surface and incubated at room temperature for 2 h. The surface was then inverted into a solution of pH7 SSC and 1% (w/v) BSA (bovine serum albumin, fraction V + 96%, Sigma) for 1 min, flipped face up and left for 1 h, followed by rinsing in fresh buffer.

The interaction of these arrayed surfaces with antibody IgG entailed immersion into a 0.5mgml^{-1} solution of Alexa Fluor 633 goat anti-mouse IgG (Molecular Probes) in combination with 0.1% (w/v) Tween-20 (Aldrich) in pH7 SSC for 1 h, and finally washing three times in pH7 SSC, 0.1% (w/v) Tween-20.

4.2.2 Immobilization of amino-dextran sugar

Amino-dextran (MW = 70,000 $gmol^{-1}$, Molecular Probes) has been successfully attached to SAM aldehyde functionalized surfaces in the past[2]. For the pulsed plasma polymer surface, the aldehyde functionalized substrate was immersed in a solution comprising 0.05g amino-dextran, 10ml of high purity water, and 0.15g $Na(CN)BH_3$ for 24 h. The dextran functionalized surfaces were then washed thoroughly in H_2O for 16 h.

4.2.3 Surface characterization

Surface characterisation by XPS, FT-IR, sessile-drop contact angle, reflectometry and fluorescence microscopy is as described in Chapter 2.

The hybridized DNA polymer microbeads were imaged using the Raman microscope system, which was fitted with a 10x lens and a 20 mW HeNe laser (632.817 nm wavelength), which corresponds to the excitation range of the Cy5 fluorophore. A polarization of 500:1 was employed, and the laser beam passed through a diffraction grating of 1800 lines mm^{-1}; a filter permitting 1% laser energy transmission was used unless otherwise stated.

4.2.4 Microwell formation

A robotic microarray spotter (Genepak) was used to manufacture microwells. A stainless steel pin was utilized and wells printed at a pitch of 350 µm. The pin head dwell time was restricted to 1 ms. The 384-well sample plate was loaded with a Cy5-fluorophore tagged oligonucleotide (Sigma-Genosys Ltd., oligonucleotide sequence: 5'-3' AACGATGCACGAGCA, desalted, reverse phase purified with 3' terminal primary amine and 5' terminal Cy5 fluorophore). Imine formation took place at 42 ℃ for 16 h in saline sodium citrate buffer at pH4.5 (citric acid 99%, Aldrich; NaCl 99.9%, Sigma). Subsequently 3.5 mg ml^{-1} $NaCN(BH_3)$ (Aldrich, 99%) was added and the solution gently stirred for 3 h. Excess physisorbed probe oligonucleotides were removed by sequential washing in high purity water; saline sodium citrate buffer (SSC, 0.3M Sodium Citrate, 3M NaCl, pH7, Sigma) with 1% sodium dodecyl sulphate (Sigma, 10% solution); high purity water; solution of 10% stock SSC buffer in high purity water with 0.1% (w/v) sodium dodecyl sulphate; and finally, high purity water; 5% stock SSC buffer in high purity water; high purity water.

Fluorescently labeled oligonucleotides attached to the surface were identified using a fluorescence microscope as described in Chapter 2

4.3 Results

4.3.1 Pulsed Plasma Polymerization of 3-Vinylbenzaldehyde

The deposition of 3-vinylbanzaldehyde was optimised for DNA immobilisation (see following sections). XPS elemental surface analysis of the optimum 3-vinylbenzaldehyde pulsed plasma polymer for DNA immobilisation (t_{on} = 50 µs, t_{off} = 4 ms, and P_p = 40 W) was measured to be 89 ± 2% carbon and 11 ± 2% oxygen. This was found to be in good agreement with the predicted theoretical composition of 90% carbon and 10% oxygen derived from the monomer structure. The accompanying deposition rate was measured to be 70 nm min^{-1}.

The 3-vinylbenzaldehyde precursor proved to be robust to the plasma deposition process. Even 5W continuous wave plasma deposited layers showed good structural retention by XPS, with 91 ± 2% carbon and 9 ± 2% oxygen. This is also apparent in the high resolution C1s envelopes where differences observed were minimal (Figure 4.1). Modelling the C1s envelopes also showed very little variation in the structure of the plasmachemical layers (Table 4.1).

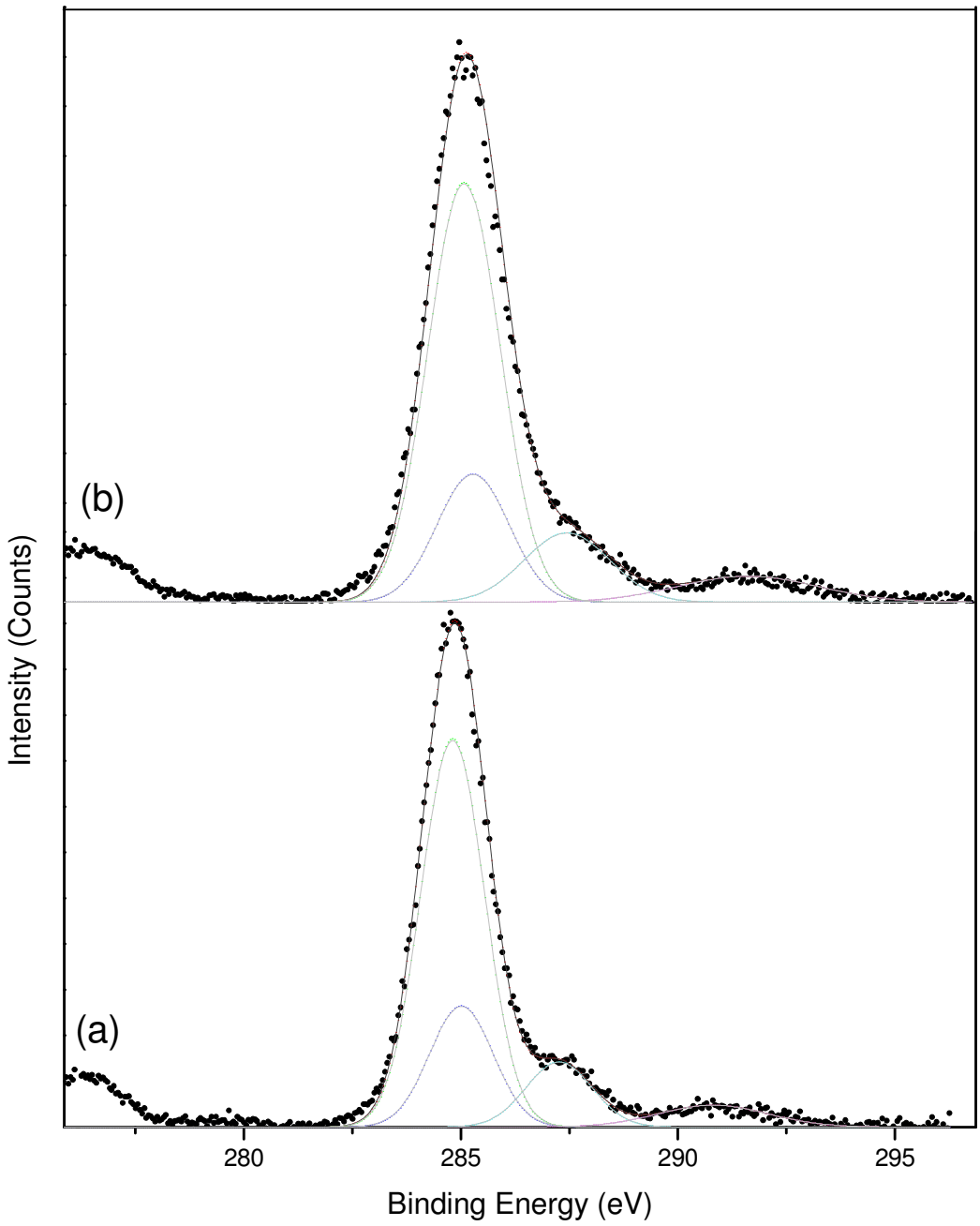

Figure 4.1. 3-Vinylbenzaldehyde Plasma Polymer Carbon XPS Envelopes. (a) 50μs-on, 4ms-off Pulsed Plasma Polymer. (b) 5W Continuous Wave Plasma Polymer.

Binding Energy (eV)	285	284.8	287.5
Assignment	CyHx	Aromatic C	Ar-C=O
Theoretical (%)	22	67	11
5W Continuous Wave (%)	22 ± 1	67 ± 1	10 ± 1

Table 4.1. Peak fitting of C1s envelopes.

A comparison of the infrared spectra obtained for the optimum pulsed plasma deposited films with the 3-vinylbenzylaldehyde precursor shows that the characteristic aldehyde CHO stretches (2815 cm^{-1} and 2723 cm^{-1}) and the aldehyde C=O stretch (1695 cm^{-1}) are retained relative to the C-H stretch region (2836-3030 cm^{-1}), Figures 4.2, 4.3 and Table 4.2. Further confirmation of good structural retention is evident from the resolved meta-substituted phenyl ring bands which include semicircle stretches (1446 cm^{-1} and 1478 cm^{-1}) and quadrant stretches (1581 cm^{-1} and 1595 cm^{-1}). The alkene C=C stretch at 1650 cm^{-1} is absent in both plasma deposited films. Note that the resolution of the spectra of the precursor is superior as both plasmachemical layers are comparatively thin at 100 nm, compared to a bulk droplet of the precursor. There is also considerable loss of resolution in the fingerprint region (less than 1600 cm^{-1}), which is particularly pronounced in the case of the continuous wave plasma polymer layer. A strong degradation here is attributed to the increased fragmentation and cross-linking occurring in the plasma, and is expected to be more pronounced in the case of continuous wave plasma polymers, with their relatively high power input.

More variation is visible in FTIR than XPS, although effects are still subtle. With varied t_{on}, it can be seen that the intensity of the aldehyde CHO stretches at 2815 cm^{-1} and 2723 cm^{-1} is highest at t_{on} between 50 µs and 100 µs. This indicates that whilst carbonyl function and the aromatic structure are largely retained irrespective of duty cycle, the aldehyde function itself is vulnerable. This is presumably due to loss of the aldehyde hydrogen which would not be observable with XPS.

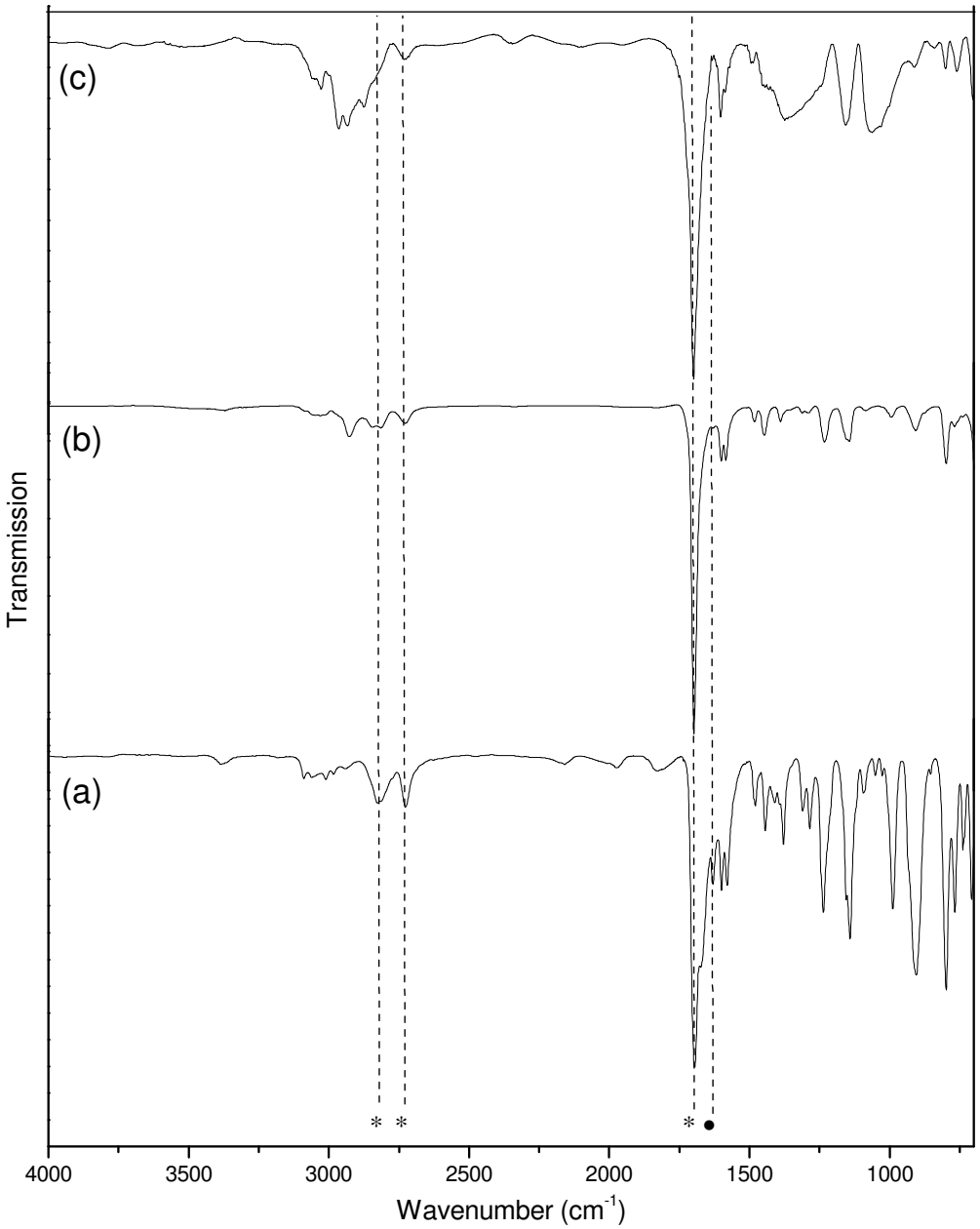

Figure 4.2. FT-IR spectra of: (a) 3-vinylbenzaldehyde monomer; (b) 3-vinylbenzaldehyde 50 µs-$_{on}$, 4 ms-$_{off}$ pulsed plasma polymer; and (c) 5W continuous wave 3-vinylbenzaldehyde plasma polymer. * denotes aldehyde absorbances; and ● denotes polymerizable alkene C=C band.
1650 cm^{-1} seen for the 3-vinylbenzaldehyde monomer is absent due to polymerization.

Wavenumber (cm^{-1})	Assignment
2836-3030	C-H stretches
2815	CHO stretch *
2723	CHO stretch *
1695	C=O stretch *
1650	C=C stretch ●
1595	Di-substituted benzene quadrant stretch
1581	Di-substituted benzene quadrant stretch
1478	Meta-substituted benzene semicircle stretch
1446	Meta-substituted benzene semicircle stretch
1410	$C=CH_2$ scissors deformation
1386	Aldehyde CH rock
1309	C=CH rock
1145	Meta ring stretch
992	Meta in-phase CH wag
908	Meta single CH wag

Table 4.2. Assignment of 3-vinylbenzaldehyde infrared absorbances[34]. (* Denotes aldehyde absorbances, and ● denotes polymerizable alkene C=C band in Figure 4.2).

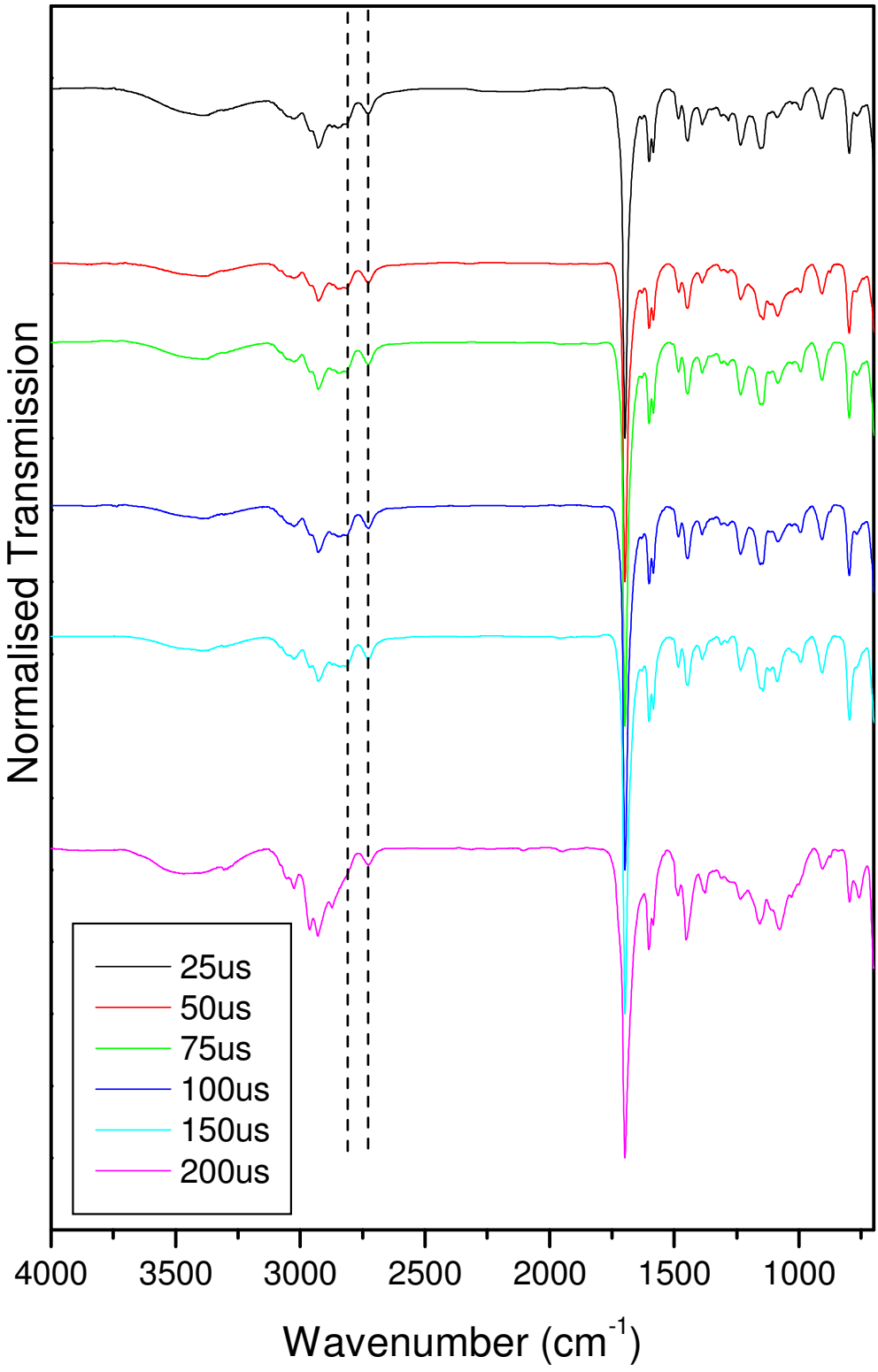

Figure 4.3 FTIR of plasmachemical films with varied pulse t_{on}. The aldehyde CHO stretch is again highlighted.

4.3.2 DNA immobilization

Pulsed plasma deposition conditions corresponding to a duty cycle of t_{on} = 50 µs, t_{off} = 4 ms, and P_p = 40 W were shown by fluorescence intensity measurements to be optimum for both oligonucleotide immobilization and subsequent hybridization, Figure 4.4. The viability of these aldehyde group functionalized films for microarrays was tested by microspotting DNA. Examination of these spots by fluorescence microscopy shows good homogeneity and sharp contrast between the plasma polymer background and the spots of hybridized DNA, Figure 4.5.

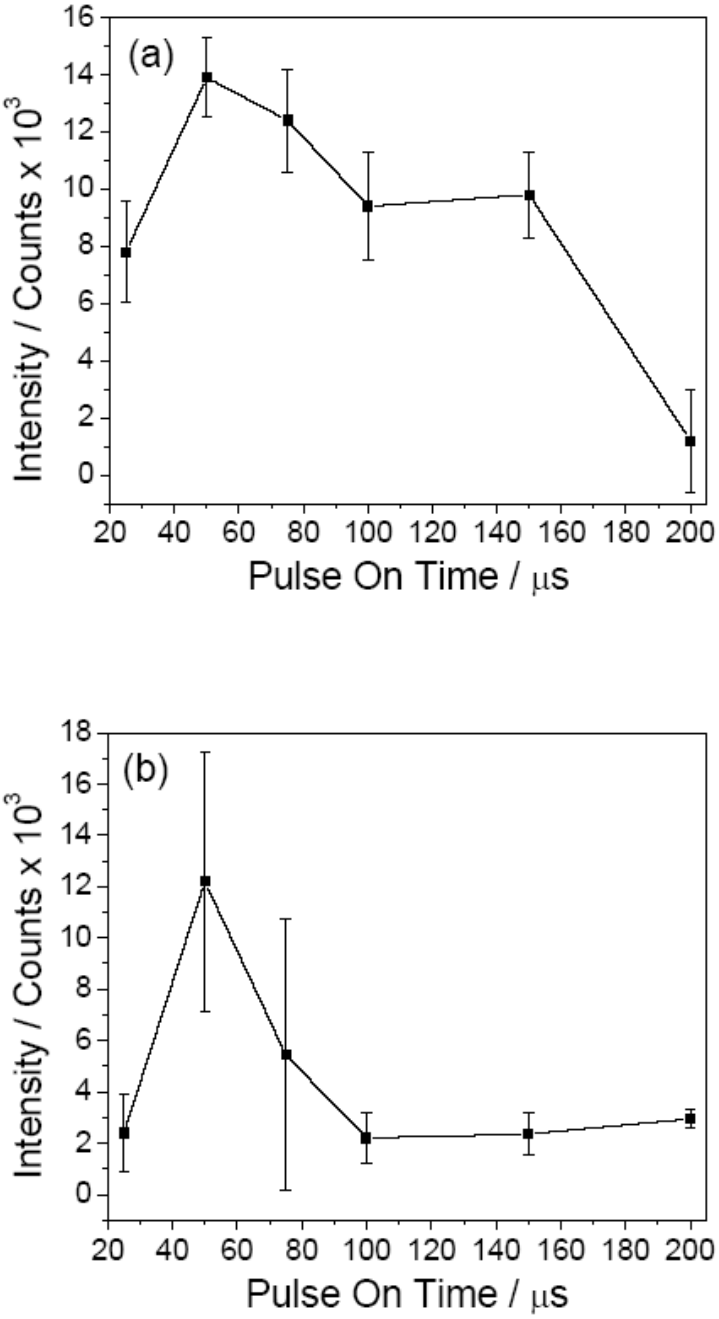

Figure 4.4. Fluorescence intensity variation with pulse on-time (*ton*) for: (a) immobilization of Cy5 tagged DNA onto 3-vinylbenzaldehyde plasma polymer surfaces (1% excitation laser intensity); and (b) hybridization of Cy5 tagged DNA to surface immobilized DNA (10% excitation laser intensity). *Pp* = 40 W and *toff* = 4 ms.

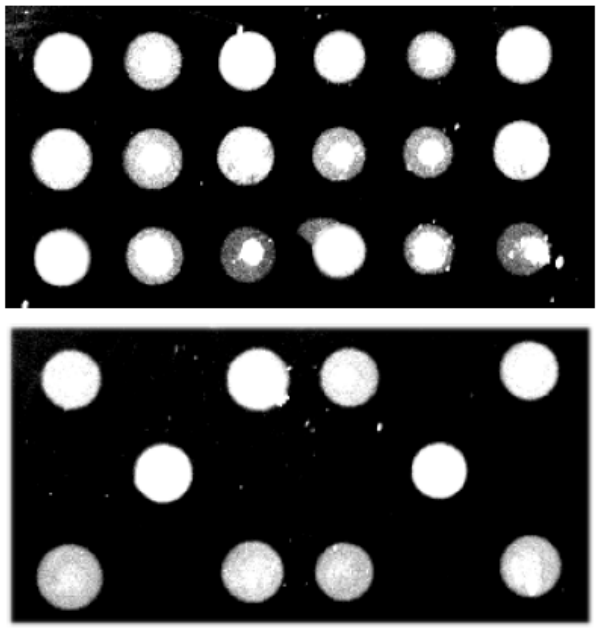

Figure 4.5. (a) Cy5 Tagged DNA, AMIPROBEIII, hybridized to spots of UAPROBEII DNA on 3-vinylbenzaldehyde pulsed plasma polymer surfaces (50 µs *ton*, 4 ms *toff*, 40 W Pp); and (b) alternate spots of non-complementary immobilized ssDNA show no hybridization.

Comparison of fluorescence intensities between plasmachemically functionalised aldehyde surfaces and commercially available slides aldehyde functionalised slides showed that, after hybridisation, plasmachemical slides yielded 500 ± 140 counts, whilst commercially available slides yielded 70 ± 11 counts. This difference is attributed to two factors. Firstly, the plasmachemical functionalisation in this case has been tailored towards reducing the cross-linking of the polymer units and thus also minimise cross-linking to generate a flexible film – both in the repeat units and the polymer backbone itself. Commercial slides utilise a glass-SAM system, which tends to restrict flexibility to that offered by individual molecules only. Secondly, a SAM is by definition a monolayer. Plasmachemical layers used in this work have a thickness in the order of 100 nm. This offers a potential reservoir of reactive groups lying just below the surface. Assuming that flexibility and reaction conditions allow reactants to reach these, then the use of plasmachemical layers potentially gives a thin three-dimensional sponge.

Functionalisation of single walled carbon nanotubes was monitored by Raman spectroscopy. Surface immobilized ssDNA and the 3-vinylbenzaldehyde pulsed plasma polymer were found to be invisible, and only the single walled carbon nanotube powder was Raman active (1322cm-1 and 1563cm-1 corresponding to single walled carbon nanotube D-band and G-bands[5]), Figure 4.6. On hybridization with complementary ssDNA strands, a sharp increase in counts is observed due to the fluorescent Cy5 tag, which drowns the single walled carbon nanotube bands, Figure 4.6. Exposure of single walled carbon nanotubes or aldehyde functionalized single walled carbon

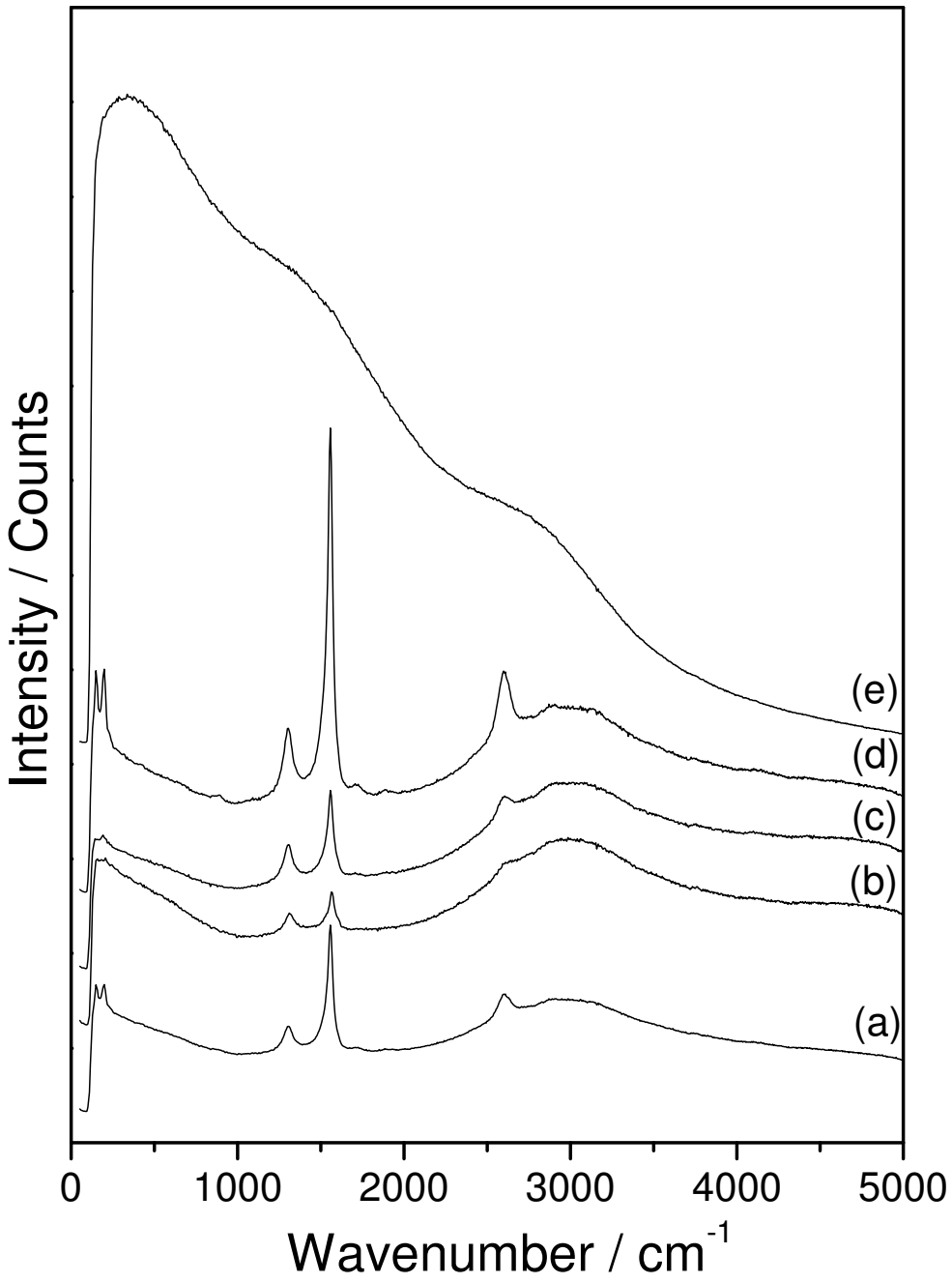

Figure 4.6. Raman spectra of 3-vinylbenzaldehyde pulsed plasma polymer modified carbon nanotubes (20 mW HeNe laser, 632.817 nm wavelength, 1% power): (a) untreated CNT on a glass slide; (b) as deposited; (c) control-exposed to 1 µm Cy5-tagged ssDNA; (d) following immobilization of untagged ssDNA; and (e) after immobilization of ssDNA and hybridization with Cy5-tagged ssDNA.

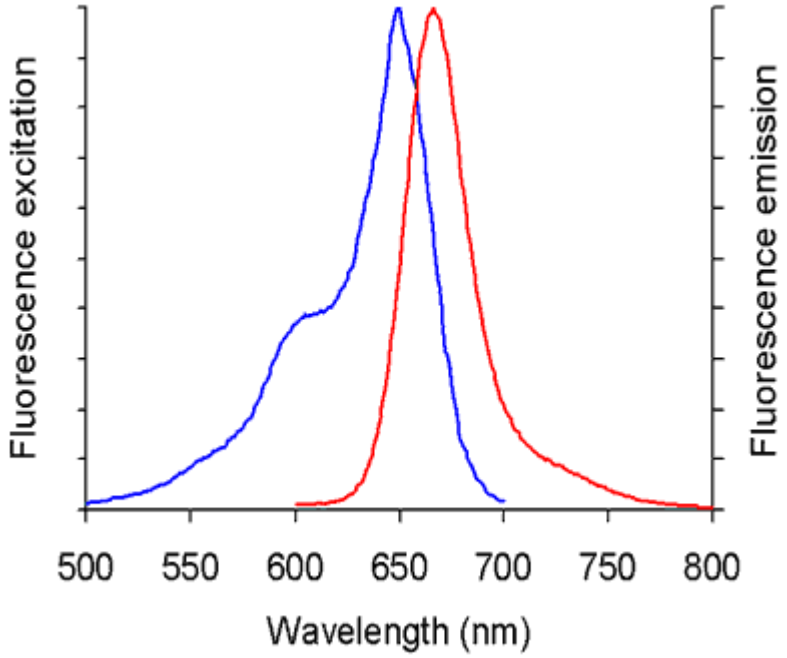

Figure 4.7 Absorption and Emission spectra of Cy5 dye in pH 7.2 buffer.[6]

nanotubes to the complementary fluorescently tagged ssDNA, without prior surface immobilization of probe ssDNA, resulted in no observed increase in counts, indicating that the increase is due solely to DNA hybridization rather than physisorption onto the single walled carbon nanotube or aldehyde functionalized single walled carbon nanotube surfaces.

Pulsed plasmachemical functionalized polymer microspheres were also found to be suitable for ssDNA immobilization and subsequent hybridization, Figure 4.8. The mircrotomed (cross sectioned) porous beads clearly show both immobilisation and hybridisation of Cy5 tagged DNA molecules onto the surface. There also appears to be a more intense signal in the outer layers of the beads, to approximately 10 µm. Other substrate materials functionalized using this approach included copper wire and non-woven polypropylene. The Cy5 fluorescent group has an adsorption maximum at 643 nm, with its emission peak at 667 nm (Figure 4.7).

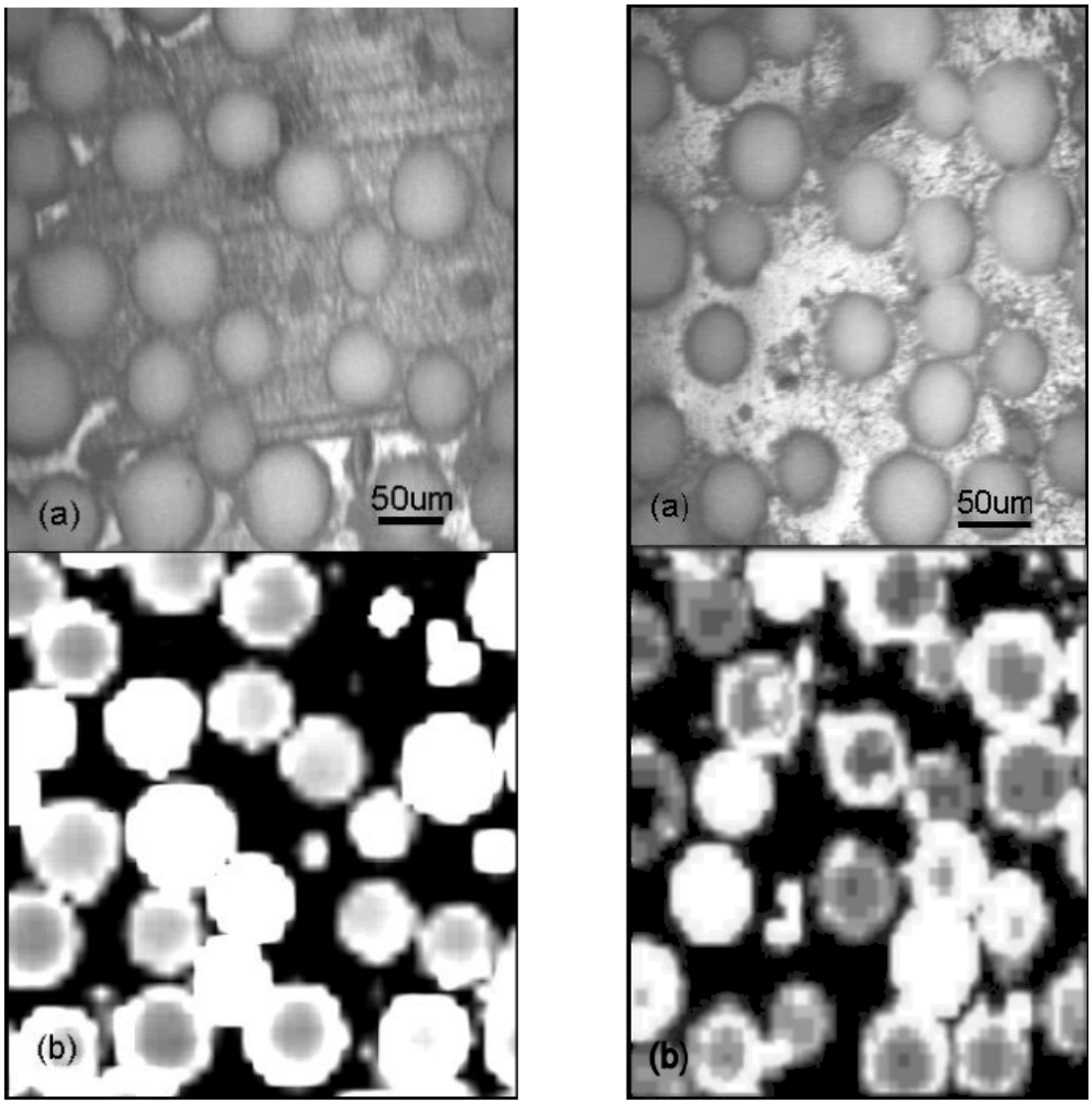

Figure 4.8. Cy5-tagged ssDNA immobilization (LHS) and hybridisation to complementary ssDNA (RHS) for 3-vinylbenzaldehyde pulsed plasma polymer functionalized polystyrene beads: (a) visible; and (b) fluorescence microscopy.

4.3.3 Protein-protein interactions

Interaction of antibody IgG with the robotically spotted protein G surface produced clear fluorescent spots with a sharp contrast between the background and surface immobilized IgG regions, Figure 4.9.

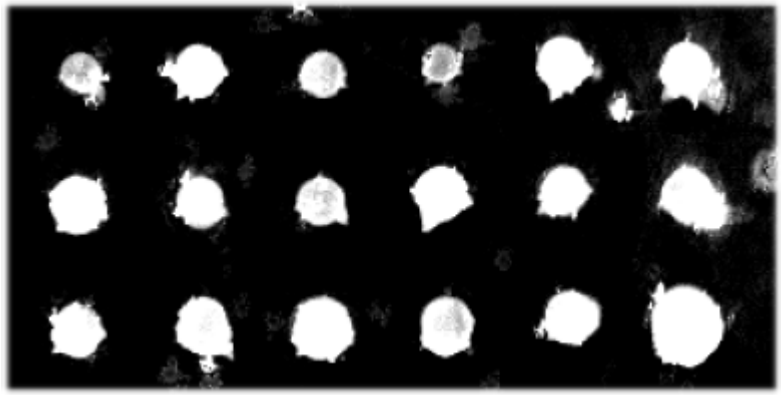

Figure 4.9. Fluorescently tagged IgG binds preferentially with robotically spotted Protein G immobilized on pulsed plasma polymerized 3-vinylbenzaldehyde surfaces.

4.3.4 Dextran immobilization

The presence of nitrogen on the dextran treated plasma polymer surface was taken to indicate the immobilization of aminodextran. The surface elemental composition was determined to be 71 ± 4 : 25 ± 4 : 4 ± 1 for C : O : N. A sharp drop in the sessile drop water contact angle was observed from 76 ± 2° for the plasma polymer to 53 ± 6° for the dextran functionalized surface.

4.3.5 Microwell Formation

Microwell formation takes place when the microarray pin comes into direct contact with a suitable substrate, leaving a physical three dimensional structure. It is a different process to classic microarray printing such as that observed in Chapter x, in which the objective is simple deposition of a liquid droplet, leaving substrate topography unchanged.

Microwell manufacture takes place in two steps. Firstly, a suitable polymer film is deposited onto the substrate by plasma polymerisation. In this case a hard borosilicate glass microscope slide was the substrate, with a relatively thick 3-vinylbenzaldehyde plasmachemical layer. The thickness of this coating was measured by reflectometry as 205 nm. Secondly, wells are printed into the polymer surface using a robot (Figure 4.10). As the robot uses a split pin to

deliver the liquid droplets, the produced microwells show a distinctive pairing of two adjacent wells. It is not expected that a split pin is required to form the microwells; it is simply the smallest pin head that was available at the time of manufacture. Examination of derivatized microwells by fluorescence microscopy showed a regular array of microwells, with each point containing the expected two wells formed by the split pin (Figure 4.11).

Examination of the surface by AFM shows the dual microwell structure clearly (Figure 4.12). Section analysis of the height image showed that the wells are 178 nm deep and surrounded by a rim of 0.3-3.0 μm height (Figures 4.13 and 4.14). This well depth also corresponds closely to the plasmachemical layer thickness.

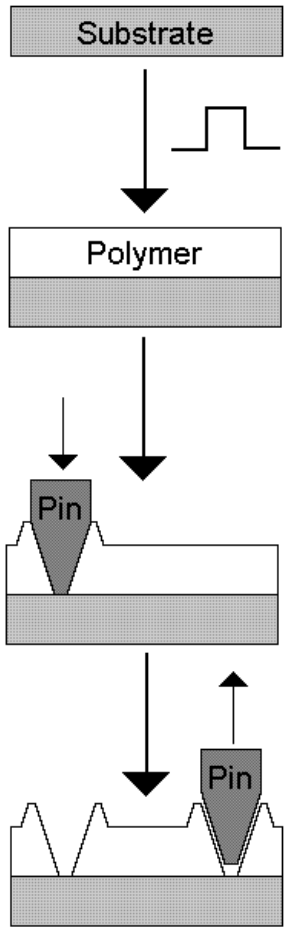

Figure 4.10. Manufacturing microwell arrays. The substrate is first treated with a plasma polymer, a robot is then used to drop a steel pin onto the surface. Repeated punching with the pin results in array formation

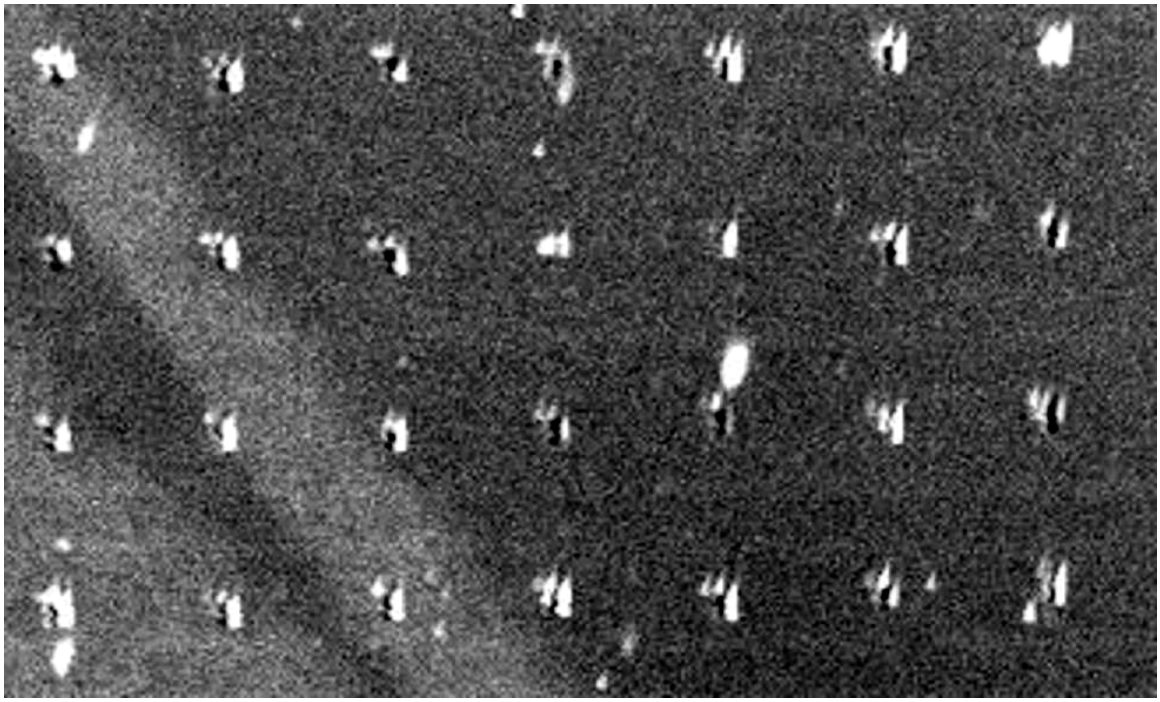

Figure 4.11. Fluorescent microscopy map of derivatized microwell array on a 3-vinylbenzaldehyde surface. The print pitch of the array is 350 μm. The dual punctures at each point correspond to the split in the pin used during manufacture.

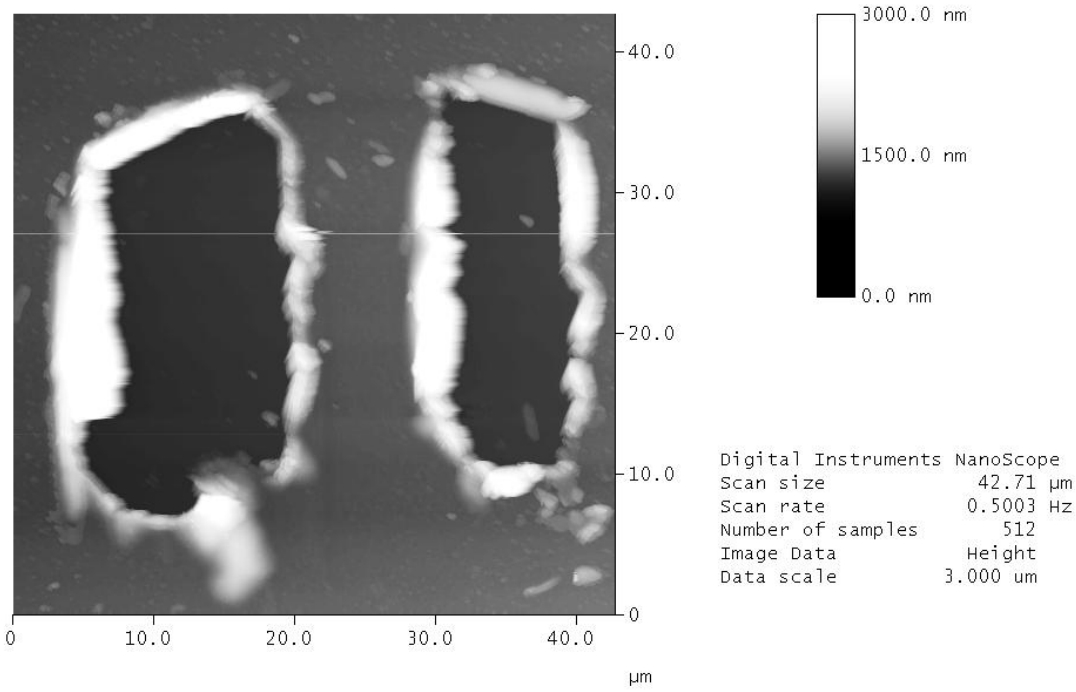

Figure 4.12. AFM height study of a microwell pair formed by the split-pin.

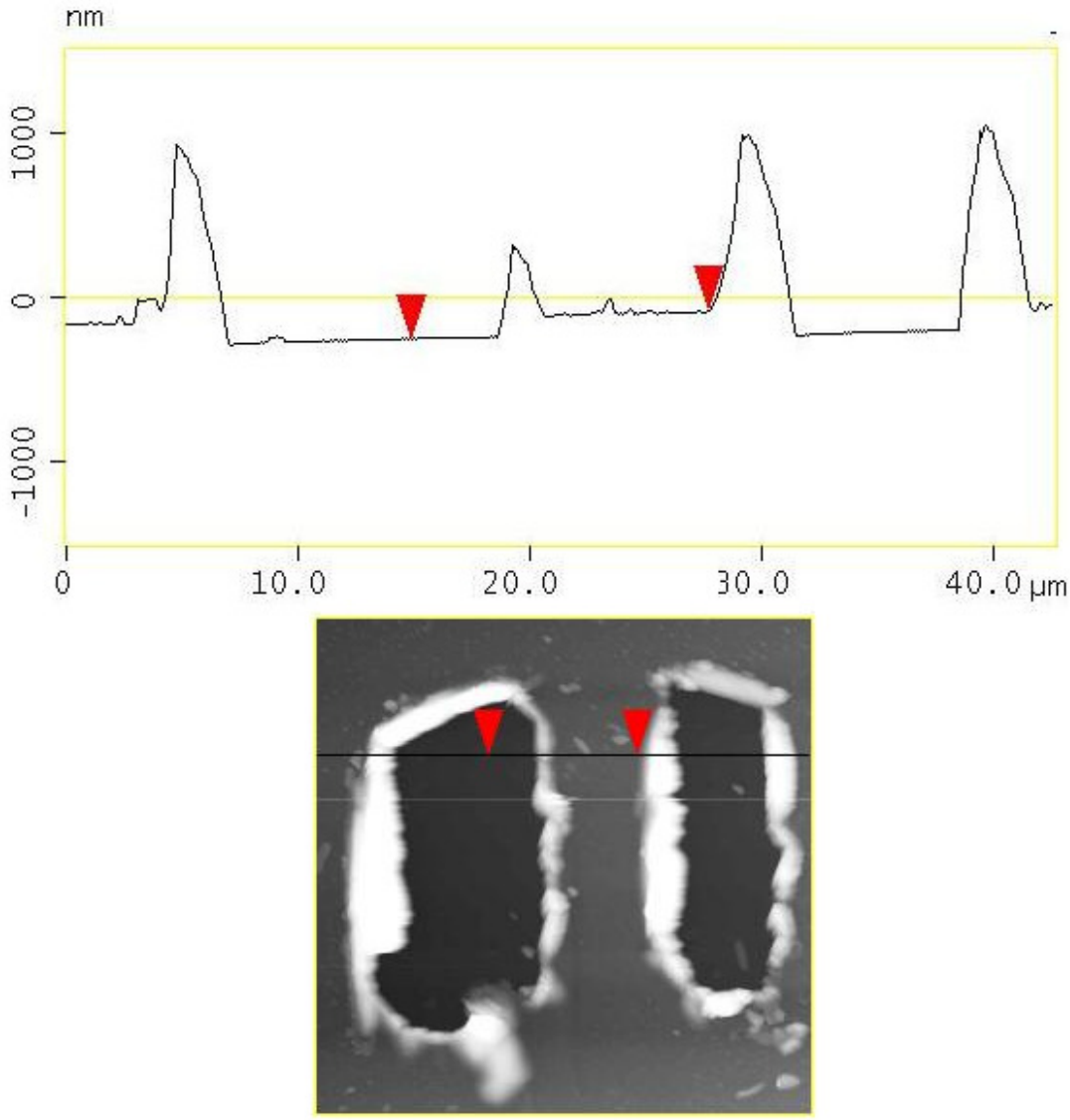

Figure 4.13. AFM section analysis of a microwell pair formed on 3-vinylbenzaldehyde plasma polymers. The height difference between the two arrows is 178 nm.

4.4. Discussion

Introduction of aldehyde functions to surfaces was again demonstrated, albeit via the styrene-like precursor 3-vinylbenzaldehyde. The precursor itself appears more robust than the previously utilised undecen-1-enal, with the optimum duty cycle utilising a longer pulse on time of 50 µs. Even using a 5W continuous wave plasmachemical layer very little variability in chemical composition is observed by XPS. Examination by FTIR also showed a strong preservation of the aldehyde functions in the precursor at the 50-100 µs, with very little change in the C-H fingerprint region (below about 1600 cm^{-1}). Given the subtle differences observed, it was decided to pick the optimum

deposition conditions based on the immobilisation and hybridisation of oligonucleotides onto the surface (Figure 4.4). The pulse t_{on} of 50 µs shows a marginal peak in immobilization intensity, although the errors (one standard deviation of the data) are large enough to suggest that 75 µs would also be applicable for DNA immobilization.

A similar trend is also observed for the hybridisation of complimentary DNA onto surface immobilized DNA strands. Again the relatively wide errors observed do not preclude the use of 75 µs as t_{on}. In many respects Figure 5.xb represents the critical measure of the substrate performance for use in DNA chips, as the ability of the immobilized DNA to hybridize with the unknown probe is the critical function of a DNA chip. This maxima observed in both the case of immobilisation and hybridisation of DNA was sufficient to justify this duty cycle as the optimum for DNA immobilization and hybridisation.

Previous attempts to form plasmachemical layers with aldehyde functions have had only limited success as discussed previously. The closest analogous precursor benzaldehyde[7], suffered particularly in that the optimum route for aldehyde retention requires disruption of the benzene ring to initiate cross-linking and polymerisation. Thus deposition conditions cause extensive fragmentation of the molecule structure and loss of aldehyde function. It is believed that the loss of aldehyde groups observed in the current work at longer pulse t_{on} were due to mild fragmentation of the CHO group, presumably with the loss of the aldehyde hydrogen. An interesting future experiment would be to produce thick enough plasmachemical layers to allow recovery for NMR experiments. ^{1}H NMR would provide a potential tool to predict the potential efficiency of the plasmachemical layer for DNA immobilisation, by identifying the number of aldehyde functions.

The use of 3-vinylbenxaldehyde for functionalisation of porous beads was also examined (Figure 4.8). Again strong signals are clearly observed for both immobilization and hybridization. Interestingly the intensity is noticeably higher in the outer layers to approximately 10 µm depth into the beads. This difference could be due to two reasons, both due to penetration into the

bead bulk structure. Firstly, the depth of plasmachemical functionalisation with the precursor may be limited by the rate of diffusion into the beads whilst the precursor is simultaneously reacting. Secondly, the ability of large molecules such as oligonucleotides to diffuse deep into the beads themselves may be limiting. If the first case is limiting then using milder duty cycles would be expected to result in deeper penetration of the aldehyde function.

Reductive amination via imines is a widely-used route to yield amines from aldehydes and ketones[8]. As well as its wide use in classic synthetic chemistry, Schiff-base chemistry has been utilized extensively in the immobilization of biomolecules such as DNA[9] or proteins[10] to aldehyde functionalized surfaces. One interest in the current Chapter was whether the very specific chemistry generated for the use of immobilising single-stranded DNA onto plasmachemical DNA chips could be extended to other commonly used biological systems. Hence the use for protein-protein interactions in which the IgG and protein G interaction acted as a model reaction. Figure 5.6 shows clearly that the Cy5 tagged IgG react preferably with the surface immobilised protein G. Again, this reaction is spatially resolved. This demonstrates that the plasmachemical substrate is applicable to other chip types and that the optimal substrate is applicable for use in other non-DNA based systems.

Dextran surfaces have been widely reported as being protein-repellent, and thus are of major interest in anti-fouling coatings – where prevention of non-specific adsorption of proteins from biological media is a key step in preventing colonization by cells[11121314]. These include SPR chips and low-protein binding substrates for column chromatography[15].

Interaction of even 3% of bases contained in a DNA strand with the surface has been previously shown to make DNA inaccessible to hybridization[1617]. The hybridization of surface immobilized ssDNA verifies that the Schiff-base reaction proceeds predominantly through the terminal amine of the oligonucleotide strand. Figure 4.5b shows that the spotted DNA chip is capable of differentiating between different DNA strands immobilised on the

surface. The deposition technology thus gives a functional DNA chip, with relatively simple manufacturing methodology, that is widely applicable to a range of substrates.

Carbon nanotubes are of particular interest due to their unique physical and chemical properties, including exceptional mechanical properties[18], and electrical[19] and thermal conductivity[20]. The introduction of ssDNA onto SWCNTs has already been shown to enhance CNT dispersion in aqueous media for nanodevice fabrication[21], and opens the door to precise patterning of CNT layers. Indeed, the use of DNA as a template for molecular electronic devices[22] DNA functionalized beads have potential use in the field of combinatorial chemistry[23]. Unfortunately, CNTs are difficult to functionalise, and this route allows simple introduction of aldehyde functions. Given the nature of plasmachemical functionalisation this also allows any plasmachemical function to be introduced onto the CNTs with analogous methodology, without any complex chemistry. Further, the use of such a plasmachemical layer is applicable to either powders or bulk materials containing CNTs, such as electrodes.

The flexibility of plasmachemical functionalized layers is an advantageous factor. Biologists have recognised the need for flexible linker layers to improve hybridization efficiency, showing that even linkers of <28Å can increase hybridization four fold[24], whilst linkers >40Å offer a 150-fold increase in hybridization efficiency[25]. This superior flexibility leads to improved hybridisation efficiency observed in comparison with commercial silane-based slides. The efficiency of the current methodology is demonstrated by the formation of arrays that are capable of immobilising DNA, and critically, hybridising tagged DNA. Interestingly, the flexibility of the plasmachemical layer can also be exploited to yield three dimensional structures on the substrate surface.

Suitably thick aldehyde films from a 3-vinylbenzaldehyde precursor can also be punched to form 3-dimensional structures on the substrate surface. In this case an arraying pin is utilized to punch a 350 µm pitched array of wells into a glass substrate. The as-produced wells are 10 x 25 µm, with a depth of 178 nm, and

are functionalized with the oligonucleotides present on the pin. The formation of such three dimensional structures with such a simple methodology would be expected to be applicable to other similar plasmachemical layers. Indeed, it can be speculated that multiple plasmachemical layers could be deposited onto one substrate, with subsequent microwell formation allowing multiple chemistries to be presented at once, with controlled spatial resolution. For instance it might be desirable to utilize a surface hydrophobic layer[26] over the 3-vinylbenzaldehyde in order to prevent spot spreading during hybridization, and to reduce the non-specific adsorption of molecules onto the bulk DNA chip surface. Critically, plasmachemical fictionalization allows excellent control of layer chemistry and thickness, whilst the combination with robotic spotting allows this to be combined with precise spatial resolution.

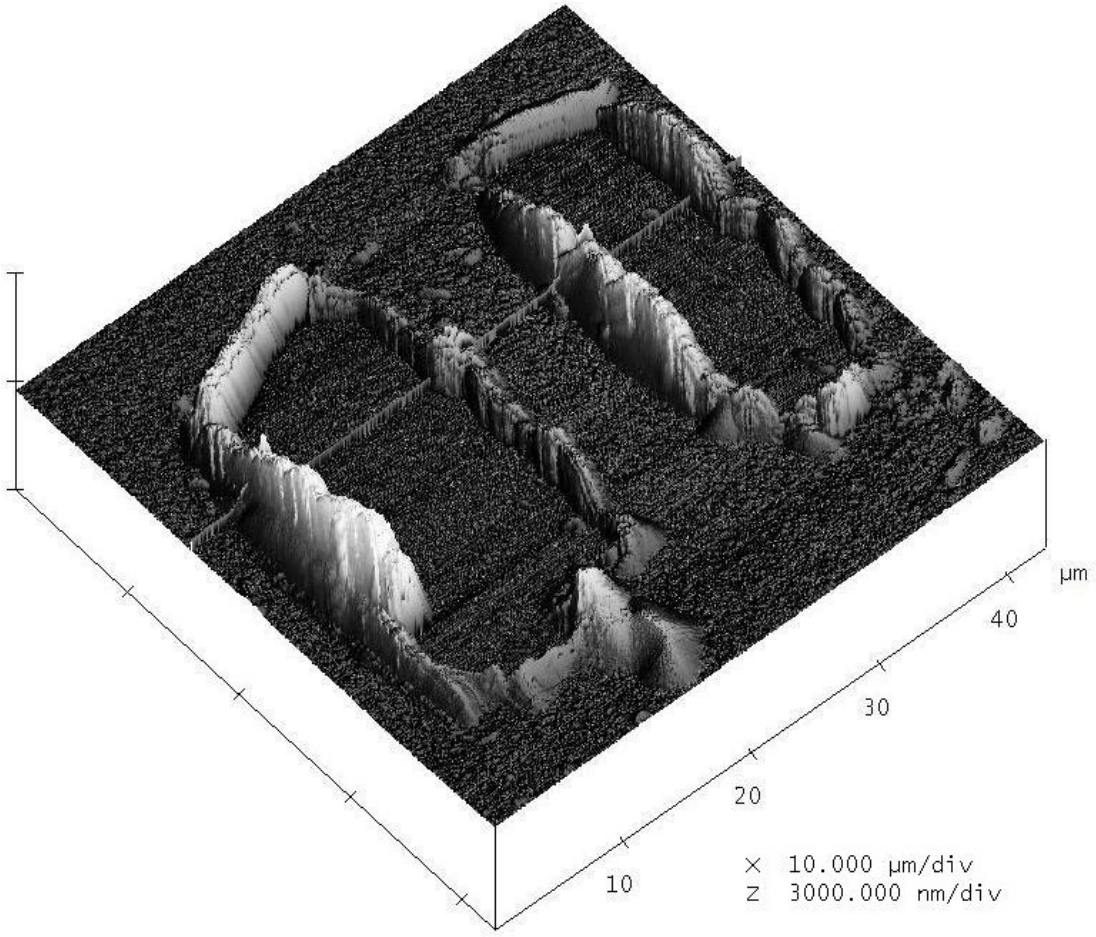

Figure 4.14. 3D AFM image of a microwell which emphasizes the height of the continuous rim formed around the well.

4.5. Conclusions

Aldehyde functionalized surfaces can be prepared by pulsed plasmachemical deposition using 3-vinylbenzaldehyde precursor. The duty cycle was optimised to produce surfaces suitable for both DNA immobilization and hybridisation. Subsequent Schiff-base chemistry leads to the efficient surface immobilization of oligonucleotides, proteins, and sugars onto a range of substrates which includes glass, silicon, polymer microspheres, and carbon nanotubes. The formation and functionalisation of microwells on the plasma polymer surface is also demonstrated.

1 Chen, Q.; Dai, L.; Gao, M.; Huang, S.; Mau, A. *J. Phys. Chem. B* **2001**, *105*, 618.

2 Chen, Q.; Dai, L.; Gao, M.; Huang, S.; Mau, A. *J. Phys. Chem. B* **2001**, *105*, 618.

3 Colthup, N. B.; Daly, L. H.; Wiberley, S. E., Introduction to Infrared and Raman Spectroscopy, 3rd ed., Academic Press, London **1990**.

4 Lin-Vein, D.; Colthup, N. B.; Fateley, W. G.; Grasselli, J. G., The Handbook of Characteristic Frequencies of Organic Molecules, Academic Press, London **1991**.

5 Dresselhaus, M. S.; Dresselhaus, G.; Jorio, A.; Souza Filho, A. G.; Saito, R. *Carbon* **2002**, *40*, 2043.

6 Product Technical Resources, www.invitrogen.com 24.02.2010

7 Leich, M. A.; Mackie, N. M.; Williams, K. L.; Fisher, E. R. *Macromolecules* **1998**, *31*, 7618.

8 For recent reviews see eg.: Baxter, E. W.; Reitz, A. B. *Organic Reactions* **2002** *59*, 1; Salvatore, R. N.; Yoon, C. H.; Jung, K. W. *Tetrahedron* **2001**, *57*, 7785.

9 Chapter 3

10 MacBeath, G.; Schreiber, S. L. *Science (Washington, DC, U.S.)* **2000**, *289*, 1760.

11 Massia, S. P.; Stark, J.; Letbetter, D. S. *Biomaterials* **2000,** *21*, 2253.

12 Österberg, E.; Bergström, K.; Holmberg, K.; Riggs, J. A.; Van Alstine, J. M.; Schuman, T. P.; Burns, N. L.; Harris, J. M. *Colloids Surf. A* **1993**, *77* ,159.

13 Marchant, R. E.; Yuan, S.; Szakalas-Gratzl, G. *J. Biomater. Sci. Polym. Ed.* **1994**, *6*, 549.

14 Österberg, E; Bergström, K.; Holmberg, K.; Schumann, T. P.; Riggs, J. A.; Burns, N. L.; Van Alstine, J. M.; Harris, J. M. *J. Biomed. Mater. Res.* **1995**, *29*, 741.

15 Sosa, J. M. *Anal. Chem.* **1980**, *52*, 910.

8 Bünemann, H.; Westhoff, P.; Herrman, R. G. *Nucleic Acids Res.* **1982**,*10*, 7163.

17 Bünemann, H. *Nucleic Acids Res.* **1982**, *10*, 7181.

18 Salvetat, J.-P.; Bonard, J.-M.; Thomson, N. H.; Kulik, A. J.; Forró, L.; Benoit. W.; Zuppiroli, L. Appl. Phys. A: Mater. Sci. Process. **1999**, 69, 255.

19 Dai, H.; Wong, E. W.; Lieber, C. M. *Science (Washington, DC, U.S.)* **1996**, *272*, 523.

20 J. Hone, M. Whitney, C. Piskoti, and A. Zettl, *Phys. Rev. B: Condens. Matter Mater. Phys*. **1999,** 40, R2514.

21 Talin, A. A.; Dentinger, P. M.; Jones, F. E.; Pathak, S.; Hunter, L.; Léonard, F.; Morales, A. M. *J. Vac. Sci. Technol. B* **2004**, *22*, 3107.

22 Keren, K.; Berman, R. S.; Buchstab, E.; Sivan, U; Braun, E. *Science* **2003**, *302*, 1380

23 Feldhaus, M. J.; Lualhati, M.; Cardon, K.; Roth, B.; Kamb, A. *Nucleic Acids Res.* **2000**, *28*, 534.

24 Zhang, Y.; Coyne, M. Y.; Will, S. G.; Levenson, C. H.; Kawasaki, E. S. *Nuc. Acids Res.* **1991**, *19*, 3929.

25 Shchepinov, M. S.; Case-Green, S. C.; Southern, E. M. *Nuc. Acids Res.* **1997**, *25*, 1155.
26 Coulson, S. R.; Woodward, I. S.; Brewer, S. A.; Willis, C.; Badyal, J. P. S. *Chem. Mater.* **2000**, *12*, 2031

5. A Substrate independent route for DNA surface hybridisation using 2-bromoethylacrylate

5.1 Precursor choice and immobilization chemistry

The use of surface immobilised bromine groups for DNA microarray construction is relatively rare, with few previous reports of such systems in use[14,1,2]. Bromine is a widely used leaving group in organic chemistry, so the introduction of bromine onto a surface should allow a nucleophile, such as the commonly available thiol-modification on oligonucleotides to covalently immobilise onto the functionalised surface (Scheme 5.1, Figure 5.1).

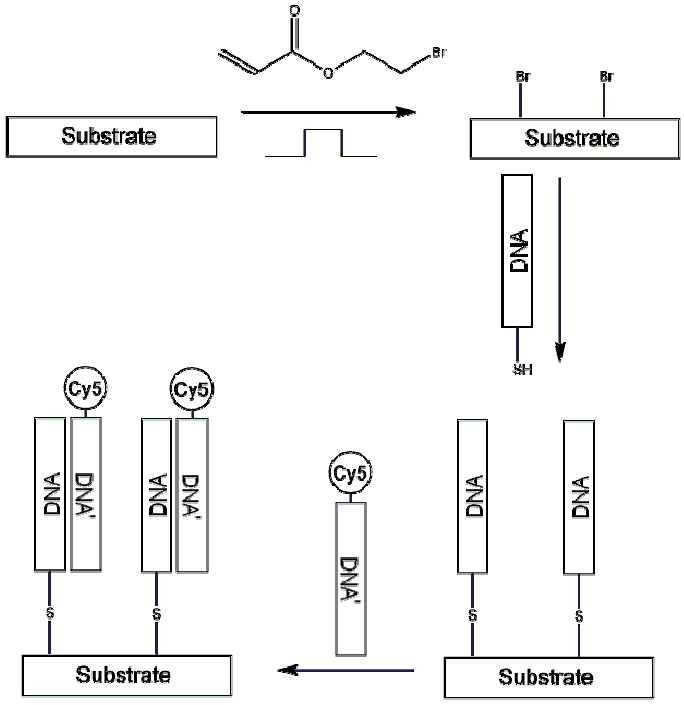

Scheme 5.1. Construction of DNA chips via plasmachemical functionalisation with 2-bromoethyl acrylate.

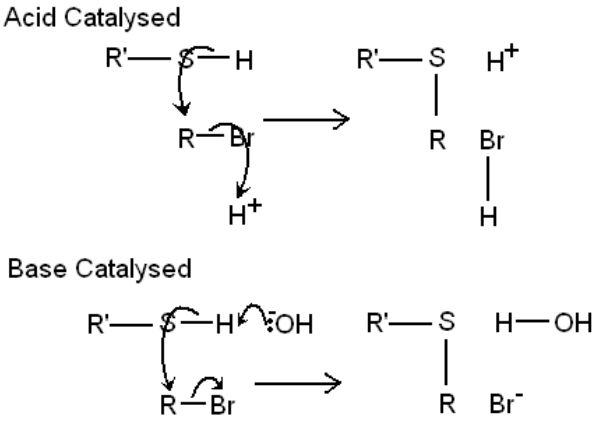

Figure 5.1. Acid/base catalysed reaction of a thiol with a C-Br bond

Pulsed plasmachemical functionalisation offers a simple potential route to brominated surfaces with good structural retention. 2-bromoethyl acrylate was selected as a suitable precursor – the acrylate group being particularly suitable for plasma functionalisation. The acrylate group has been used successfully in a number of plasmachemical functionalisations[3,4,5,6,7], and it is hoped that the presence of the classically polymerisable acrylate function will help to protect the C-Br functional group.

With regards to the choice of reaction chemistry, it should be noted that a thiolated substrate surface presents an attractive choice for thiolated DNA immobilisation, but that this chemistry has already been accomplished via the plasmachemical route[8].

In a more general sense, bromination of a polymer surface is known to improve properties such as adhesion[9] or wettability[10] when applied to a polymeric substrate. As such there has been considerable interest in bromination reactions, although the survival of the relatively weak C-Br bond (~366 KJ mol^{-1}) through multiple reaction steps (or generation in situ) is problematic. UV and thermal activated grafting of bromine gas to polyethylene[11], has allowed a bromine loading of 4.6-6.6 bromine atoms per 50 monomer units is reported.

Bromine-containing molecules have also been tethered directly to cellulose substrates by esterification of the cellulose –OH groups[12,13]

In the biological field, self-assembled monolayers of brominated silanes have been utilised to surface tether thiolated oligonucleotides[14] or proteins via the thiolated side chains naturally present on the cysteine amino acid[15,16,17]. However, as the immobilization chemistry is based on the formation of a silane network, this technology is only applicable to glass substrates. Surface bromine loading levels are typically not reported, but assuming complete functionalisation would amount to 7 atomic%[17].

Finally pulsed plasma polymerisation of species such as bromoform ($HCBr_3$) allows the introduction of C-Br bonds directly to the polymer surface, where up to 40 C-Br functions are present per 100 C atoms. However, this is typically reduced to about 20 C-Br (or ~17 At% bromine) functions after immersion in solvent removes weakly bound small molecular fragments[18]. This process produces multiple reaction pathways as the weak C-Br bond breaks, leaving a structure of $(CBr_x)_n$ (x = 0, 1, 2, 3; crosslinking and hydrogen atoms forming the remaining bonds). A more ideal case would be the use of a carefully tailored pulsed plasma polymer containing a readily polymerisable function to encourage structural retention.

5.2 Experimental

Pulsed plasma polymerisation of 2-bromoethyl acrylate, (Aldrich +99%), was carried out in an electrodeless cylindrical glass reactor as described in Chapter 2. 2-bromoethyl acrylate monomer vapour was introduced into the reactor at a pressure of 0.30 mbar and 5.2 x 10^{-9} mol s^{-1} flow rate for 5 minutes prior to reaction.

The immobilisation of DNA and subsequent hybridisation follow the method outlined in Chapter 2, except that oligonucleotide strands were modified with 3'-

terminal thiol modifications. Arrays were incubated at 60℃, pH9.0 unless otherwise stated.

Surface characterization techniques are outlined in Chapter 2.

5.3. Results

5.3.1. Plasmachemical Functionalisation with 2-Bromoethyl Acrylate

XPS analysis of plasmachemical functionalised 2-bromoethylacrylate surfaces deposited onto borosilicate glass coverslips showed excellent retention of the precursor structure. Bands corresponding to Br (3d) (71 eV), Br (3p) (184 eV), C (1s) (285 eV), and O (1s) (533 eV) were observed in survey spectra (Figure 5.2)[19]. Plasmachemical functionalisation yielded surface compositions that closely correspond to that of the theoretical polymer, although with a small increase in bromine content at the surface (Table 5.1).

	Surface Concentration (Atomic %)		
	C (1s)	O (1s)	Br (3d)
t_{on} = 20 µs, t_{off} = 10 ms, 40W P_P	60 ± 3	23 ± 4	17 ± 4
t_{on} = 30 µs, t_{off} = 10 ms, 40W P_P	61 ± 2	23 ± 3	16 ± 5
Continuous Wave (10W)	60 ± 1	23 ± 3	18 ± 3
Theoretical	62.5	25	12.5

Table 5.1. Surface atomic composition of plasmachemical functionalised 2-bromoethyl acrylate surfaces on silicon wafers.

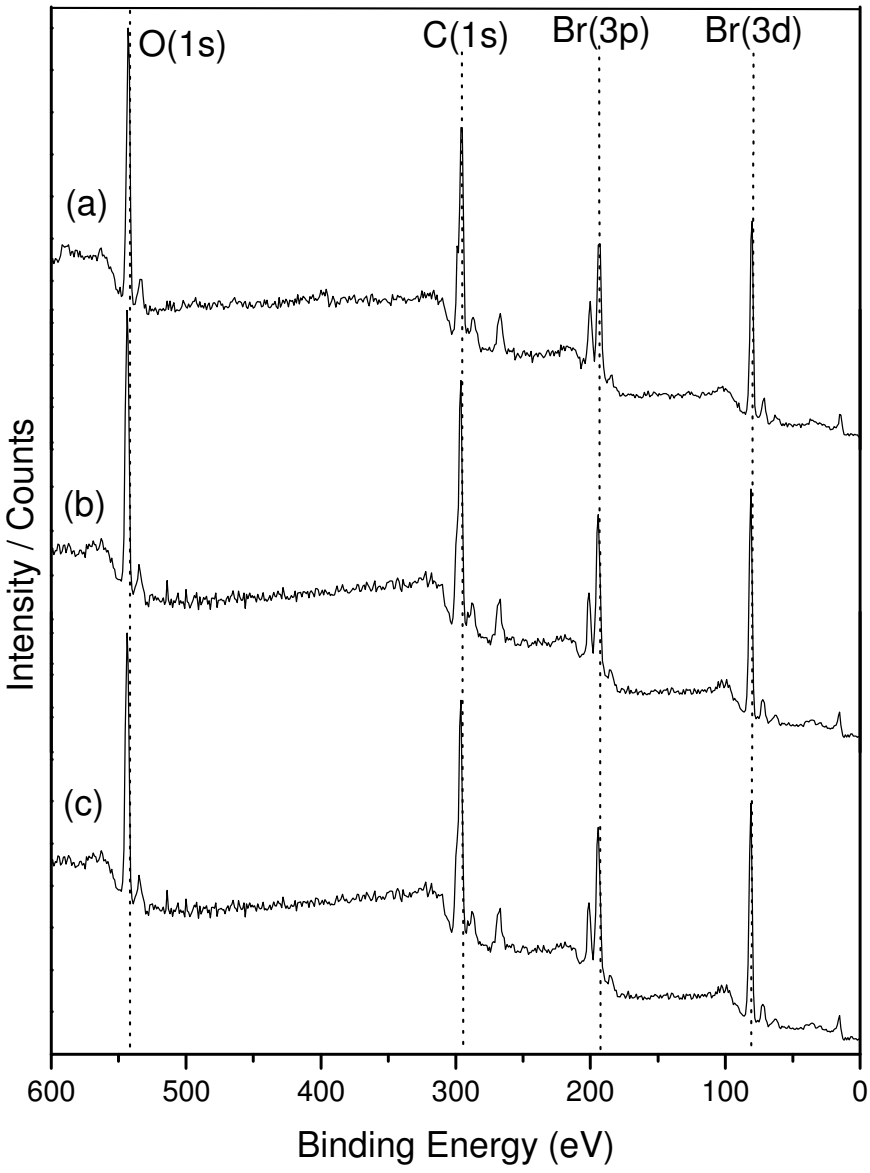

Figure 5.2. XPS survey scans of bromoethyl acrylate plasmachemical surfaces under various deposition regimes (a) Pulsed deposition (t_{on} = 30 µs), (b) Pulsed deposition (t_{on} = 20 µs), (c) 10 W continuous wave deposition. Bands corresponding to Br (3d) (71 eV), Br (3p) (184 eV), C (1s) (285 eV), and O (1s) (533 eV) are highlighted.

High resolution C (1s) envelope scans of the functionalised surfaces confirmed the superior structural retention of the pulsed plasmachemical systems when compared to the continuous wave system (Figure 5.4). In particular, the side band in the C (1s) envelope at 288.5 eV (O-C=O) is pronounced in the pulsed systems but largely absent in the oxygenated tail due by precursor fragmentation in the continuous wave plasma. The remainder of the envelope is attributed to the five carbon environments below: C_xH_y (285.0 eV), C-C=O (285.6 eV), C-O (286.4 eV), C-Br (286.0eV) (Figure 5.3)[20].

Examination of the high resolution Br (3d) envelope shows a single peak at 69.4 eV (Figure 5.5)[21]. This is consistent with ionic Br^- rather than C-Br, suggesting that significant loss of C-Br function has taken place at the plasmachemical layer surface.

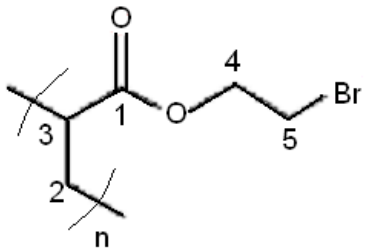

Figure 5.3. C(1s) environments present in the theoretical polymer

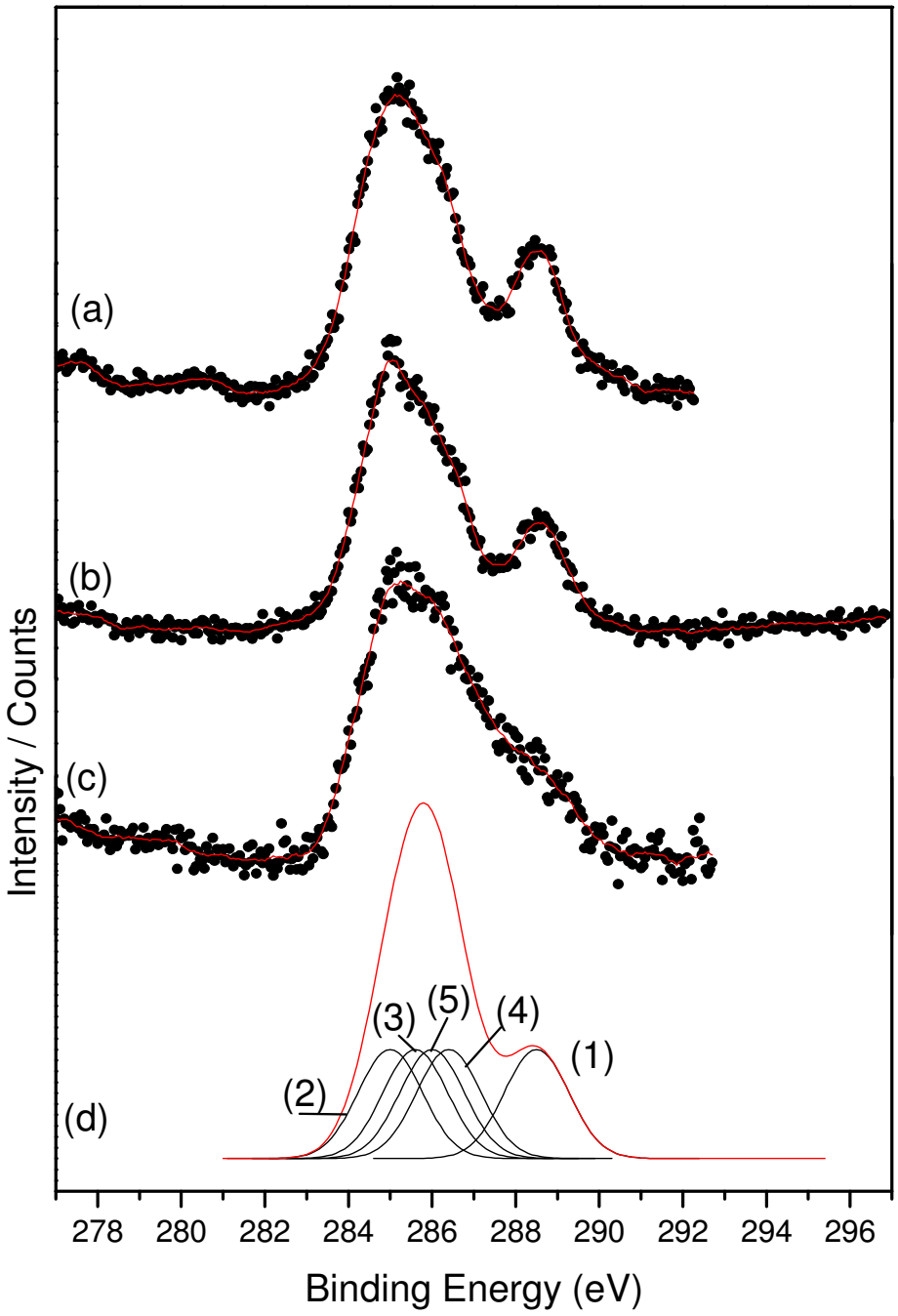

Figure 5.4. C(1s) envelopes by XPS of plasmachemical functionalised bromine surfaces (a) pulsed (t_{on} = 30 μs), (b) pulsed (t_{on} = 20 μs), (c) 5 W continuous wave, (d) theoretical C(1s) envelope assuming no monomer fragmentation.

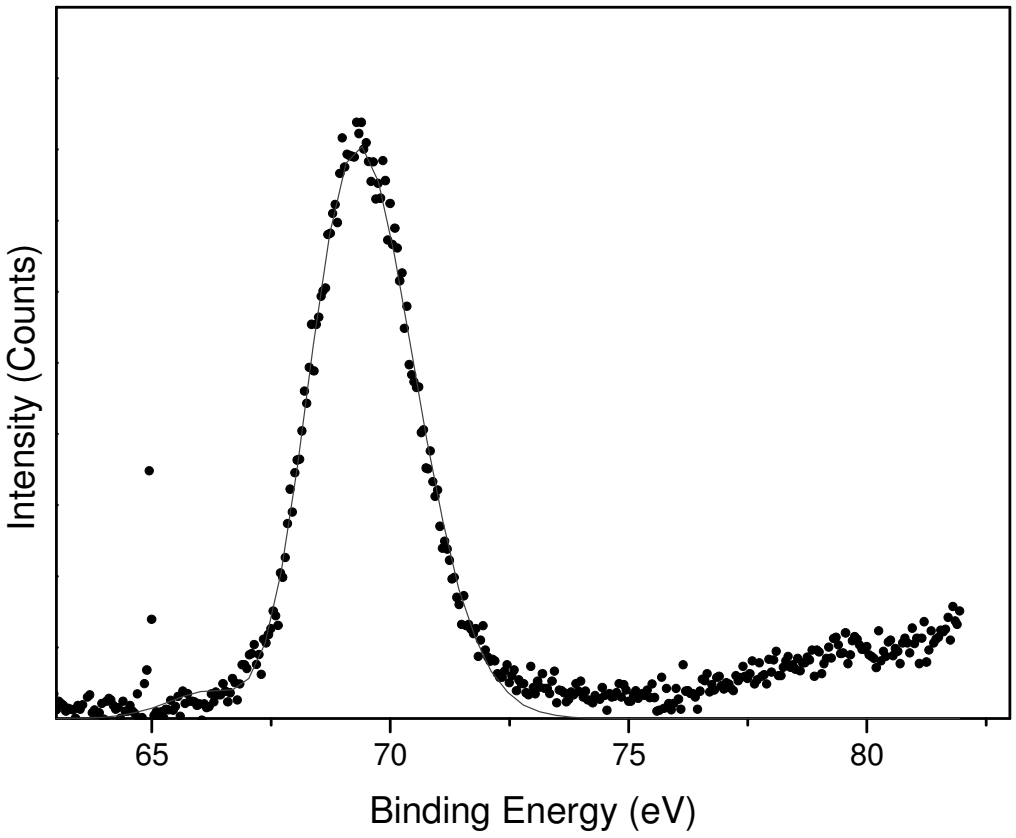

Figure 5.5 Br (3d) envelope of pulsed plasmachemical functionalised bromine surface (t_{on} = 30 µs).

FT-IR analysis of the plasmachemically functionalised surfaces also indicated superior structural retention in the pulsed systems. The pulsed systems give sharp, strong signals with bands closely corresponding to those observed in the monomer (Figure 5.6). In particular the C-Br stretch (570 cm^{-1}) and bands corresponding to the ester group (C=O stretch, 1728 cm^{-1}; C-O stretch, 1180 cm^{-1}) are retained in the pulsed system. Bands observed in the monomer from the alkene (e.g. C=C stretch, 1620 cm^{-1} & 1636 cm^{-1}; CH deformation, 1409 cm^{-1}; trans =CH rock, 1297 cm^{-1}; cis =CH rock, 1267 cm^{-1}; $=CH_2$ rock, 1079 cm^{-1}) are absent in the functionalised surfaces, indicating loss of the alkene functional group.

By contrast, the continuous wave system shows significant loss of bands and broadening in the spectrum. A significant band is observed in the –OH region (3400 cm^{-1}) suggests the creation of significant alcohol functionality in the surface polymer. Although broadened, the C=C bands at 1620 & 1633 cm^{-1} are retained, indicating that the continuous wave conditions were not conducive to reaction through the double bond.

Examination of the surfaces by sessile drop contact angle showed a marked difference between the pulsed and continuous wave systems, with the 10W continuous wave system giving a contact angle of 73 ± 1° and the pulsed 61 ± 3° (t_{on}=30 µs). Deposition rates as measured by reflectometry were 30 ± 3.3 nm min^{-1} for the continuous system (10W), with pulsed functionalisation proceeding markedly slower – 1.4 ± 0.3 nm min^{-1} at t_{on}=20 µs, and 7.5 ± 1.0 nm min^{-1} at t_{on}=30 µs.

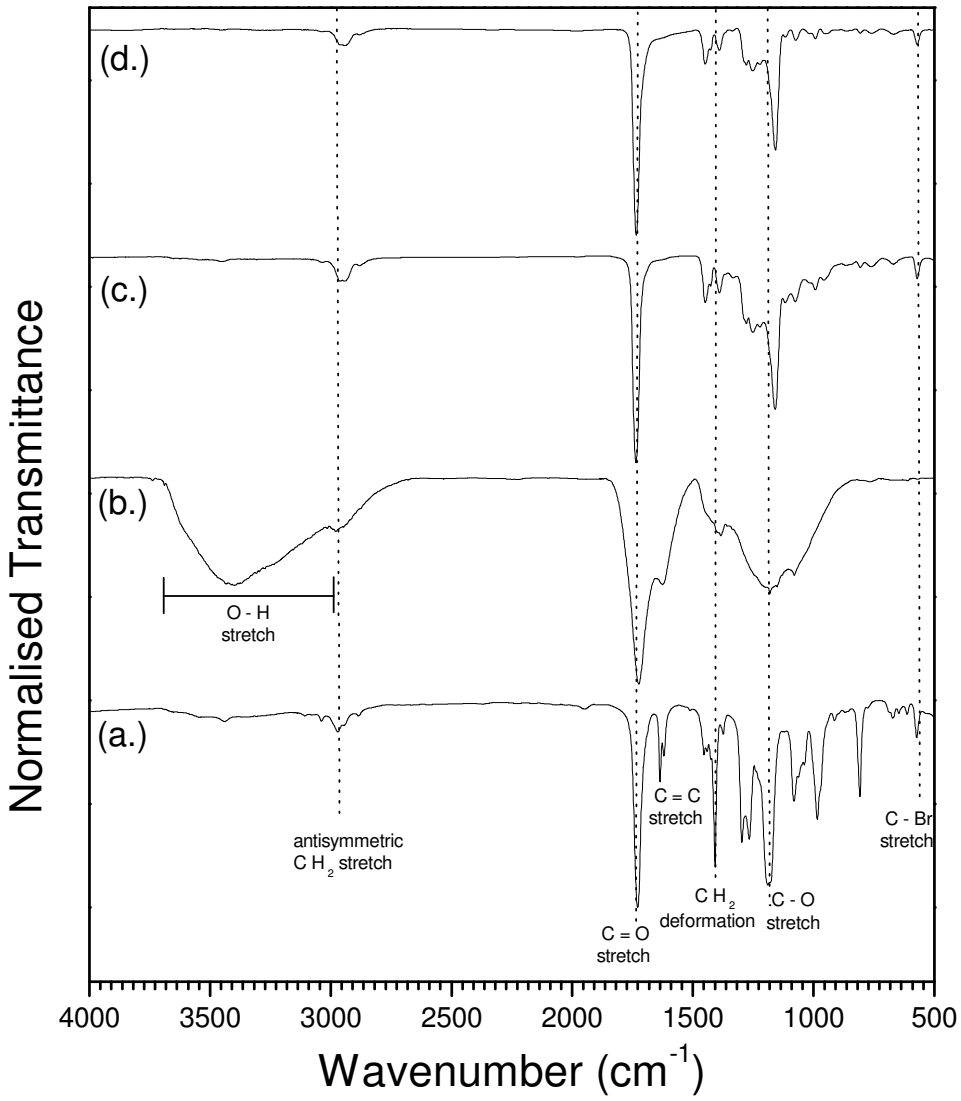

Figure 5.6. Infrared spectra of (a.) 2-bromoethylacrylate monomer, (b.) 10 W continuous wave plasma polymer, (c.) pulsed plasma polymer (time on = 20 μs, time off = 10 ms, peak power = 40 W), and (d.) pulsed plasma polymer (time on = 20 μs, time off = 10 ms, peak power = 40 W) [22,23].

5.3.2 DNA immobilization

The effect of various reaction parameters on immobilisation efficiency of the thiol modified probe TH1 (for probe structures see Table 5.2) was followed by fluorescence spectroscopy of the Cy5 tag. The intensity of immobilised oligonucleotides were highest at increased temperature (60°C), although a significant rise in immobilised DNA was also observed below freezing (-18°C, Figure 5.7). pH also had a marked effect upon the intensity of the observed fluorescence signal, with a strong peak at pH 9.00, with immobilisation particularly poor at neutral pH (Figure 5.8). The reaction was observed to reach completion after 5 hours (Figure 5.9).

	5' Modification	5'-3' Base Sequence	3' Modification
TH1	Cy5	AACGATGCACGAGCA	C13 Thiol
TH2	C13 Thiol	GCTTATCGAGCTTTC	-
TH3	Cy5	GAAGCTCGATAAGC	-

Table 5.2. Oligonucleotide Probe Structures

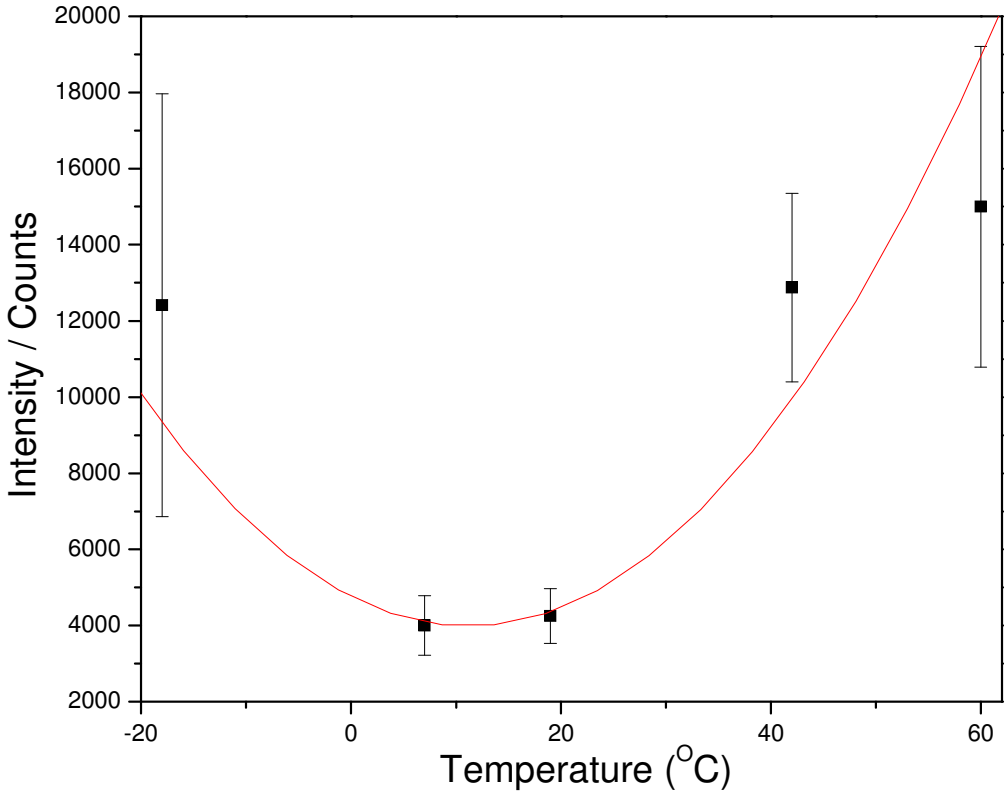

Figure 5.7. Fluorescence intensity as a function of temperature for Cy5 tagged oligonucleotide reaction with pulsed plasmachemical 2-bromoethyl acrylate surfaces (20 µs t_{on}, 10 ms t_{off}, 40W PP). Probe concentration 200 nmol dm^{-3}, incubation time 24 hours, pH 9.33.

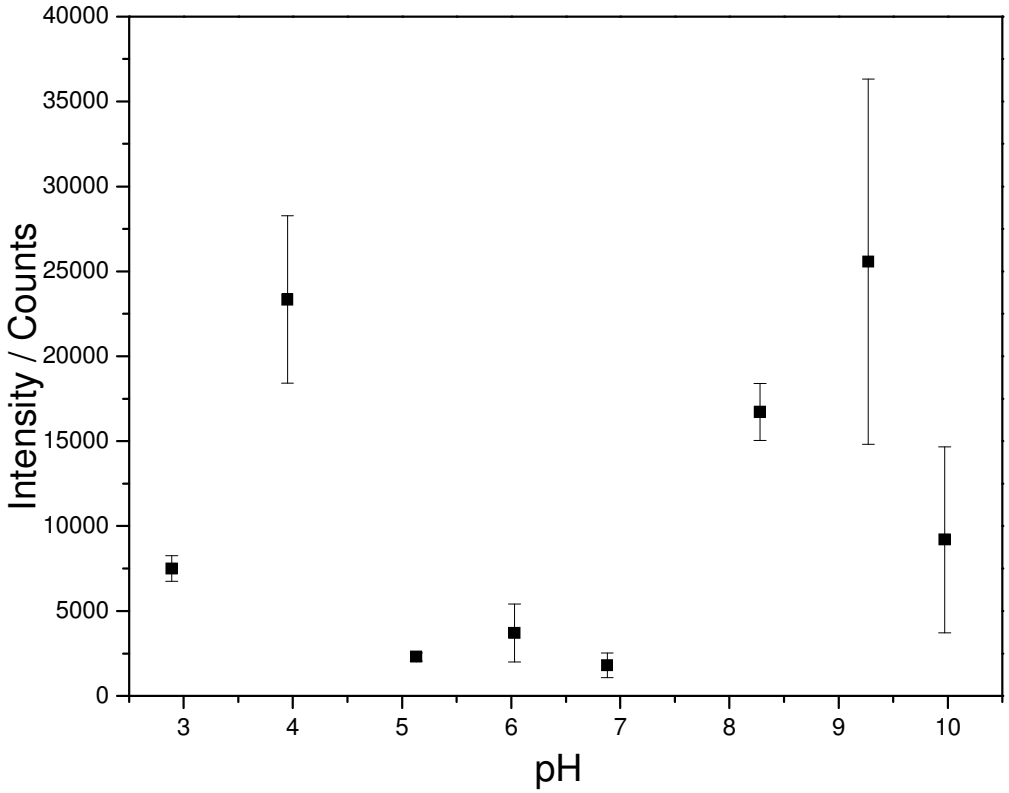

Figure 5.8. Fluorescence intensity as a function of pH for Cy5 tagged oligonucleotide reaction with pulsed plasmachemical 2-bromoethyl acrylate surfaces (20 μs t_{on}, 10 ms t_{off}, 40W P_P). Probe concentration 200 nmol dm^{-3}, incubation time 24 hours, incubation temperature 60℃.

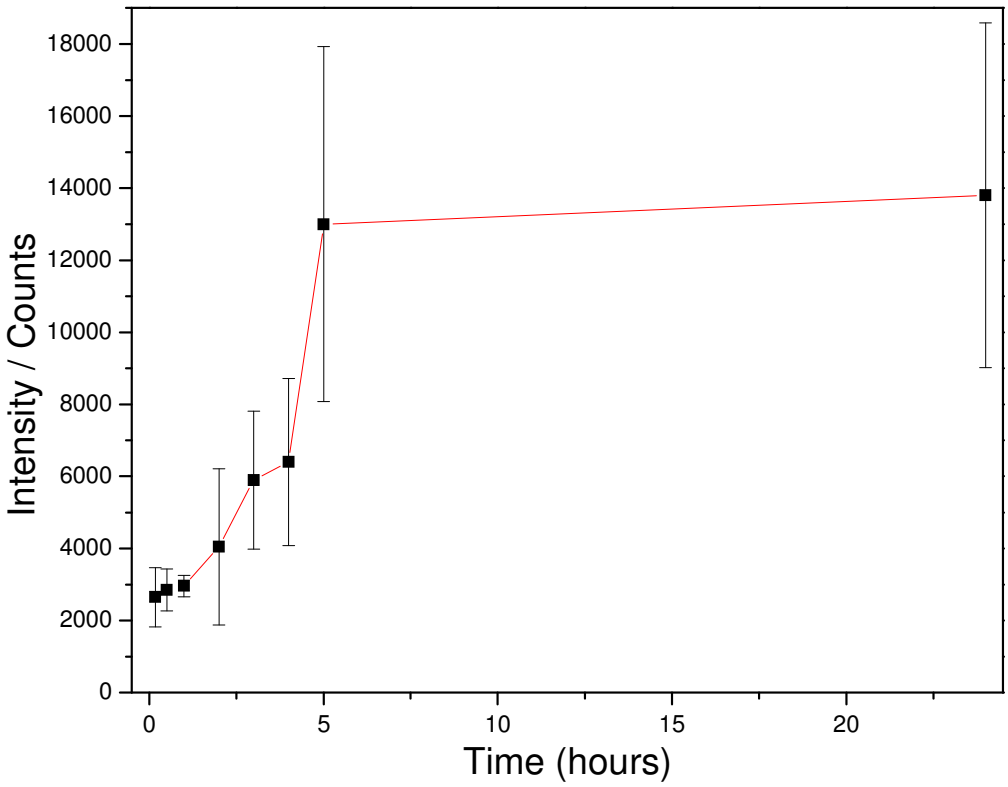

Figure 5.9. Fluorescence intensity as a function of time for Cy5 tagged oligonucleotide reaction with pulsed plasmachemical 2-bromoethyl acrylate surfaces (20 μs t_{on}, 10 ms t_{off}, 40W P_P). Probe concentration 200 nmol dm^{-3}, incubation temperature 60℃, pH 9.33.

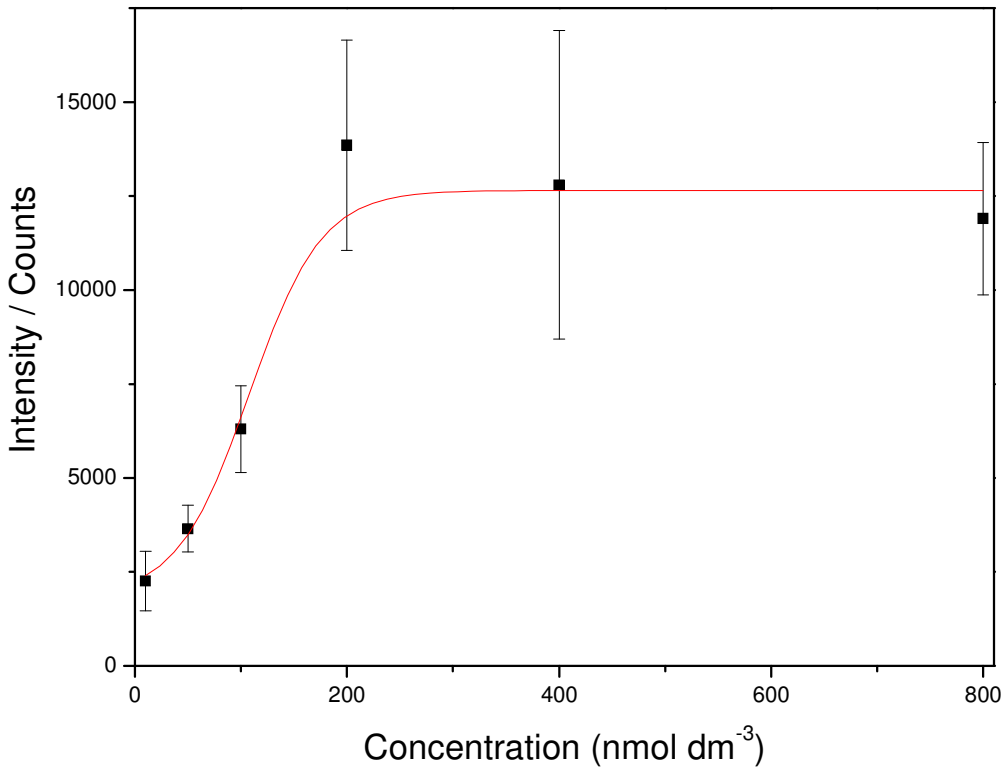

Figure 5.10. Fluorescence intensity as a function of probe concentration for Cy5 tagged oligonucleotide reaction with pulsed plasmachemical 2-bromoethyl acrylate surfaces (20 μs t_{on}, 10 ms t_{off}, 40W P_P). pH 9.33, incubation time 24 hours, incubation temperature 60°C.

200 nmol dm^{-3} of probe allowed the reaction to reach completion (Figure 5.10).

5.3.3 DNA hybridisation on bromine functionalised surfaces

The probe TH2 was immobilised onto the 2-bromoethyl acrylate functionalised surfaces for the hybridisation of the complimentary TH3 target. This reaction was followed by fluorescence microscopy and yielded 14,000 ± 8000 counts (85 % of the peak immobilisation signal at pH 9.0) indicating that the surface immobilised TH2 is suitable for hybridisation reactions.

The optimal conditions yielded above were then applied to production of an array of TH2 on a 2-bromoethyl acrylate functionalized surface. Arrays formed using this system proved to be difficult to image, with high background signals being observed across the whole substrate surface and very poor definition of individual spots. Close examination of the surface shows a distinctive mottled texture across the whole surface, with the hybridised probe showing as more intense signals on the mottled background (Figure 5.11). No signal was observed from control surfaces of 2-bromoethyl acrylate lacking surface immobilised TH2 oligonucleotides.

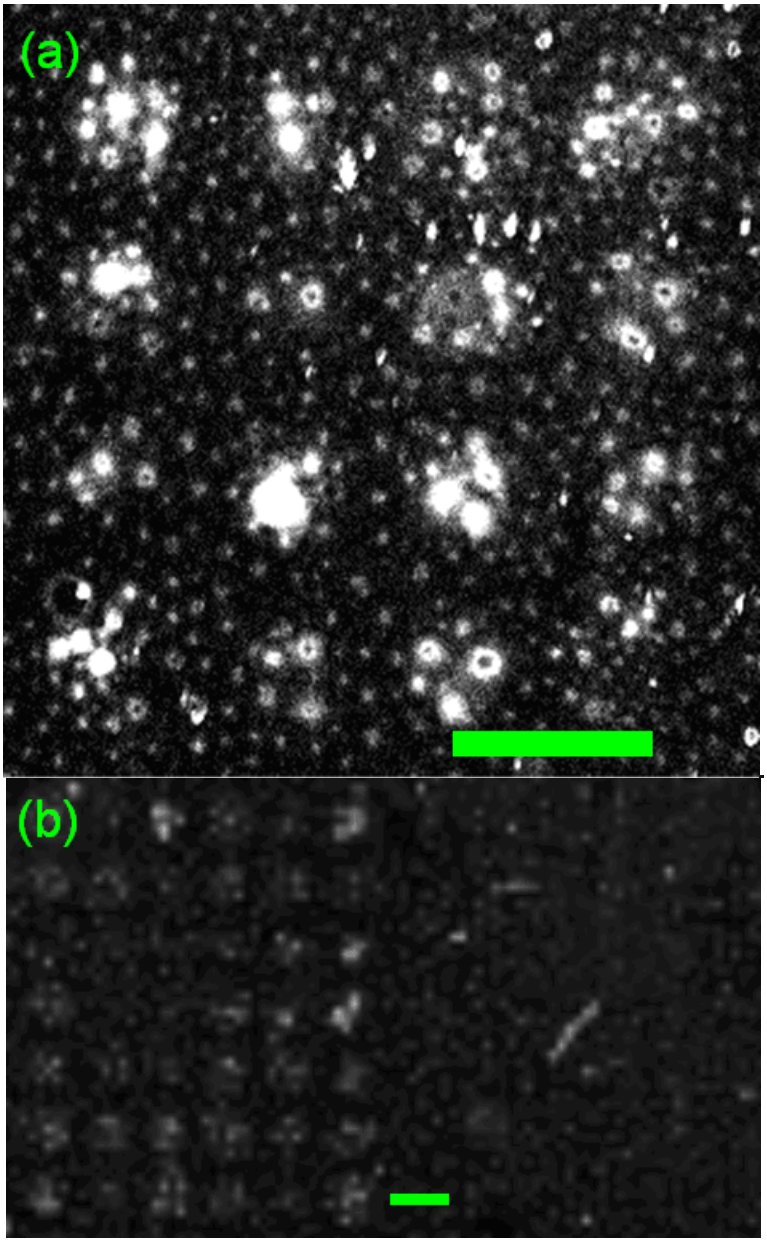

Figure 5.11. Typical fluorescent image of an arrays on the 2-bromoethyl acrylate surfaces (20 µs t_{on},10 ms t_{off}, 40W P_P). Surface tethered probe concentration 200 nmol dm^{-3}, incubation time 24 hours, incubation temperature 60℃, pH 9.27, 100 µm diameter head pin used. Hybridisation under conditions outlined in Chapter 3. (a) High resolution image of an array, (b) large detail of an array on a microscope slide, showing the mottled appearance of the background. Scale bars 750 µm.

5.4. Discussion

5.4.1 Bromoethyl acrylate functionalization

Production of bromine functionalised surfaces by pulsed plasmachemical functionalisation yielded good structural retention when compared to the continuous wave system. The improved structural retention of the pulsed system is a significant improvement over previous continuous wave functionalisations of precursors, with polymerisation primarily taking place through the C=C group. However, the relatively weak C-Br bond is not retained on the functionalised surface, with bromine content observed to be higher than expected from the theoretical monomer structure. This observation is consistent with previous plasmachemical functionalisation methods used to produce bromine-containing surfaces, especially at low duty cycles[24]. The significantly higher contact angle for the continuous wave system also indicates structural damage and a more cross-linked polymer layer.

There is something of a contrast between the XPS data, particularly the Br (3d) envelope, and the bulk FT-IR data. The Br (3d) envelope suggests an almost complete loss of the C-Br function, with only a single peak corresponding to bromine salts or ionic bromine at 69.4 eV, rather than the C-Br peak expected at 76-77 eV (Figure 5.5). Conversely, the FT-IR shows retention of the C-Br band at 570cm^{-1}, albeit with a possible reduction in intensity compared with the precursor (Figure 5.6). These results would suggest that whilst C-Br functions are retained in the bulk, there is little retention within the outer 10 nm of the plasmachemical layer. However, the flexible nature of plasmachemical layers has already been discussed in previous chapters, which might still allow access of the thiolated DNA to the functional groups deeper into the bulk of the plasmachemical layer. Secondly, with reference to Figure 5.1, an ionic Br function might also leave reactive groups present on the substrate surface. In retrospect, a washing experiment might also have helped to highlight any

presence of loose fragments on the substrate surface such as H-Br or ionic species.

The pulsed plasma polymerisation of 2-bromoethylacrylate presents a relatively attractive method when compared to others in the literature (Table 5.3). Pulsing is crucial for structural retention, as is the monomer choice –the polymerisable acrylate group allows improved structure retention, as opposed to H_3CBr[18], dibromomethane (CH_2Br_2)[24], or allyl bromide[24]. The relatively high Br loading compares favourably with other methodologies, and the pulsed plasma technology is more generally applicable than many of the alternatives which require specific substrate surfaces.

Br Reported (Atomic %)	Br Estimated[a] (Atomic %)	Method	Reference
7.00	N/A	Esterification of cellulose	12
N/A	6.19	UV/thermal graft to polyethylene	11
N/A	3.3	UV/thermal graft to polyaminonitrile	25
N/A	10	UV bromination of silane SAM	26
N/A	6.25	Silane SAM	27
6.69	N/A	Thermal graft on carbon black	28
N/A	10	Vapour adsorption to poly[1(trimethylsilyl)-1-propyne	29
42	N/A	Pulsed plasma polymerisation	14
16 ± 5	N/A	Pulsed plasma polymerisation	Present

Table 5.3. Typical bromine loadings by various techniques. a) As % Br is often not reported, this estimated value is based on the maximum reported Br loading in each case.

Equation (1) was again applied in order to establish the power applied during the deposition. The continuous wave system of <P> = 5W, compares to <P> = 0.08W (t_{on} = 20 µs) or 0.12W (t_{on} = 30 µs). The relatively gentle power input of the pulsed systems results in a lower degree of fragmentation and a better structural retention in the plasmachemical surface. The corresponding deposition efficiencies of 6 ± 0.7 nm min^{-1} W^{-1} (5W CW), 173 ± 4 nm min^{-1} W^{-1} (t_{on} = 20 µs) and 63 ± 9 nm min^{-1} W^{-1} (t_{on} = 20 µs) illustrate the superior efficiency of the pulsed plasmachemical technology.

5.4.2 DNA immobilization

Whilst the increase in immobilisation intensity at higher temperatures can be attributed to improved reaction due to the extra energy, this explanation is insufficient at lower temperatures where the intensity would be expected to be

lower still. The increase in observed immobilisation of thiol (and phosphorthioate) modified oligonucleotides to brominated surfaces at low temperatures has been observed previously - this is attributed the reagents being forced into intimate contact as the lattice of ice forms, resulting in an increase in signal[14,1]. The use of sub-zero temperatures also resulted in film surface damage, with consequent reproducibility problems.

The influence of pH – which results in reaction maxima in both acidic (pH = 3.95) and basic (pH = 9.33) conditions, with very little reaction at neutral pH. At basic pH deprotonation of the thiol –SH occurs to allow nucleophilic attack, with bromine acting as a leaving group. Similarly at acidic pH, protonation of the Br atom can occur, which weakens the C-Br bond and again allows nucleophilic attack by lone pairs on the sulphur.

Extreme pH values (<3.96 , >9.33) were observed to result in damage to the plasmachemical layer, and were therefore not suitable for microarray the immobilisation reaction. However, these pH ranges lie significantly outside the range expected in the working life of microarray systems which typically operate at neutral pH to simulate biological processes.

Array manufacture proved to be extremely difficult with the 2-bromoethylacrylate system. The poor resolution and apparent spreading of the oligonulcleotides to cover the entire surface could be attributable to several factors. The most common cause of noise in microarray systems is non-specific adsorption of tagged oligonucleotides onto the surface, but control experiments in which the plasmachemical layer is exposed to TH3 resulted in no signal indicating that this is unlikely to be the cause. The (relatively) high contact angle of the plasmachemical layer suggests that complete wetting of the surface as drops are applied should not be an issue. Spot spreading and surface wetting due to excess humidity would not result in the observed mottling on the surface. Another possibility is that the heating cycle employed during oligonucleotide immobilisation results in rearrangement of the

plasmachemical layer, either by chemical reaction and crosslinking, or physical segregation into regions.

An interesting avenue of future research might be to investigate the effect of plasma crosslinking on the spot formation in the arrays. If the heating cycle is causing rearrangements in the plasma functionalised layer, then the introduction of additional deliberate cross-linking should reduce or eliminate the problem, although with the sacrifice of structural retention.

5.5. Conclusions

The plasmachemical functionalisation of surfaces with 2-bromoethyl acrylate is demonstrated, but with evidence that significant C-Br loss may have taken pleace, albeit to leave other bromine functions on the surface. In spite of this, the plasmachemical layer is suitable for the immobilisation and hybridisation of thiol-terminated oligonucleotide strands. The immbolisation of DNA to the plasmachemical surface was optimised, bur clear array reading is inhibited by deterioration of the plasmachemical surface under the immobilisation conditions.

5.6. Discussion – comparison of systems

All three systems were found to be suitable for DNA immobilization and hybridisation. 3-vinylbenzaldehyde functionalisation allowed a maximum hybridisation of 500 ± 140 counts, with an excellent deposition rate and structural retention (see section 3). This corresponds to a significantly larger than that hybridisation intensity observed on commercially available aldehyde functionalised DNA chips (see Table 5.4).

Surface Function	Precursor	Immobilsation Counts	Hybridisation Counts	Fluorophore
Aldehyde	3-vinylbenzaldehyde	14000 ± 1000	500 ± 140	Cy5
Aldehyde	Undec-1-enal	9000 ± 1500	700 ± 70	Cy5
Aldehyde	ALS-25		70 ± 11	Cy5
Bromine	2-bromoethylacrlate	17000 ± 1500	14000 ± 8000	Cy5

Table 5.4 Comparison of different surface functionalisations: immobilisations and hybridisations.

Undec-1-enal was also suitable for DNA chips, although the observed hybridisation was as intense in this system at 700 ± 70 counts. Although the undec-1-enal surface also retains much of precursor structure, aldehyde intensity is notably reduced in the FT-IR (Chapter 3). Undec-1-enal also suffers from a relatively slow deposition rate when compared to the other monomers.

Both the aldehyde functionalised surfaces show relatively low hybridisation counts compared to the level of immobilisation. There are several factors that can reduce hybridisation efficiency. Firstly, high immobilisation efficiencies do not translate directly into superior hybridisation as too tightly packed a network of oligonucleotides on the surface can inhibit the hybridisation reaction. Further, flexible polymer layers also give improved hybridisation, It can be speculated that the slightly higher efficiency observed for the undec-1-enal is due to the

long flexible carbon chain as opposed the rigid aromatic structure of the 3-vinylbenzaldehyde. The commercial slide shows even poorer results, presumably as the surface is a SAM, which lacks the flexibility of a pulsed plasma polymer.

Bromine functionalised surfaces offer the superior surface for DNA immobilisation, which is attributed to several factors. Firstly there is a relatively high Br concentration on the pulsed plasmachemical surface when compared to the aldehyde loading of either 3-vinylbenzaldehyde or undece-1-enal. Secondly the polymer is observed to be slightly soft & sticky, which suggest a highly flexible substrate that allows rearrangement and/or solvation of the surface bound structures (see Chapter 5).

Whilst plasmachemical functionalised 2-bromoethyl acrylate also allows good hybridisation, fluorescence intensity 14000 + 8000 counts, there are several drawbacks to this technology in comparison to the aldehyde functionalisations. The major problem is the difficulty in producing clear, crisp microarrays and the distinctive mottling of the surface that occurs on heating which render this particular plasmachemical layer unsuitable for microarray manufacture, with only weak differentiation between hybridisation and non-specific adsorbtion of the target (Chapter 5).

Unfortunately, direct comparison between different methods present in the literature is extremely difficult due to the wide array of tags (fluorophores & radioactive labels), substrates, excitation methods. Even where fluorophores are identical, it is usual for results to be normalised[30] The short 15-base oligonucleotides chosen in the present study also represent the most difficult hybridisation conditions – with very unstable duplexes being formed, *any* binding through the DNA side chains will result in hybridisation failure. Using longer oligonucleotides or DNA strands for the array (commonly observed in the literature) will result in improved signals. However, on a qualitative level, these results do compare favourably with those mentioned in the introduction.

1 Kang, S.; Xu, X.; Heidenreich, O.; Gryaznov, S.; Nerenberg, M. Nucleic Acids Res. **1995**, *23*, 2344.

2 Fahy, E.; Davis, G. R.; DiMichele, L. J.; Ghosh, S. S. *Nucleic Acids. Res.* **1993**, *21*, 1819.

3 Ward, A. J.; Short, R. D. *Polymer* **1995**, *36,* 3439

4 Coulson, S. R.; Woodward, I. S.; Badyal, J. P. S.; Brewer, S. A.; Willis, C. *Chem. Mater.* **2000**, *12*, 2031

5 France, R, M.; Short, R. D.; Dawson, R. A.; MacNeil, S. *J. Mater. Chem.* **1998**, *8*, 37

6 O'Toole, L.; Beck, A. J.; Short, R. D. *Macromolecules* **1996**, *29*, 5172

7 Tarducci, C.; Schofield, W. C. E.; Badyal, J. P. S.; Brewer, S. A.; Willis, C. *Chem. Mater.* **2002**, *14*, 2541

8 Schofield, W. C. E.; McGettrick, J.; Bradley, T. J.; Badyal, J. P. S.; Przyborski, S. *J. Am. Chem. Soc.* **2006**, *128*, 2280

9 Chew, A.; Dahm, R. H.; Brewis, D. M.; Briggs, D.; Rance, D. G. *J. Colloid Interface Sci.* **1986**, 110, 88-95.

10 Shah, C. D.; Jain, D. K. *Textile Res. J*. **1984**, *54*, 742-748.

11 Noppavan Chanunpanich, Abraham Ulman, Y. M. Strzhemechny, S. A. Schwarz, A. Janke, H. G. Braun, T. Kraztmuller *Langmuir*, **1999**,*15*, 2093

12 Zampano, G.; Bertoldo, M.; Bronco, S.; *Carbohydrate Polymers* **2009**, *75*, 22

13 Lee, S. B.; Koepsel, R. R.; Morley, S. W.; Matyjaszewski, K.; Sun, Y.; Russell. A. J. *Biomacromolecules* **2004**, *5*, 877

14 Pirrung, M. C.; Davis, J. D.; Odenbaugh, A. L. *Langmuir* **2000**, *16*, 2185

15 Balachander, A.; Sukenik, C. N. *Langmuir* **1990**, *6*, 1621.

16 Yong Woo Lee, Joseph Reed-Mundell, Chaim N. Sukenik, James E. Zull *Langmuir* **1993*, 9,*** 3009

17 Andreas Heise, Henning Menzel, Hyun Yim, Mark D. Foster, Reinier Hendrik Wieringa, Arend Jan Schouten, Volker Erb, Manfred Stamm *Langmuir* **1997,** *13,* 723-728

18 Kühn, G.; Ghode, A.; Weidner, St.; Retzo, I.; Unger, W. E. S.; Friedrich, J. F.; *Polymer Surface Modification: Relevance to Adhesion Vol. 2 pp 45-64 VSP, Utrecht, The Netherlands,* **1996**

19 Beamson, G.; Briggs, D. High *Resolution XPS of Organic Molecules the Scienta ESCA 300 Database*; John Wiley & Sons : New York, **1992**.

20 Briggs, D.; Seah, M. P. (eds) *Practical Surface Analysis 2nd Ed.* John Wiley & Sons, Chichester, **1990**.

21 Briggs, D.; Seah, M. P. (eds) *Practical Surface Analysis 2nd Ed.* John Wiley & Sons, Chichester, **1990**.

22 Colthup, N. B.; Daly, L. H.; Wiberley, S. E., Introduction to Infrared and Raman Spectroscopy, 3rd ed*.,* Academic Press, London **1990**.

23 Lin-Vein, D.; Colthup, N. B.; Fateley, W. G.; Grasselli, J. G., The

Handbook of Characteristic Frequencies of Organic Molecules, Academic Press, London **1991**.

24 Wang, J.; Chen, X.; Chen, J.; Calderon, J. G.; Timmons, R. B. Plasmas and Polymers' **1997**, *2*, 245.

25 Ulbricht, M.; Oechel, A. *European Polymer Journal* **1996,** *32*, 1045

26 Baker, M. V.; Watling, J. D. *Tetrahedron Letters*, **1995**, *36*, 4623

27 Faucheux, N.; Schweiss, R.; Lützow, K.; Werner, C.; Groth, T. **2004,** *25,* 2721.

28 Paprier, E.; Lacroix,; Donnet, J. –B. *Carbon*, **1996,** *34* 1521

29 Xu, G.; Sun, X.; Qiu, X.; Zhang, J.; Zheng, G. *Chinese Journal of Polymer Science* **1994**, *12*, 180.

30 Dolan, P. L.; Wu, Y.; Ista, L. K.; Metzenberg, R. L.; Nelson, M. A.; Lopez, G. P. *Nucleic Acids Research* **2001**, *29(21)*, e107

6. A plasmachemical route to smart wound dressings – some initial results.

6.1 Introduction

Wound healing is a complex process. To compliment the complexity of wound healing, a wide range of commercial wound dressing products are available which act to improve the wound healing process, particularly in chronic wounds such as ulcers or burns[1]. Typically these wound dressings either act as a replacement skin layer, or contain biologically derived chemicals that promote accelerated wound healing[2,3], or allow the targeted delivery of drugs or scaffolds for tissue growth[4,5], although a wide range of products are available[6]. Another approach is to surface tether other biologically active molecules such as antibiotics[7]. Ultimately wound infection & complications even with commonly available graft materials such as muscle tissue[8], animal tissue[9], polytetrafluoroethylene[10,11], or Dacron (a trade name for polyethylene[12] terephtalate) can result in the need for extra treatment, loss of limbs, or even patient mortality.

Enzymes are complex proteins that act to catalyse specific reactions in biological systems. The specificity of enzyme action is well-reported, and is described by the lock-and-key model – the active site of the enzyme is geometrically structured to accept the desired substrate. A simple generic reaction scheme is then that the substrate and enzyme bind, a reaction takes place, and the product(s) are then released. However, the enzyme itself is a large, flexible system and the induced-fit model factors this flexibility into the traditional lock-and-key model by allowing for changes in the geometry of the enzyme active site that will promote reaction of the substrate[13].

One enzyme known to cause problems in wound healing is elastase, which has been shown to attack the bio-molecules that promote wound healing such as elastin, coagulation factors, cytokine growth factors, or fibronectin can be degraded in the presence of excess elastase. The elastase family acts by hydrolysing the amide bonds that form the backbones of any protein-

based molecule (Figure 6.1). Introduction of elastase recognition sites on cotton was one tactic adopted for the inhibition of elastase activity by inducing enzymatic binding to the fabric[14]. Another novel approach to the construction of smart wound dressings involves the surface tethering of an elastase inhibitor to hydroxyl groups in cotton[15].

Enzyme inhibitors are molecules that act to prevent the catalytic process reducing or totally preventing the binding of the substrate to the enzyme active site. There are four main types of inhibitors: 1) Competitive inhibitors that compete directly with substrate molecules by binding in the enzyme's active site, and often have a similar physical structure to the substrate; 2) Uncompetitive inhibitors which bind to the enzyme-substrate complex to form an inactive enzyme-substrate-inhibitor complex; 3) Non-competitive inhibitors can bind either to the enzyme or enzyme-substrate complex, but never compete with the substrate as they do not bind directly to the enzyme active site; 4) Mixed inhibitors typically form enzyme-substrate-inhibitor complexes in the same manner as non-competitive inhibitors, but this complex retains at least some of its catalytic properties. Inhibitors that form a strong covalent bond with the enzyme are known as irreversible inhibitors.

In the case of the elastase family of proteins, one group of irreversible inhibitors that has proven effective in reducing catalytic activity are the chloro methyl ketones (CMKs)[16], which bind directly to the elastase active site as a competitive inhibitor[17]. Studies have suggested that CMKs, and other electrophilic ketones, act to produce a bridge between two amino acids present at the enzymes active site, whilst the small peptide chain acts as a recognition unit (Figure 6.1)[18,19,20,21].

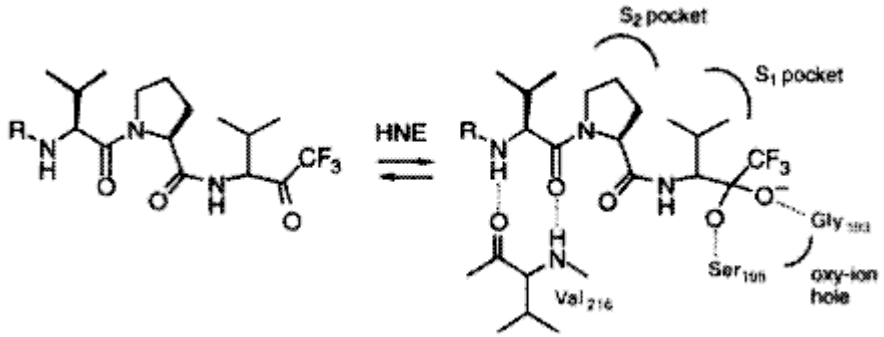

Figure 6.1. Inhibition of human neutrophil elastase by an electrophilic ketone[22].

In this work, initial results suggesting the feasibility of using plasmachemical technology for wound dressings are presented. A plasmachemical hydroxyl surface is generated from the pulsed plasmachemical functionalisation of 2-hydroxyethylacrylate[23]. The peptide chloromethylketone (CMK) is then surface tethered under acidic conditions, which drives the formation of a hemi-acetal (Figure 6.2), with hydrogen bonding between hydroxyl groups on the surface and the peptide carbonyls contributing to the surface tethering. This binding is weak, so that the surface-bound CMK can then be introduced into neutral solution where it will be released. The CMK then permanently inhibits any elastase present by binding with the active site of the enzyme.

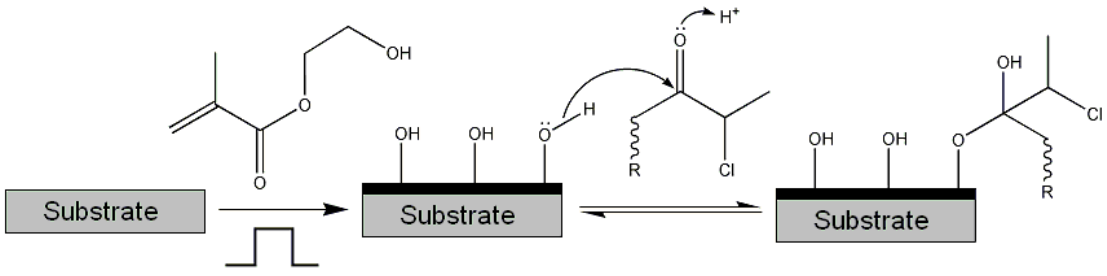

Figure 6.2. Tethering of CMK to a plasmachemically modified surface.

The CMK inhibition can be demonstrated by monitoring the decomposition of a suitable substrate. One method adopted for monitoring the catalytic effects of the porcine pancreatic elastase is to monitor the release of *p*-nitroaniline from the hydrolysis of a suitably modified peptide substrate[15]. The small peptide chain allows recognition of the molecule as a substrate by the

porcine pancreatic elastase, which then acts to hydrolise the peptide link between the peptide chain and the aromatic anilide, to release *p*-nitroaniline in an identical manner to the hydrolysis of peptide bonds in a protein chain (Figures 6.1 & 6.3). The *p*-nitroaniline is a yellow-coloured compound that can then be monitored through UV-Vis spectrometry to assess the level of porcine pancreatic elastase activity.

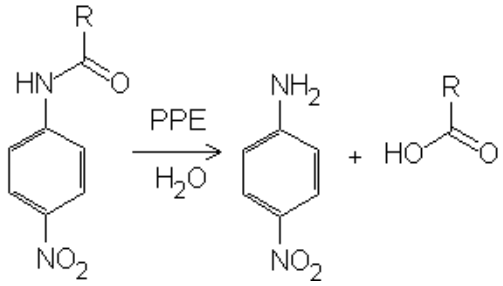

Figure 6.3. Hydrolysis of the peptide link between the peptide side chain (R) and the *p*-nitroanilide group.

6.2 Experimental

Plasma polymerization of 2-hydroxyethylmethacrylate (Aldrich, 95%) was carried out in an electrodeless cylindrical glass reactor as described previously[23]. Substrates included borosilicate glass cover slips and polished silicon. Substrates were subjected to an additional 5 minute continuous wave air plasma at 40W power prior to HEMA deposition in order to improve adhesion of the plasmachemical layer to the substrate.

The surface tethering method of CMK onto the hydroxyl surface was modified from that used previously[15]. HEMA-modified surfaces were immersed in pH 4.5 SSC for 1 h. For borosilicate glass coverslips, 10 µL of 1.2 $mgml^{-1}$ CMK in acetonitrile was dropped onto the coverslip surface, with a second coverslip used to cover the first (like a sandwich). The second coverslip was removed after 1 or 24 h by brief (30s) immersion of the sandwich in acetonitrile.

Porcine pancreatic elastase was obtained as an affinity chromatography purified, lyophilized powder possessing 3–6 units per mg protein (Sigma). Stock buffer consisted of 0.1M sodium phosphate, 0.5 M NaCl, 3.3% (v/v) DMSO, pH7.6. In a typical experiment 72 µM of substrate (MeOSuc-Ala-Ala-Pro-Val-*p*-nitroanilide) in 1250 µL buffer was combined with 250 µL enzyme solution. Surface tethered CMK was introduced on glass substrates by immersion in the substrate solution immediately prior to mixing.

Surface characterisation by XPS, FT-IR, sessile drop contact angle and reflectometry is described in previous chapters.

UV-vis measurements were taken on an ATI Unicam UV/Vis Spectrophotometer UV2-100 with Unicam Vision version 3.41 software in fixed λ mode at 410 nm. Buffer solution was used as a reference for each experiment. Readings were taken once every 5s for 15 min. Surface tethered CMK on glass coverslip substrates were weighed and then introduced directly into the reaction cell.

6.3 Results and Discussion

XPS of plasmachemically functionalised hydroxyl surfaces correspond closely to those observed previously[23] (Table 6.1, Figure 6.5a). The C(1s) envelope of the pulsed plasmachemical layer (t_{on} = 20 µs, t_{off} = 20 ms, 40 W) showed a strong correspondence to the theoretical spectra based on the precursor structure (Figure 6.6a and b). Four peaks were used to create the theoretical model: (1) C_xH_y (285.0 eV), (2) C-C=O (285.6 eV), (3) C-O (286.4 eV), (4) O-C=O (288.5 eV)[24], as suggested based on the theoretical polymer structure (Figure x.x).

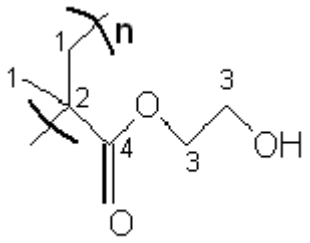

Figure 6.4 Carbon environments in the theoretical poly-HEMA

The continuous wave hydroxyl film was deposited at a rate of 20 ± 2 nm, whilst the pulsed hydroxyl layer (t_{on} = 20 µs, t_{off} = 20 ms, 40 W) was deposited at a rate of 8 ± 6 nm. FT-IR spectra also corresponds to those observed previously, with bands corresponding to O-H stretches (3500 cm^{-1}), C-H stretching (3000-2800 cm^{-1}), C=O stretching (1728 cm^{-1}). As observed previously, the peaks for the pulsed film are sharper than those observed for the continuous wave film (Figure 6.7). The observed contact angle for the continuous wave film was 57.8 ± 0.8°, whilst the less cross-linked pulsed film was 41.0 ± 0.7°. These results indicate good retention of structure and correspond well with those previously observed.

Polymer	%C	%O
Theoretical	66.6	33.3
Pulsed	67 ± 1	33 ± 1
CW	73 ± 1	27 ± 1

Table 6.1. XPS Atomic Composition for 2-hydroxyethylmethacrylate.

Reaction of the HEMA substrates with the CMK was monitored by XPS (Table 6.2). Bands corresponding to the Cl(1s) and N(1s) appear on XPS survey spectra when treated with CMK. Minimal Na(1s) bands are observed from the buffer salt solutions (Figure 6.5). After 24h exposure to the reaction solution, the 2.2% N is observed is 18% of the theoretical CMK structure. The lack of Si(2p) signal from the substrate was taken to indicate survival of the hydroxyl film under the reaction conditions. There is no visible change in the C(1s) envelope (Figure 6.6).

	%Cl	%C	%N	%O
Untreated PPP HEMA	0	76	0	24
1h Exposure to CMK	0.34	76	1.3	22
24hExposure to CMK	0.63	77	2.2	20
Theoretical CMK	2.1	65	12	21

Table 6.2. XPS elemental atomic composition of HEMA surfaces treated with CMK.

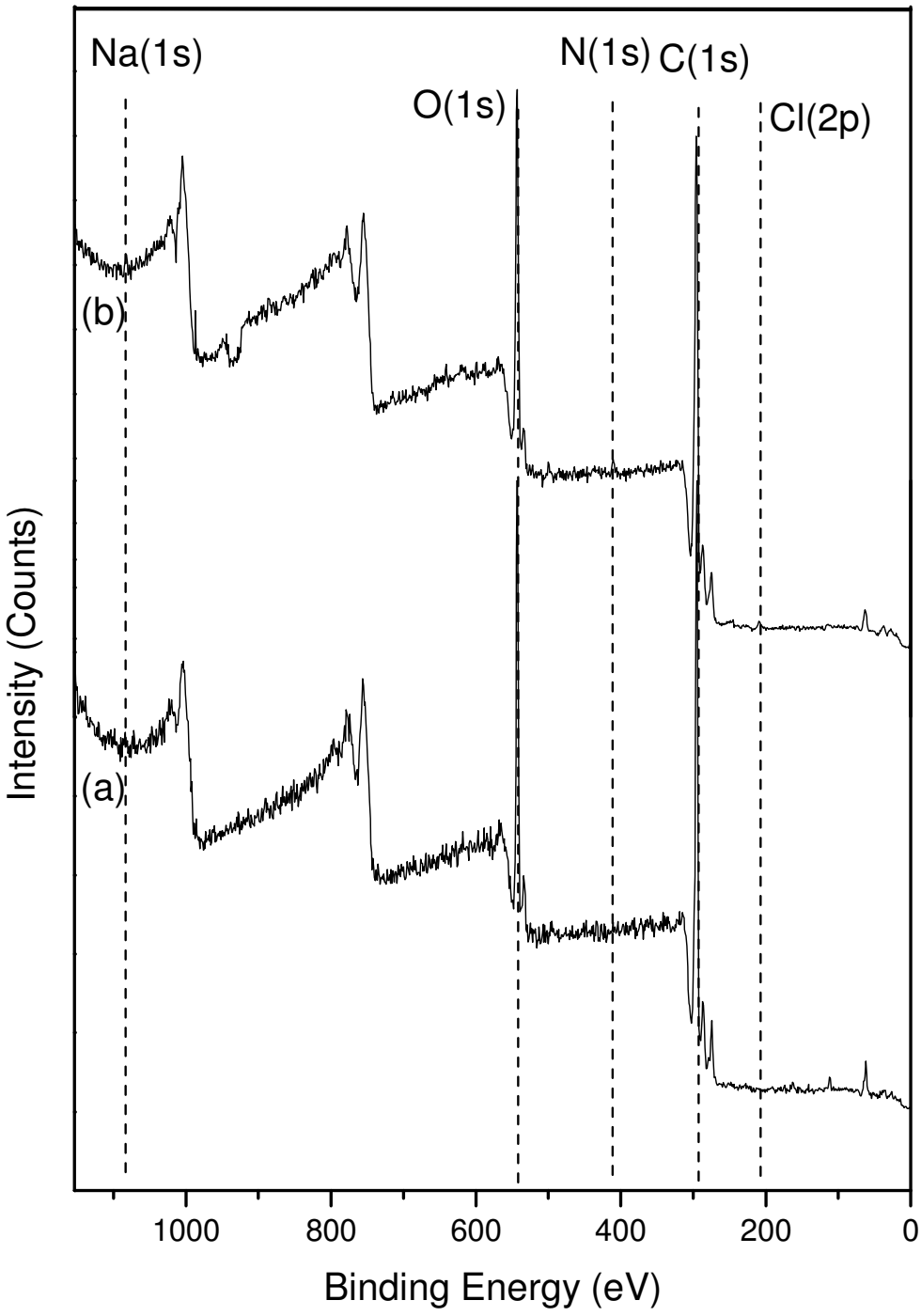

Figure 6.5 XPS wide scans of (a) Pulsed Plasmachemical Film (time on = 20 µs, time off = 20 ms, peak power = 40 W) on glass coverslip; (b) The same film following CMK immobilisation.

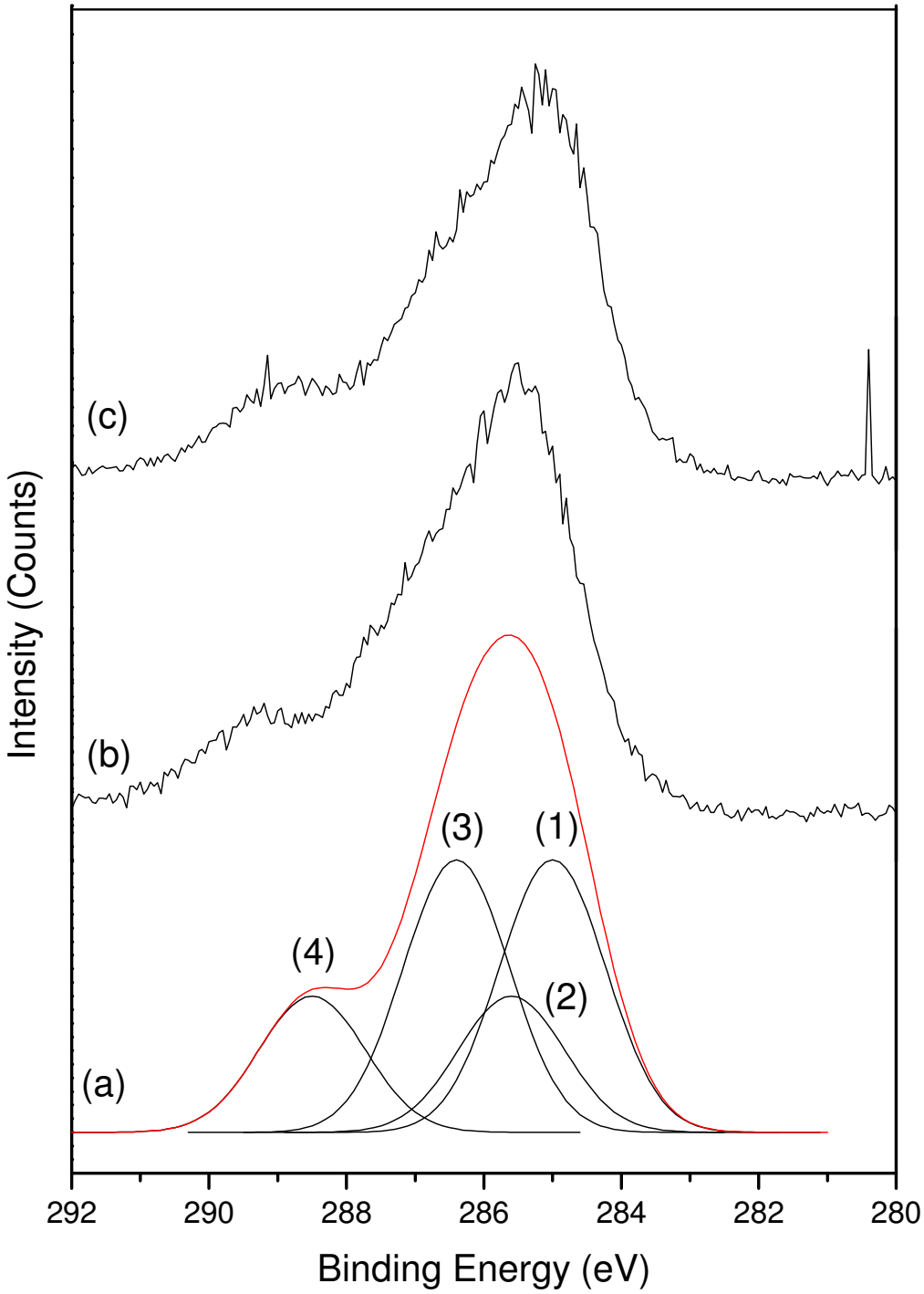

Figure 6.6. C(1s) envelopes by XPS of plasmachemical functionalised bromine surfaces (a) theoretical C(1s) envelope assuming no monomer fragmentation, (b) Pulsed Plasmachemical Film (time on = 20 µs, time off = 20 ms, peak power = 40 W) on glass coverslip; (c) The same film following CMK
immobilisation.

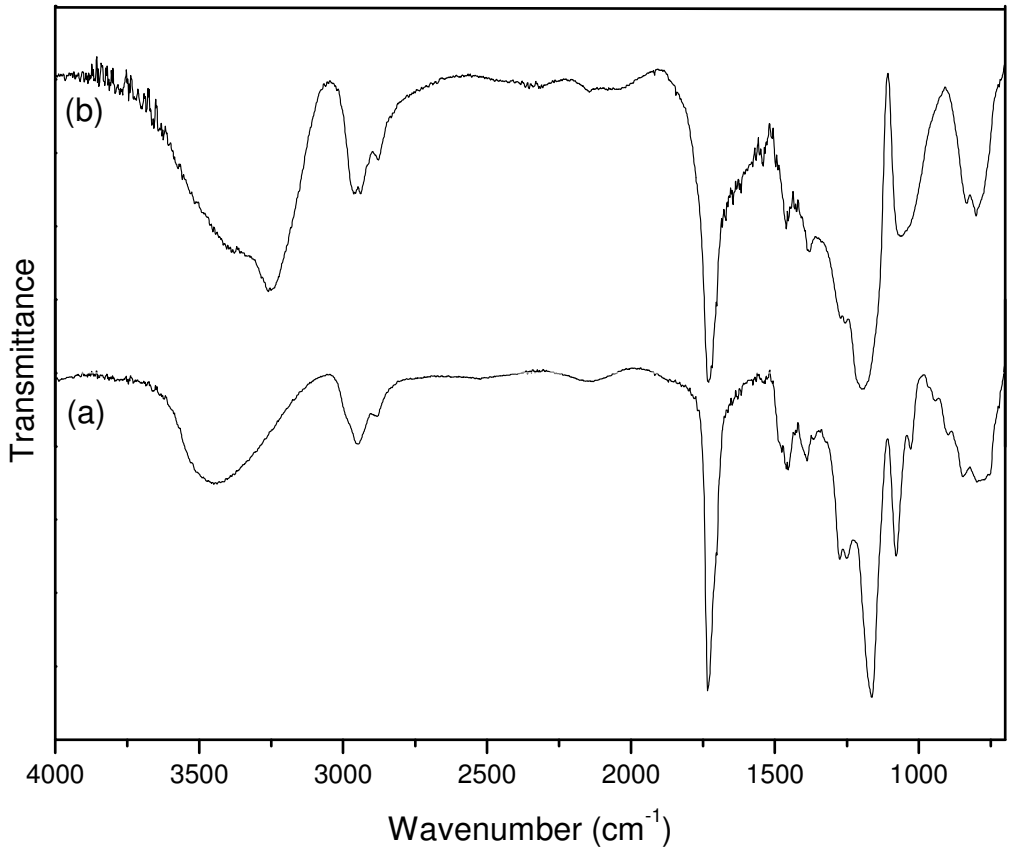

Figure 6.7. Infrared Spectra of (a) Pulsed Plasmachemical Film (time on = 20 µs, time off = 20 ms, peak power = 40 W), (b) 5 W Continuous Wave Film.

In order to confirm the presence and release of the CMK from the surface, samples of HEMA-treated borosilicate glass slides were treated with CMK and exposed to a solution containing porcine pancreatic elastase. The inhibitive effect of the CMK was monitored by following the hydrolysis of a peptide substrate. The hydrolysis reaction resulted in the production of UV-vis active *p*-nitroaniline, which allowed the progress of the reaction to be followed.

The introduction of CMK treated HEMA glass slides clearly reduces the formation of *p*-nitroaniline compared to untreated control glass coverslips. This inhibitive effect is increased as the mass of CMK modified HEMA glass substrate increases, and hence as the surface area of plasmachemical hydroxyl functions and associated CMK on the surface is increased. This

greater surface area of CMK with all other experimental conditions being equal results in a further reduction of enzyme activity (Figure 6.8).

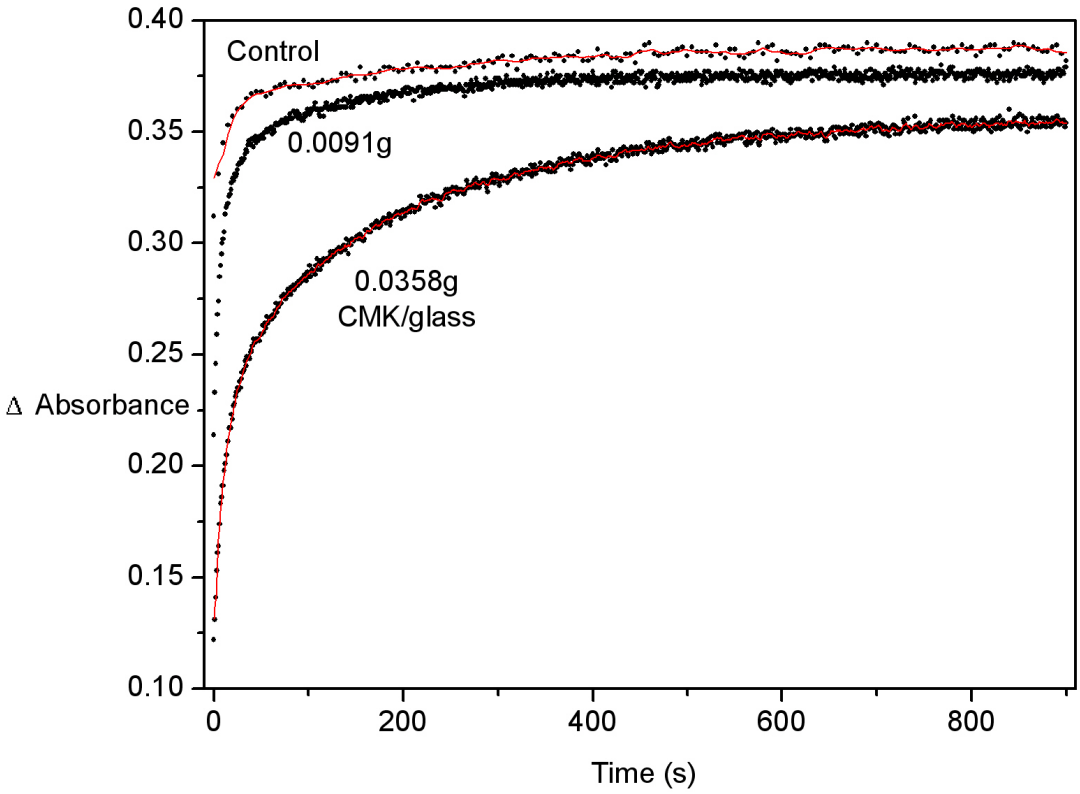

Figure 6.8. UV-Vis absorbance against time for inhibition of *p*-nitroaniline formation for various masses of CMK-HEMA treated glass cover slips of various weights introduced directly into the reaction cell. The control sample contains no CMK-glass inhibitor.

Pulsed functionalisation shows a greater inhibitive effect than the equivalent continuous wave system (Figure 6.9). This increase in enzyme inhibition probably stems from the superior structural retention offered by pulsed plasmachemical functionalisation, with a high density of hydroxyl groups and chain flexibility retained due to the relative lack of cross-linking[23]. This allows for more efficient binding and release of the CMK species in the first instance. Table 6.3 shows the initial change in absorbance as a function of time, which shows the large reduction in the initial reaction rate for both

plasmachemical routes, with a larger increase for the pulsed plasmachemical system.

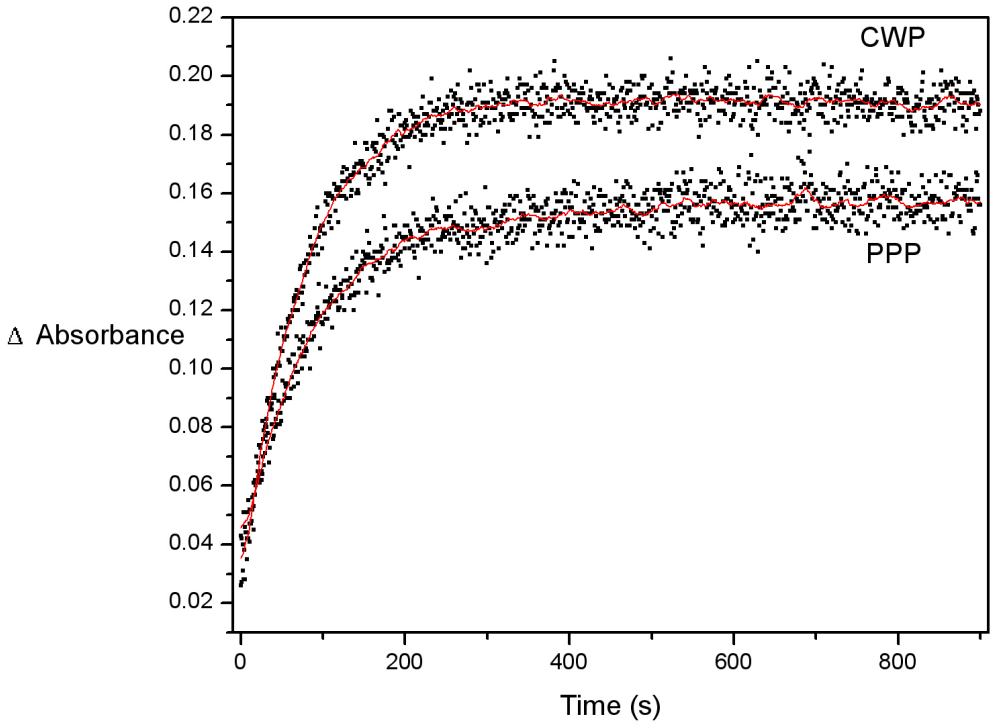

Figure 6.9. UV-Vis absorbance against time for inhibition of *p*-nitroaniline formation, a comparison of continuous wave (CWP, 5W power) and pulsed plasma (PPP, time on = 20 µs, time off = 20 ms, peak power = 40 W) HEMA layers.

	Initial Gradient ($\Delta abs.s^{-1}$)
Control	1284.7
5W CW	725.95
PPP t_{on} = 20 µs, t_{off} = 20 ms, P_p = 40 W	518.53

Table 6.3. Initial reaction gradients for porcine pancreatic elastase inhibition various CMK modified substrates

Whilst these initial results show the promise of the suggested synthetic route, there remains much work to be done to prove and to understand the binding of CMK to the hydroxyl modified surfaces. In particular the kinetics of the reaction need to be established, by a more in depth study relating absorbance to both CMK and p-nitroaniline concentrations. Hence the effect of important reaction parameters such as time, CMK concentration, and pH on the amount of CMK bound to the hydroxyl substrate could be fully studied. These parameters could then also be related to the release of CMK into a model system such as the porcine pancreatic elastase system used in this work. Studying the effect of CMK loading on the modified surface, and the amount of CMK-substrate present in the reaction system, on the inhibition of the elastase would also be desirable. Finally, once control of the CMK loading and understanding of its relation to inhibition is established, trials on actual wound fluids could be arranged to verify the activity of the smart dressing on actual patients.

A further approach might be to develop a more acidic hydroxyl surface to facilitate CMK attachment. A suitable precursor might include 4-vinylphenol, which should be readily polymerisable under pulsed conditions.

6.4 Conclusion

Initial results for the surface tethering of a CMK onto a plasmachemical hydroxyl layer confirm the promise of the proposed synthetic route for smart wound dressings. Further work is required to quantify the reactions kinetics, optimise the system and provide more control over construction.

1 Ruszczak, Z.; Schwartz, R. A. *Dermatol. Surg.* **2000**, *26*, 219

2 CIGNA HealthCare Coverage Position, Coverage Position Number 0068: "Wound Healing: Tissue Engineered Skin Substitutes and Growth Factors".

3 Gharaee-Kermani, M.; Phan, S. H. *Current Pharmaceutical Design* **2001**, *7*, 1083

4 Roy, I.; Gupta, M. N.; *Chem. & Biol.* **2003**, *10*, 1161

5 Taylor, L. M.; Mueller-Velten, G.; Koslow, A.; Hunter, G.; Naslund, T.; Kline, R. *J. Vascular Surgery* **2003**, *38*, 766

6 Kumar, S.; Wong, P. F.; Leaper, D. J. *Turk. J. Med. Sci.* **2004**, *34*, 147

7 Ozaki, C. K.; Phaneuf, M. D.; Bide, M. J.; Quist, W. C.; Alessi, J. M.; LoGerfo, F. W. *J. Surgical Res.* **1993**, *55*, 543.

8 Treiman, G. S.; Copland, S.; Yellin, A. E.; Lawrence, P. F.; McNamara, R. M.; Treiman, R. L. *J. Vascular Surgery* **2001**, *33*, 948

9 Mostow, E. N.; Haraway, G. D.; Dalsing, M.; Hoddle, J. P.; King, D. *J. Vascular Surgery* **2005**, *41*, 837

10 Kreienberg, P. B.; Clement Darling III, R.; Chang, B. B.; Champagne, B. J.; Paty, P. S. K.; Roddy, S. P.; Lloyd, W. E.; Ozsvath, K. J.; Shah, D. M. *J. Vascular Surgery* **2002**, *35*, 299

11 Fox, C. J.; Gilespie, D. L.; O'Donnell, S. D.; Rasmussen, T. E.; Goff, J. M.; Johnson, C. A.; Galgon, R. E.; Sarac, T. P.; Rich, N. M. *J. Vascular Surgery* **2005**, *41*, 638

12 Calligaro, K. D.; Veith, F. J.; Valladares, J. A.; McKay, J.; Schindler, N.; Dougherty, M. J. *J. Vascular Surgery* **2000**, *31*, 245

13 Koshland, D. E. *Proc. Nat. Acad. Sci. USA* **1958,** *44*, 98

14 Edwards, J. V.; Batiste, S. L.; Gibbins, E. M.; Goheen, S. C. *J. Peptide Res.* **1999**, *54*, 536

15 Edwards, J. V.; Bopp, A. F.; Batiste, S.; Ullah, A. J.; Cohen, I. K.; Diegelmann, R. F.; Montante, S. J. *Wound Repair and Regeneration* **1999**, *7*, 106

16 Thompson, R. C.; Blout, E. R. *Biochemistry* **1973**, *12*, 44

17 Remold-O'Donnell, E. *J. Exp. Med.***1985**, *162*, 2142

18 Navia, M. A.; McKeever, B. M.; Springer; J. P.; Lin, T.-Y.; Williams, H. R.; Fluder, E. M.; Dorn, C. P.; Hoogsteen, K. *Proc. Natl. Acad. Sci. USA* **1989**, *86,* 7

19 Bode, W.; Meyer, E.; Powers, J. C. *Biochemistry*, **1989**, *28*, 1951

20 Metz, W. A.; Peet, N. P. in "High Throughput Screening for Novel Anti-Inflammatories" Kahn, M. (ed.), Birkhäuser, **2000**, p49

21 Polgár, L. *Cell. Mol. Life Sci.* **2005**, *62*, 2161

22 Metz, W. A.; Peet, N. P. in "High Throughput Screening for Novel Anti-Inflammatories" Kahn, M. (ed.), Birkhäuser, **2000**, p49

23 Tarducci, C.; Schofield, W. C. E.; Brewer, S. A.; Willis, C.; Badyal, J. P. S. *Chem. Mater.* **2002**, *14*, 2541

24 Briggs, D.; Seah, M. P. (eds) *Practical Surface Analysis 2nd Ed.* John Wiley & Sons, Chichester, **1990**.

7. Plasmachemical functionalisation of single walled carbon nanotubes

Carbon nanotubes are attracting much interest due to their excellent mechanical and electrical properties, however a major difficulty with carbon nanotube systems is the introduction of chemical functionality onto the nanotube surface. Pulsed plasmachemical functionalisation is an ideal methodology for the modification of three dimensional structures such as carbon nanotubes. This use of plasmachemical technology is demonstrated by the electroless deposition of copper onto surface tethered pyridine functions and silver onto surface tethered aldehyde functions.

7.1. Introduction

Carbon nanotubes (CNTs) are part of the fullerene family of chemicals: long, thin, tube-like structures formed from a continuous sheet of hexagonal carbon atoms; essentially a simple sheet of graphite rolled to form a tube. CNTs can be found as single-walled structures (SWCNTs) or multi-walled structures (MWCNTs) formed when multiple concentric SWCNTs are held together by van der Waals interactions. The complexity of MWCNTs, particularly for modelling, has meant that research often focuses on the more simple SWCNTs.

CNTs are of great interest at the current time due to the many unique properties that they offer. They offer both a large surface area and superior mechanical strength. Their elastic modulus is equivalent to that of diamond and the strength of CNTs far surpasses that of materials such as steel[1]. Thus CNTs are attractive as scaffolds for nanodevice construction, and additives in composite materials[2]. The strength of CNTs is also combined with surprising flexibility[3] that allows bends of 110°.

As well as their mechanical properties, CNTs are excellent electrical conductors[4], with current capacity reported to be 1000 times that of copper[5], and thermal stability up to 2800°C. In short, CNTs offer a fertile ground for research[6,7,8], particularly for novel devices with the drive for miniaturisation[9].

However, chemical modification and processing of such inert structures is difficult. Consequently, treatment conditions are extremely difficult and typically include refluxing in acids[10], use of high temperatures[11], or the use of extremely reactive species[12].

In this section we deal with the potential benefits of plasmachemical functionalisaton for SWCNT modification. Pyridine and aldehyde functions are introduced onto SWCNTs in order to allow metallization with copper and silver respectively. By functionalising the surface of CNTs with metal it is suggested that wetting properties can be improved during composites manufacture, and the introduction of metals to the surface could allow construction of nanodevices.

The effect of plasmachemical modification on bulk carbon fibres has been examined previously and shown viable[13]. Similarly, the plasmachemical route to modifying surfaces for copper electroless deposition has already been examined in the case of continuous wave glycidyl methacrylate deposition onto PTFE[14]. Continuous wave methods have also been applied to as produced carbon nanotubes for the introduction of organic molecules[15].

Electroless deposition techniques have allowed functionalisation of CNTs with cobalt, nickel[16], gold[17], and encased in copper matrices[18]. Previous methods for the electroless deposition of copper have typically required extremely vigorous activation by refluxing in acid[19]. The root of the problem is that the substrates typically require an activation step to generate particulate Pd^0 on the substrate surface, which both acts as an initial nucleation point and also catalyses the formation of the electroless metal layer. The use of suitable ligands, such as the surface tethered pyridine ligand generated in this work, allow relatively mild conditions to be employed[20]. The electroless deposition of copper in a basic medium can then take place:

$$Cu^{2+} + 2HCHO + 4HO^- \rightarrow Cu + 2HCOO^- + 2H_2O + H_2$$

The Tollens silver mirror test is an old and widely used test for aldehyde functions in which 5% aqueous silver nitrate solution is used to form the Tollens reagent, which forms a silver mirror on the introduction of aldehyde functions[21]:

$$R\text{-}CHO + 2Ag(NH_3)_2^+ + H_2O \rightarrow R\text{-}COOH + 2Ag + 2NH_4^+$$

7.2 Experimental

Unless otherwise stated functionalisations and reactions are as outlined in previous chapters.

7.2.1 Metallization via 4-vinylpyridine functionalisation

Plasma polymerization of 4-vinylpyridine (Aldrich, 95%, H2C=CH(C_5H_4N), purified by several freeze-pump-thaw cycles) was carried out in an electrodeless cylindrical glass reactor as described in Chapter 2.

4-vinylpyridine was introduced into the reactor at a pressure of 0.22 mbar and a flow rate of 9.3 x 10^{-8} mol s^{-1} for 15 min prior to reaction. Deposition took place over 60 min in a t_{on} = 100 µs, t_{off} = 4 ms pulsing regime and a peak power of 40 W. Subsequent to reaction the chamber was flushed with monomer for 15 min. Substrates included borosilicate glass cover slips, polished silicon wafers and SWCNTs. In order to ensure uniformity of coating, only small masses of SWCNTs (<0.03g) were used in each deposition, spread thinly and evenly across the reactor plate.

0.0100 g of functionalised SWCNTs were immersed in a 0.1 % (w/v) solution of $PdCl_2$ in pH 4.5 SSC for 16 h, then filtered and washed with high purity water. SWCNTs were then immersed in 1.5% (w/v) $CuSO_4.5H_2O$, 7% (w/v) K/Na tartrate, 1% (w/v) NaOH, 50% (v/v) formaldehyde (aq. 37% concentration), 40.5% H_2O for 60min. SWCNTs were again filtered and excess reaction solution removed by copious washing with high purity water.

7.2.2 Metallization via 3-vinylbenzaldehyde functionalisation

Deposition of aldehyde functions from 3-vinylbenzaldehyde precursors is described in Chapter 4.

0.0100g of functionalised SWCNTs were immersed in a solution containing 4.532 ml H_2O, 0.468 ml NH_4OH (Aldrich, 25% - in H2O), 0.0850 g $AgNO_3$ (Apollo 97%) for 16 h. SWCNTs were filtered and washed in excess high purity water.

7.2.3 Surface Analysis

The surface analysis conditions used for XPS, FT-IR, and reflectometry were as outlined in previous chapters.

7.3. Results

7.3.1 Metallization via 4-vinylpyridine functionalisation

The plasmachemical functionalisation of surfaces with 4-vinylpyridine (t_{on} = 100 µs, t_{off} = 4ms, P_P = 40 W) was followed by XPS, which showed good correspondence with the expected surface atomic composition (77% C, 12%N, 10%O), with the C(1s) envelope lacking any major oxygenated components (Figure 7.1, FWHM 2.4). Separate peaks relating to the aromatic carbons (284.6 eV), C_xH_y (285.0 eV), and aromatic CN (286.4 eV) are not resolved. In each case a simple Gaussian was used to model the observed spectra. The N(1s) peak at 398.8 eV (FWHM 2.3) in consistent with aromatic nitrogen. The O(1s) signal peaks at 532.0 eV (FWHM 1.7) [22,23]. A corresponding deposition rate of 8 ± 1 nm min^{-1} was observed.

Analysis of the as-deposited films by FT-IR confirmed deposition of 4-vinylpyridine with good structural retention (Figure 7.2), with the major bands from the monomer retained and only minor line broadening. In particular, bands from the aromatic pyridine function are retained at 1600 and 1410 cm^{-1}. Both monomer and functionalised layer show broad bands in the 3000-3500 cm^{-1} region, which are attributed to adsorbed water on the hydrophilic surface.

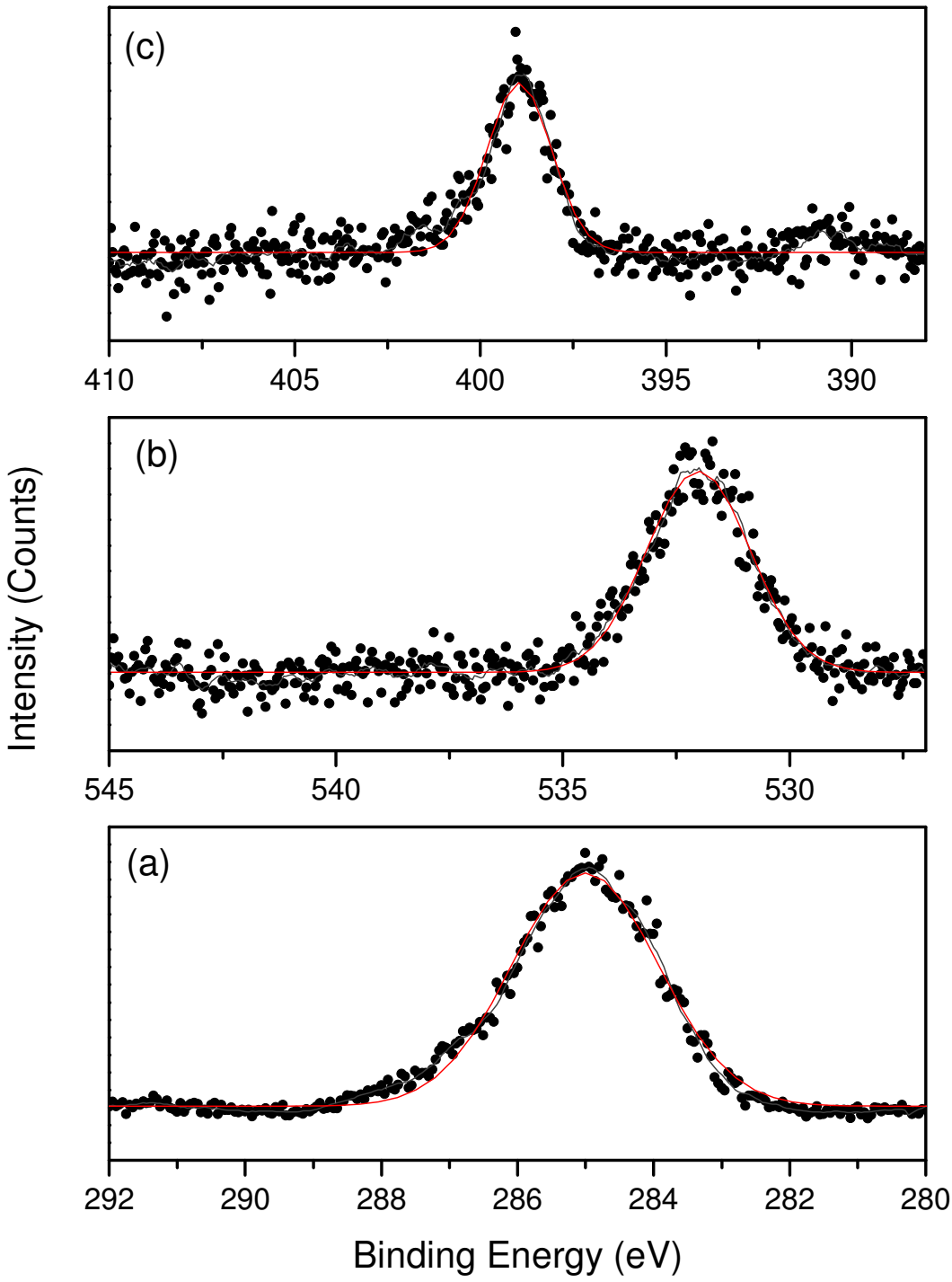

Figure 7.1 High resolution XPS spectra of plasmachemical pyridine elemental envelopes. (a) C1s; (b) O1s; (c) N1s. Data fitting in each case is a single Gaussian peak.

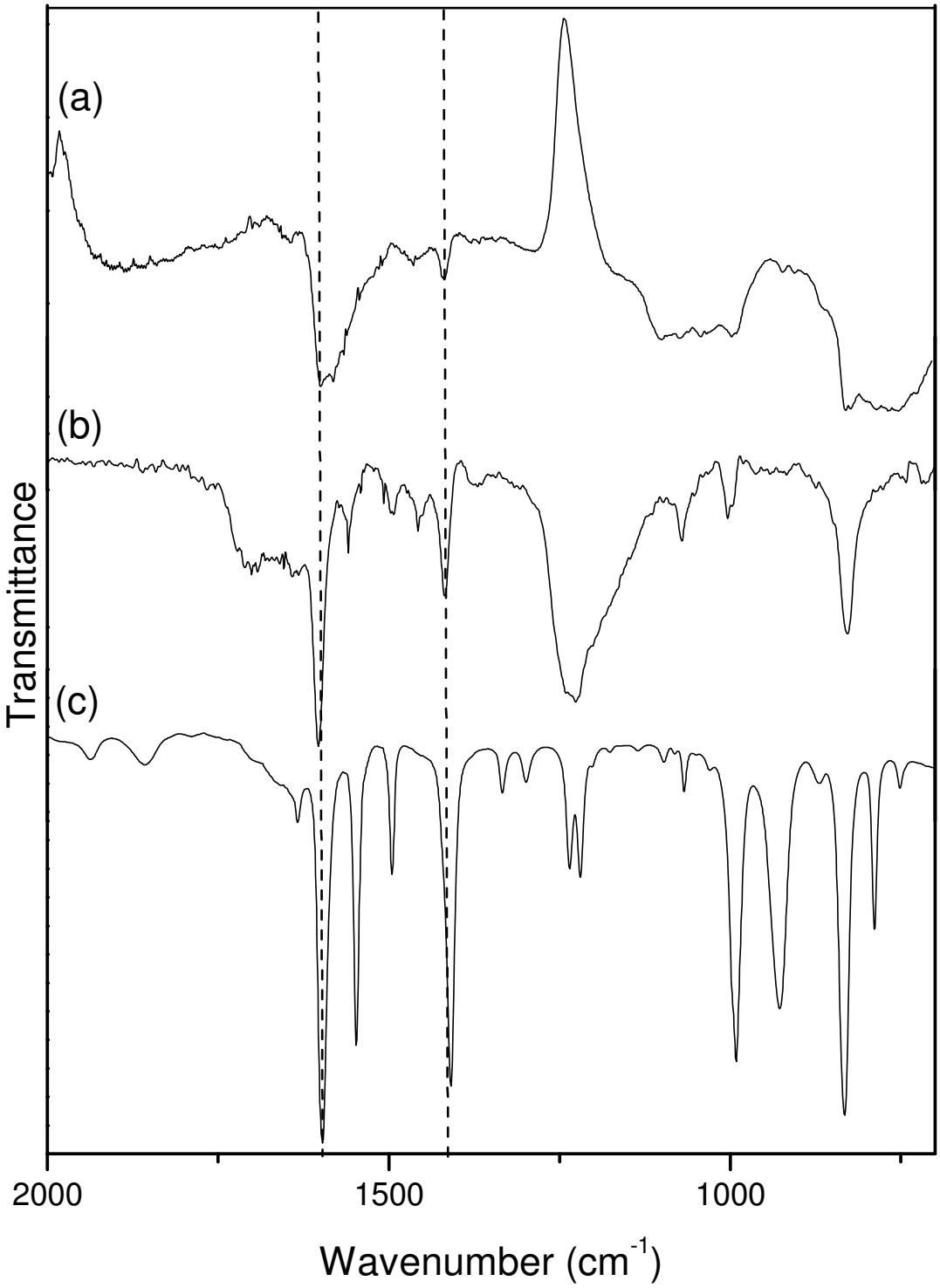

Figure 7.2. FT-IR of 4-vinylpyridine (a) as deposited on SWCNT, (b) as deposited on silicon wafer, and (c) 4-vinylpyridine precursor. Highlighted are the characteristic pyridine ring stretches at 1600 cm^{-1} and 1410 cm^{-1}.

System	C (1s) %	N (1s) %	O (1s) %	Cu (2p3/2) %
Unmodified SWCNT	100	0	0	0
SWCNT with plasmachemical vinylpyridine layer	77 ± 8	12 ± 7	10.2 ± 0.2	0
SWCNT, pyridine functionalised, exposed to metallization solution	76 ± 8	0	21 ± 8	2.6 ± 0.5

Table 7.1. Surface atomic composition of SWCNT powders.

The metallization reaction resulted in visible changes. Copper mirrors were observed for Si substrates modified with vinyl pyridine and $PdCl_2$ and flecks of copper were observed in the resulting CNT powder. Exposure of as-produced vinyl pyridine and unmodified control surfaces to the reaction solution did not result in a visible change.

The metallization reaction was also followed by XPS. Flat silicon substrates confirmed the deposition of copper, showing only carbon (84 %) and copper (16%). XPS of plasmachemical functionalised SWCNTs themselves also showed copper (3%), carbon (76%) and oxygen (21%) (Table 7.1). High resolution examination of the Cu ($2p_{3/2}$) envelope shows a noisy peak at 933.0 eV (Figure 7.3).

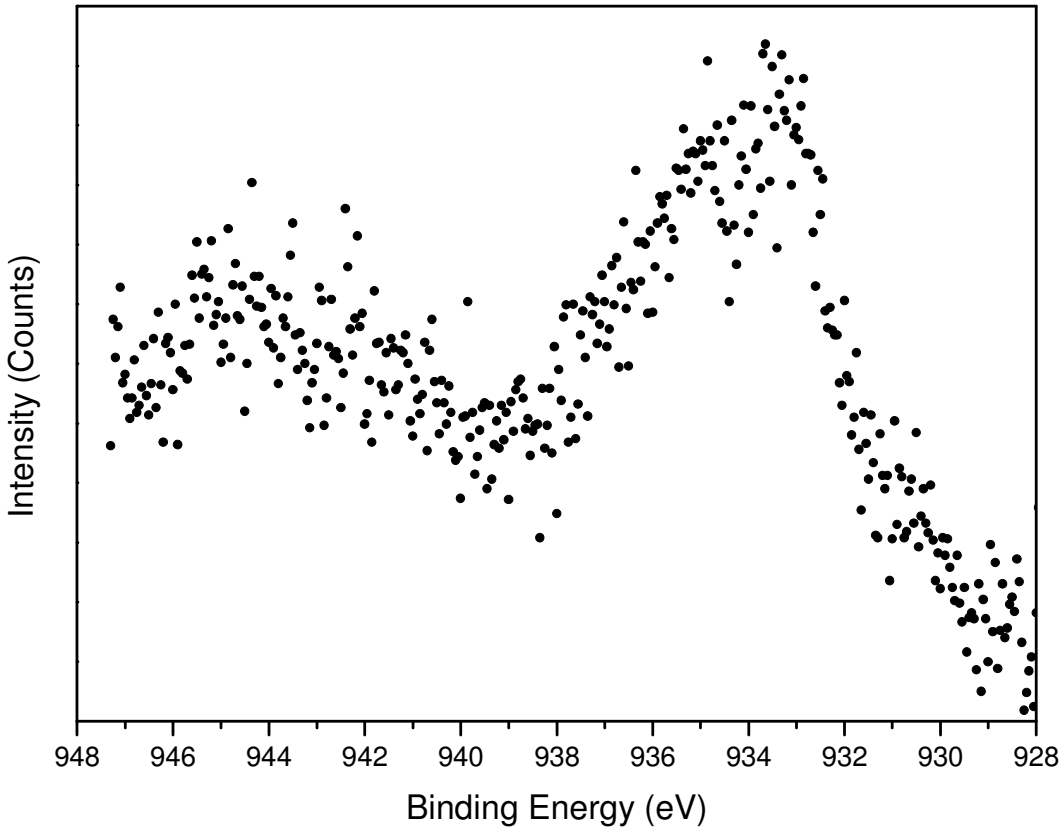

Figure 7.3 Cu ($2p_{3/2}$) envelope of metalized CNTs.

The functionalisation was also monitored by SEM and backscattered electron imaging. SEM imaging of the unmodified SWCNT showed both individual SWCNTs and regions of bulk carbon (Figure 7.4a), the SWCNTs were from the same batch as those used in Chapter x, and the bulky features are attributed to amorphous carbon. BEI showed no presence of heavy elements, with only the cloudy background of the bulk carbon visible.

Plasmachemical functionalisation with 4-vinylpyridine shows no discernable difference from the unmodified SWCNTs by either SEM or BEI imaging (Figure 7.5). The surface appearance of the metallized SWCNT's differs markedly from both the untreated SWCNT substrate and plasmachemically functionalised SWCNT's. A bulbous texture is observed and individual bundles are coated to tens of nanometers thickness. This bulbous appearance is attributed to the merging of individual copper nucleation/growth sites along the functionalized SWCNT surface. The BEI is

clearly resolved, with intense signals corresponding to the thick coating (Figures 7.6 and 7.7)

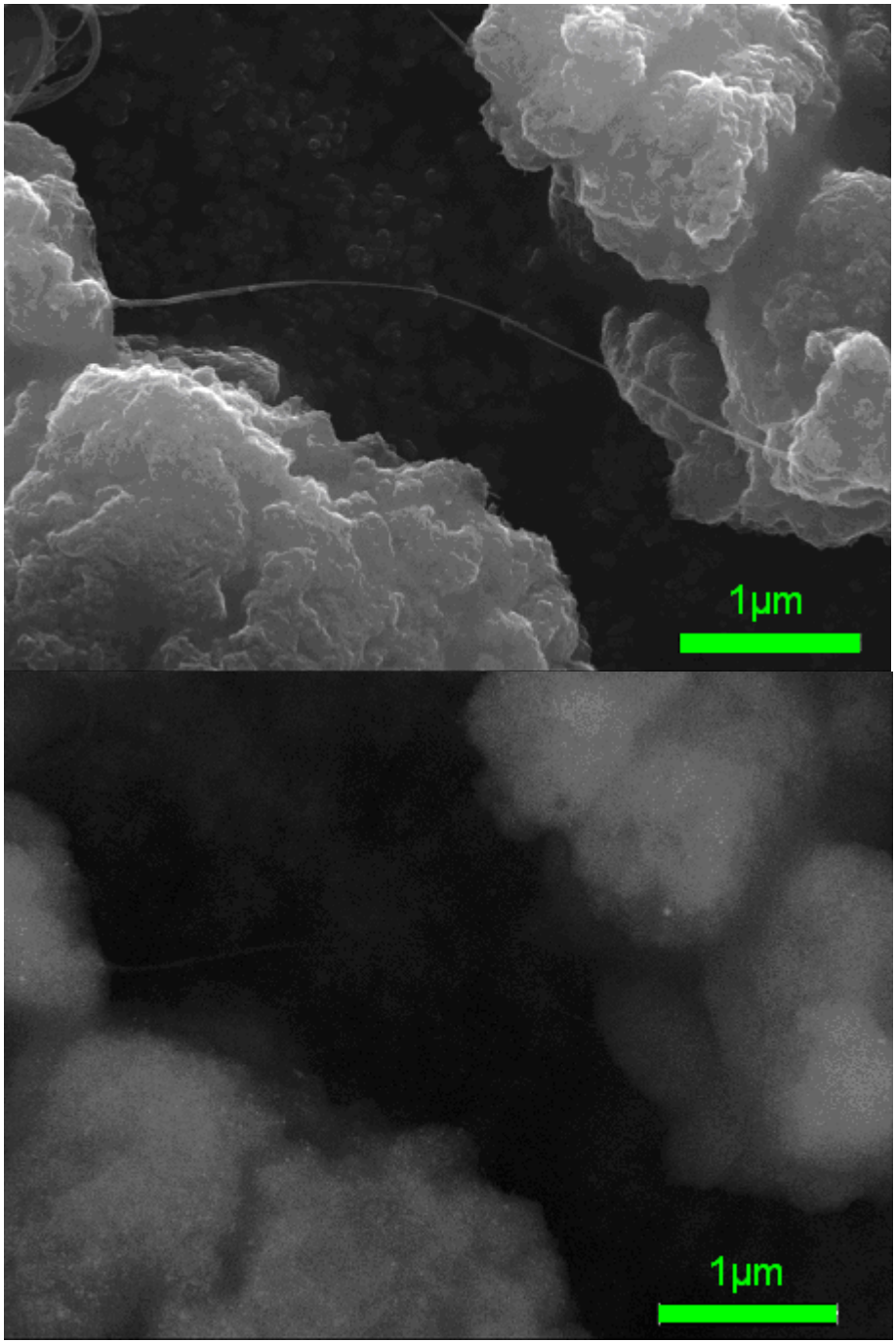

Figure 7.4. a) SEM of unmodified SWCNT powder shows both individual bundles and bulky carbon deposits. b) Resolution by BEI shows few features, with only the bulk substrate weakly visible.

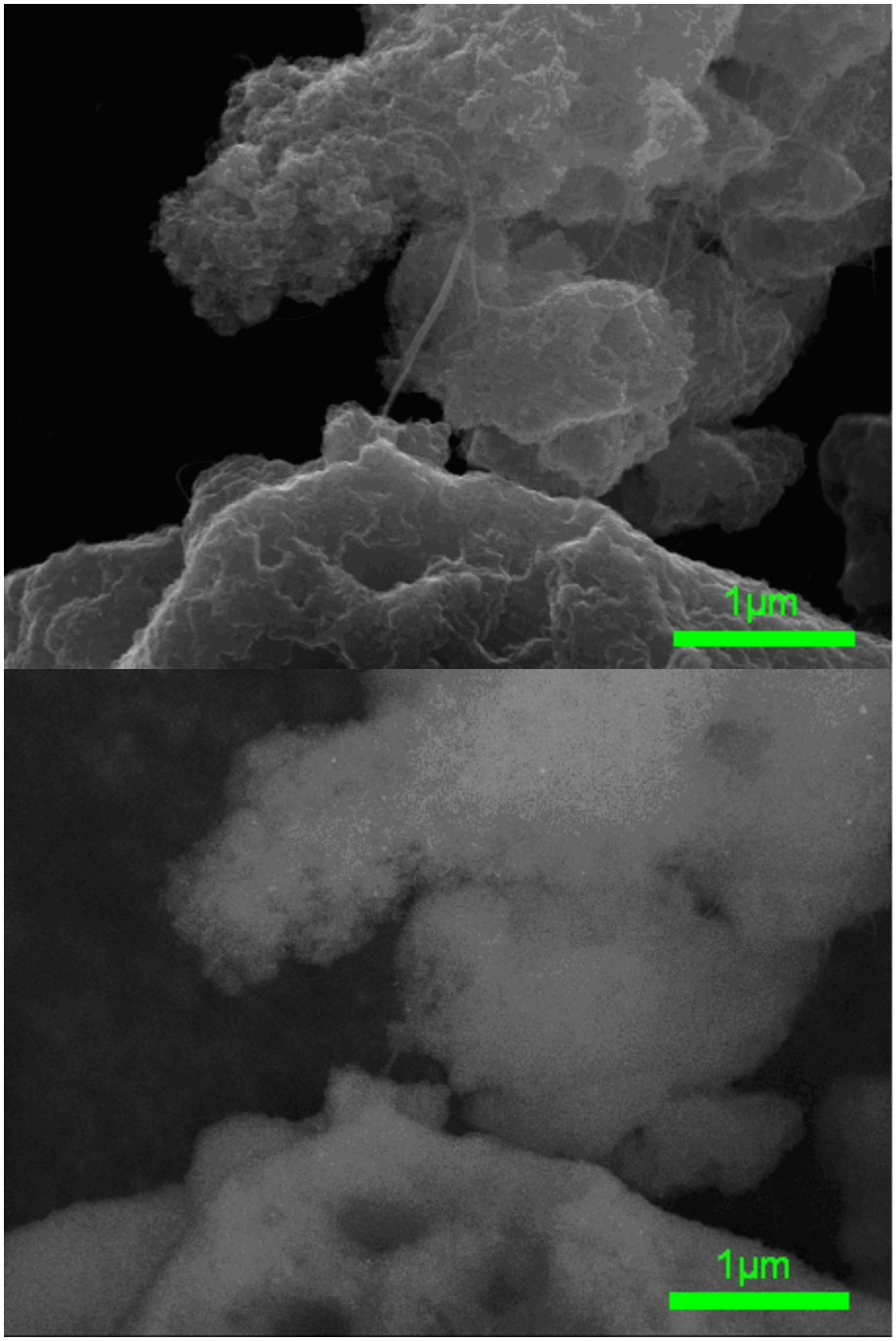

Figure 7.5. Plasmachemical functionalisation of SWCNT substrate. No significant change is visible either by a) SEM imaging or b) BEI imaging.

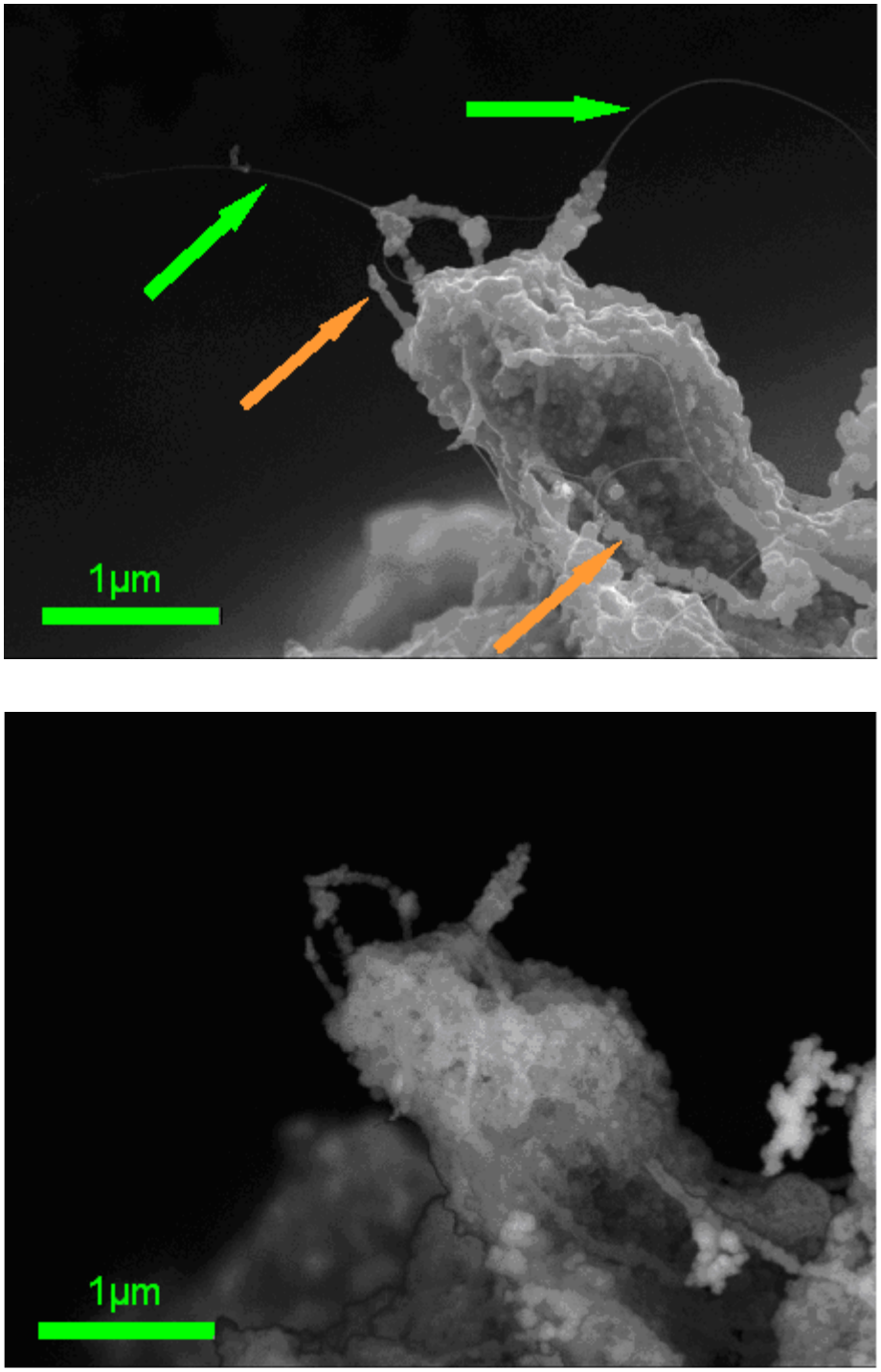

Figure 7.6. Metallization of vinylpyridine plasmachemical functionalised SWCNT substrate. a) SEM image showing deposits (green arrows showing uncoated, and orange arrows coated carbon nanotubes). b) The corresponding BEI showing an intense response from regions in which bulbous deposition is observed.

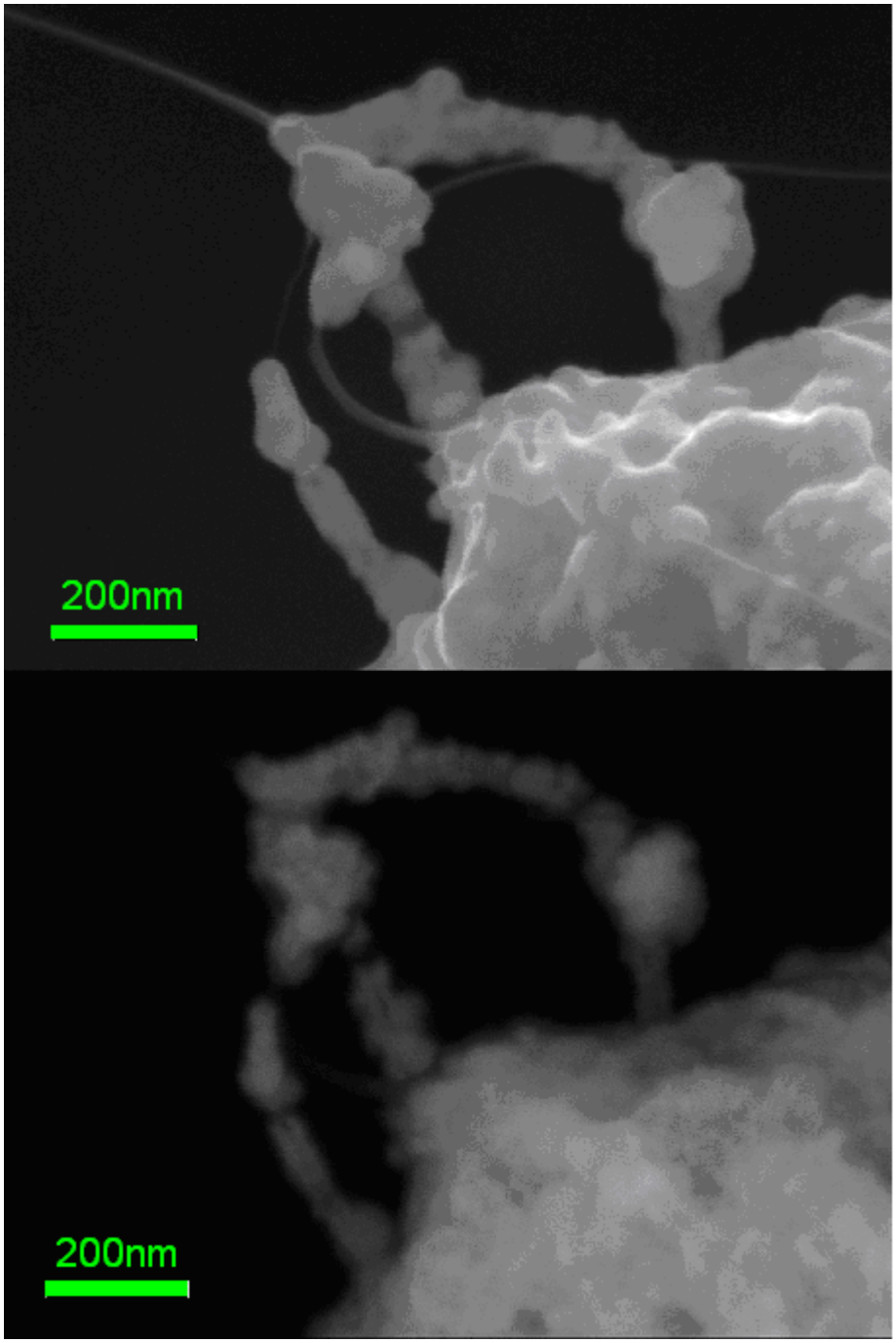

Figure 7.7. High resolution detail of vinylpyridine plasmachemical functionalised SWCNT. a) SEM image showing metal coated bundles. b) Corresponding BEI image showing signal only from metal layer, with the SWCNT ‘core’ clearly visible.

7.3.2 Metallization via 3-vinylbenzaldehyde functionalisation

The plasmachemical functionalisation of SWCNTs with 3-vinylbenzaldehyde (t_{on} = 50 µs, t_{off} = 4ms, P_P = 40 W) was monitored by XPS and showed excellent correspondence with the expected polymer structure (C = 90%, O = 10%), with the well resolved C(1s) envelope previously observed on flat substrates retained[24] (Figure 7.8). The functionalisation was also followed by FT-IR which also confirmed excellent structural retention (Figure 7.9). The vinyl stretch at 1650 cm^{-1} in the monomer is not present on in the SWCNT powder, although bands corresponding to the aldehyde CHO function at 2815 cm^{-1} and 2723 cm^{-1} are retained, as is the carbonyl band at 1695 cm^{-1}.

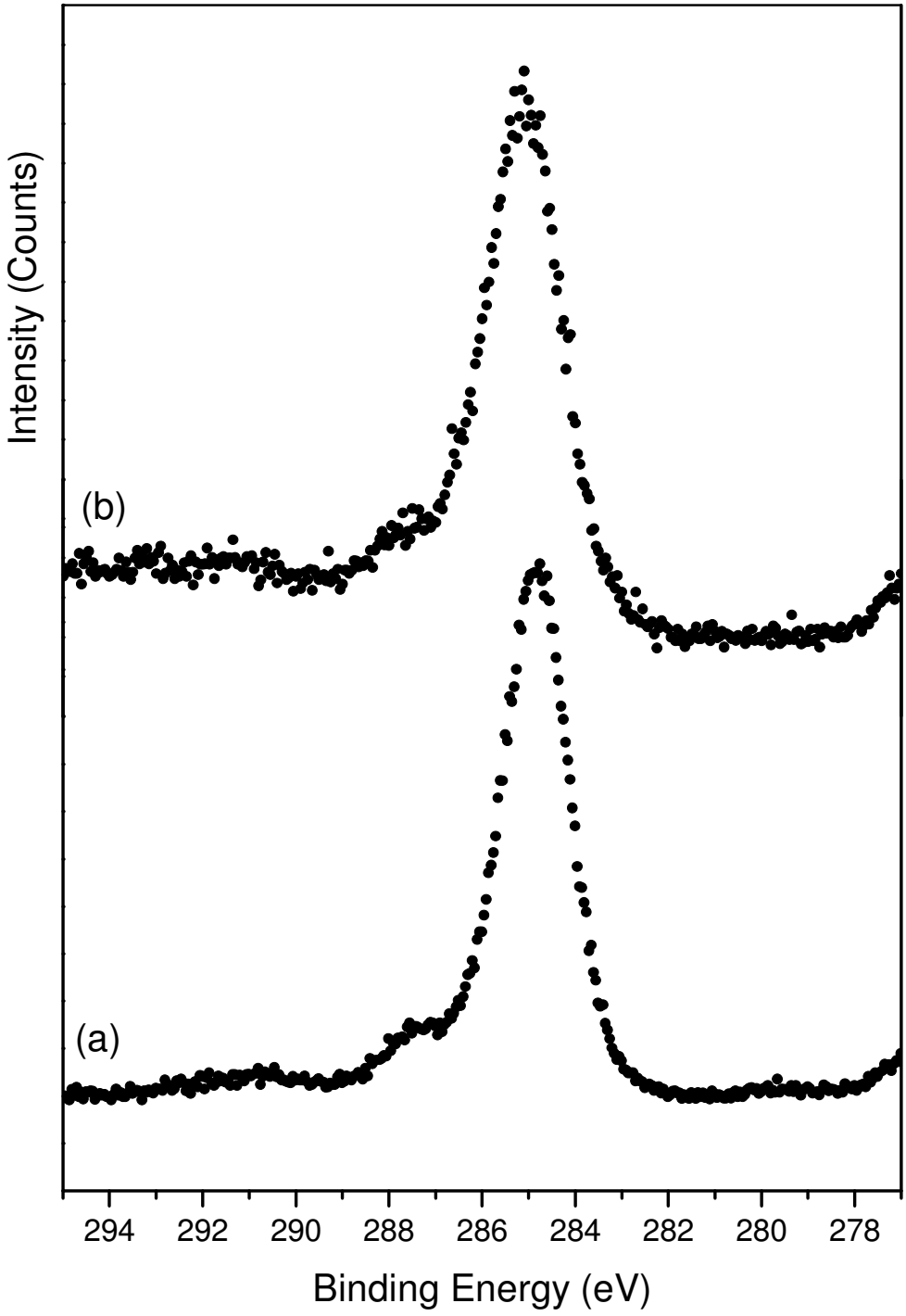

Figure 7.8. C(1s) envelopes of (a) pulsed plasmachemical 3-vinylbenzaldehyde on borosilicate glass substrate. (b) pulsed plasmachemical 3-vinylbenzaldehyde on CNTs.

The metallization of SWCNT was monitored by XPS. Silver is clearly observed on all SWCNT samples (Table 7.2). The high resolution Ag (3d) envelope shows two peaks corresponding to metallic Ag; Ag $3d_{5/2}$ at 369.2 eV and Ag $3d_{3/2}$ at 375.2 eV (Figure 7.10). The metallization was also monitored by SEM and BEI. Plasmachemical functionalisation of the SWCNTs produced no apparent change in their appearance by SEM, and the BEI retained its cloudy appearance (Figure 7.11). The metallization reaction produces a strong change in physical appearance, with several apparently cubic features now present, although the bulk is unmodified. Examination of the same region by BEI highlights these same features strongly, indicating the presence of a heavy element. The bulk retains the cloudy, indistinct appearance, showing no observable change (Figure 7.12).

System	C (1s) %	O (1s) %	Ag (p3/2) %
Unmodified SWCNT	100	0	0
SWCNT with plasmachemical 3-vinylbenzaldehyde layer	90 ± 2	10 ± 2	0
Silver metalized with 0.25 M silver nitrate solution	68 ± 5	28 ± 4	4 ± 2
Silver metalized with 1.0 M silver nitrate solution	77 ± 7	20 ± 5	3 ± 2
Silver metalized with 1.5 M silver nitrate solution	76 ± 3	23 ± 3	1 ± 1

Table 7.2. Surface atomic composition of SWCNT powders obtained during metallization with silver nitrate.

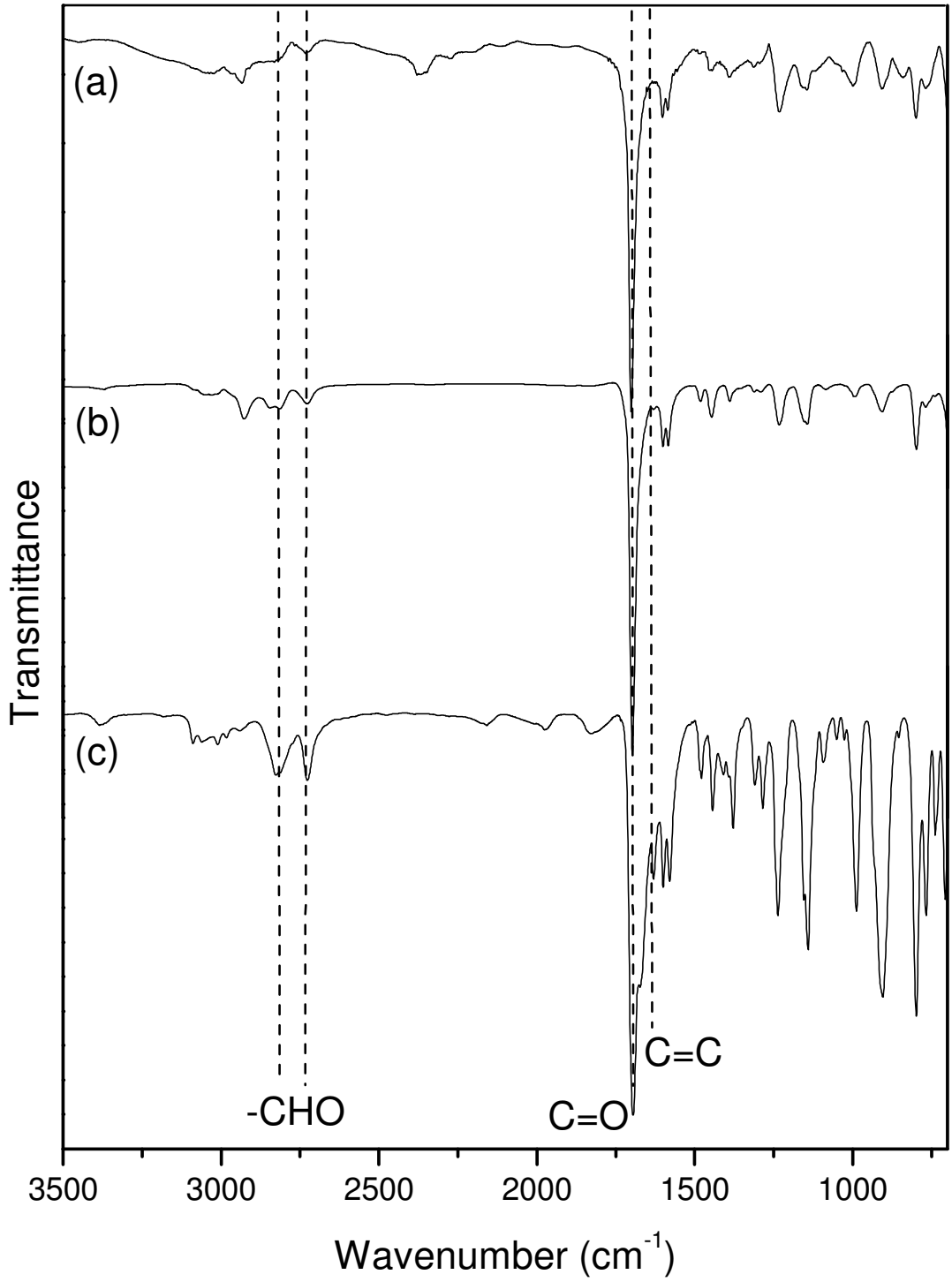

Figure 7.9. FT-IR of 3-vinylbenzaldehyde (a) as deposited on SWCNT, (b) as deposited on silicon wafer, and (c) 3-vinylbezaldehyde precursor. Highlighted are the aldehyde CHO stretches at 2815 and 2723 cm^{-1}, and the carbonyl stretch at 1695 cm^{-1}. Also highlighted is the C=C bond (1650 cm^{-1}) present in the monomer which is lost in the polymers.

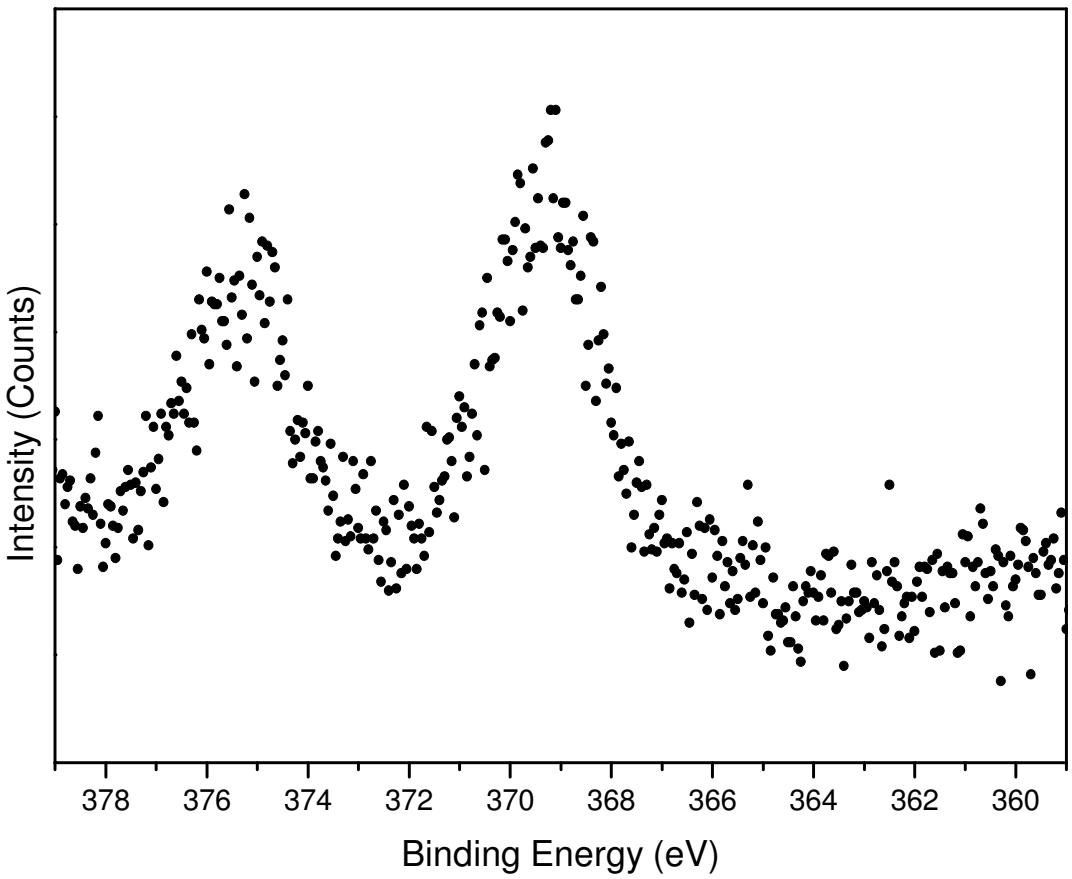

Figure 7.10 High resolution Ag (3d) envelope of silver deposited on CNTs via Tollens reaction with suface immobilised 3-vinylbenzaldehyde.

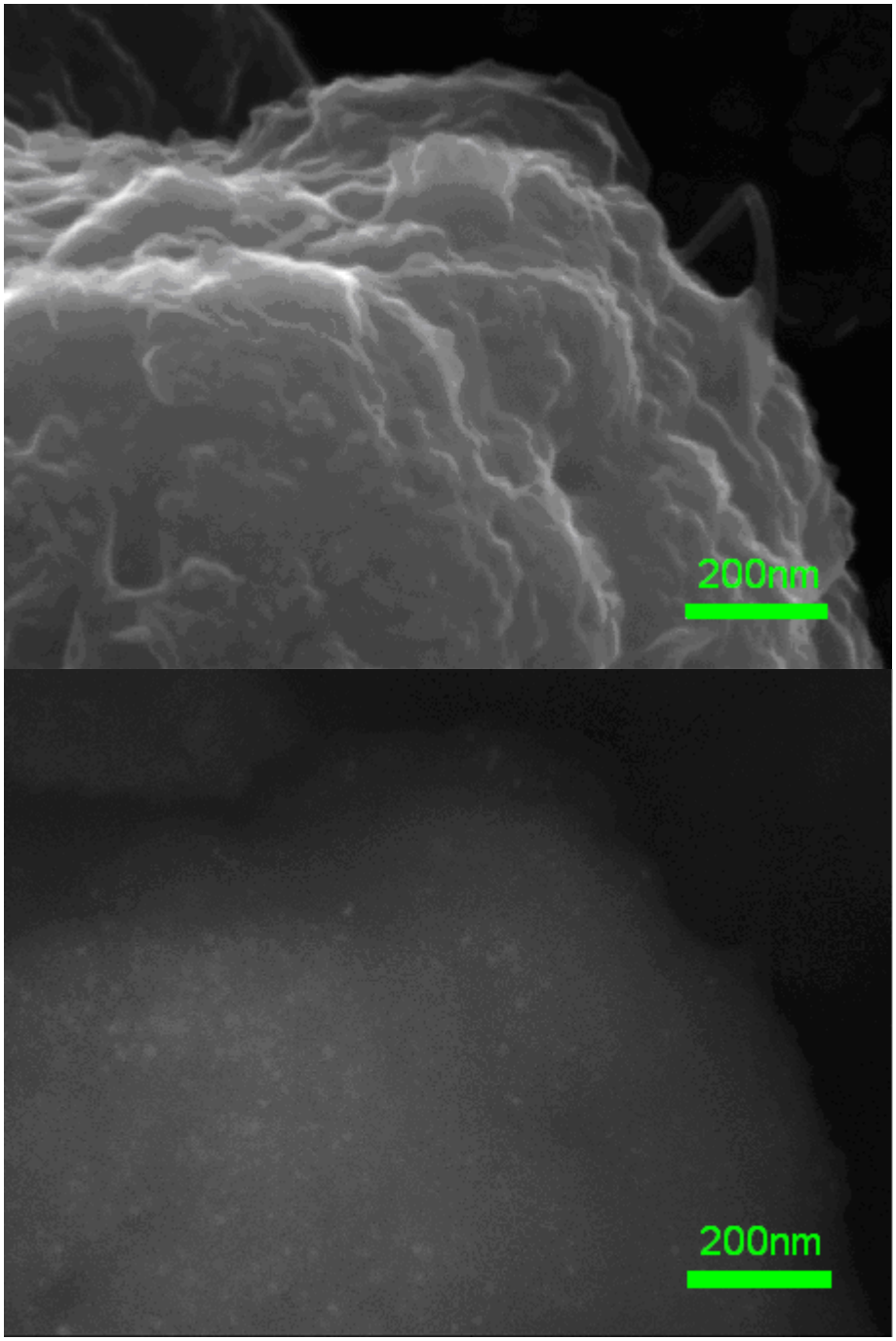

Figure 7.11. Plasmachemical functionalisation of SWCNTS with 3-vinylbenzaldehyde as observed by a) SEM and b) BEI

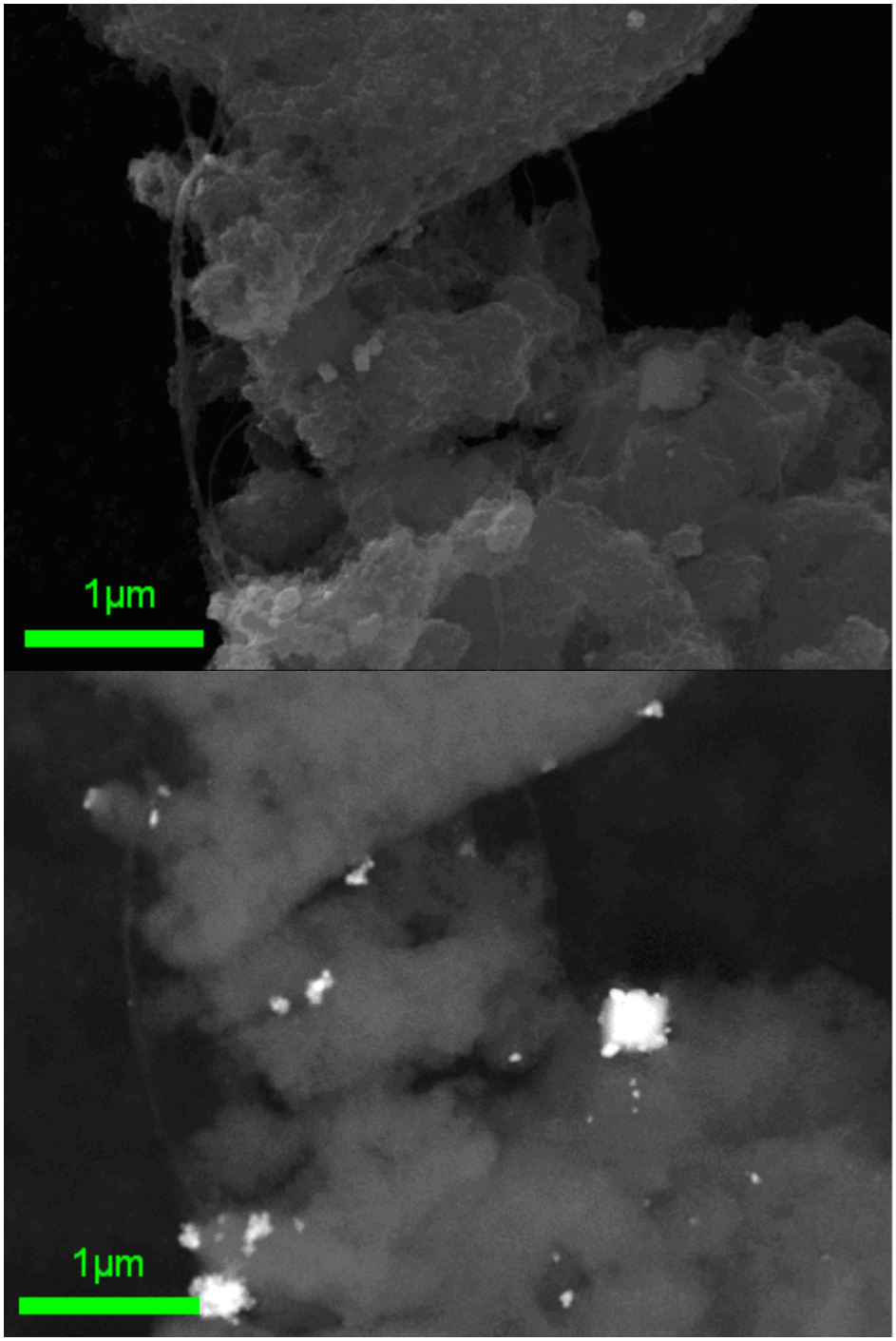

Figure 7.12. Silver metallization of aldehyde functionalised SWCNT's as observed a) SEM and b) BEI

7.4. Discussion

Plasmachemical functionalisation is not applicable only to a range of surface chemistries, but as modification takes place using monomer vapour, is also suitable for the modification of varied substrate architectures. Substrates such as SWCNT's with high surface area and unique physical properties are one novel architecture that is attracting much interest.

Plasmachemical functionalisation of SWCNTs with monomers such as 4-vinylpyridine and 3-vinylbenzaldehyde demonstrate the applicability of this technique to introduce chemical functionality onto SWCNT surfaces. The introduction of plasmachemical functionalised layers onto the SWCNT substrate was confirmed both by both XPS and FT-IR, with the monomer structures largely retained, except for the alkene C=C which is lost as the polymerisation reaction proceeds.

The metallization of the pyridine functionalised SWCNT surface was confirmed by both XPS and SEM. The coating of the SWCNTs is observed in the SEM images (Figure 7.7) where the bulbous sheath on the SWCNTs is attributed to surface immobilised copper. The high resolution images of the bundles show that the coating is tens of nanometres in diameter, leaving the uncoated SWCNT cores and the amorphous carbon deposits visible by XPS, resulting in a low observed copper signal. As part of any future work it would be desirable to establish if increased, or repeated, treatment resulted in superior surface coverage, particularly given the large surface area of the SWCNTs in comparison to flat substrates.

The uniform surface appearance is marred only by the bulbous appearance of the coating that is attributed to the coalescing of individual nucleation sites during the metallization reaction. For application of this process to, for instance, the construction of copper molecular wires via plasmachemical functionalisation an annealing step might be required to produce a wholly uniform surface. Also, a minority of the CNT bundles are not treated – the large surface area of the CNTs probably requires a slightly higher metallization solution to SWCNT ratio. The largely complete, largely uniform

appearance indicates the benefits of introducing a suitable chemical function to the surface of substrates such as SWCNTs for the controlled construction of nano-scale devices. The plasmachemical route compares favourably with traditional electroless methods, where coatings are also polycrystalline[25], and of varied thicknesses of 40 – 300 nm[2627]. The coating thickness is also comparable to that reported previously for Ni-P coatings of 70-90 nm with comparable uniformity[18].

This route would be worth exploring in more depth as the vigorous activation steps utilised for nanotube activation in other methods[19] are avoided by the plasmachemcial route. The loading of CNT's and the composition of the reaction solution could be varied to produce wires with differing copper thickness, and the effect of an annealing step examined.

Metallization with silver via a 3-vinylbenzaldehyde plasmachemically modified substrate provided a less uniform result. Although the functionalisation is confirmed again by XPS and FT-IR, the metallization reaction does not result in surface coverage of the modified SWCNT substrates. Rather than the desired metal deposition along the substrate, the silver forms distinctive particles that do not appear to be associated with any particular surface feature such as the nanotube bundles. Electroless deposition of conducting materials onto insulating substrates tends to proceed via an island growth mechanism whereby the rate of growth of crystal nuclei is faster than the rate of nucleation onto the surface[28]. The observed particles of silver on the SEM images are consistent with this preferential growth.

Whilst the introduction of silver particles onto the surface in such a manner is less applicable to nanodevice construction, it does offer some potential use for antibacterial surfaces where the release of silver is a key requirement. The use of this synthetic route to produce antibacterial surfaces, such as smart wound dressings as highlighted in Chapter 6, should be considered for the future as it would require little modification of the current method. Optimisation of the reaction on fabric surfaces would probably be required, followed by testing on bacteria cultures.

7.5. Conclusions

The applicability of the plasmachemical functionalisation technology to SWCNT's has been demonstrated by the metallization of pyridine modified SWCNTs with copper to form wire like structures, and by the introduction of silver particles onto the nanotube surface. The copper was demonstrated to be in metallic form and form a sheath like structure around the SWCNT to give a wire like structure. The metallization with silver also resulted in metallic silver deposition but this was not resolved as being specifically bound to the SWCNTs but is present as particles within the SWCNT powder.

---

1 Falvo, M. R.; Clary, G. J.; Taylor, R.; Chi, V.; Brooks, F. P. J.; Wasburn, S.; Superfine, R. *Nature* **1997**, *389*, 62

2 Thostensona, E, T.; Renb, Z.; Choua, T.-, W. *Composites Science and Technology* **2001,** *61*, 1899

3 Iijima, S.; Brabec, C.; Maiti A.; Bernholc, J. *J. Chem. Phys.* **1996**, *104*, 2089

4 Odom, T. W.; Huang, J. L.; Kim, P.; Lieber, C. M. *Nature* **1998**, *391*, 62

5 Collins, P. G.; Avouris, P. *Scientific American* **2000**, *283*, 62.

6 Fuhrer, M. S.; Nygard, J.; Shih, L.; Forero, Y. G.; Yon, Y. G.; Mazzoni, M. S.; Zettl, A.; McEuen, P. *Science* **2000**, *288*, 294

7 Rosen, R.; Simendinger, W.; Debbault, C.; Shimonda, H.; Stoner, L.; Zhou, O *Appl. Phys. Lett.* **2000**, *76*, 1668

8 Smith, B.; Luzzi, D. *Chem. Phys. Lett.* **2000**, *321*, 169

9 Seidel, R. V.; Graham, A. P.; Duesberg, G. S.; Liebau, M.; Unger, E.; Kreupl, F.; Wolfgang Hoenlein, W. 12th GAAS Symposium - Amsterdam, **2004**

10 Dai, L. *Polym. Adv. Technol.* **1999**, *10*, 357

11 Chen, J.; Hamon, M. A.; Hu, H.; Chen, Y.; Rao, A. M.; Eklund, P. C. **1998**, *282*, 95

12 Bannerjee, S.; Wong, S. S. *J. Phys. Chem. B* **2002**, *106*, 12144

13 Kettle, A. P.; Beck, A. J.; O'Toole, L.; Jones, F. R.; Short, R. D. *Comp. Sci. Technol.* **1997**, *57*, 1023

14 Yang, G. H.; Kang, E. T.; Neoh, K. G. *J. Polym. Sci.A: Polym. Chem.***2000**, *38*, 3498

15 Chen, Q.; Dai, L.; Gao, M.; Huang, S.; Mau, A. *J. Phys. Chem. B* **2001**, *105*, 618

16 Li, J., Haslett, T. L., Moskovits, M., ***Chem.*** Mater., 1998, 1963.

17 Lü, W Mat. Res. Soc. Symp. Proc. **2004**, 820 ©

18 Chen, W. X.; Tu, J. P.; Wang, L. Y.; Gan, H.Y.; Xu, Z. D.; Zhang, X.B. *Carbon* **2003**, *41*, 215

19 Probst, C.; Goujon, C.; Gauvin, R.; Drew, R. A. L. *J. Am. Chem. Soc. 26*, 263

20 Djokic, S. in *Modern aspects of Electrochemistry*, Conway, B. E.; White, R. E. (eds) **2002,** Kluwer Academic / Plenum Publishers, New York.

21 Sigga, S.; Segal, E. *Anal. Chem.* **1953**, *25*, 640

22 Beamson, G.; Briggs, D. *High Resolution XPS of Organic Polymers The Scienta ESCA300 Database*, Wiley, Chichester **1992**.

23 Cecchet, F.; Pilling, M.; Hevesi, L.; Schergna, S.; Wong, J. K. Y.; Clarkson, G. J.; Leigh, D. A.; Rudolf, P. *J. Phys. Chem. B* **2003**, *107*, 10863

24 Chapter 5

25 Ang, L. M.; Hor, T. S. A.; Xu, G. Q.; Tung, C. H.; Zhao, S. P.; Wang, J. L. S. *Carbon* **2000**, *38*, 363

26 Wang, F.; Arai, S.; Endo. M. *Electrochem. Comms* **2004**, *6*, 1042

27 Xu, C.; Wu, G.; Liu, Z.; Wu, D.; Meek, T. T.; Han, Q. *Mater. Res. Bull.* **2004**, *39*, 1499

28 Zhao, H.; Cui, J. *Surf. Coat. Technol*. **2007,** *201*, 4512

8. Conclusions and Future Work

8.1 Plasmachemical Functionalisation

The preceding experimental chapters outline the key strengths of plasmachemical functionalisation. As well as the ability to introduce specific chemistries onto a surface, the various plasma parameters can be adjusted in order to tailor material response to specific tasks. For instance, the ability to introduce a degree of cross-linking to the plasmachemical layer would allow more robust layers where exposure to damaging environments was of concern, albeit with some sacrifice to structural retention. Additionally, the plasmachemical route has several key strengths such as substrate material independence and ability to treat three dimensional features.

The choice of precursor is one of the critical factors, both for plasmachemical functionalisation, and for chemical vapour deposition techniques in general. Continuous wave plasma has tended to small, saturated organic molecules, with high volatility. The use of such molecules is convenient when the incident energy will largely, or completely, fragment the molecule anyway. The relatively mild energy input of the pulsed plasma polymerisation allows a broad range of organic precursors to be used. Critically, it also introduces a strong degree of control on the subsequent surface. The use of molecules based around acrylate and styrene functionalities, with multiple double bonds and delocalisation of electrons, allows polymerisation reactions with chain growth via radical chain growth. Compare for instance the relatively slow deposition of undecenal (Chapter 4) and the fast growth of 3-vinylbenzaldehyde (Chapter 5). The structural retention is sufficient that 3-vinylbenzaldehyde was even observed to fluoresce under laser illumination.

The extensive range of coated substrates presented in the work includes silicon, glass, carbon nanotubes, polystyrene beads, but is essentially only limited by the imagination of the author and reactor size. The ability to use exactly the same deposition route on multiple substrate architectures and materials is obviously an extremely desirable feature for potential use of any technology on an industrial scale.

Of course, pulsed plasmachemical functionalisation does have limitations. The relatively mild power input, that allows structural retention and use of fairly complex organic precursors, also means that some areas suffer. Production of robust layers, and the adhesion of the layers to a substrate are potentially weakened. There are routes to reduce or eliminate these problems, but only at the cost of decreased structural retention or extra process steps. Use of the technology for deposition of layers requiring extensive molecular rearrangement, such as the deposition of inorganic layers from organometallic precursors would be extremely challenging if not impossible. Also, whilst more complex precursors are of great interest to the pulsed plasma chemist, there is also the need to deliver a suitable vapour of a precursor into the reactor.

8.2 Key Findings

The use of plasmachemical functionalisation for the manufacture of DNA microarrays was demonstrated. This route relies on the use of the precursors undecenal (Chapter 4), 3-vinylbenzaldehyde (Chapter 5) and 2-bromoethyl acrylate. The previous plasmachemical routes towards either aldehyde or bromine functionalised surfaces have suffered from relatively poor structural retention, either through the use of continuous wave plasmas or the introduction of precursors that lack the polymerisable carbon-carbon double bond of the precursors used in this work.

The generation of functional surfaces with high structural retention and low crosslinking are key in generating suitable substrates of DNA immobilisation and hybridisation. For this reason the particularly challenging situation of 15-base oligonucleotides was chosen for the current work. The base pairing between two oligonucloetide strands relies on two or three hydrogen bonds between each base pair, so is relatively weak for such small oligonucleotide chains. So, the observation of hybridisation in this case gives strong confidence that the majority of oligonucleotides are bonded through the linker, rather than non-specifically adsorbed onto the surface, and so are suitable for use in even the more challenging screening experiments. Critically, for the aldehyde surfaces, a relatively low level of non-specific

adsorption to the surface was also observed. Without this, there would be little chance of achieving a suitable spatial resolution to allow the observation of hybridisation on the surface. The adhesion of proteins and dextrans to the surface was also demonstrated, and shows the versatility of the surface.

Whilst this work concentrated on this tough scenario, an interesting piece of further work would be to specifically tailor a surface for non-specific adsorption of larger DNA strands, which allows experimentally simpler screening. Another interesting route that might result in higher hybridisation densities would be to co-polymerise two molecules together. For instance the co-polymerisation of styrene and 3-vinyl benzaldehyde could potentially allow a reduction in the density of DNA immobilisation – however this might then result in more hybridisation overall.

Initial results for the use of plasmachemical functions for the reversible immobilisation of chloromethyl ketone (CMK) enzyme inhibitors to 2-hydroxyethyl methacrylate (HEMA) surfaces also demonstrates the potential of plasmachemical technologies for wound recovery. Although these initial results were obtained on glass and silicon rather than the gauzes and fabrics commonly used in wound dressings, the inhibitive effect of the CMK's on the activity of elastase has been demonstrated. A priority for any further work would be to establish the kinetics of the inhibition and, to relate this back to surface loading of CMK.

Understanding how factors such as substrate surface area, the parameters used in the plasmachemical deposition of HEMA, would allow this approach to be extended to actual dressing materials. As discussed above the move from a glass or silicon substrate to a fabric or fabric-like substrate should be relatively simple, although a fabric would be expected to have a much larger surface area than a flat piece of silicon or glass. This would need to be factored into both the plasmachemical functionalisation with HEMA and the subsequent loading of the substrate with CMK.

Further, the stability of the plasmachemical layer to long term liquid exposure in a wound environment will be critical. The hydroxyl layer produced by

plasmachemical functionalsation is hydrophilic, presenting two potential problems. The plasmachemical layer itself might act as a sponge and contribute to wound drying, or be preloaded with aqueous solution to maintain a moist wound environment. Also there is potential for any small fragments of poorly cross-linked material to desorb from the bulk plasmachemical layer into the wound itself, with the hydroxyl tail helping to solvate the small fragments.

Also presented are initial results which utilise plasmachemically functionalised layers as centres for the immobilisation of metals. These originally span out of the work presented in Chapters 3 and 4 on the deposition of aldehyde surfaces and the Tollens silver mirror test for an aldehyde. The metallization of CNT's via the silver route was not particularly successful, leaving only crystals with no discernable relationship to the plasmachemically modified CNT substrate. The electroless copper deposition via the vinyl pyridine proved to be extremely successful leaving copper deposited along the length of individual CNT bundles.

These initial promising results should be presented of course with the caveat that very little optimisation of the metallisation wet chemistry was performed. CNT's are a substrate with massive surface areas so driving reactions to completion on a whole batch of CNT's may be challenging even with relatively small masses. In particular, the relatively low loading of Cu seen by XPS suggest that there is significant room for improvement, and that the Cu loading could be significantly increased. However, it should be remembered that in spite of the many exciting suggestions for the potential use of CNTs, processability remains a major hurdle. This work has highlighted one simple approach to treating CNTs, which should be easily applicable to the introduction of any functional group available in the plasmachemical library. The use of the plasmachemical route also offers a potential route to bulk CNT-organic composites. Combination of CNT's with a relatively long deposition of a plasmachemical layer with a high deposition rate, such as 3-vinylbenzaldehyde, could potentially allow for the cross-linking of a CNT

powder and the formation of such a composite layer measuring depths of hundreds of nanometres, or even microns.

Further, the relatively mild conditions offered by the pulsed plasmachemical route offer one of very few vapour deposition routes to the functionalisation with relatively complex molecules. Another extension of this work would be to identify relatively volatile organo-metallics which could be introduced into the plasma to form a suitable layer. Ferrocene is one such molecule that is volatile, subliming at relatively low temperature. However, care would need to be taken to introduce a suitable polymerisable function to the organic ligands to allow the classical polymerisation reactions to occur without major fragmentation of the molecule.

Overall a broad range of applications have been studied, springing both from targeted precursor selection of the aldehyde, bromine or hydroxyl groups, based on the already existing body of work in the scientific literature. There is also an extension of the function of such layers, which sprang originally from the Tollens test for aldehydes, but extended to the immobilisation of other metals to the plasmachemical layers.

Appendix 1. Some initial results demonstrating heterogeneous catalysis using methylrheniumtrioxide co-ordinated to plasma polymerised 4-vinylpyridine

1. Introduction

A technology is presented in which a plasmachemical pyridine surface is utilised as a substrate for methyl rhenium trioxide (MTO) immobilisation onto a substrate of interest. The reactions are characterised by XPS, FT-IR, sessile drop contact angle and PIXE analysis, and the generated surfaces proved suitable for catalysis of the styrene vinyl group to the epoxy and diol products.

1.1 MTO Catalysis

MTO ($(CH_3)ReO_3$) is a well known transition metal catalyst that has been demonstrated to catalyse numerous organic transformations, with particular use in catalytic oxidations (see Abu-Omar *et al* for a review[1]). Recent applications include in epoxidation of glycals[2]; the Bayer-Villiger reaction (oxidation of cyclic ketones to cyclic esters) in ionic liquid[3], selective oxidation of terminal alcohols[4]; oxidation of arenes to p-benzoquinones[5].

As well as the extensive use of MTO in oxidative reactions, MTO is has proven versatile enough to catalyse the reduction of epoxides in the presence of triphenylphosphine for Vitamin E synthesis[6,7].

1.2. MTO on Surfaces for Heterogeneous Catalysis.

Heterogenization of the MTO catalytic process presents potential benefits in recovery of catalyst and improved reactivity.

1.2.1 *Polymeric Substrates*

Saladino and co-workers have carried out extensive work based on incorporating MTO catalysts into polymeric substrates. These heterogeneous catalysts are manufactured using commercially available pVP (polyvinylpyridine) cross-linked with 2% / 25% divinylbenzene, pVPN (poly(4-

vinylpyridine-*N*-oxide) (2% crosslinked)), pS (polystyrene (2% crosslinked)). These polymer based heterogeneous catalysts are suitable for a variety of reactions, including C-H insertion reactions[8,9]; oxidation of cardanol derivatives[10]; epoxidation of terpenes[11]; epoxidation and ring opening of glycals[12]; epoxidation of olefins[13]; oxidation of phenols and anisoles to quinones[14].

The efficiency of these reactions is high. In the case of epoxidation of olefins the reaction will proceed slowly in the absence of MTO, with <2% conversion of substrates. Introduction of heterogeneous MTO under identical conditions results in >98% conversion, with high selectivity of the epoxide over the diol (>98% preference in the case of styrene, cis-cyclooctene, α-methylstyrene, and *trans*-stilbene in the presence of 25% cross linked pVP-MTO)[13]. Crucially, the catalyst retained stability over successive oxidations.

Via Pyridine (and pyridine-N-oxide) Ligands

The chemistry utilised in the preparation pVP/pVPN-MTO catalysts systems is simple (Figure 1).

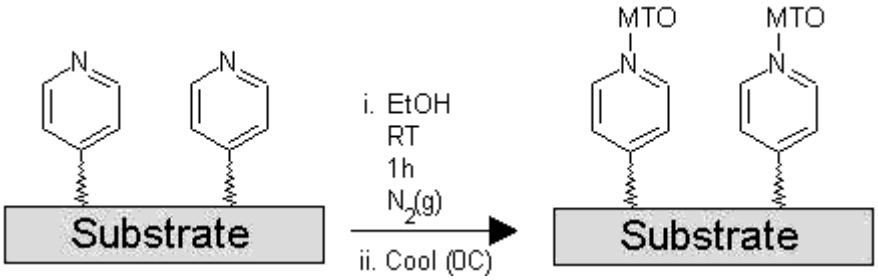

Figure 1. Immobilisation of MTO via Pyridine Ligands[13].

In the first step the pVP/pVPN is suspended in ethanol at room temperature and powdered MTO added to the reaction mixture, which is then stirred for 1h. Typically, a loading factor (mmol MTO per gram of support) of 0.5-1.0 was used. The reaction was then cooled to 0℃ and the polymers were observed to change from colourless to bright yellow (only weak colour for pVPN). pVP/pVPN-MTO catalysts were recovered by filtration, washed with ethyl

acetate several times, and used without further purification. No trace of MTO was recovered with the organic solvent.

Via Polystyrene Encapsulation

Again, simple preparation of the heterogeneous catalyst is presented (Figure 2).

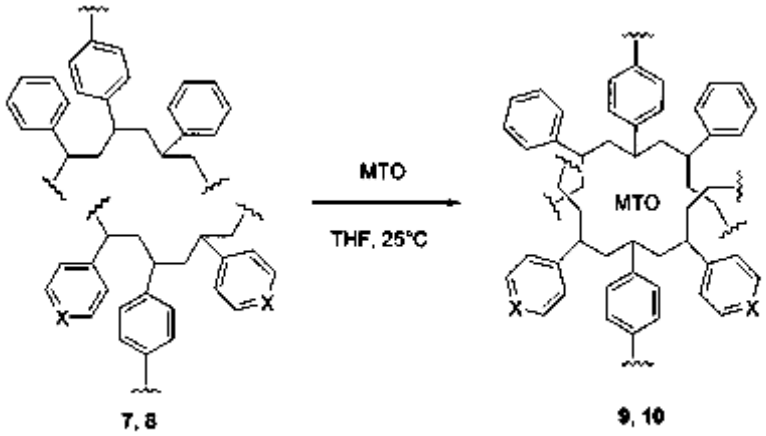

Figure 2. MTO Encapsulation in pS or pS/pVP Mixtures[13]

The substrate was suspended in THF at room temperature, causing the polystyrene to swell, powdered MTO was added to the suspension under a nitrogen atmosphere. On addition of hexane and stirring for 1 hour, polymers were observed to change from colourless to bright blue. No trace of MTO was recovered in the organic phase.

1.2.2 *Zeolite Supported Re Catalysts*

MTO can be physisorbed onto zeolites by CVD[15]. MTO heated to 333 K at 10^{-3} Pa sublimes and is allowed to enter a reaction chamber in which zeolite is present (pretreated at 673 K for 4 h at 10^{-3} Pa). Deposition takes place over a period of 14 h at RT and samples are evacuated to remove undeposited MTO. These are subsequently used in oxidation of propene to acrolein at 673 K. Note that although the major CVD product is MTO co-ordinated to the surface,

subsequent treatments yield tetrahedral ReO_4 that is chemically bound to the surface.

1.2.3 *Niobia Substrates*

Catalytic activity of MTO on niobia (Nb_2O_5) has been reported[16]. The niobia acts as a Lewis base in an analogous manner to the pyridine ligands, producing similar fast reactions and high (100%) conversions as pVP systems[17].

1.3. Potential Benefits of Pulsed Plasmachemical Route to Surface Tethered MTO.

The excellent structural retention in, and wide the variety of functional groups available for, pulsed plasmachemical functionalisation make this technology a strong candidate for use in catalytic systems such as the vp-MTO system. The substrate independence of pulsed plasmachemical functionalisation allows a wide range of potential substrate architecture and chemistry whilst retaining identical MTO immobilisation chemistry and catalysis conditions to those available in the literature. Candidate substrates in the field of catalysis could include any high surface area architectures such as beads, carbon nanotubes, or more macroscopic structures such as the surface of standard reaction glassware.

Alongside the massive potential of plasmachemical technology for use with any substrate, the proven structural retention in films formed from precursors such as 4-vinylpyridene allows high yields. Further, there is potential to ‘tune’ the environment in which a catalyst such as MTO operates by adjusting parameters of the deposition, with a view to improving reaction efficiency or selectivity.

In this chapter results for the surface immobilisation of MTO onto 4-vinylpyridene and subsequent catalytic action of the prepared surfaces are presented. Substrates include glass, silicon, polystyrene beads.

2. Experimental

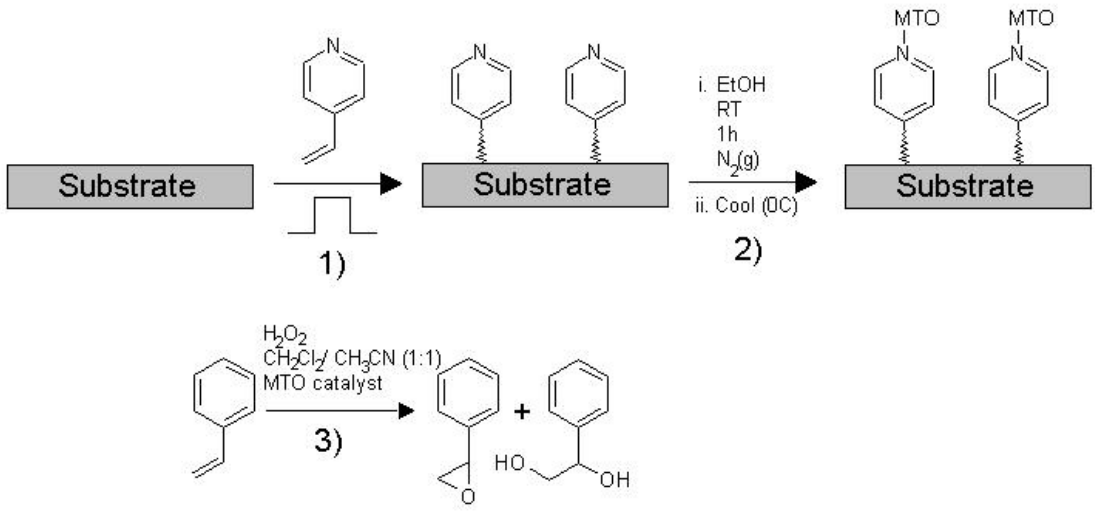

Scheme 1. 1) Pulsed plasmachemical functionalisation of substrates to create pyridine groups on the surface. 2) Attachment of MTO via nitrogen lone pair. 3) Surface bound catalyst is then suitable for epoxidation of olefins such as styrene to give phenol oxirane or phenyl ethanediol.

Reaction 1.

Plasma polymerization of 4-vinylpyridine (Aldrich, 95%, H2C=CH(C_5H_4N), purified by several freeze-pump-thaw cycles) was carried out in an electrodeless cylindrical glass reactor as described in Chapter 2.

4-vinylpyridine was introduced into the reactor at a pressure of 0.22 mbar and a flow rate of 9.3 x 10^{-8} mol s^{-1} for 15 min prior to reaction. Deposition took place over 60 min in a t_{on} = 100 µs, t_{off} = 4 ms pulsing regime and a peak power of 40 W. Subsequent to reaction the chamber was flushed with monomer for 15 min. Substrates included borosilicate glass cover slips, polished silicon wafers and SWCNTs.

Reaction 2.

Previously described loading of pVP was be repeated[13]. 369.8 mg of resin was suspended in 4 mL methanol. To this was added 140 mg of MTO and the

mixture stirred for 1h using a magnetic stirrer and then slowly cooled to 0 ℃. Solvent was removed by filtration and the solid residue washed five times with 20 mL ethanol and dried under high vacuum. A yellow coloured powder remained and was used without further purification.

Reaction 3.

Previous heterogeneous catalysis with MTO was repeated[13]. 1 mmol of styrene in 2 mmol of H_2O_2 (30% aqueous solution), to 5.0 ml CH_2Cl_2 / CH_3CN (1:1 v/v) in which 120mg of the MTO catalyst was suspended. After reaction, the catalyst was recovered by filtration, and washed 5 times in 10 ml ethanol. The filtrate was treated with a small amount of manganese dioxide (MnO_2) at 25 ℃ and filtered. The solvent was dried with Na_2SO_4 after removal of the solvent the crude product was analysed by GC-MS.

Surface Analysis

Surface analysis by XPS, FT-IR, sessile drop contact angle and reflectometry is described in previous chapters.

3. Results

3.1. Plasmachemical Functionalisation of Surfaces with 4-Vinylpyridene

The plasmachemical functionalisation of surfaces with 4-vinylpyridene (t_{on} = 100 µs, t_{off} = 4ms, P_P = 40 W) was followed by XPS, which shows good correspondence with the expected surface atomic composition (Table 1), with the C(1s) envelope lacking any major oxygenated components. A corresponding deposition rate of 8 ± 1 nm min^{-1} was observed.

	C(1s) (%)	N(1s) (%)	O(1s) (%)
Theoretical	88	13	0
100 µs t_{on}, 4 ms t_{off} Plasmachemical Functionalisation	83 ± 2	11 ± 1	5 ± 1

Table 1. Surface composition of plasmachemically functionalised pyridine surfaces.

Analysis of the as-deposited films by FT-IR confirms deposition of 4-vinylpyridene with good structural retention (Figure 3), with the major bands from the monomer retained and only minor line broadening. In particular, bands from the aromatic pyridine function are retained. Both monomer and functionalised layer show broad bands in the 3000-3500 cm^{-1} region, which are attributed to adsorbed water on the hydrophilic surface.

As deposited pyridine surfaces gave a contact angle of 27 ± 1°.

3.2. Complexation of Methyl Rhenium Trioxide.

The reaction of pyridine functionalised surfaces with MTO was monitored by XPS which showed inclusion of 0.5 ± 0.2 % Re on the surface and a marked increase in oxygen content (Table 2). Particle induced X-ray emission analysis also confirmed the presence of Re at 41,371 ppm ± 3.17 % (or an contribution of 4.1 ± 0.1 wt%).

The reaction was also followed by FT-IR (Figure 4) which showed a marked reduction of the pyridine ring stretch at 1600 cm^{-1} and the introduction of a band at 1640 cm^{-1} corresponding to the coordinated ring. The strong band at 912 cm^{-1} is attributed to Re=O asymmetric stretching.

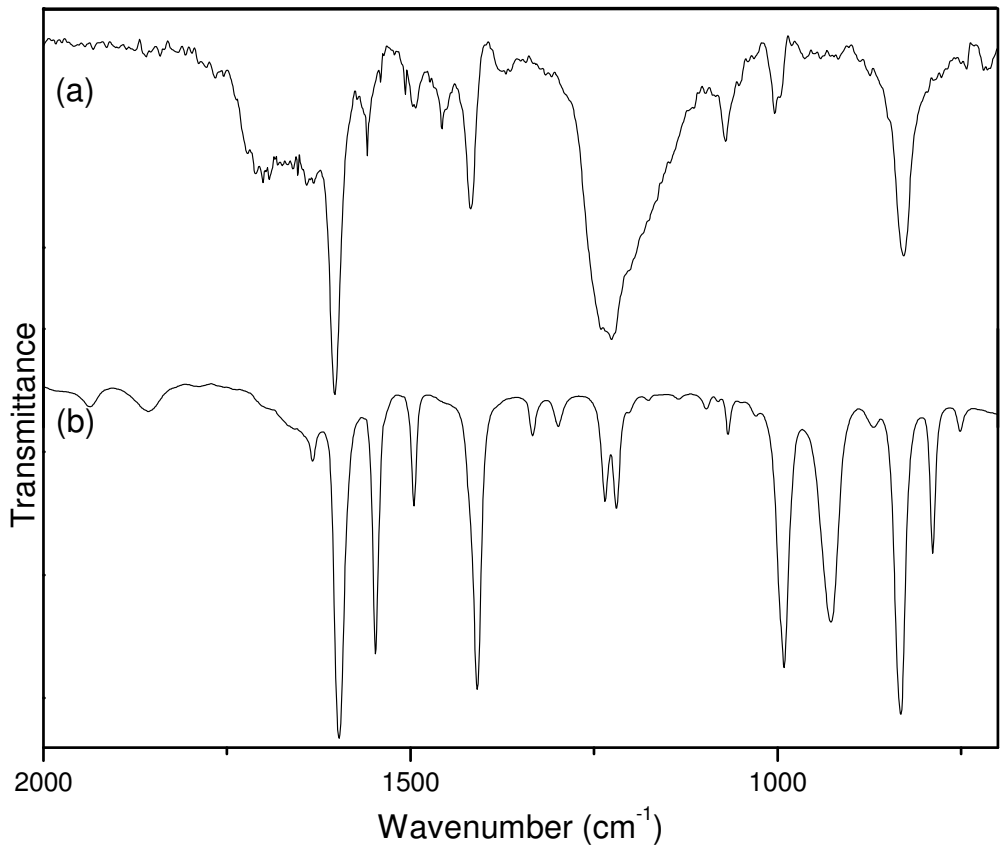

Figure 3. FT-IR spectra of vinyl pyridine (t_{on} = 100 µs, t_{off} = 4ms, P_P = 40 W). (a) Plasmachemical functionalised pyridine surface. (b) 4-vinyl pyridine monomer.

	C(1s) (%)	N(1s) (%)	O(1s) (%)	Re (%)
Theoretical	62	8	23	8
Observed	65 ± 6	12.2 ± 0.1	22 ± 6	0.5 ± 0.2

Table 2. Surface composition of plasmachemically functionalised pyridine surfaces after reaction with MTO.

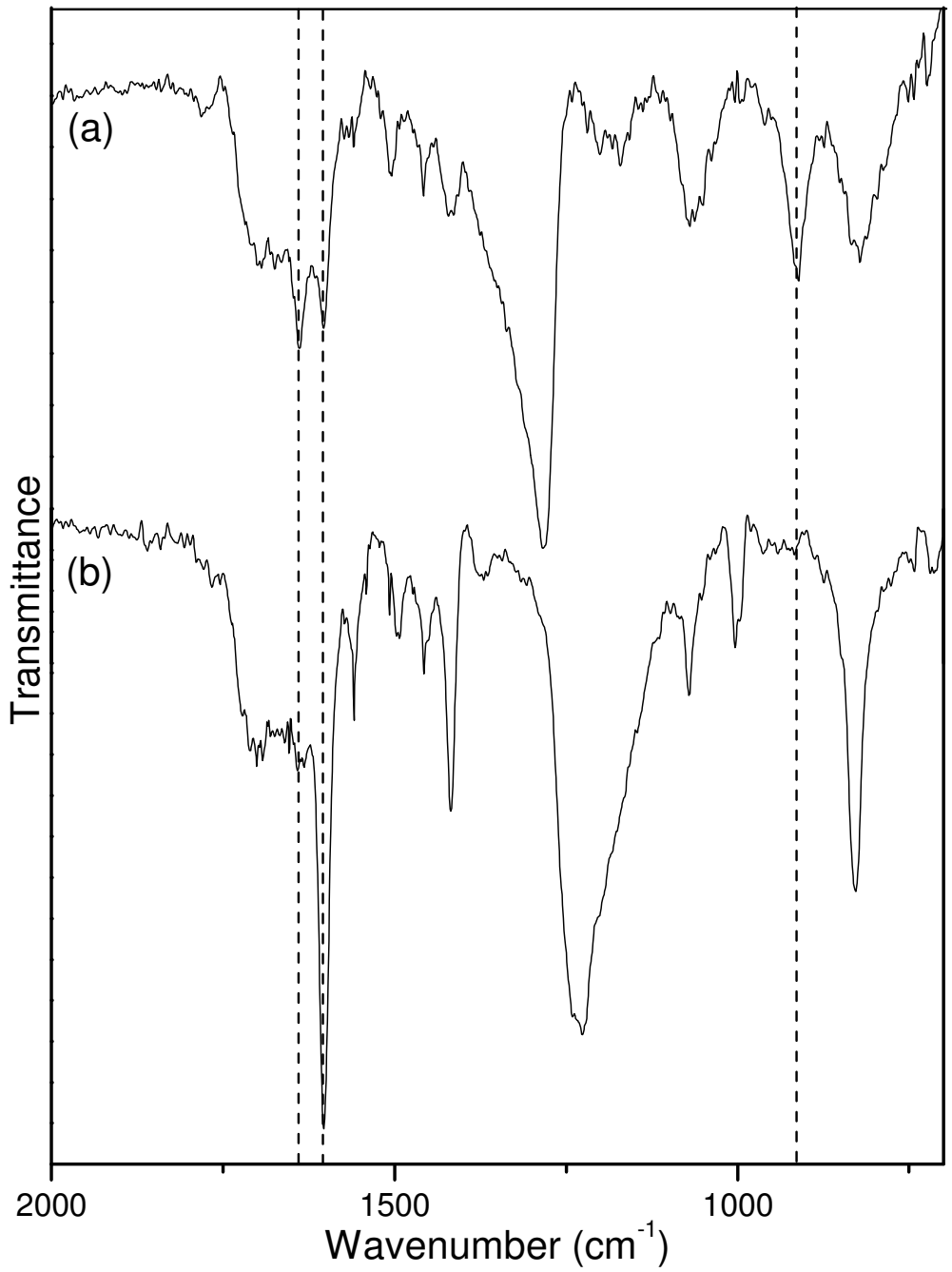

Figure 4. FT-IR spectra of vinyl pyridine (t_{on} = 100 µs, t_{off} = 4ms, P_P = 40 W). (a) After reaction with MTO. (b) As produced plasmachemical functionalised pyridine surface.

	Product (%)		
	Run1	Run2	Error
Styrene	22	49	1
Phenol Oxirane	37.2	34.3	0.5
Phenyl ethanediol	40.7	16.6	0.7

Table 3. Catalysis products of styrene oxidation with MTO surface immobilised to plasmachemical pyridine functions.

After reaction, substrates were observed to change colour to a rich yellow-orange, and the contact angle on flat substrates was observed to increase to 46 ± 2° for the MTO treated plasmachemical surface. Elemental analysis of washings suggested reaction of 96.06 % MTO to give an average loading of 2.13 mg cm^{-2}.

3.3. Heterogeneous Catalysis of Styrene with Surface Immobilised MTO

The epoxidation of styrene was followed by GC-MS (Figure 5). The resultant product mixture was observed to contain three major regions at 6.5 min, 10.5 min and 12 min. The region at 6.3 min corresponded to the styrene control, and MS of this peak confirmed fragments at m/z 105 (C_6H_7, styrene), 78 (C_6H_6), 77 (C_6H_7), and 52 (C_4H_4) (Figure 6). The band at 10.7 min returned fragments at 121 (C_8H_9O, Phenol oxirane-H^+) (Figure 7) and the band at 12 min returned the molecular ion at 138 ($C_8H_{10}O_2$, phenylethanediol), 91 (C_7H_6), and 77 (Figure 8).

Re-running the catalysis with the same MTO-substrate showed a 20% decrease in the converted styrene %, and a marked increase in the selectivity of epoxide from 1:1 epoxide:diol to 2:1.

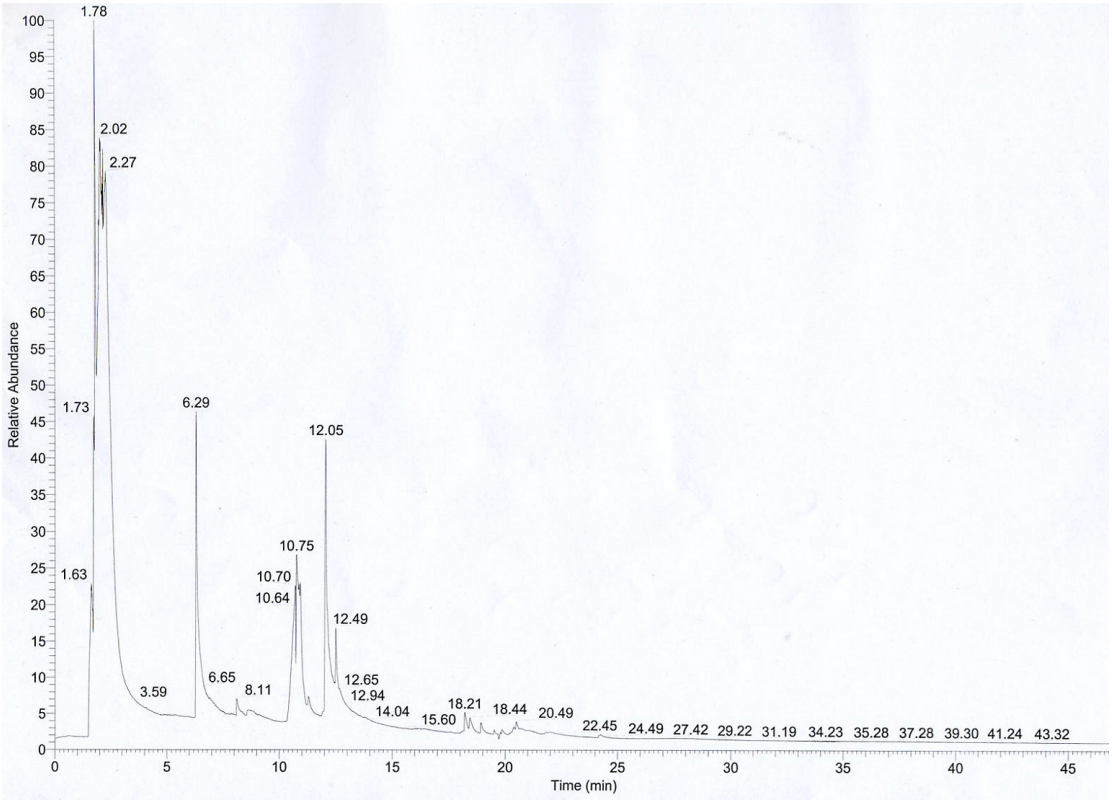

Figure 5. GC-MS of reaction products from heterogeneous catalysis of styrene.

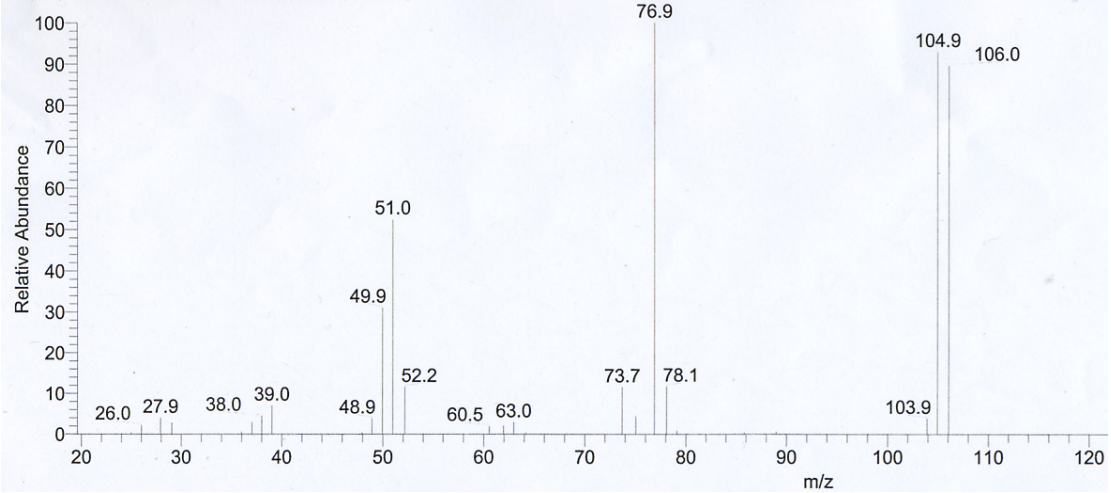

Figure 6. MS of reaction products from heterogeneous catalysis of styrene in the 6.3 min region.

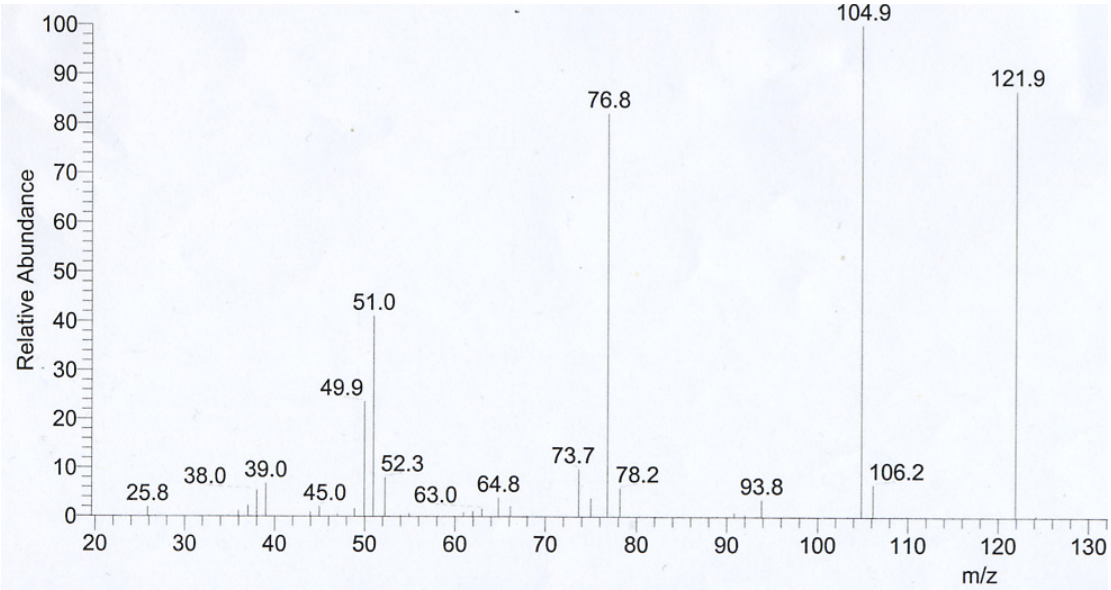

Figure 7. MS of reaction products from heterogeneous catalysis of styrene in the 10.7 min region.

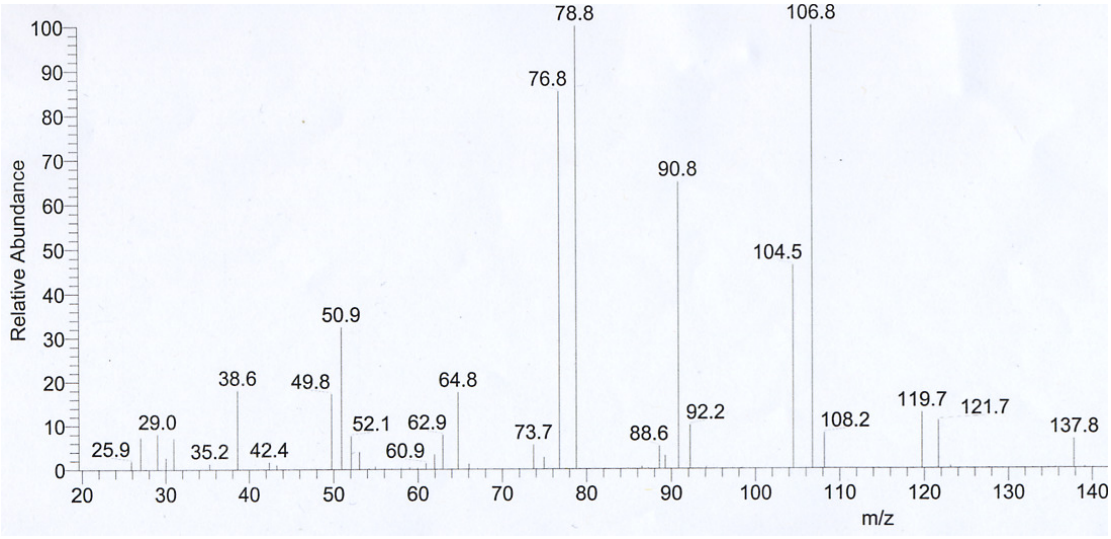

Figure 8. MS of reaction products from heterogeneous catalysis of styrene in the 12 min region.

4. Discussion

The deposition of 4-vinylpyridene proceeds with excellent structural retention. Crucially, FT-IR confirms that the aromatic pyridine structure is retained, with XPS identifying only minor oxygen incorporation. The pyridine functions give the surface a distinctive hydrophilicity as identified both by sessile drop contact angle and from large water bands observed in the FT-IR. This hydophilicity is compromised by the subsequent complexation of the catalyst MTO onto the surface via the electron lone pair on the nitrogen group, and results in the observed increase in the sessile drop contact angle in the immobilisation reaction.

XPS analysis of the prepared MTO-pyridine surfaces suggests a surprisingly small amount of MTO on the surface, a meagre 6 % of the theoretical Re present on the surface. However, PIXE analysis suggests that 4% Re is present (50% of the theoretical surface). This discrepancy is probably due to the UHV conditions employed by XPS analysis – and the relatively long time the substrate is retained at UHV. The known volatility of MTO suggests that it could be stripped from the substrate surface. PIXE also has a greater penetration depth than XPS, so can sample deeper into the substrate.

The presence of a sizable amount of MTO is further confirmed by FT-IR, where the appearance of the MTO band at 912 cm^{-1} is accompanied by a marked reduction of the pyridine ring stretch at 1600 cm^{-1}. The disruption of the aromaticity of the pyridine ring when complexation occurs causes a shift to 1640 cm^{-1} which strongly confirms the reaction has proceeded.

The observed loading of MTO onto the substrate compares favourably to those observed previously (0.5 or 1.0 mmol MTO for each 1g of support) and suggest that enough MTO is present to initiate catalysis – the strong colour change in the treated substrate is also a good indication that complexation has occurred.

The catalysis of styrene epoxidation does not result in the yield or selectivity that would be required to utilise the plasmachemical system in the laboratory for catalysis. Desired conversion and selectivity are in the region of 99%. However, one of the advantages of the plasmachemical technology is the ability to tailor surfaces via optimising pulsing parameters. Whilst the plasmachemical pyridine surface in this work was optimised for structural retention a promising line of future inquiry is likely to be how the pulsing parameters of the deposition modify the ultimate yield and conversion of the catalysis. In particular, the degree of crosslinking in the substrate has a demonstrable effect on the catalysis and switching to more rigorous deposition conditions (longer t_{on}, shorter t_{off}, greater power, or even continuous wave deposition) would allow the degree of crosslinking to be increased.

Increasing crosslinking density might also be a solution to the reduction in catalytic activity observed when the substrate is re-used a second time. The relatively destructive conditions used in the epoxidation reaction might have caused some surface damage, and crosslinking would minimise this. However, the reaction does still proceed and surprisingly becomes more selective for the epoxide. The decrease in styrene conversion also matches the reduction in observed diol yield, suggesting that either some of the catalyst (corresponding to the diol conversion) is lost or that rearrangements in the surface structure, such as swelling in solvent, are changing the chemical environment around the catalyst.

Exploring the effect of cross-linking by varying deposition parameters would provide a good starting point for future work. Also of interest would be the effects of the catalyst on other alkenes, as previous literature indicates that the extent and selectivity of conversion can depending on the substrate structure.

5. Conclusion

The applicability of pulsed plasmachemical technology to heterogeneous catalysis has been demonstrated. The use of a plasmachemical film to

provide a ligand for the surface immobilisation of a transition metal catalyst such as MTO and its subsequent catalytic action were demonstrated.

1 Owens, G. S.; Arias, J.; Abu-Omar, M. M. *Catalysis Today*, **2000**, *55*, 317

2 Soldaini, G.; Cardona, F.; Goti, A. *Tetrahedron Letters* **2003**, *44*, 5589

3 Bernini, R.; Coratti, A.; Fabrizi, G.; Goggiamani, A. *Tetrahedron Letters* **2003**, *44*, 8991

4 Herrmann, W. A.; Zoller, J. P.; Fischer, R. W. *J. Organometallic Chemistry* **1999**, *579*, 404

5 Jacob, J.; Espenson, J. H. *Inorganica Chimica Acta* **1998**, *270*, 55

6 Hyatt, J. A.; Kottas, G. S.; Effler, J. *Organic Process Research and Development* **2002**, *6*, 782

7 Hyatt, J. A.; US6156913, WO0001649

8 Bianchini, G.; Crucianelli, M.; De Angelis, A.; Neri, V.; Saladino, R. *Tetrahedron Letters* **2005**, *46*, 2427

9 Bianchini, G.; Crucianelli, M.; De Angelis, A.; Neri, V.; Saladino, R. *Tetrahedron Letters* **2004**, *45*, 2351

10 Saladino, R.; Mincione, E.; Attanasi, O. A.; Filippone, P. *Pure Appl. Chem.* **2003**, *75*, 265

11 Saladino, R.; Neri, V.; Pelliccia, A. R.; Mincione, E; *Tetrahedron* **2003**, *59*, 7403

12 Saladino, R.; Cardona, F.; Goti, A. *Tetrahedron Letters* **2003**, *44*, 5589

13 Saladino, R.; Neri, V.; Pelliccia, A. R.; Caminiti, R.; Sadun, C. *J. Org. Chem.* **2002**, *67*, 1323

14 Saladino, R.; Neri, V.; Mincione, E.; Filippone, P. *Tetrahedron* **2002**, *58*, 8493

15 Viswanadham, N.; Shido, T.; Sasaki, T.; Iwasawa, Y. *J. Phys. Chem. B* **2002**, *106*, 10955

16 Li, M.; Espenson, J. H. *J. Molecular Catalysis A: Chemical* **2004**, *208*, 123

17 Bouh, A. O.; Espenson, J. H. *J. Molecular Catalysis A : Chemical* **2003,** *200*, 43